CLIMATE-DRIVEN LANDSCAPE CHANGE AND THAW SLUMP IMPACTS ON HIGH ARCTIC STREAM SYSTEMS IN EUREKA, NUNAVUT, CANADA.

Kethra Campbell-Heaton

Thesis submitted to the University of Ottawa
in partial fulfillment of the requirements for the
Doctor of Philosophy in Geography.

Department of Geography, Environment and Geomatics
Faculty of Arts
University of Ottawa

© Kethra Campbell-Heaton, Ottawa, Canada, 2026

Abstract

Permafrost thaw is increasingly threatening infrastructure, ecosystem function and freshwater security. Retrogressive thaw slumps (RTS), for example, are increasing in frequency across the Canadian Arctic, including High Arctic locations. Most knowledge of the hydrological impacts of thaw slumping is based on studies in the Western Canadian and Alaskan Arctic, where thaw slumping is pluvial driven. In the Eureka region, thaw slumping is widespread and linked to warmer summer air temperatures. However, the hydrological impacts of thaw slumps on local streams remain unquantified. This PhD thesis therefore (1) quantifies regional landscape change, (2) isolates the geochemical effects of thaw slumping on nival streams, and (3) evaluates how regional climate influences stream activity in the region of Eureka, Ellesmere Island, Nunavut.

Landsat trend analysis spanning from 1999 to 2024 shows that 79.3% of the Fosheim Peninsula experienced significant positive change in greening (vegetation increase), 42.3% in brightness (surface reflectance) and 31.2% in wetness (surface water and ground moisture). Notably, 26% of areas with positive greening trends occur on barren land. Random-forest classification indicates aridification processes on 3.7% of the peninsula. LARCH visual analysis shows substantial geomorphic reorganization, including widespread fluvial erosion and channel migration in the Slidre River system. Over the 25-year period, nine lakes fully or partially drained, and 139 thaw slumps were identified, 60 of which were active in 2024. Stream chemistry from two nival-dominated streams shows that RTS had no impact on stream δD-$\delta^{18}O$ but increased dissolved organic carbon and solute concentrations, including elevated chloride downstream of disturbances. Stream-climate interactions indicate that intra-stream temperature variability is governed primarily by channel morphology and temperature inversion rather than thermokarst activity. Climate–temperature relationships shifted between years: air temperature strongly controlled stream temperature in the cold–wet year (avg among sites $r = 0.76$), whereas solar radiation dominated in the warm–dry year (avg among sites $r = 0.56$). Stream discharge was greater and more variable in 2022, while suspended sediment and dissolved particulate loads were significantly elevated downstream of RTS during the dry 2023 season ($p < 0.001$). Collectively, these results show that the region is undergoing rapid climate-driven landscape change, RTS significantly alters stream geochemistry and sediment loads, whereas climatic conditions directly control stream discharge and temperature.

Acknowledgements

First and foremost, I would like to thank my supervisor, Dr. Denis Lacelle for his support and guidance over the course of this project. Denis, thank you for the opportunity to study this unique landscape and for giving me the space to learn. Thank you for helping me take my idea and turn it into reality – and then some. Thank you for encouraging my involvement in volunteer activities, participating in national conferences and furthering my training with graduate level courses. Most of all thank you for your patience and support over the years.

I'd like to thank Dr. Konrad Gajewski, who has been my sounding board over the last few years. KG, thank you for your wisdom, your jokes and always asking "Is your thesis done yet?". Thank you for your friendship and support, words cannot express how much you've helped me, thank you.

Thank you to Jean Bjornson for your friendship and aid in organizing my field campaigns. I am very grateful that you didn't get angry (at least that I saw) after I broke the velocity meter, sorry about that! Thank you to Dr. Bernard Lauriol and Jacob Prest for your assistance in the field. BL, thank you for your patience while I searched for my lost phone. Thank you for showing me how you conduct field research, how you look at an area and say, "let's go over here and just take a peek". Your curiosity was infectious and awe-inspiring. JP, I would probably still be stuck in that creek without your help. Thank you for accompanying me to this remote region and sticking it out with me for the three weeks, without a shower and a bucket for a w/c. I want to also thank PCSP for the logistical support of both field campaigns, the staff were amazing and supportive. Thank you for helping me get up to Eureka, making sure I had all the equipment I needed and making sure myself and field assistants were safe. Much appreciated, I hope I get to work with you all again in the future.

I want to express my appreciation for the laboratory support I have received over the last few years. The Ján Veizer and Geochemical laboratories at uOttawa were wonderful and prompt with analyses; thank you for your support. Thank you to Simiarani Mohanty and Dr. Nimal De Silva for always being so kind when I showed up to run another batch of samples.

Thank you to my peers in my lab and volunteer groups over the years. Thank you to E. Carrière, B. Faucher, R. Frappier, G. Gaudreau, Y. Wu, G. Richardson, and so many others for your camaraderie. Thank you to my colleagues with the Parks Canada Wood Buffalo Action Plan Team, I am so fortunate to have had the opportunity to work with you all; big shout out to P. Wilson – thank you for your unwavering support and encouragement.

This research would not have been possible without the support from the Natural Sciences and Engineering Research Council of Canada (NSERC), the Northern Scientific Training Program (NSTP), the Royal Canadian Geographical Society (RGS), the Association of Canadian Universities for Northern Studies (ACUNS) and the Ontario Graduate Scholarship (OGS). Additional logistical support was provided by the Polar Continental Shelf Program (Natural Resources Canada).

Finally, I would like to thank my parents, Mark and Abi, for their support and encouragement as I found footing in this field I love. Thank you to J. Prest for never letting me quit… every few months… and, encouraging me to go after what I want. Thank you for putting up with the late-night r-coding sessions, giving me the space to get sucked into whatever part of this project that held my attention and listening to me ramble about my findings. Wow, it has been a journey (and it's just getting started).

This thesis is dedicated to my daughter Aura. Girlie, you can do anything.

I would also like to acknowledge you, the reader. My hope is that this document provides clarity, insight, and a useful contribution to our understanding of a rapidly changing Arctic landscape. The Fosheim Peninsula is highly sensitive to climate warming, and the changes documented here are part of broader transformations occurring across many regions of the world. As scientists, we have a responsibility to report these changes with accuracy and care; as people, we share a responsibility to steward the environments we depend on.

Finally, to any graduate student reading this: you are not alone in the challenges of graduate studies. The process can be demanding, but it is worth the effort. I hope your own work brings you the same sense of purpose and discovery that this project has brought me.

Table of Contents

Abstract....ii
Acknowledgements....iii
List of Figures....x
List of Tables....xiii
List of Abbreviations....xiv
Chapter 1....1
1.1 Introduction....1
1.2 Background Literature....4
1.2.1 Introduction to Permafrost Landscapes....4
1.2.2 Remote Monitoring of Arctic Landscapes....6
1.2.3 Terrestrial Hydrology in Permafrost Environments....8
1.2.3.1 Atmospheric Water....9
1.2.3.2 Surface Water....10
1.2.3.3 Ground Ice....11
1.2.3.4 Ground Water....12
1.2.4 Nival Streams....14
1.2.5 Permafrost Thaw Detection in Streams....15
1.3 Study Area....16
1.3.1 Glaciation and Surficial Sediments....16
1.3.2 Modern Climate....17
1.3.3 Modern Vegetation....17
1.3.4 Permafrost and Ground Ice....18
1.3.5 Watershed Characteristics....19
1.3.5.1 Blacktop Creek Watershed:....19
1.3.5.2 Station Creek Watershed:....20
1.3.5.3 Historical water quality data of Station and Blacktop Creeks....20
1.4 Thesis Organization and Research Objectives....21
1.5 Authorship and Co-authorship contributions....24
1.6 References....25
1.7 Figures....33
Chapter 2....36

2.1 Introduction....37
2.2 Study Area....38
2.3 Methods....40
2.3.1 Imagery Acquisition....40
2.3.2 Landscape change detection....41
2.3.3 Classification of Landscape Changes....41
2.3.4 Multi-scale Image Analysis....43
2.4 Results....43
2.4.1 Significant changes in TCG, TCB and TCW....43
2.4.2 Classified Landscape Change....44
2.5 Discussion....46
2.5.1 Response of the Fosheim Peninsula to Warmer-Wetter Climate....46
2.5.2 The Fosheim Peninsula as a Predictor of Changes in the High Arctic....48
2.6 Conclusions....50
2.7 Acknowledgements....50
2.8 References....52
2.9 Captions....56
2.10 Tables....57
2.11 Figures....59
Chapter 3....67
3.1 Introduction....68
3.2 Study Area....69
3.3 Methods....71
3.3.1 Site Description....71
3.3.2 Sample Collection....72
3.3.3 Laboratory Analyses....72
3.3.4 Data Analysis....73
3.4 Results....73
3.4.1 Potential Source Chemistry:....73
3.4.2 Geochemistry Of Ice-Rich Permafrost Exposed in Headwalls....74
3.4.3 Hydrochemistry Of Slump Runoff and Streams....75
3.4.3.1 Interannual stream hydrochemistry variations....75
3.4.3.2 Hydrochemistry of undisturbed sites....75

3.4.3.3 Hydrochemistry of Slump Runoff: 76
3.4.3.4 Hydrochemistry of Disturbed Sites: 76
3.5 Discussion 79
3.5.1 Above Disturbance Stream Conditions 79
3.5.2 Slump Runoff Conditions 80
3.5.3 Below Disturbance Stream Conditions 81
3.6 Conclusion 84
3.7 Acknowledgments 85
3.8 References 85
3.9 Captions 91
3.10 Tables 92
3.11 Figures 94
Chapter 4 99
4.1 Introduction 100
4.2 Study Site 101
4.2.1 Watershed Characteristics 102
4.3 Methods 103
4.3.1 Passive Stream Monitoring 103
4.3.1.1 Logger deployment: 103
4.3.1.2 Water-level data processing: 103
4.3.2 Total Suspended Sediment and Total Dissolved Particulates 103
4.3.3 Manual Discharge 104
4.3.4 Data Analysis 105
4.4 Results & Discussion 106
4.4.1 Temperature Response of Two Nival-Dominated Streams. 106
4.4.2 Stream Temperature Climate Forcings 107
4.4.3 Stage-Discharge Relationship of Nival Dominated Streams 108
4.4.4 Suspended Sediment and Dissolved Particulate Load of Nival Fed, RTS Impacted Streams 110
4.5 Conclusion 111
4.6 Acknowledgments 112
4.7 References 112
4.8 Captions 116
4.9 Tables 117

4.10 Figures 118
Chapter 5 123
5.1 Summary and Conclusions 123
5.2 Limitations and Future Research Directions 125
5.3 Key Contributions 128
5.4 References 129
Appendix A : Data Download 131
Appendix B : Chapter 2 Code 132
Appendix C : Chapter 3 Code 148
Appendix D : Chapter 4 Code 155

List of Figures

Figure 1.1. Project study region (A) is the Canadian Arctic Archipelago, and (B) the Fosheim Peninsula with Station Creek and Blacktop Creek basin and course outlines. Geospatial data (populated areas, watercourses, digital terrain model, Northern Canada outline, Canada outline) provided by Natural Resources Canada. 33
Figure 1.2. Active thaw slumps monitored in Chapters 3 and 4. (A) Nunavut Slump – Blacktop Creek; (B) BL Slump - Station Creek; (C) CHP Slump – Station Creek. All photos were captured in July 2023 by author or J. Prest. 34
Figure 1.3. Slump runoff sample locations and runoff-stream mixing sites. (A) Nunavut Slump – Blacktop Creek; (B) BL Slump – Station Creek; (D) CHP Slump – Station Creek. 35
Figure 2.1. Map of study area, (A) shows study site in relation to Canadian Arctic Archipelago and Canada; (B) shows Fosheim Peninsula, labelled, elevation (ArcticDEM 4) with maximum extent of marine inundation (150m asl in black). Data for large water bodies and water courses from Natural Resources Canada (Government of Canada, 2019a; 2022). 59
Figure 2.2. Annual image collection used for this analysis. Images filtered from July 10 (192) to August 10 (223), number of images per collection indicated at the top of figure..... 60
Figure 2.3. Results of Mann-Kendell analysis; displayed is the significant ($p<0.05$) slope values. (A) illustrates the RGB (R = TC Brightness, G=TC Greenness and B=TC Wetness). (B) TC Greenness, (C) TC Wetness and (D) TC Brightness. Watercourses outlined in grey, marine limit (146m a.s.l.) denoted by black dashed line..... 61
Figure 2.4. Results of Random Forest land change classification, marine limit denoted by dashed line. Stable and bedrock classes are omitted. 62
Figure 2.5. LARCH result, map illustrating the RGB (Brightness slope – red, Greenness slope – green, and Wetness slope – blue) for the Fosheim peninsula (A) and subsequent focus areas (B-D). Extent labels correspond to features highlighted in Figures 6 and 8..... 63
Figure 2.6. Examples of lake dynamics in the region. Visual comparison provided for LARCH composite results, false-colour Landsat 1999 and 2023 mosaic and model predicted landscape change classification. Lake dataset provided by Government of Canada (2022). 64
Figure 2.7. Locations of identified thaw slumps with dashed black line indicating approximate marine limit (145 m a.s.l.) overlain the elevation profile for the region (ArcticDEM 4). 65

Figure 2.8. Examples of active thaw slumps in the region. Visual comparison provided for LARCH RGB image, false-colour Landsat 1999 and 2023 and high-resolution planet imagery from July 30th, 2022 (5 m resolution). Random forest change classes and aerial image from July 2019. 66
Figure 3.1. Site map of Eureka and surrounding area. Extent of Station Creek watershed outlined by large black dashes, small black dashes indicate the extent of Blacktop creek watershed. Marine limit (~146 m asl) outlined by grey dashed lines. Elevation presented in meters above sea level. Slumps monitored in this study are indicated with a black star. 94
Figure 3.2. $\delta^{18}O$~D for Station creek and Blacktop creek in 2022 and 2023. Data is coloured by sampling day (dark - early to light -late) and symbol (circle/triangle) represents disturbed and undisturbed sites. Local Meteoric water line (LMWL; blue; IAEA/WMO, 2018) and Global Meteoric Water Line (GMWL; black). 95
Figure 3.3. Scholler plot of major ions from stream chemistry for Station creek and Blacktop creek. Plots divided by disturbance and coloured by site, mean value presented per ion, mean Total Dissolved Solids (TDS) per site also included. 96
Figure 3.4. Time series of molar ratio between (A) sulphate and chloride and (B) sodium and chloride for Station creek and Blacktop creek for July 2022 and 2023. Data is divided by disturbance (shape) and sampling location (colour). 97
Figure 3.5. Time series of stream chloride (Cl^-), sulphate (SO_4) and TDS concentrations (mg/L) for July 2022 and 2023.....98
Figure 4.1. Study site (A) Canadian Arctic Archipelago; (B) watershed extent with elevation underlay, dashed black line indicates marine limit; (C) sample locations, true colour composite satellite image underlain. Satellite image captured July 30, 2022, by Planet Labs PBC (2024). Ephemeral creeks represented by blue dashed line, continuous flowing streams by the solid blue line; (D) images of sample locations, site numbers correspond numbers in Fig, 1C. Images were taken in July 2023, photo credit Jacob Prest. All images are taken downstream. 118
Figure 4.2. Climate and stream component comparison left panel illustrates July 2022, right July 2023. A) TOA Radiation (W m^{-2}); B) Hourly Air temperature (°C) recorded at Eureka Weather Station (black) and Eureka Air Strip (red; data collected from Government of Canada); C) Hourly precipitation (mm) collected at Weather station (data collected from Government of Canada); D) Blacktop Creek recorded stream temperature (30 min interval); E) Station Creek recorded stream temperature (30 min interval); F) Blacktop Creek calculated discharge (m^3/s); G) Station Creek calculated discharge (m^3/s); H) Blacktop Creek sediment and dissolved particulate load (mg/L); I) Station Creek sediment and dissolved particulate load (mg/L). 119

Figure 4.3. Mean annual stream temperature (labelled) for each study site overlying the lidar-derived elevation (ArcticDEM Version 4.1; Porter et al., 2023) for (A) 2022 and (B) 2023, Site 7 in inset map. (C) shows watershed extent with digital elevation model, dashed line indicates extent of marine sediments (~146 m asl). 120
Figure 4.4. Hourly stream temperature for 2022 and 2023 against recorded air temperature (°C; A & B) and estimated top of atmosphere (TOA) solar radiation (W m^{-2}; C & D). 121
Figure 4.5. Log-transformed stream sediment and dissolved particulate load against log-transformed stream discharge. Data illustrated per year, per stream. 122

List of Tables

Table 2.1. Landscape change classes included is the number of training points (No. TP) per class and the mean index value per class. 57
Table 2.2. Confusion Matrix for Random Forest Model results for each land change class. Class-specific performance metrics for Random Forest model. Includes model sensitivity, precision, overall accuracy and f1 score also included.....58
Table 3.1. Slump characteristics, approximate size in hectares evaluated via satellite imagery, status and approximate straight-line distance to the respective stream. Evaluated 2023 from high-resolution imagery. 92
Table 3.2. Average concentration of major ions for massive ice and ice wedges for Eureka, Nunavut. Concentrations reported in mg/L, massive ice samples collected in July 2017, ice wedges collected in July 2019. 92
Table 3.3. Average ion concentrations (Cl^-, Ca, Mg and Na) for undisturbed, thaw runoff and disturbed study sites within the Blacktop and Station creek watersheds. Ion concentrations in ppm.....93
Table 4.1. Stage-Discharge equation components, number of manual measurements and the average difference between the estimated and measured discharge. Note, if the number of manual measurements is 5 or less, they were not included. 117

List of Abbreviations

a.s.l.	Above Sea Level
ALD	Active Layer Depth
BC	Blacktop Creek
B1-B7	Landsat Spectral Bands
BP	Before Present
CAA	Canadian Arctic Archipelago
CRREL	Cold Regions Research and Engineering Laboratory
$\delta^{13}C$	Carbon-13 isotope ratio
$\delta^{18}O$	Oxygen-18 isotope ratio
δD	Deuterium isotope ratio
d	D-excess (‰)
DP	Dew Point
DOC	Dissolved Organic Carbon
ESL	Eureka Sound Lowlands
ETM+	Enhanced Thematic Mapper Plus (Landsat 7)
GEE	Google Earth Engine
GMWL	Global Meteoric Water Line
L7/ L8	Landsat 7/ Landsat 8
LMWL	Local Meteoric Water Line
LARCH	Landsat Arctic RBG Change
MAAT	Mean Annual Air Temperature
m a.s.l.	Metres above sea level
NDVI	Normalized Difference Vegetation Index
NHN	National Hydro Network
NWT	Northwest Territories
OLI	Operational Land Imager (Landsat 8)
POC	Particulate Organic Carbon
‰	Parts per million
RF	Random Forest
RH	Relative Humidity
RTS	Retrogressive Thaw Slump
SC	Station Creek
TCB	Tasseled Cap Brightness
TCG	Tasseled Cap Greenness
TCW	Tasseled Cap Wetness
TDD	Thawing Degree Days
TDS	Total Dissolved Solids
TSS	Total Suspended Solids
TOA	Top of Atmosphere
kyr BP	thousand years before present
VPDB	Vienna Pee Dee Belemnite
VSMOW	Vienna Standard Mean Ocean Water

Chapter 1

1.1 Introduction

Warmer summers in the Arctic, attributed to global climate change, are predicted to increase regional precipitation; triggering a positive shift toward a warmer ground thermal regime and an increase in thermokarst activity (Box et al., 2019; Jones et al., 2022; Walvoord & Kurylyk, 2016). In Northern Russia and Siberia, permafrost has been warming since the 1980s at varying rates (0.1-0.4°C/decade) and dependent on site conditions (i.e., topography, vegetation, and sediment characteristics; Drozdov et al., 2015). Comparably, permafrost in Nordic regions is warming at a higher rate (0.4-0.7°C/decade) as the permafrost in this region is warmer (above -3°C) and isolated to bog environments (Christiansen et al., 2010; Farbrot et al., 2013). In the Canadian sub-Arctic, observed permafrost warming rates are less than 0.3°C/decade. Comparatively, in the high Canadian Arctic, where permafrost is colder (<-10°C), observed rates of warming are significantly greater (~1°C/decade; Smith et al., 2012, 2015, 2022). Warming temperatures in deep permafrost are important when considering future long-term changes to the ground thermal regime. However, a more pressing concern is the impact of thawing near-surface permafrost on the Arctic's hydrological cycle.

The presence of permafrost in a region has a significant impact on the local water table. In cold climate conditions, permafrost acts as an impermeable layer by restricting water flow and storing water on the surface as lakes, ponds, and wetlands (Woo, 2012). With warmer climate conditions, the depth to the permafrost table can deepen and allow for more water to infiltrate the ground, thereby reducing the volume of water stored on the surface (Woo, 1990; Walvoord & Kurylyk, 2016; Webb et al., 2022). This redistribution of water changes the ground moisture levels (wetter conditions in some areas and drier conditions in others) which can significantly alter a landscape and disturb the plant and animal communities of these ecosystems. Likewise, a decline in the permafrost table will impact northern communities whose infrastructure is not equipped to access ground water.

An increase in the depth to permafrost table in continuous permafrost is a direct result of changing active layer conditions (Shiklomanov & Nelson, 2013). Circumpolar active layer depth data is showing consistent deepening since the late 1990s at varying rates depending on site conditions (Christiansen et al., 2010; Smith et al., 2010, 2015, 2016). Current research reveals that

degrading surface permafrost and thicker active layers influence surface water chemistry and availability (Hobbie et al., 2017; MacDonald et al., 2018), plant diversity (Hobbie et al., 2017; Liljedahl et al., 2016), and accelerating coastal erosion (Dallimore et al., 1996; Lantuit & Pollard, 2008; Wolfe et al., 1998).

An increase in active layer depth in a region can thaw long-lived surficial ground ice which raises the moisture content of the active layer and leads to an increase in the risk of slope failure, slope runoff, and sediment transfer (Woo, 1990). Further, thaw slumps are considered one of the most rapid erosional processes occurring in permafrost landscapes with observed retreat rates as high as 6-8 m yr^{-1} (French, 2017; Lewkowicz, 1987; Mackay, 1966). These thermokarst features are ubiquitous to the Arctic and typically found in regions where ice-rich permafrost is exposed to thaw (French, 2017). There are several known trigger mechanisms for thaw slumps, including: 1) undercutting of a steep bank by lateral stream erosion (Balser et al., 2014; Lewkowicz & Way, 2019); 2) thermally driven lakeshore subsidence (Burn & Kokelj, 2009); 3) wave action (Lantuit & Pollard, 2008); 4) extreme thaw or precipitation (Lacelle et al., 2010). In some cases, thaw slumping can occur randomly with no known trigger mechanism (French, 2017). The recession of a slump can last multiple decades but usually ceases (stabilizes) once the ground ice is completely thawed or enough sediment has covered the melting ice in the head wall to insulate and prevent further recession. In cases where the ground ice beneath the slump floor is preserved, a new slump may be initiated, termed polycyclic retrogressive thaw slumps, this may result in the formation of multiple slumps within the existing slump and which can continue to erode beyond the primary slump headwall (Mackay, 1966; Wolfe et al., 2001; Lantuit & Pollard, 2008). These thermokarst features pose a significant risk to regional hydrology, infrastructure, atmospheric carbon concentrations and methylmercury (Dixon, 2013; Doré et al., 2016; Frey & McClelland, 2009; Kokelj et al., 2015; Ward Jones & Pollard, 2021).

In the last decade, the frequency of thaw slump occurrences in the Canadian Arctic are increasing (Lewkowicz & Way, 2019; Ward Jones et al., 2019). Research on the hydrological impact of slump activity in Canada is limited to the Western Canadian Arctic. Studies in the Peel plateau show that the presence of thaw slumps will significantly impact stream geochemistry by increasing the solute load well above the 'normal' load in pristine streams (Malone et al., 2013). The authors used a two-component mixing equation to estimate the spatial extent to which slump runoff is impacting streams, with a higher stream solute load indicative of a nearby active thaw slump (Malone et al., 2013). Moreover, SO_4/Cl is a reliable solute tracer in surface waters for

thermokarst slump activity in Western Arctic Canada (Peel Plateau and Mackenzie delta). Kokelj et al (2005; 2013) found that the concentration of SO_4 in thaw-effected surface waters is several orders of magnitude greater than pristine (unaffected) surface waters. Their work showed that the ratio of SO_4/Cl can be used to determine the influence of thaw slumping in glaciogenic landscapes (Kokelj et al., 2013). Moreover, thaw-effected streams exhibited diurnal fluctuations in water level, solute load, and sediment flux, attributed entirely to ground ice thaw (Kokelj et al., 2013). Higher rates of rainfall in the Peel Plateau were found to accelerate the recession of slump headwalls by removing sediment away from the slump headwall and exposing ground ice. Rainfall accelerates slump growth and initiates the development of 'mega-slumps' (5-40 ha; Kokelj et al., 2015). Solute analysis of nearby streams showed up to a three-day lag in some areas for slump materials to be transported from the scar zone to the stream (Kokelj et al., 2015). Lacelle et al. (2019) shows that sediment in the thaw slump scar zone has a higher concentration of solutes than the undisturbed permafrost due to evaporation. Therefore, slump wash downstream contributes a higher concentration of solutes than other moisture sources and poses a higher risk to freshwater invertebrate and vertebrate communities (Lacelle et al., 2019).

In comparison, retrogressive thaw slump activity in the Canadian High Arctic (Eureka, Nunavut) is directly influenced by increasing air temperatures, as precipitation in the region is extremely low (<80 mm/yr.; Ward Jones et al., 2019). Slump activity in the Eureka Sound Lowlands has been monitored since 1991 with the number of observed slumps increasing by 10% annually since 2005 (Pollard et al., 2015). Between 2011 and 2018, Ward Jones et al. (2019) observed an average headwall retreat rate of 6.2 m yr^{-1} with individual slump annual ranges up to 26 m yr^{-1} and maximum retreat for a few specific slumps observed as high as 79 m yr^{-1} over a seven year-period (Ward Jones et al., 2019). This high slump activity is attributed to the combined effects of melting massive intrasedimental ice and ice wedge ice (Grom, 2008). Ground ice in Eureka is estimated to constitute 30.8%$_{vol}$ of the upper 5.9 m of permafrost and in regions below marine limit (~146m a.s.l.) 48.6%$_{vol}$ of frozen materials is comprised of pore ice or ice lenses (Couture & Pollard, 1998). Wedge ice only comprises a small fraction of the total ground ice volume (3.3%) however, the near purity of this type of ice makes it highly susceptible to any disturbance leading to ground subsidence or triggering a retrogressive thaw slump (Couture & Pollard, 1998).

Ice wedges in Eureka were formed after the last glaciation. Observed ages range from 14 - 2.5 kyr BP and formed from the infilling of spring snowmelt (mid/late-Holocene) and glacial meltwater (early-Holocene; Campbell-Heaton et al., 2021). Although the Eureka ice wedges are active (Ward Jones et al., 2020; Campbell-Heaton et al., 2021), they are degrading because of warming air

temperatures (Ward Jones et al., 2020). Ice wedge melt-outs are a frequent occurrence in Eureka (Pollard et al., 2015) but there is currently no known information on the hydrological impact of these events or of thaw slumps to this polar desert watershed. This project seeks to understand the impacts of thermokarst processes (ice wedge degradation and thaw slumping) on the regional hydrology and overall water quality in Eureka, Nunavut.

The focus area for this project is located on the Fosheim Peninsula which is surrounded on three sides by the Arctic Ocean and separated from the rest of Ellesmere Island by the Sawtooth Mountain range (max. elv. 1000 m a.s.l.). The region is described as a polar desert where mean annual air temperature (MAAT) is -18.0±1.2°C (1991-2021), winters average around -35.1±1.9°C, and summers are cool, averaging around 4.5±1.4°C but can exceed 15°C (Government of Canada, 2025). Total annual precipitation is low (77.0 ± 23.0 mm y^{-1}) with the majority falling as snow. The depth of the permafrost in the region exceeds 500m, characterized as continuous permafrost (Pollard et al., 2015). The active layer depth averages 60cm but can range between 10-100cm in depth (Hodgson and Nixon, 1998). Ground ice is estimated to occupy 30%$_{vol}$ of the upper most 6m of the region (Couture and Pollard, 1998). Recently, the occurrence of thaw slumps and ice wedge melt outs have been increasing in the region, this is synchronous with a thickening of the active layer (Pollard et al., 2015). Consequently, it is critical to characterize the hydrological effects of permafrost degradation in a polar desert environment.

1.2 Background Literature

1.2.1 Introduction to Permafrost Landscapes

Permafrost is defined as any ground (soil or bedrock) that remains below 0 °C for two or more consecutive years (French, 2017). Constrained primarily to polar and alpine regions, permafrost underlies approximately 24% of the Earth's surface and about 50% of Canada (Stott & Huddart, 2010). This proportion, however, is somewhat overstated as it assumes a uniform distribution, whereas in reality, permafrost occurrence varies substantially across northern Canada and other circumpolar regions. Four general classifications of permafrost coverage are recognized: (1) continuous (90–100%), (2) discontinuous (50–90%), (3) sporadic (10–50%), and (4) isolated (0–10%). On a broad scale, these zones correspond to mean annual air temperature (MAAT) isotherms (French, 2017).

The presence of permafrost in a given region is not solely dictated by temperature but also by factors such as soil type, snow cover, vegetation composition and density, topography, and

drainage (French, 2017). Although climate conditions are central to permafrost formation, stability, and degradation, localized ecosystem characteristics can allow permafrost to persist under relatively warm climates, though typically only over short timescales (Shur & Jorgenson, 2007). Long-term monitoring of permafrost relies on ground temperature measurements at depth, and studies indicate that even deep permafrost layers are responding to ongoing climatic shifts (Smith et al., 2010).

Permafrost in northern Russia and Siberia has been warming since the late 1980s, with rates varying from 0.1–0.4 °C decade^{-1} depending on local site conditions (Drozdov et al., 2015). In Nordic regions, where permafrost is relatively warm (> –3 °C), ground temperatures have increased by 0.4–0.7 °C decade^{-1} since the early 2000s (Christiansen et al., 2010; Farbrot et al., 2013). Similarly, permafrost in northern Alaska and the Mackenzie Valley has warmed at rates between 0.4–0.8 °C decade^{-1} (Romanovsky et al., 2020; Smith et al., 2022), while northern Quebec exhibits even higher rates of approximately 0.7 °C decade^{-1} (Smith et al., 2022). In the Canadian High Arctic (Alert), permafrost has warmed by 0.4–0.6 °C decade^{-1} since 1978, with accelerated warming of 0.6–1.1 °C decade^{-1} observed in recent decades (Romanovsky et al., 2020). Across the circumpolar Arctic, permafrost temperatures have increased at variable rates ranging from 0.1–1.1 °C decade^{-1} since 2000, with slower warming observed in regions of warmer permafrost. This is attributed to the increased latent heat requirements of phase change near the 0 °C threshold, which buffers further temperature rise (Romanovsky et al., 2020).

The active layer represents a dynamic component of permafrost environments. It consists of the uppermost soil, bedrock, or organic material that undergoes annual freeze–thaw cycles and interacts directly with the atmosphere. Active layer thickness varies from roughly 0.15 m to over 1 m depending on local climate and environmental conditions such as vegetation cover, soil moisture, topography, and substrate type. In continuous permafrost zones, the active layer directly overlies the permafrost table, whereas in discontinuous and sporadic zones, it may be separated from permafrost by a zone of permanently thawed ground, known as a talik (French, 2017).

Studies have identified a third subsurface component: the transient layer, which marks the interface between the active layer and the permafrost table (Shur et al., 2005; French, 2017). This layer freezes and thaws over multi-decadal to centennial timescales and typically contains more ground ice than either the active layer or the deeper permafrost. Thawing of the transient layer poses particular concern because it can lead to slope instability, rapid mass movements, solifluction, changes in soil hydrology, and the release of stored carbon (French, 2017).

As a response to climate change, active layer depth (ALD) has been increasing across the circumpolar Arctic (Romanovsky et al., 2020). The most pronounced deepening has occurred in the Russian Arctic—particularly the Russian European North and western Siberia—where average ALD increased by 0.4 m between 1999 and 2019 (Smith et al., 2022). In Alaska, 2020 measurements from the North Slope were near the 2003–2012 mean and slightly (0.06 m) lower than the 2019 record, while interior Alaska recorded its deepest average ALD of 0.92 m in 2020 (Smith et al., 2021; Romanovsky et al., 2020). In northwestern Canada, ALD has been gradually increasing since 2014, with similar thickening observed at monitoring sites in Greenland and Svalbard, although these regions exhibit high interannual variability (Smith et al., 2021). Furthermore, Smith et al. (2022) highlight that both the maximum thaw depth and refreezing depth are changing unevenly across Arctic regions. Warmer ground temperatures are delaying freeze-up in autumn, resulting in deeper seasonal thaw penetration and incomplete refreezing in some years. These processes promote talik formation and perennially thawed zones, further accelerating permafrost degradation and altering subsurface hydrology. Consequently, permafrost degradation and active layer deepening have wide-ranging ecological and biogeochemical effects. Hobbie et al. (2017) documented increases in lake alkalinity associated with deeper active layers, while permafrost thaw has been linked to altered surface hydrology (MacDonald et al., 2018), enhanced plant diversity (Liljedahl et al., 2016; Hobbie et al., 2017), and increased carbon dioxide and methane emissions (Schuur et al., 2015).

1.2.2 Remote Monitoring of Arctic Landscapes

Researchers rely on satellite imagery to assess the health and function of remote ecosystems. The term "Arctic Greening or Browning" is frequently used to describe visual changes identified in satellite images from a time series analysis. The change in Normalized Difference Vegetation Index (NDVI) between years is the most common method to remotely assess landscape changes. NDVI is calculated as:

$$NDVI = (NIR - RED) / (NIR + Red) \quad (1)$$

Where NIR corresponds to near-infrared reflectance (~0.77-0.90 μm) and Red corresponds to red reflectance (~0.63-0.69 μm). Healthy vegetation strongly reflects near-infrared wavelengths while absorbing red wavelengths, resulting in high positive NDVI values. Therefore, a positive NDVI trend is interpreted as ecosystem productivity (greening), and a negative NDVI trend is interpreted as reduced productivity (browning; Wang and Friedl, 2019). While NDVI is useful for quantifying vegetation productivity, it provides limited information on

other environmental changes. Consequently, many Arctic remote sensing studies employ the Tasseled Cap transformation, which combines Landsat spectral bands into three interpretable indices: Brightness, Greenness, and Wetness (Crist and Cicone, 1984). Greenness is associated primarily with vegetation abundance and productivity, Wetness is related to surface and near-surface moisture conditions, and Brightness represents overall surface reflectance. In permafrost environments, changes in these indices may reflect shifts in vegetation change (greening, fires), active layer moisture, thermokarst activity, hydrological reorganization, exposed sediments, and surface conditions associated with thawing ground ice (Fraser et al., 2012; Brooker, et al., 2014; Fraser et al., 2014; Olthof & Fraser, 2014; Frappier et al., 2023).

Remotely observed widespread greening of the circumpolar Arctic in recent decades correlates strongly with increasing summer air temperatures, annual soil temperatures and summer soil moisture (Berner et al., 2020). However, not all areas within the Arctic are greening with no observed positive trends in some tundra locations whilst others were browning; attributed to a lag in vegetation response and/or the importance of other factors (i.e., hydrological changes associated with permafrost thaw, drought, and fire). Moreover, Bi et al. (2013) found that Arctic-Boreal regions in North America and Northern Eurasia exhibited contrasting vegetation responses to temperature, with significant greening in Eurasia and more browning in North America's boreal zones. They linked these regional differences to climate variability, highlighting precipitation as a key driver of vegetation growth, particularly in North America. Similarly, Wang and Friedl (2019) analyzed NDVI trends across Northwestern Canada and Alaska from 1984 to 2012 and found substantial greening and browning patterns—often linked to forest disturbance and recovery—with rates significantly higher than in stable landscapes. They concluded that while land cover changes and disturbances like fires and harvesting played major roles, complex ecological factors such as drought and permafrost thaw also contributed to boreal browning. On a smaller scale, Miles and Esau (2016) focus on NDVI change over northern West Siberia, an area considered a hot spot of extensive landcover change due to rapid resource development, geomorphic change, climate change, and reindeer grazing. They found that only 18% of the total northern West Siberia area had statistically significant changes in productivity, with 8.4% increasing (greening) and 9.6% decreasing (browning). Browning was found to be the most prominent in areas of denser tree coverage, particularly in evergreen coniferous forest and evergreen-majority mixed forests (Miles and Esau, 2016). In contrast, low density deciduous needleleaf forest dominated by larch (*Larix sibirica*), showed a significant increase in productivity, even while neighbouring species show decreased productivity (Miles and Esau, 2016). The observed trends were attributed to climatic

changes, site factors (soils, permafrost, hydrology, etc.) and plant factors (structure, health, phenology, species composition, etc.) which they found determined the vegetation vitality, growth, and productivity in their study region. Lara et al. (2018) examined NDVI change over 15 years (1999-2014) across the Arctic Coastal Plain of northern Alaska. Their results found that greening at the landscape scale increased if precipitation decreased more than -10mm relative to the normal precipitation patterns whereas browning increased with precipitation (Lara et al., 2018). At this scale, they suggest that trends in NDVI are typically due to local processes such as the frequency and magnitude of wildfires, regional climate change, infrastructure development and shrubification. Their study also suggests the importance of tundra geomorphology as another factor which affects NDVI trends. At the regional scale, Arndt et al. (2019) found that NDVI increase or greening closely correlated with the number of thawing degree days which was found to increase in a similar trend for the same period. These findings suggest that Arctic ecosystem greening is occurring due to a lengthening growing season which stimulated plant productivity without any significant change in vegetation community (Arndt et al., 2019). In addition, plant communities in wetter communities were found to green nearly twice as fast as those found in drier conditions, supporting the idea that wetter communities respond more strongly to warming. The stage of ice wedge degradation (as outlined by Liljedahl et al. (2016)) controlled the distribution of water on the surface and thus, the soil moisture. They isolated that soil moisture was the main factor driving the separation between wet and dry vegetation communities. The faster green-up in wetter communities confirms future predictions which show an increase in moisture for the northern Alaska region (Zhang et al., 2008). In addition, Larking et al. (2021) examined rapid greening near Nain, Nunatsiavut for 1985-2018. They used NDVI to determine areas of high and low shrub growth and field analysis to identify vegetation composition. The causes of the variable greening rates were attributed to natural growth difference: alder grew at a rate between 4.69-8.88 cm yr^{-1} where dwarf shrubs were 0.65-1.82 cm yr^{-1} (Larking et al., 2021). Snow redistribution and local microclimates were also an important factor in moderating winter extremes and influencing the distribution of different shrub species. Overall, the factors controlling Arctic and sub-Arctic greening and browning trends vary depending on the study's scale. At the broad scale, temperature and precipitation dominate NDVI trends whereas, at the regional scale, NDVI trends are more associated with landscape heterogeneity and species physiology.

1.2.3 Terrestrial Hydrology in Permafrost Environments

1.2.3.1 Atmospheric Water

Low temperatures in Arctic regions limit atmospheric moisture, and most areas north of 70° N are considered polar deserts, with precipitation increasing toward lower latitudes (Woo, 2012). Sea ice restricts water vapour exchange between ocean and atmosphere, and prevailing winds transport low-moisture air inland unless open-water areas (polynyas) are nearby. Precipitation patterns vary across the Arctic depending on the position of the Arctic front and cyclonic activity. Winter cyclones bring heat and moisture along continental margins, but interior regions remain arid under high-pressure systems (Woo, 2012). Continuous permafrost zones experience roughly 250 days of snow cover annually, while discontinuous zones experience over 200. Spring melt in northern and alpine regions is delayed by persistent cold and high surface albedo, and the main melt period lasts only a few weeks before cooler temperatures return (Woo, 2012).

Climate change is projected to increase both snowfall and rainfall intensity in high-latitude regions (Hoegh-Guldberg et al., 2018). Deeper snowpacks insulate the ground, altering subsurface thermal regimes and increasing near-surface temperatures—particularly in discontinuous permafrost zones—while continuous zones show smaller changes (French, 2017; Williams & Smith, 1989). Such thermal shifts threaten the stability of infrastructure that relies on frozen ground for structural support (Streletskiy et al., 2015).

Snowmelt infiltration strongly influences early-season thaw. As snowpack melts, percolating water refreezes within frozen soil, releasing latent heat that raises ground temperatures and produces a “thermal pulse” accelerating active layer warming (Kane & Stein, 1983; Hinkel et al., 1997; 2001). Kane (1980) found infiltration in pre-wetted soils to be an order of magnitude slower than in dry soils, while Zhu et al. (2017) showed that meltwater entering very cold (< –6°C) soil refreezes and stores latent heat that persists for weeks, with effects governed by soil porosity, water volume, and temperature. In the Mackenzie Delta and Alaska, meltwater has been observed moving rapidly through microcracks formed by winter desiccation, enhancing runoff and thaw (Hinkel et al., 1997).

Summer rainfall exerts similar effects on active layer temperatures. Infiltration depth depends on soil type, moisture, rainfall intensity, and vegetation, as plant roots and fissures provide preferential flow paths (Woo, 2012). Rainwater infiltration releases convective heat, warming the active layer and deepening thaw (Hinkel & Outcalt, 1994). Studies show that rain warmed at the surface transfers sensible heat downward, though this effect diminishes with depth (Hinkel et al., 1997). On the Tibetan Plateau, Wen et al. (2014) found that rainfall infiltration reduced temperature

gradients and modified near-surface heat fluxes, while Zhu et al. (2017) demonstrated that rainfall timing affects freeze–thaw dynamics: early-season rains enhance thaw, whereas late-season events delay freeze-back and increase soil water retention, prolonging the energy required to refreeze (Woo & Xia, 1996). Collectively, snow and rainfall infiltration represent key pathways linking atmospheric water to ground thermal dynamics in permafrost regions. Their timing, intensity, and duration govern the rate and depth of thaw, exerting strong controls on permafrost stability and the hydrological and ecological responses of northern landscapes.

1.2.3.2 Surface Water

In the Arctic, surface water regimes differ than in temperate regimes because of cold climates and the existence of permafrost. Surface water runoff on tundra slopes for example accumulates in runnels (Woo, 2012). These are poorly defined shallow linear depressions where water collects on steep permafrost slopes, the high soil moisture in these runnels allows vegetation growth (Woo, 2012). Large cracks surrounding ice wedge polygons provide troughs for channeled flow, with ice wedge degradation, these tracks will link up to form a gully-system that conveys the flow to a stream or fans out to inundate depressions downslope (Woo, 2012; Liljedahl et al., 2016). Pipeflow occurs beneath the surface in mineral or organic medium to fine grained soils, these pipes range in length from several to tens of centimeters and transport subsurface water. Soil moisture in the circumpolar Arctic is expected to decline over the next century because of increase in drainage and redistribution of water in the soil column (Andresen et al., 2020). A decrease in soil moisture will have negative effects on plant biomass and negatively impact the rest of the food web.

Vast tracts of wetland are found in permafrost regions, with the areal extent of saturated land tending to be dynamic, expanding in the wet period and shrinking in the dry period (Woo, 2012). The existence of permafrost below wetlands inhibits the percolation of water and the relatively thin active layer restricts water storage. Therefore, hydrological activities, concentrated within a few months a year, exhibit strong seasonal and inter-annual variability (Woo, 2012). The irregularities in surface microtopography of wetlands, differential thaw of the active layer and seasonal variation in storage control the timing of water release to local streams and rivers. With climate change, degrading permafrost will allow for better ground water flow and will subsequently dry wetlands which could have a major impact to the communities downstream which rely on that late season water storage. The fate of patchy wetlands is particularly uncertain as their preservation is easily jeopardized by loss of late-lying snowbanks, changes in river courses and lakeshores or a

rise in sea level, and human activities (i.e., oil exploration, mining, housing development; Woo, 2012).

Rivers and streams in the Arctic operate on a similar basis to their southerly counterparts in the warm seasons. However, in the Arctic, river ice duration and thickness intensifies with an increase in latitude except for some Arctic rivers in continuous permafrost which ceases to flow and therefore has very thin or no ice (Woo, 2012). Breakup of Arctic rivers is changing because of more frequent mild winters days that are causing an increased frequency of mid-winter breakup events, increased flooding and ice jams, delayed freeze-up dates, and advanced break-up dates. These changes affect fluvial geomorphology, aquatic ecology, and infrastructure damages (McBean et al., 2005). Moreover, climate change is expected to affect glacier-fed rivers in Kazakhstan. Shahgedanova et al. (2020) project that stream discharge will decline by 2050 due to glacial retreat, with the most significant decline (20-37%) observed in catchments with low glacierization (2-4%). In Alberta, projected glacier streamflow contributions in are expected to decline by the end of this century, from 1.1 $km^3 a^{-1}$ in the early 2000s to 0.1 $km^3 a^{-1}$ (Marshall et al., 2011). This will have significant effects on societies which rely on this water source.

The origin of lakes in the Arctic varies more than lakes in temperate regions, i.e., formation from thermokarst processes, glaciers, isostatic rebound, artificially created by animals or humans (Woo, 2012). Once formed, these lakes undergo modification by physical or biological processes such as enlargement by erosion or shrinkage due to sedimentation and encroachment of plant growth (Woo, 2012). With climate change, thermokarst processes because of thawing permafrost are responsible for both the creation and disappearance of lakes. The thickening in suprapermafrost taliks will lead to drawdown or drainage of the lake. This loss has been observed in discontinuous permafrost regions of both Siberia and north America (Smith et al., 2005; Yoshikawa and Hinzman, 2003). Lake drawdown and disappearance can have substantial impacts to neighbouring communities which rely on these lakes for freshwater.

1.2.3.3 Ground Ice

A significant characteristic of permafrost environments is ground ice. The quantity of ground ice in a region varies depending on soil structure, texture, and moisture. The classification of ground ice is based on the source of water prior to freezing and the principal transfer process which moves water to the freezing plane (French, 2017). There are four main types of ground ice: pore ice, segregated ice, intrusive/injection ice, and vein ice. Except for pore ice, most of the ground

ice is visible to the naked eye. In the Canadian Arctic, the volumetric ice content is usually between 40-60% and is mostly pore and segregated ice (French, 2017).

Pore ice is the ice that occupies the pore space between sediment grains. Segregated ice forms when water from the active layer will move towards a freezing front (typically at lower depth) and refrozen. The speed of the freezing front (moving upwards or downwards) will influence the amount of water frozen at depth (French, 2017). With intrusive ice, water is expelled under high pressure into the active layer or permafrost. This type of ice is typically associated with surface landforms such as pingos. Vein ice forms from infilling meteoric water within thermal contraction cracks, repeated cracking in the same location results in large ice wedges (French, 2017). Massive ice is typically found as large bodies of ice in the ground often consisting of different types of ice (ie. segregated, intrusive, vein) and/or buried ice from a perennial snowpack, glacial ice, and lake, sea or river ice (Woo, 2012). Most of the ground ice is found within the top 1-3m of permafrost and is therefore highly sensitive to climate changes (French, 2017). Permafrost thaw in ice-rich regions will often form thermokarst landforms such as thaw ponds and thaw slumps. Thawing of soils with large quantities of ground ice will yield a significant amount of water and enable the expansion of moisture elsewhere in the soil profile and the replenishment of ground water. Westerman et al. (2016) projected changes (from 1901 to 2100) to the Arctic hydrological cycle from permafrost thaw. Their results suggest that the trajectories of future permafrost that are strongly influenced by ground ice contents. Thawing permafrost and subsequent ground ice can have significant negative effects on societies living on ice rich permafrost as disruptions to the thermal regimes from infrastructure development and land use changes can trigger thaw events and impact the overall stability of the land (Hjort et al., 2018).

1.2.3.4 Ground Water

The ground conditions of permafrost varies throughout the Arctic, but, in most regions, the ice and water content of permafrost acts to block the soil pores and significantly reduces the permeability of the soil (Woo, 2012). Permafrost is generally considered an aquiclude (poor in the transmission and retention of water) or an aquitard (relatively impervious to water transmission; Woo, 2012). Therefore, ground water and its movement is typically limited to thawed regions.

Movement of groundwater can occur above, within or beneath permafrost, called suprapermafrost, intrapermafrost and subpermafrost groundwater. Suprapermafrost groundwater occurs mostly in the active layer and thus is subjected to seasonal freeze and thaw, water is this layer in winter is either stored as ground ice or extruded above the ground (Woo, 2012). This

groundwater is typically recharged by meteoric water with snowmelt and rain the primary sources and glacial melt in glacierized areas. Suprapermafrost groundwater can also exist in suprapermafrost taliks, regions of unfrozen ground above permafrost formed typically below deep lakes or when active layer freeze back does not reach the permafrost table (Woo, 2012). Intrapermafrost groundwater occurs in taliks within the permafrost. This groundwater is perennially unfrozen though it can be below 0°C if it has a high concentration of dissolved solids (Woo, 2012). The talik within the permafrost can be a through-following talik (intrapermafrost talik) which traverses the entire length of the permafrost and provide passage for groundwater to connect with the water above and below the permafrost (Everdingen, 2005). The talik can also be closed or isolated which may be due to the localized presence of highly mineralized water. Closed taliks are frequently found beneath recently drained lakes where the aggrading permafrost encroaches and cuts off flow connections.

Subpermafrost groundwater is above 0°C but is confined by permafrost and is under hydrostatic pressure and has artesian conditions (Williams and Waller, 1996). Where the permafrost is thin, this ground water can be stored in unconsolidated materials or bedrocks. Where the permafrost is thick, this groundwater is limited to aquifers in sedimentary beds or in igneous rock sufficiently fractures to store water (Woo, 2012). Subpermafrost groundwater can be relatively fresh in karst landscapes but more often this water is high in concentrations of dissolved solids, concentrations are dependent on the composition of the aquifer and the residence time (Woo, 2012). recharge of this groundwater in discontinuous permafrost regions can be directly from adjacent non-permafrost upland or through supra and intrapermafrost connections. In continuous permafrost landscapes, recharge is restricted but can be enhanced through fractures or solution conduits such as sinkholes (Woo, 2012)

Discharge of groundwater occurs as springs or seeps that rise above ground, it also supports river flow and supplies water to tundra ponds and lakes. Icings are formed during the winter from groundwater seeps, flows from a spring or emerges from beneath a riverbed or through fractures in river ice. There are three types of icings: ground, spring and river. Ground and spring icings are difficult to distinguish (Carey, 1973). Ground icings are produced by the seepage of groundwater that saturates the ground surface in the winter while spring icings are due to the discharge of groundwater that leads to well-defined channels on the ground. The water supply for ground and spring icings is usually limited and often exhausted before the end of winter (Woo, 2012). River icings occur when the hydrostatic pressure of water is increased by the hydraulic gradient in the stream channel and groundwater is pushed through a confining cap which may be a frozen

streambed or river ice (Woo, 2012). Recently, the distribution of icings in northwestern Canada have been affected by winter air conditions and winter baseflow conditions (Crites et al., 2020).

Arctic climate change will have direct and indirect impacts on groundwater availability and movement in the Arctic. Zhang et al. (2008) projected permafrost thaw from the surface propagating downwards for 1990 to 2100 with a 0.3-0.7 m increase in active layer thickness and a depth to permafrost table increase by 1.9-5.0 m. Such change would have a significant impact on ground water movement in the Arctic including more sub-surface flow, increased lake drawdown and less surface water storage. This would have significant societal impacts, especially to those communities which rely on the fresh-surface water.

1.2.4 Nival Streams

Nival streams are predominantly snowmelt fed, have high spring freshets, are intermittently peaked by summer rain events, and taper off quickly to low baseflow or no flow in the winter. The majority (90%) of continuously monitored (by the Canadian Hydrometric Service) nival streams are in Atlantic Canada near the St. Lawrence (Zaerpour et al., 2021). In the Arctic and subarctic, nival streams are affected by permafrost, which restricts ground water movement and as a result, baseflow. Nival subarctic streams can be characterized as winter dry or perennial flow. Winter dry indicating an absence of flow during the winter, resulting in dry, ice-less riverbeds (Church, 1974). Large, subarctic rivers with perennial flow will have a low baseflow throughout the winter, often flow will occur under ice cover (Church, 1974). The freshet of Arctic nival streams is typically the most severe flooding as rain events in the Arctic are less intense and infrequent (Church, 1974). This spring flood is the main mechanism for sediment transport in High Arctic nival streams (McDonald & Lamoureux, 2009; Woo, 2012).

With climate change, Western Arctic nival streams are responding to an earlier spring runoff (Dery et al., 2009). This has also been observed in the High Arctic (Melville Island), Favaro and Lamoureux (2015) record a decline in snowmelt driven runoff and stream sediment yield between 2010 and 2012. This decline is attributed the presence of snowbanks in the stream channel which buffer the stream bed and bank from erosion during the bulk melt period (Favaro & Lamoureux, 2015). In that year, the sediment yield of the stream was greater post-melt due to permafrost degradation and related localized disturbances (Favaro & Lamoureux, 2015). However, the effect of permafrost disturbance to stream sediment yield is suspected to be much weaker than the shift towards a pluvial-dominated hydrological regime in the High Arctic (Beel et al, 2018). More recent research from this region is showing a shift in hydrological regime from nival to pluvial

and nival dominated, a shift which is ubiquitous to watersheds in the high and low Arctic (Beel et al., 2021). A warmer, wetter thaw season is increasing the stream's erosive power later in the year, resulting in greater sediment and carbon transfer (Beel et al., 2021). This increase in summer and fall rain events is expected to have a significant effect to landscape change, stream sediment yield and carbon exchange than Arctic greening and thermokarst activity (Beel et al., 2018; 2021).

1.2.5 Permafrost Thaw Detection in Streams

Most of the research on the hydrological impact of slump activity in Canada is limited to the Western Canadian Arctic and Alaska, with very few focused on the Canadian High Arctic. Studies in the Peel Plateau (NWT) show that the presence of thaw slumps will significantly impact stream geochemistry by increasing the solute load well above the normal load in pristine streams (Malone et al., 2013). Using the molecular ratio between sulphate (SO_4) and chlorine (Cl^-) proved to be an effective tracer to identify slump-effected streams where disturbed streams had SO_4 concentrations several magnitudes greater than pristine streams (Kokelj et al, 2005; 2013). Thaw-effected streams also exhibited diurnal fluctuations in water level, solute load, and sediment flux, attributed entirely to ground ice thaw (Kokelj et al., 2013). Higher rates of rainfall in the Peel Plateau were found to the accelerate the recession of slump headwalls by removing sediment away from the slump headwall and exposing ground ice. Rainfall accelerates slump growth and initiates the development of 'mega-slumps' (5-40 ha; Kokelj et al., 2015). Solute analysis of nearby streams showed up to a three-day lag in some areas for slump materials to be transported from the scar zone to the stream (Kokelj et al., 2015). Lacelle et al (2019) showed that sediment in the thaw slump scar zone has a higher concentration of solutes than the undisturbed permafrost due to evaporation. Moreover, in North Slope Alaska, Bowden et al (2008) identified higher concentrations of ammonium, nitrate and phosphate downstream of active thermokarst features, earlier work of theirs showed that a small increase in stream nutrient loading can stimulate primary and secondary production. Therefore, the moisture released from active thermokarst (slump activity) poses a high risk to freshwater invertebrate and vertebrate communities via changes to stream nutrient levels (Bowden et al., 2008; Lacelle et al., 2019). To date, very few studies have investigated hydrochemical indicators of thermokarst activity in High Arctic polar desert environments. Where low precipitation and high ground-ice content may lead to substantially different hydrological responses.

1.3 Study Area

Field research for this project took place in the Eureka Sound Lowlands (80˚00'N, 85˚56'W), an area c. 750 km^2 covering Axel Heiberg and the Fosheim peninsula in the Canada Arctic Archipelago. The region is underlaid by the Sverdrup basin, a folded and faulted Carboniferous to Paleogene sedimentary bedrock comprised of sandstone, siltstone, and shale strata (Bell, 1996; Embry & Beauchamp, 2008; Hodgson & Nixon, 1998; Miall, 1986). The study site is located on the Fosheim Peninsula, surrounded on three sides by the Arctic Ocean (Fig. 1.1A) and isolated from the rest of Ellesmere Island by the Sawtooth Mountain range to the south-east. The region is dissected by gullies and shallow, snowmelt streams (nival) that flow for 3 months of the year (Young and Woo, 2000). Two of these streams (Station creek and Blacktop creek) will be the focus of study for this project (Fig. 1.1B).

1.3.1 Glaciation and Surficial Sediments

The most recent glacial reconstructions for the Eureka Sound Lowlands suggest that the Innuitian Ice Sheet covered much of the Queen Elizabeth Islands reaching a maximum extent (1.6 km thick) by 15.8 ka BP (Blake Jr., 1970; Dyke et al., 2002; England et al., 2006; Hodgson, 1985; Huges et al., 1977; Simon et al., 2015). In the Eureka Sound Lowlands, deglaciation began between 10.3-8.7 ka BP and retreated inland to current extents on Ellesmere and Axel Heiberg Island (England et al., 2006). Marine inundation of the Eureka Sound Lowlands occurred until 8.8-7.8 ka BP and covered approximately a third of the peninsula. As a result, Holocene marine limit varies between 139 -150 m asl on the FP; near the Eureka Weather station, the marine limit reaches 143 m asl (Bell, 1996). The rate of post-glacial isostatic rebound in the region was high between 10-8 ka BP after deglaciation of the IIS and complete by 2.5 ka BP (Simon et al., 2015).

Severely weathered bedrock is the most common surficial sediment on the FP, the severity of weathering is evident on most bedrock outcrops and glacial erratics in the region (Bell & Hodgson, 2000; Young & Woo, 2000). Two types of till deposits are present on the Fosheim Peninsula; Blanket (>2m thick) and Veneer (Bell & Hodgson, 2000). Glaciofluvial sediments are present in meltwater channels above marine limit with large gravel deposits found in northeastern side of the FP (Bell & Hodgson, 2000). Holocene marine sediments ranging in size from clay to sand are located below marine limit, deposits are between 5-10m thick (Hodgson & Nixon, 1998; Bell & Hodgson, 2000). Minor surficial units on the FP are fluvial, eolian, organic deposits and colluvium (Bell & Hodgson, 2000). Following marine emergence, soluable salts

remained within fine-grained marine sediments throughout the Eureka Sound Lowlands. Disturbance of these sediments through active-layer deepening, ice-wedge degradation, and thaw slumping commonly produces salt efflorescence at the ground surface; development of salt efflorescence is limited to marine sediments, located below regional marine limit (Kokelj & Lewkowicz, 1999).

1.3.2 Modern Climate

The Eureka Sound Lowlands is a polar desert (Edlund et al., 2000), with a cold winter and cool summer temperatures and little precipitation. Atmospheric parameters (temperature, pressure, relative humidity, wind speed and precipitation) have been recorded in the region (Eureka, Nunavut) since 1947 (Rae, 1951). Between 1991-2021, the mean annual air temperature (MAAT) for Eureka was -18.0±1.2°C; mean winter air temperature (DJF) was -35.1±1.9°C; mean summer air temperature (JJA) was 4.5±1.4°C but can exceed +15°C on a given day (Atkinson et al., 2000). The MAAT at Eureka shows strong inter-annual variations and has experienced a general increase in MAAT since the 1980s at a rate of 0.53°C decade^{-1} over the period 1980-2019.

Average annual precipitation for Eureka is low (1991-2021: 77.0 ± 23.0 mm y^{-1}, with ~80% falling as snow; Government of Canada, 2025). The average snow depth in Eureka is 12.1 ± 8.3 cm between 1991-2021 (Government of Canada, 2025). Maximum snow depths are reached in early April and decrease rapidly with spring snowmelt (Alt & Maxwell, 2000). Rainfall events are typically low (<0.03mm) but can reach >10mm. Total precipitation increased at a rate of 1.26mm decade^{-1} over the period 1950 to 2019. The low precipitation around Eureka is attributed to the surrounding topography which blocks cold ocean air masses and creates a rain-shadow (Alt & Maxwell, 2000; Bell, 1996; Edlund & Alt, 1989).

1.3.3 Modern Vegetation

The FP is classified as Enriched Prostrate Shrub Zone, characterized as having the greatest diversity and density of vascular plant species of the Queen Elizabeth Islands (Edlund et al., 2000; Edlund & Alt, 1989). Woody plants (i.e., *Salix arctica* and *Dryas integrifolia*) dominate the moderate to well-drained soils below 300-500 m a.s.l. (Edlund et al., 2000). *Salix arctica* dominates most slopes, rooting in shallow troughs, major cracks between hummocks and in shallow depressions, whereas *Dryas integrifolia* is more common in sandier soils and in more microhabitats (Edlund et al., 2000). Vegetation in low-centred polygons is characterized by the grasses

Alopecurus alpinus and *Poa alpigena*, the woody low-lying shrub *Salix arctica* and the herbaceous *Stellaria longipes*. Thegrasses *Puccinella* (i.e., *P. augustate, P. langeana* and *P. poacea*) and *Poa* (*P. hartzii* and *P. glauca*) dominate silty knolls and slopes where the surface has salt accumulations (Edlund et al., 2000). Wetlands are common to lowland areas, are in poorly drained troughs and trough junctions or near a headwater lake or pond. These wetlands are dominated by sedge-meadow vegetation with thick bryophytic mats (Edlund et al., 2000).

1.3.4 Permafrost and Ground Ice

The Eureka Sound Lowlands is located within the continuous permafrost zone, with permafrost >500m thick (Pollard et al., 2015). The active layer depth is between 10 and 100 cm and averages ~60 cm (Hodgson & Nixon, 1998). The mean annual ground temperature (measured at depth of zero annual amplitude) remains <-10ºC (Hjort et al., 2018). The tundra polygon (formed by ice wedge activity) is the main periglacial landform in the region, covering approximately 50% of the Fosheim Peninsula, with the majority found within marine limit (140m a.s.l.; Bernard-Grand'Maison and Pollard, 2018). Thaw slumps and active layer detachment slides are the other main permafrost landforms found in the area. Ground ice in the Fosheim region is estimated to occupy 30% $_{vol}$ of the uppermost 6 m of permafrost (Couture & Pollard, 1998). Of that, 3.5% $_{vol}$ is estimated to be wedge ice and the remaining occurs mostly as tabular bodies of massive ice (Couture & Pollard, 1998). Ice wedges in the region were formed during the Holocene between 9-2.5 Cal ka BP from spring snowmelt (Campbell-Heaton et al., 2021). Tabular massive ice in the region was formed during the same period from ground water inclusion (Roy, 2018). Average concentration of DOC (dissolved organic carbon) within studied ice wedges is 2.70±3.02 ppm (Campbell-Heaton et al., 2021), studied massive ice/ intrasedimental ice has a much higher DOC concentration which ranged between 1.01-31.61ppm and averaged 6.67ppm (Roy, 2018). Below, Table 1 details the average concentration for major ions in massive ice samples and ice wedges from Roy (2018) and Campbell-Heaton (2020). Most reported concentrations are greater in the ice wedge samples than the massive ice. This difference is attributed to the moisture source of the respective ground ice types (i.e., meteoric, ground water).

The increasing MAAT over the past 40 years has implications on the stability of permafrost in the Eureka Sound Lowlands (ex. Pollard et al., 2015). In recent years, tundra polygons and ice wedges were found to be degrading at a rate synchronous with the active layer thickening; the number of active thaw slumps have also been increasing (Pollard et al., 2015). The troughs of tundra

polygons in the Eureka Sound Lowlands experienced a significant amount of degradation for a cold polar desert, such changes include trough subsidence, increase in ponding water and an increase in melt out events (Ward Jones et al., 2020). However, troughs with a greater vegetation cover experienced less degradation than troughs with little to no vegetation due to the insulating property of vegetation during the summer which in turn reduced active layer thaw depth (Becker et al., 2016; Ward Jones et al., 2020). Degradation of the troughs that lack vegetation results from a combination of higher soil moisture content that delays freezing in the winter and increases thaw depth in the summer, and from an increase in snow thickness within the troughs that leads to warmer winter ground temperatures (Ward Jones et al., 2020). Thaw slump activity in the region has been well documented since the 1990s. Between 1990-2015, average headwall retreat rate was 6.9 m yr^{-1}, between 2010-15 average retreat rates increased to 7.5 m yr^{-1} with the highest observed annual rate of 23.9m (Pollard et al., 2015). Ward Jones et al (2019) observed thaw slump initiation in the eureka region is driven by warm summer air temperatures over a period of several years. Once initiated, slump activity is observed to decouple from a climate influence and rely more on the terrain factors, i.e., slope, aspect, and morphology (Ward Jones et al., 2019). Comparatively, weekly headwall retreat rates observed over one summer (2017) are significantly correlated to thawing degree days and mean daily temperatures, no correlation was found with precipitation (Ward Jones & Pollard, 2021). Permafrost in this region is extremely responsive to changing climate conditions because of the thin (if any) organic soil layer and low vegetation cover which provides an insulation layer in lower latitudes (Ward Jones et al., 2019).

1.3.5 Watershed Characteristics

1.3.5.1 Blacktop Creek Watershed:

Blacktop Creek watershed is approximately 98 km^2. The watershed is underlain by colluvial rubble at higher elevations and at lower elevations, by colluvial fine-grained and glacio-marine sediments. There are two known active retrogressive thaw slumps, Blacktop slump and Nunavut slump. Blacktop slump headwall retreat rate between 2011-2018 was monitored by Ward Jones et al. (2019), the slump retreated an average of 8m yr^{-1}. At present, no known retreat rates exist for Nunavut slump, as the slump initiated between 2017 and 2018. Blacktop slump is approx. 97m wide, the headwall is approx. 671 m away from Blacktop Creek, this slump in 2023 was no longer active. Nunavut is significantly larger than Blacktop, the slump is approximately 230m wide, with a headwall of 5-6m high and located 656 m away from Blacktop Creek (Fig. 1.2A). Slumps in this

watershed range in elevation from 60-100m asl. The headwall exposes an active layer 60 cm thick, the headwall is composed of segregated and reticulate ice in marine sediments (<1m), massive ice (~5m) and ice wedges. In summer 2022 and 2023, the headwall of this slump retreat by about 5 m and rillwash was observed along the slump floor. Slump runoff (rillwash) travelled approximately 700 m downhill from headwall to Blacktop Creek, observed flow was low and inconsistent (Fig. 1.3A)

1.3.5.2 Station Creek Watershed:

Station Creek watershed is approximately 111 km^2, primarily underlain by colluvial rubble in higher elevations (above marine limit) and fine grained (glacio) marine sediments at lower elevations (below marine limit). Ward Jones et al. (2019) monitored six-known retrogressive thaw slumps between 2011 and 2017. By the end of the study, five of the six thaw slumps were inactive (retreat rates of <1m yr^{-1}). Field observations in 2019 revealed that the sixth slump, station creek slump was no longer active. Between 2011-2018, retrogressive thaw slump retreat in the Station creek watershed averaged 4.7 m yr^{-1}. Station creek slump is approximately 105m wide and located approx. 236m away from Station Creek. Slumps in this watershed range in elevation between 43-60m asl, all well below marine limit. In July 2022, a small slump (BL slump; Fig. 1.2B) developed downstream (~10 m) of the Station Creek slump (within the same slump complex). This slump is ~100 m wide and 6-10 m high. The headwall exposes an active layer 60 cm thick and is composed of reticulate ice formed in marine sediments (4-5m thick) and massive ice (~5m). The slump debris outwashes directly into this creek (Fig. 1.3B). In 2023, this slump was active and the slump runoff completely blocked Station Creek (Fig. 1.3B), creating a pond upstream. In July 2023, another large thaw slump (CHP slump) was found 4.2 km upstream of the Eureka Weather Station (Fig. 1.2C). Satellite imagery shows that this slump initiated in 2012, see Table 1 for slump characteristics. The headwall of the slump is 490 m wide and 6-8 m tall. The headwall exposes an active layer ~60 cm thick and comprised mostly of massive (3-4 m) and wedge ice (~1 m). In summer 2023, this slump was very active, with slump runoff consistently flowing almost a kilometer before entering Station Creek (Fig. 1.3C).

1.3.5.3 Historical water quality data of Station and Blacktop Creeks

Water quality monitoring was conducted in August 2010 of Station Creek to ensure the water meet the Canadian Drinking Water Quality Guidelines (Arcadis Canada Inc., 2016). Recorded water temperature for Station Creek was 5.9°C, electrical conductivity was 797 µs/cm, pH 7.49,

turbidity 3.27 NTU, TDS 544 mg/L, dissolved sodium ranged between 333 to 507 mg/L and aluminum 0.215 mg/L (Arcadis Canada Inc., 2016). All other water quality parameters for Station Creek were below the Aesthetic Objective (a threshold to monitor water quality). In July 2018, water samples were collected by K. Campbell-Heaton near the outlet of Station Creek and Blacktop Creek. Recorded $\delta^{18}O$ for Station Creek and Blacktop Creek was -25.25±0.11‰ and -23.90±0.12‰, d-excess is 1.88 and 1.15, respectively. Recorded dissolved organic carbon (DOC) concentrations for Station Creek and Blacktop Creek were 2.21 ppm and 1.84 ppm, respectively. Moreover, $\delta^{13}C$ values for Station Creek and Blacktop Creek are similar, -28.64‰ and -28.16‰. Both creeks were only sampled once in 2018. In addition, the 2018 stream samples were analyzed for major ions. Sodium (Na^{2+}), chloride (Cl^{-}) and sulphate (SO_4^{-2}) were the ions with the highest concentrations in both streams.

1.4 Thesis Organization and Research Objectives

This doctoral thesis was written in article format. Each of the following chapters addresses knowledge gaps related to landscape change on the Fosheim Peninsula and how these changes influence hydrological processes in the downstream nival systems of Eureka, Nunavut. Chapter 2 quantifies the landscape change on the Fosheim Peninsula using Landsat-derived time series trend analysis (LARCH). Chapter 3 evaluates the hydrogeochemical influence of retrogressive thaw slumps to two nival-dominated streams in Eureka. Chapter 4 examines the combined climate and thermokarst controls on nival stream dynamics. Chapter 5 synthesizes the key findings, contributions, and limitations of Chapters 2-4. The following section outlines the research questions and methodological approaches addressed in these manuscripts. References, tables, and figures are provided at the end of each chapter.

Objective 1: *Quantify long-term landscape change on the Fosheim Peninsula using Landsat-based LARCH analysis.*

Chapter 2 examines the multi-decadal landscape evolution of the Fosheim Peninsula using a 25-year Landsat 7 and 8 time series (1999-2024). While previous studies in the region have documented thermokarst activity, ice wedge degradation, and geomorphic change through field observation and short-term remote sensing (e.g., Lewkowicz & Duguay, 1999; Pollard et al., 2015; Rudy et al., 2016; Ward Jones et al., 2020), no study has produced a peninsula-wide, long-term, multispectral trend analysis. This chapter addresses this gap by applying the LARCH framework to quantify monotonic and non-monotonic changes in surface greenness, brightness and wetness.

It is hypothesized that: (1) directional changes in vegetation, surface reflectance and moisture occur across significant portions of the Fosheim Peninsula and are detectable using Landsat-derived trend metrics; (2) LARCH trend metrics differentiate geomorphic and thermokarst processes – specifically fluvial reorganization, lake drainage and retrogressive thaw slump activity – based on their characteristic spectral trajectories; and (3) a Random Forest classifier trained on LARCH trend metrics can accurately predict dominant landscape change processes across the Fosheim Peninsula. These hypotheses are evaluated using Tasseled Cap indices, Mann-Kendall significance testing, Theil-Sen slope estimation, and a Random Forest model trained with high-resolution imagery and field-validated change-class polygons.

Findings from this chapter provide the first peninsula-scale assessment of landscape change for the Fosheim Peninsula and establish a remote sensing foundation for hydrological analyses presented in subsequent chapters.

Objective 2: *Determine the hydrochemical impacts of retrogressive thaw slumps on two High Arctic nival streams.*

Chapter 3 investigates how retrogressive thaw slumping influences the hydrochemistry of two nival-fed streams in the Eureka Sound Lowlands. The hydrochemical influence of thaw slumps on stream quality is well documented in the Western Canadian Arctic and Alaska (i.e., Kokelj et al., 2005, 2012; Malone et al., 2013; Bowden et al., 2008), but very little is known in the Canadian High Arctic where summer precipitation is very low and ground ice content is high. Previous work in Eureka has documented rapid increases in thaw slump activity, high ground ice volumes and accelerated slump headwall retreat (Pollard et al., 2015; Ward Jones et al., 2019), yet, no study has quantified how slump-derived moisture and solutes alter stream water quality in this polar desert environment. This chapter addresses this knowledge gap by comparing upstream (undisturbed) and downstream (disturbed) hydrochemistry in Blacktop Creek and Station Creek.

It is hypothesized that: (1) retrogressive thaw slump rillwash increases the dissolved organic carbon (DOC) concentrations in receiving streams; (2) slump-derived water does not substantially modify stream δD-$\delta^{18}O$ signature because these are nival-fed streams; and (3) slump activity increases major ion concentrations in receiving streams due to the addition of solute-rich runoff. These hypotheses are evaluated using daily water sampling above and below active slump inputs during July 2022 and 2023, combined with analyses of DOC, δD-$\delta^{18}O$, $\delta^{13}C_{DOC}$, major ions, and continuous measurements of conductivity, temperature, and water level from Solinst loggers.

Geochemical profiles of exposed ground ice (massive ice, intrasedimental ice, and ice wedges) are also used to identify potential solute sources.

Findings from this chapter provide the first assessment of thaw-driven hydrochemical change in nival streams for Eureka, Nunavut and provide geochemical context for subsequent hydrological change presented in the final manuscript.

Objective 3: *Evaluate how climate variability and permafrost thaw disturbances influence the thermal, hydrological and sedimentary regimes of High Arctic nival streams.*

Chapter 4 examines the combined influence of climate forcing and permafrost thaw disturbances on the summer behaviour of two nival dominated streams in the Eureka Sound Lowlands. Although several studies have documented climate-stream interactions and sediment dynamics in High Arctic nival streams - most notably on Melville Island (ie., Favaro & Lamoureux, 2015; Beel et al., 2018; 2021)- the hydrological and thermal regimes of streams in the polar desert environment of Eureka remain largely uncharacterized. Existing work shows that High Arctic streams are sensitive to shifts in snowmelt timing, rainfall intensity, and permafrost degradation, yet no studies have quantified how these factors jointly influence stream temperature, discharge and particulate transport in this cold, low-precipitation environment. This chapter addresses this gap by comparing stream responses across toe contrasting summers – a cold - wet 2022 and warm – dry 2023 – while accounting for the influence of nearby retrogressive thaw slumps.

It is hypothesized that: (1) stream temperature regimes are primarily controlled by climate forcing (air temperature, solar radiation, humidity), with thermokarst disturbances exerting secondary controls; (2) discharge and water-level recession rates differ substantially between cold-wet and warm-dry summers, reflecting shifts between rainfall-driven and snowmelt-dominated hydrological regimes; and (3) suspended sediment and dissolved particulate loads increase downstream of active thaw slumps, particularly under warm, low-flow conditions. These hypotheses are tested using continuous Solinst Levellogger-5 measurements of water temperature, stage and conductivity; manual discharge measurements used to construct site-specific rating curves; and gravimetric analysis of total suspended and dissolved particulate load collected daily at seven stream sites. Climate variables (air temperature, humidity, precipitation and solar elevation/azimuth) were integrated to evaluate the relative influence of different forcings on stream thermal behaviour.

Findings from this chapter provide the first process-level assessment of climate-stream interactions in High Arctic nival systems and clarify how thermokarst disturbances modulate sediment and solute transport under contrasting climate regimes.

1.5 Authorship and Co-authorship contributions

The three manuscripts presented in this thesis (Chapters 2-4) are first authored by the PhD Candidate, Kethra Campbell-Heaton. Research objectives, field data collection and statistical analysis approaches were developed by K. Campbell-Heaton and in consultation with Dr. Denis Lacelle, her supervisor. Field data was collected by K. Campbell-Heaton with help from field assistants in 2022 and 2023. Contributions presented in each chapter originate from original ideas by K. Campbell-Heaton and D. Lacelle (a co-author of each chapter).

K. Campbell-Heaton wrote the manuscript presented in Chapter 2 with contributions from thesis supervisor, D. Lacelle. Spatial and statistical analysis were conducted by KCH. W. Pollard provided logistical field support.

K. Campbell-Heaton wrote the manuscript presented in Chapter 3 with contributions from thesis supervisor, D. Lacelle. Field data was collected by KCH with help from field assistants, W. Pollard provided logistical field support. KCH conducted laboratory analysis with support from Ján Viezer and Geochemistry laboratories at the University of Ottawa. Statistical analysis was conducted by KCH.

K. Campbell-Heaton wrote the manuscript presented in Chapter 4 with contributions from thesis supervisor, D. Lacelle. Field data was collected by KCH with help from field assistants, W. Pollard provided logistical field support. KCH conducted the laboratory and statistical analysis.

Artificial intelligence tools were used in this thesis to assist with text clarity, grammar and organization during the writing process. These tools were not used to generate research content, data, analyses, figures or interpretations. All research design, data collection, coding, analyses and conclusions are my own with intellectual and analytical contributions from co-authors. Occasional AI use was also employed to assist with code debugging and syntax clarification within workflows that I designed; this use was approved by my supervisor (D. Lacelle) and all code is provided in Appendix of this thesis. This use complies with the uOttawa's Academic Regulation A-4 on Academic Integrity.

1.6 References

Alt, B. T., & Maxwell, B. (2000). Overview of the modern arctic climate. *Bulletin of the Geological Survey of Canada*, *529*, 17–36.

Andresen, C.G., Lawrence, D.M., Wilson, C.J., McGuire, A.D., Koven, C., Schaefer, K., Jafarov, E., Peng, S., Chen, X., Gouttevin, I. and Burke, E. (2020). Soil moisture and hydrology projections of the permafrost region–a model intercomparison. *The Cryosphere*, 14(2), pp.445-459.

Arcadis Canada Inc. (2016). *Environmental Impact Assessment - High Arctic Weather Station Project Improvments* (Issue September).

Arndt, K.A., Santos, M.J., Ustin, S., Davidson, S.J., Stow, D., Oechel, W.C., Tran, T.T., Graybill, B. and Zona, D. (2019). Arctic greening associated with lengthening growing seasons in Northern Alaska. *Environmental Research Letters, 14*(12), p.125018.

Atkinson, D. E., Alt, B., & Gajewski, K. (2000). A New Database of High Arctic Climate Data from the Polar Continental Shelf Project Archives. *Bulletin of the American Meteorological Society*, *81*(11), 2621–2629. https://doi.org/10.1175/1520-0477(2000)081<2621:ANDOHA>2.3.CO;2

Balser, A. W., Jones, J. B., & Gens, R. (2014). Timing of retrogressive thaw slump initiation in the Noatak Basin, northwest Alaska, USA. *Journal of Geophysical Research: Earth Surface*, *119*(5), 1106–1120. https://doi.org/10.1002/2013JF002889.

Becker, M. S., Davies, T. J., & Pollard, W. H. (2016). Ground ice melt in the high Arctic leads to greater ecological heterogeneity. *Journal of Ecology*, *104*(1), 114–124. https://doi.org/10.1111/1365-2745.12491

Beel, C. R., Heslop, J. K., Orwin, J. F., Pope, M. A., Schevers, A. J., Hung, J. K. Y., ... & Lamoureux, S. F. (2021). Emerging dominance of summer rainfall driving High Arctic terrestrial-aquatic connectivity. *Nature Communications, 12*(1), 1448.

Beel, C. R., Lamoureux, S. F., & Orwin, J. F. (2018). Fluvial response to a period of hydrometeorological change and landscape disturbance in the Canadian High Arctic. *Geophysical Research Letters, 45*(19), 10,446-10,455.

Bell, T. (1996). The last glaciation and sea level history of. *Fosheim Peninsula, Ellesmere Island, Canadian High Arctic. Canadian Journal of Earth Sciences*, *33*, 1075–1086.

Bell, T., & Hodgson, D. A. (2000). Quaternary geology and glacial history of Fosheim Peninsula, Ellesmere Island, Nanavut. In *Bulletin of the Geological Survey of Canada* (Issue 529). https://doi.org/10.4095/211957

Bernard-Grand'Maison, C., & Pollard, W. (2018). An estimate of ice wedge volume for a High Arctic polar desert environment, Fosheim Peninsula, Ellesmere Island. The Cryosphere, *12*(11), 3589-3604. https://doi.org/10.5194/tc-2018-29.

Berner, L.T., Massey, R., Jantz, P., Forbes, B.C., Macias-Fauria, M., Myers-Smith, I., Kumpula, T., Gauthier, G., Andreu-Hayles, L., Gaglioti, B.V. and Burns, P. (2020). Summer warming explains widespread but not uniform greening in the Arctic tundra biome. *Nature communications*, *11*(1), pp.1-12.

Bi, J., Xu, L., Samanta, A., Zhu, Z. and Myneni, R. (2013). Divergent arctic-boreal vegetation changes between North America and Eurasia over the past 30 years. *Remote Sensing*, *5*(5), pp.2093-2112.

Blake Jr., W. (1970). Studies of glacial history in Arctic Canada. I. Pumice, radiocarbon dates, and differential postglacial uplift in the eastern Queen Elizabeth Islands. *Canadian Journal of Earth Sciences, 7*(2). https://doi.org/10.1139/e70-065

Bowden, W. B., Gooseff, M. N., Balser, A., Green, A., Peterson, B. J., & Bradford, J. (2008). Sediment and nutrient delivery from thermokarst features in the foothills of the North

Slope, Alaska: Potential impacts on headwater stream ecosystems. *Journal of Geophysical Research: Biogeosciences*, *113*(G2).

Box, J. E., Colgan, W. T., Christensen, T. R., Schmidt, N. M., Lund, M., Parmentier, F.-J. W., Brown, R., Bhatt, U. S., Euskirchen, E. S., Romanovsky, V. E., Walsh, J. E., Overland, J. E., Wang, M., Corell, R. W., Meier, W. N., Wouters, B., Mernild, S., Mård, J., Pawlak, J., & Olsen, M. S. (2019). Key indicators of Arctic climate change: 1971–2017. *Environmental Research Letters*, *14*(4), 045010. https://doi.org/10.1088/1748-9326/aafc1b

Brooker, A., Fraser, R. H., Olthof, I., Kokelj, S. V., & Lacelle, D. (2014). Mapping the activity and evolution of retrogressive thaw slumps by tasselled cap trend analysis of a Landsat satellite image stack. *Permafrost and Periglacial Processes*, *25*(4), 243-256.

Burn, C. R., & Kokelj, S. v. (2009). The environment and permafrost of the Mackenzie Delta area. *Permafrost and Periglacial Processes*, *20*(2), 83–105. https://doi.org/10.1002/ppp.655

Campbell-Heaton, K. (2020). *Ice wedge activity in the Eureka Sound Lowlands, Canadian High Arctic* (Master's dissertation, Université d'Ottawa/University of Ottawa).

Campbell-Heaton, K., Lacelle, D., Fisher, D., & Pollard, W. (2021). Holocene ice wedge formation in the Eureka Sound Lowlands, high Arctic Canada. *Quaternary Research, 102,* 175-187. https://doi.org/10.1017/qua.2020.126

Carey, K. L. (1973). *Icings developed from surface water and ground water* (Monograph III-D3). U.S. Army Cold Regions Research and Engineering Laboratory. https://trid.trb.org/view/123493

Christiansen, H. H., Etzelmüller, B., Isaksen, K., Juliussen, H., Farbrot, H., Humlum, O., Johansson, M., Ingeman-Nielsen, T., Kristensen, L., Hjort, J., Holmlund, P., Sannel, A. B. K., Sigsgaard, C., Åkerman, H. J., Foged, N., Blikra, L. H., Pernosky, M. A., & Ødegård, R. S. (2010). The thermal state of permafrost in the nordic area during the international polar year 2007-2009. *Permafrost and Periglacial Processes*, *21*(2), 156–181. https://doi.org/10.1002/ppp.687

Church, M. (1974). Hydrology and Permafrost with Reference to Northern North America. In *Proceedings of workshop seminar "Permafrost Hydrology"*. (pp. 7-15). Ottawa: Canadian National Committee of the International Hydrological Decade.

Couture, N. J., & Pollard, W. H. (1998). An assessment of ground ice volume near eureka, northwest territories. *In Permafrost - Seventh International Converence*, *55*, 195–200.

Crist, E. P., & Cicone, R. C. (1984). A physically-based transformation of Thematic Mapper data---The TM Tasseled Cap. *IEEE Transactions on Geoscience and Remote sensing*, (3), 256-263.

Crites, H., Kokelj, S.V. & Lacelle, D. (2020). Icings and groundwater conditions in permafrost catchments of northwestern Canada. *Sci Rep* **10,** 3283. https://doi.org/10.1038/s41598-020-60322-w

Dallimore, S. R., Wolfe, S. A., & Solomon, S. M. (1996). Influence of ground ice and permafrost on coastal evolution, Richards Island, Beaufort Sea coast, N.W.T. *Canadian Journal of Earth Sciences*, *33*(5), 664–675. https://doi.org/10.1139/e96-050

Déry, S. J., Stahl, K., Moore, R. D., Whitfield, P. H., Menounos, B., & Burford, J. E. (2009). Detection of runoff timing changes in pluvial, nival, and glacial rivers of western Canada. *Water Resources Research*, *45*(4). doi:10.1029/2008WR006975.

Dixon, J. C. (2013). Response of Periglacial Geomorphic Processes to Global Change. *Treatise on Geomorphology*, *13*, 176–189. https://doi.org/10.1016/B978-0-12-374739-6.00351-1

Doré, G., Niu, F., & Brooks, H. (2016). Adaptation Methods for Transportation Infrastructure Built on Degrading Permafrost. *Permafrost and Periglacial Processes*, *27*(4), 352–364. https://doi.org/10.1002/ppp.1919

Drozdov, D. S., Malkova, G. v., Romanovsky, V. E., Rumyantseva, Ya. v., Abramov, A. A., Konstabtinov, P. Ya., Sergeev, D. O., Shiklomanov, N. I., Kholodov, A. L., Ponomareva, O. E., & Streletskiy, D. A. (2015). Monitoring of permafrost in Russia. Russian database and the international GTN-P project. 68e Conférence Canadienne de Géotechnique et 7e Conférence Canadienne Sur Le Pergélisol, 20 Au 23 Septembre 2015, Québec, Québec., 3–9.

Dyke, A. S., Andrews, J. T., Clark, P. U., England, J. H., Miller, G. H., Shaw, J., & Veillette, J. J. (2002). The Laurentide and Innuitian ice sheets during the Last Glacial Maximum. Quaternary Science Reviews, 21.

Edlund, S. A., & Alt, B. T. (1989). Regional congruence of vegetation and summer climate patterns in the Queen Elizabeth Islands, Northwest Territories, Canada. *Arctic*, *42*(1), 3–23. https://doi.org/10.14430/arctic1635

Edlund, S. A., Alt, B. T., & Garneau, M. (2000). Vegetation patterns on Fosheim Peninsula, Ellesmere Island, Nunavut. In *Bulletin of the Geological Survey of Canada* (Issue 529).

Embry, A., & Beauchamp, B. (2008). Chapter 13 Sverdrup Basin. Sedimentary Basins of the World, 5(C), 451–471. https://doi.org/10.1016/S1874-5997(08)00013-0

England, J., Atkinson, N., Bednarski, J., Dyke, A. S., Hodgson, D. A., & Ó Cofaigh, C. (2006). The Innuitian Ice Sheet: configuration, dynamics and chronology. Quaternary Science Reviews, 25(7–8), 689–703. https://doi.org/10.1016/j.quascirev.2005.08.007

Everdingen, V. R. (2005). Multi-language glossary of permafrost and related ground-ice terms. *International Permafrost Association*.

Farbrot, H., Isaksen, K., Etzelmüller, B., & Gisnås, K. (2013). Ground Thermal Regime and Permafrost Distribution under a Changing Climate in Northern Norway. *Permafrost and Periglacial Processes, 24*(3), 205–218. https://doi.org/10.1002/ppp.1763

Favaro, E. A., & Lamoureux, S. F. (2015). Downstream patterns of suspended sediment transport in a High Arctic River influenced by permafrost disturbance and recent climate change. Geomorphology, 246, 359-369.

Frappier, R., Lacelle, D., & Fraser, R. H. (2023). Landscape changes in the Tombstone Territorial Park region (central Yukon, Canada) from multilevel remote sensing analysis. Arctic Science, 9(4), 838-855.

Fraser, R., Olthof, I., Carrière, M., Deschamps, A., & Pouliot, D. (2012). A method for trend-based change analysis in Arctic tundra using the 25-year Landsat archive. *Polar record*, *48*(1), 83-93.

Fraser, R., Olthof, I., Kokelj, S., Lantz, T., Lacelle, D., Brooker, A., ... & Schwarz, S. (2014). Detecting landscape changes in high latitude environments using landsat trend analysis: 1. Visualization. *Remote Sensing*, *6*(11), 11533-11557.

French, H. M. (2017). *The Periglacial Environment* (4th ed.). Hoboken, NJ: John Wiley & Sons.

Frey, K. E., & McClelland, J. W. (2009). Impacts of permafrost degradation on arctic river biogeochemistry. *Hydrological Processes*, *23*(1), 169–182. https://doi.org/10.1002/hyp.7196

Government of Canada. (2025). Historical Climate Data. Retrieved from https://climate.weather.gc.ca/historical_data/

Grom, J. (2008). *Retrogressive thaw slump process and morphology, Eureka Sound Lowlands, Ellesmere Island, Nunavut, Canada* (Master's thesis, McGill University).

Hinkel, K. M., & Outcalt, S. I. (1994). Identification of heat-transfer processes during soil cooling, freezing, and thaw in central alaska. *Permafrost and Periglacial Processes*, *5*(4), 217-235.

Hinkel, K. M., Outcalt, S. I., & Taylor, A. E. (1997). Seasonal patterns of coupled flow in the active layer at three sites in northwest North America. *Canadian Journal of Earth Sciences*, *34*(5), 667-678.

Hinkel, K. M., Paetzold, F., Nelson, F. E., & Bockheim, J. G. (2001). Patterns of soil temperature and moisture in the active layer and upper permafrost at Barrow, Alaska: 1993–1999. *Global and Planetary Change*, *29*(3-4), 293-309.

Hjort, J., Karjalainen, O., Aalto, J., Westermann, S., Romanovsky, V.E., Nelson, F.E., Etzelmüller, B. and Luoto, M. (2018). Degrading permafrost puts Arctic infrastructure at risk by mid-century. Nature communications, 9(1), pp.1-9.

Hobbie, J. E., Shaver, G. R., Rastetter, E. B., Cherry, J. E., Goetz, S. J., Guay, K. C., Gould, W. A., & Kling, G. W. (2017). Ecosystem responses to climate change at a Low Arctic and a High Arctic long-term research site. *Ambio*, *46*, 160–173. https://doi.org/10.1007/s13280-016-0870-x

Hodgson, D. A. (1985). The last glaciation of west-central Ellesmere Island, Arctic Archipelago, Canada. *Canadian Journal of Earth Sciences, 22*(5), 684–693.

Hodgson, D. A., & Nixon, F. M. (1998). Ground ice volumes determined from shallow cores from western Fosheim Peninsula Ellesmere Island, Northwest Territories. *Bulletin of the Geological Survey of Canada, 507*, 1–24.

Hoegh-Guldberg, O., Jacob, D., Bindi, M., Brown, S., Camilloni, I., Diedhiou, A., Djalante, R., Ebi, K., Engelbrecht, F., Guiot, J., Hijioka, Y., Mehrotra, S., Payne, A., Seneviratne, S. I., Thomas, A., Warren, R., Zhou, G., Halim, S. A., Achlatis, M., ... Zougmoré, R. B. (2018). Impacts of 1.5°C Global Warming on Natural and Human Systems. In V. Masson-Delmotte et al., (Eds.), *Global warming of 1.5°C: An IPCC Special Report* (pp. 175-311). Intergovernmental Panel on Climate Change. https://www.ipcc.ch/sr15/

Huddart, D., & Stott, T. (2010). *Earth Environments: Past, Present and Future.* Wiley-Blackwell, Chichester, UK. 984 pp. ISBN: 978-1-4051-3592-4

Hughes, T., Denton, G. H., & Grosswald, M. G. (1977). Was there a late-Würm Arctic Ice sheet? Nature, 266(5603), 596–602.

Jones, B. M., Grosse, G., Farquharson, L. M., Roy-Léveillée, P., Veremeeva, A., Kanevskiy, M. Z., Gaglioti, B. v., Breen, A. L., Parsekian, A. D., Ulrich, M., & Hinkel, K. M. (2022). Lake and drained lake basin systems in lowland permafrost regions. *Nature Reviews Earth & Environment*, *3*(1), 85–98. https://doi.org/10.1038/s43017-021-00238-9

Kane, D. L. (1980). Hydrology of tundra ponds and lakes, Barrow, Alaska. U.S. Army Cold Regions Research and Engineering Laboratory, CRREL Report 80-26.

Kane, D. L., & Stein, J. (1983). Snowmelt runoff in the Kuparuk River Basin, Alaska, 1980. Water Resources Research, 19(3), 767–773. https://doi.org/10.1029/WR019i003p00767

Kokelj, S. V., Jenkins, R. E., Milburn, D., Burn, C. R., & Snow, N. (2005). The influence of thermokarst disturbance on the water quality of small upland lakes, Mackenzie Delta region, Northwest Territories, Canada. Permafrost and Periglacial Processes, 16(4), 343-353.

Kokelj, S. V., Lacelle, D., Lantz, T. C., & Gergel, S. E. (2013). Rapid thawing of subarctic ice-rich permafrost: Impacts on hydrology, geomorphology, and vegetation. *Geophysical Research Letters, 40*(22), 5700–5705. https://doi.org/10.1002/2013GL057642

Kokelj, S., Tunnicliffe, J., Lacelle, D., Lantz, T. C., Chin, K. S., & Fraser, R. (2015). Increased precipitation drives mega slump development and destabilization of ice-rich permafrost terrain, northwestern Canada. *Global and Planetary Change*, *129*, 56–68. https://doi.org/10.1016/j.gloplacha.2015.02.008

Lacelle, D., Bjornson, J., & Lauriol, B. (2010). Climatic and geomorphic factors affecting contemporary (1950-2004) activity of retrogressive thaw slumps on the Aklavik Plateau, Richardson Mountains, NWT, Canada. *Permafrost and Periglacial Processes*, *21*(1), 1–15. https://doi.org/10.1002/ppp.666

Lacelle, D., Fontaine, M., Pellerin, A., Kokelj, S. V., & Clark, I. D. (2019). Legacy of holocene landscape changes on soil biogeochemistry: a perspective from paleo-active layers in Northwestern Canada. Journal of Geophysical Research: Biogeosciences, 124(9), 2662-2679.

Lantuit, H., & Pollard, W. H. (2008). Fifty years of coastal erosion and retrogressive thaw slump activity on Herschel Island, southern Beaufort Sea, Yukon Territory, Canada. *Geomorphology*, *95*(1–2), 84–102. https://doi.org/10.1016/j.geomorph.2006.07.040

Lara, M.J., Nitze, I., Grosse, G., Martin, P. and McGuire, A.D. (2018). Reduced arctic tundra productivity linked with landform and climate change interactions. *Scientific reports*, *8*(1), pp.1-10.

Larking, T., Davis, E., Way, R., Hermanutz, L., & Trant, A. (2021). Recent greening driven by species-specific shrub growth characteristics in Nunatsiavut, Labrador, Canada. Arctic Science, 7(4), 781-797.

Lewkowicz, A. G. (1987). Headwall retreat of ground-ice slumps, Banks Island, Northwest Territories. *Canadian Journal of Earth Sciences*, *24*(6), 1077–1085. https://doi.org/10.1139/e87-105

Lewkowicz, A. G., & Duguay, C. R. (1999). Detection of permafrost features using SPOT panchromatic imagery, Fosheim Peninsula, Ellesmere Island, NWT. *Canadian Journal of Remote Sensing*, *25*(1), 34-44.

Lewkowicz, A. G., & Way, R. G. (2019). Extremes of summer climate trigger thousands of thermokarst landslides in a High Arctic environment. *Nature Communications (Resubmitted December 2018)*, *10*(1), 1329. https://doi.org/10.1038/s41467-019-09314-7

Liljedahl, A. K., Boike, J., Daanen, R. P., Fedorov, A. N., Frost, G. v., Grosse, G., Hinzman, L. D., Iijma, Y., Jorgenson, J. C., Matveyeva, N., Necsoiu, M., Raynolds, M. K., Romanovsky, V. E., Schulla, J., Tape, K. D., Walker, D. A., Wilson, C. J., Yabuki, H., & Zona, D. (2016). Pan-Arctic ice-wedge degradation in warming permafrost and its influence on tundra hydrology. *Nature Geoscience*, *9*(4), 312–318. https://doi.org/10.1038/ngeo2674

MacDonald, M. K., Stadnyk, T. A., Déry, S. J., Braun, M., Gustafsson, D., Isberg, K., & Arheimer, B. (2018). Impacts of 1.5 and 2.0 °C Warming on Pan-Arctic River Discharge Into the Hudson Bay Complex Through 2070. *Geophysical Research Letters*, *45*(15), 7561–7570. https://doi.org/10.1029/2018GL079147

Mackay, J. R. (1966). Segregated epigenetic ice and slumps in permafrost, Mackenzie Delta area, N.W.T. *Geographical Bulletin*, *8*, 59–80. https://cir.nii.ac.jp/crid/1570854174364600320.bib?lang=en

Malone, L., Lacelle, D., Kokelj, S., & Clark, I. D. (2013). Impacts of hillslope thaw slumps on the geochemistry of permafrost catchments (Stony Creek watershed, NWT, Canada). Chemical Geology, 356, 38-49.

Marshall, S.J., White, E.C., Demuth, M.N., Bolch, T., Wheate, R., Menounos, B., Beedle, M.J. and Shea, J.M. (2011). Glacier water resources on the eastern slopes of the Canadian Rocky Mountains. Canadian Water Resources Journal, 36(2), pp.109-134.

McBean, G., Alekseev, G., Chen, D., Foerland, E., Fyfe, J., Groisman, P.Y., King, R., Melling, H., Vose, R. and Whitfield, P.H. (2005). Chapter 2: Arctic Climate: Past and Present. *Arctic Climate Impact Assessment* (pp. 21–60). Cambridge University Press.

McDonald, D. M., & Lamoureux, S. F. (2009). Hydroclimatic and channel snowpack controls over suspended sediment and grain size transport in a High Arctic catchment. *Earth Surface Processes and Landforms*, *34*(3), 424-436.

Miall, A. D. (1986). Eureka Sound Group. *Bulletin of Canadian Petroleum Geology*, *34*(2), 240–270. http://archives.datapages.com/data/cspg/data/034/034002/pdfs/0240.pdf

Miles, V.V. and Esau, I. (2016). Spatial heterogeneity of greening and browning between and within bioclimatic zones in northern West Siberia. *Environmental Research Letters*, *11*(11), p.115002.

Olthof, I., & Fraser, R. H. (2014). Detecting landscape changes in high latitude environments using Landsat trend analysis: 2. Classification. *Remote Sensing*, *6*(11), 11558-11578.

Pollard, W., Ward, M., & Becker, M. (2015). The Eureka Sound lowlands : an ice-rich permafrost landscape in transition. *68e Conférence Canadienne de Géotechnique et 7e Conférence Canadienne Sur Le Pergélisol, 20 Au 23 Septembre 2015, Québec, Québec.*, *Figure 1*.

Rae, R. W. (1951). Joint Arctic Weather Project. Arctic, 4(1). https://doi.org/10.14430/arctic3932

Romanovsky, V. E., Smith, S. L., Isaksen, K., Shiklomanov, N. I., Streletskiy, D. A., Kholodov, A. L., ... & Marchenko, S. S. (2020). Permafrost [in "State of the Climate in 2019"]. *Bulletin of the American Meteorological Society*, *101*(8), S265-S270.

Roy, C. (2018). Origin of massive ground ice in the Eureka Sound Lowlands, Nunavut. Master's Thesis, McGill University.

Rudy, A. C., Lamoureux, S. F., Treitz, P., & Van Ewijk, K. Y. (2016). Transferability of regional permafrost disturbance susceptibility modelling using generalized linear and generalized additive models. *Geomorphology*, *264*, 95-108.

Schuur, E. A., McGuire, A. D., Schädel, C., Grosse, G., Harden, J. W., Hayes, D. J., ... & Vonk, J. E. (2015). Climate change and the permafrost carbon feedback. *Nature*, *520*(7546), 171-179.

Shahgedanova, M., Afzal, M., Hagg, W., Kapitsa, V., Kasatkin, N., Mayr, E., Rybak, O., Saidaliyeva, Z., Severskiy, I., Usmanova, Z. and Wade, A. (2020). Emptying water towers? Impacts of future climate and glacier change on river discharge in the Northern Tien Shan, Central Asia. *Water, 12*(3), p.627.

Shiklomanov, N. I., & Nelson, F. E. (2013). Active Layer Processes. In *Encyclopedia of Quaternary Science: Second Edition* (pp. 421–429). https://doi.org/10.1016/B978-0-444-53643-3.00095-9

Shur, Y. L., & Jorgenson, M. T. (2007). Patterns of permafrost formation and degradation in relation to climate and ecosystems. *Permafrost and Periglacial Processes, 18*(1), 7-19.

Shur, Y., Hinkel, K. M., & Nelson, F. E. (2005). The transient layer: implications for geocryology and climate-change science. *Permafrost and Periglacial Processes*, *16*(1), 5-17.

Simon, K. M., James, T. S., & Dyke, A. S. (2015). A new glacial isostatic adjustment model of the Innuitian Ice Sheet, Arctic Canada. *Quaternary Science Reviews*. https://doi.org/10.1016/j.quascirev.2015.04.007

Smith L.C., Sheng Y., MacDonald G.M., Hinzman L.D. (2005). Disappearing Arctic lakes. *Science, 308*(5727), 1429–1432. https://doi.org/10.1126/science.1108142

Smith, S. L., Chartrand, J., Duchesne, C., Ednie, M., Smith, S. L., Duchesne, C., & Riseborough, D. W. (2016). Report on 2013 field activities and collection of ground thermal and active layer data in the Mackenzie Corridor. *Geological Survey of Canada Open File 8125*, *7659*, 1–105. https://doi.org/10.4095/299296

Smith, S. L., Lewkowicz, A. G., & Duchesne, C. (2015). Variability and Change in Permafrost Thermal State in Northern Canada. *68e Conférence Canadienne de Géotechnique et 7e Conférence Canadienne Sur Le Pergélisol, 20 Au 23 Septembre 2015, Québec, Québec.*, *Figure 1*, 1–6.

Smith, S. L., O'Neill, H. B., Isaksen, K., Noetzli, J., & Romanovsky, V. E. (2022). The changing thermal state of permafrost. *Nature Reviews Earth & Environment*, *3*(1), 10–23. https://doi.org/10.1038/s43017-021-00240-1

Smith, S. L., Romanovsky, V. E., Lewkowicz, A. G., Burn, C. R., Allard, M., Clow, G. D., Yoshikawa, K., & Throop, J. (2010). Thermal state of permafrost in North America: A

contribution to the international polar year. *Permafrost and Periglacial Processes*, *21*(2), 117–135. https://doi.org/10.1002/ppp.690

Smith, S. L., Throop, J., & Lewkowicz, A. G. (2012). Recent changes in climate and permafrost temperatures at forested and polar desert sites in Northern Canada. *Canadian Journal of Earth Sciences*, *49*(8), 914–924. https://doi.org/10.1139/E2012-019

Streletskiy, D., Shiklomanov, N., Kokarev, V. and Anisimov, O. (2015). Arctic cities, permafrost and changing climatic conditions. *In Proceedings of the 68th Canadian Geotechnical Conference* (GEOQuébec 2015) (pp. 20-23). Canadian Geotechnical Society.

Walvoord, M. A., & Kurylyk, B. L. (2016). Hydrologic Impacts of Thawing Permafrost-A Review. *Vadose Zone Journal*, *15*(6), vzj2016.01.0010. https://doi.org/10.2136/vzj2016.01.0010

Wang, J.A. and Friedl, M.A. (2019). The role of land cover change in Arctic-Boreal greening and browning trends. Environmental Research Letters, 14(12), p.125007.

Ward Jones, M. K., & Pollard, W. H. (2021). Daily field observations of retrogressive thaw slump dynamics in the Canadian high arctic. *Arctic*, *74*(3), 339–354. https://doi.org/10.14430/arctic73377

Ward Jones, M. K., Pollard, W. H., & Amyot, F. (2020). Impacts of Degrading Ice-Wedges on Ground Temperatures in a High Arctic Polar Desert System. *Journal of Geophysical Research: Earth Surface*, *125*(3). https://doi.org/10.1029/2019JF005173

Ward Jones, M. K., Pollard, W. H., & Jones, B. M. (2019). Rapid initialization of retrogressive thaw slumps in the Canadian high Arctic and their response to climate and terrain factors. *Environmental Research Letters*, *14*(5). https://doi.org/10.1088/1748-9326/ab12fd

Webb, E. E., Liljedahl, A. K., Cordeiro, J. A., Loranty, M. M., Witharana, C., & Lichstein, J. W. (2022). Permafrost thaw drives surface water decline across lake-rich regions of the Arctic. *Nature Climate Change*, *12*(9), 841–846. https://doi.org/10.1038/s41558-022-01455-w

Wen, Z., Niu, F., Yu, Q., Wang, D., Feng, W., & Zheng, J. (2014). The role of rainfall in the thermal-moisture dynamics of the active layer at Beiluhe of Qinghai-Tibetan plateau. *Environmental earth sciences*, *71*(3), 1195-1204.

Westermann, S., Langer, M., Boike, J., Heikenfeld, M., Peter, M., Etzelmüller, B. and Krinner, G. (2016). Simulating the thermal regime and thaw processes of ice-rich permafrost ground with the land-surface model CryoGrid 3. Geoscientific Model Development, 9(2), pp.523-546.

Williams, J. R., & Waller, R. M. (1966). Ground water occurrence in permafrost regions of Alaska. In *Proceedings of the 1st International Conference on Permafrost* (pp. 159–164). National Academy of Sciences.

Williams, P. J., and Smith, M. W. (1989). The Ground Thermal Regime. In *The Frozen Earth: Fundamentals of Geocryology* (pp. 83–121). Cambridge: Cambridge University Press.

Wolfe, S. A., Dallimore, S. R., & Solomon, S. M. (1998). Coastal permafrost investigations along a rapidly eroding shoreline, Tuktoyaktuk, NWT. *Permafrost: Proceedings of the Seventh International Conference.*

Wolfe, S. A., Kotler, E., & Dallimore, S. R. (2001). *Surficial characteristics and the distribution of thaw landforms (1970 to 1999), Shingle Point to Kay Point, Yukon Territory.*

Woo, M. (1990). Consequences of Climatic Change for Hydrology in Permafrost Zones. *Journal of Cold Regions Engineering*, *4*(1), 15–20. https://doi.org/10.1061/(asce)0887-381x(1990)4:1(15)

Woo, M. K. (2012). *Permafrost Hydrology.* Springer Science & Business Media. https://doi.org/10.1007/978-3-642-23462-0

Woo, M. K., & Xia, Z. (1996). Effects of hydrology on the thermal conditions of the active layer: Paper presented at the 10th Northern Res. Basin Symposium (Svalbard, Norway—28 Aug./3 Sept. 1994). *Hydrology Research*, *27*(1-2), 129-142.

Yoshikawa K, Hinzman LD. (2003). Shrinking thermokarst ponds and groundwater dynamics in discontinuous permafrost near Council, Alaska. *Permafrost Periglacial Processes, 14*, 151–160

Young, K. L., & Woo, M. K. (2000). Hydrological environment of the Hot Weather Creek basin, Ellesmere Island, Nunavut. *Bulletin of the Geological Survey of Canada*, *529*, 347–360. https://doi.org/10.4095/211973

Zaerpour, M., Hatami, S., Sadri, J., & Nazemi, A. (2021). A global algorithm for identifying changing streamflow regimes: application to Canadian natural streams (1966–2010). *Hydrology and Earth System Sciences, 25*(9), 5193-5217.

Zhang, Y., Chen, W. and Riseborough, D.W. (2008). Transient projections of permafrost distribution in Canada during the 21st century under scenarios of climate change. *Global and Planetary Change, 60*(3-4), pp.443-456.

Zhu, X., Wu, T., Li, R., Xie, C., Hu, G., Qin, Y., ... & Yang, C. (2017). Impacts of summer extreme precipitation events on the hydrothermal dynamics of the active layer in the Tanggula permafrost region on the Qinghai-Tibetan plateau. *Journal of Geophysical Research: Atmospheres*, *122*(21), 11-549.

1.7 Figures

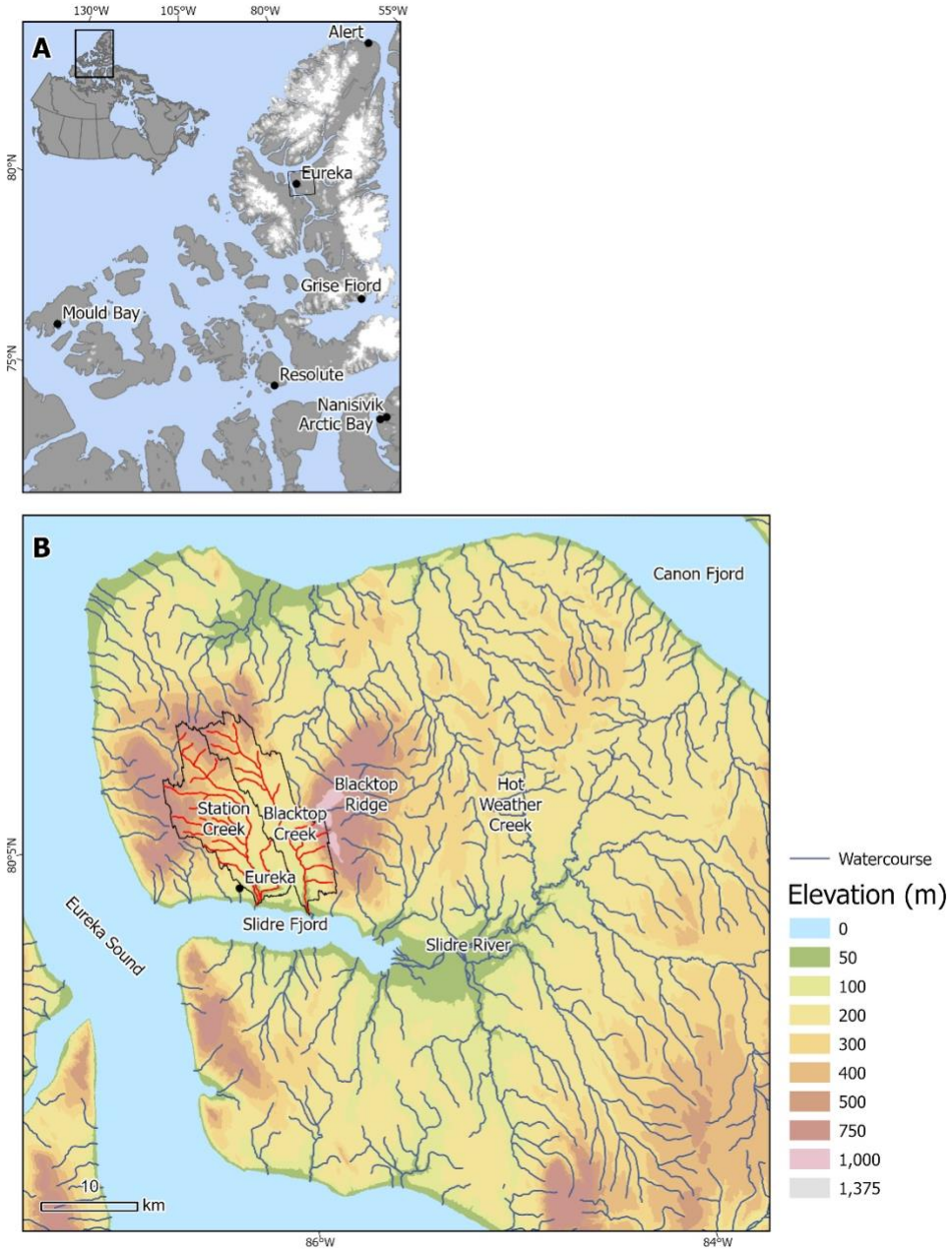


Figure 1.1. Project study region (A) is the Canadian Arctic Archipelago, and (B) the Fosheim Peninsula with Station Creek and Blacktop Creek basin and course outlines. Geospatial data (populated areas, watercourses, digital terrain model, Northern Canada outline, Canada outline) provided by Natural Resources Canada.



Figure 1.2. Active thaw slumps monitored in Chapters 3 and 4. (A) Nunavut Slump – Blacktop Creek; (B) BL Slump - Station Creek; (C) CHP Slump – Station Creek. All photos were captured in July 2023 by author or J. Prest.

A



B



C



Figure 1.3. Slump runoff sample locations and runoff-stream mixing sites. (A) Nunavut Slump – Blacktop Creek; (B) BL Slump – Station Creek; (D) CHP Slump – Station Creek.

Chapter 2

Landscape change (1999-2024) in the Fosheim Peninsula, Canadian High Arctic, using Landsat imagery.

Kethra Campbell-Heaton[1], Denis Lacelle[1]

[1]Department of Geography, Environment and Geomatics, University of Ottawa, Ottawa, ON, Canada

Abstract

Arctic climate warming is substantially changing Arctic ecosystems and geomorphology. In the Canadian Arctic especially, it is difficult to quantify these changes on a broad and uniform scale across the Arctic. This project seeks to understand the climate-driven landscape changes for the Fosheim Peninsula, Nunavut, using Landsat 7 and 8 TOA image composites from 1999 to 2024 for the summer period (July 10- August 10). Monotonic and non-monotonic reflectance trends were derived and used to train a Random-Forest based landscape classification to identify dominate land change processes. Trend analysis using Man Kendell and Theil-Sen estimators indicate that 79.3% of the Fosheim Peninsula experienced significant positive change in greening, 42.3% in brightness and 31.2% in wetness. Of that, 26% of the region showing positive greening trend is barren land. Forest-based landscape classification indicates aridfication occurring on 3.7% of the peninsula. A Landsat trend analysis visual analysis identified substantial geomorphic reorganization including widespread fluvial erosion and channel migration of the Slidre River system. Over the 25-year period nine lakes fully or partially drained and 139 thaw slumps were identified with 60-active in 2024. Together, these results indicate that the Fosheim Peninsula is undergoing a major transitional phase driven by regional warming, the distribution of Quaternary surficial deposits and a high near-surface ground ice content. The application of long-term satellite imagery and Landsat trend analysis-based change detection provides a reliable framework for Arctic landscape change monitoring.

Keywords.

Greening/Browning. High Arctic. Climate change. Landsat. Landscape change.

2.1 Introduction

The Arctic is experiencing an increase in air temperatures at a rate 2-4 times than the global average and an increase in precipitation (Dou et al., 2022; Rantanen et al., 2022; Cast et al., 2025). Given the vastness of the Arctic, historical satellite imageries have become central for monitoring long-term effects of climate change in permafrost environments. Analysis of individual indices from NOAA-AVHRR and the USGS Landsat series over the past few decades revealed shifts in vegetation structure, surface moisture, and an increase in local disturbances, such as wildfires and thaw slumps (Walvoord & Kurylyk, 2016; Hobbie et al., 2017; Box et al., 2019; Jones et al., 2022; Webb et al., 2022). For example, much of the Arctic has experienced since the 1990s widespread increase in the Normalized Difference Vegetation Index (NDVI), which was interpreted as an increase in vegetation abundance and productivity or "greening" (Wang and Friedl, 2019; Berner et al., 2020). A decrease in NDVI, or "browning", has been found mostly in localized areas following surface disturbances (Bi et al., 2013; Wang & Friedl, 2019; Phoenix et al., 2025). On a broad scale, large patterns in Arctic greening have been linked to increasing thaw degree days; however, on a more local scale, surface moisture appears as a key driver to Arctic vegetation productivity, found that greening rates in moisture-rich soil were nearly double than those in drier soil conditions (Arndt et al., 2019).

It is clear that the response of permafrost to climate change is complex and linked not only to changes in air temperature and precipitation, but also to surface moisture and vegetation through a series of intricate feedback that can amplify or dampen changes in ground temperatures and permafrost thaw (Walvoord & Kurylyk, 2016; Jones et al., 2022). For example, vegetation greening tends to have positive feedback on ground temperatures because it reduces the surface albedo, allowing the ground surface to absorb more insolation that is transferred to heat and conducted into the ground (Wang and Friedl, 2019; Berner et al., 2020). Surface moisture also tends to create positive feedback on permafrost temperatures whereby higher surface and soil moisture increases the thermal conductivity and heat capacity allowing heat to be transferred into the ground (Walvoord & Kurylyk, 2016; Hobbie et al., 2017; Webb et al., 2022). To that end, multispectral indices like the Tasseled Cap (TC) transformation can provide valuable information to assess current and future changes in permafrost environments. The TC transformation method consists of three indices: TC brightness that represents surface reflectance, TC greenness captures vegetation abundance and productivity, and TC wetness is sensitive to surface moisture (Crist and Cicone, 1984). In northwestern Canada, the TC indices have been applied to dense stacks of Landsat imageries to investigate a range of gradual and abrupt landscape changes, including vegetation change (greening, browning, fires), fluvial processes and geomorphic disturbances

such as thaw slumps, lake drainage (Fraser et al., 2012; Brooker, et al., 2014; Fraser et al., 2014; Olthof & Fraser, 2014; Frappier et al., 2023). These investigations revealed the direction and magnitude of landscape changes and the expected response of permafrost to climate change.

To date, few studies have examined changes in vegetation productivity, surface moisture and reflectivity in the High Arctic. Those that have reported a general increase in surface greening (Hobbie et al., 2017; Edwards & Treitz, 2017; Hamel Jomphe et al., 2026). In Zackenburg, Greenland (74˚28' N) the maximum NDVI (Normalized Difference Vegetation Index) values increased from 0.35 in 1994 to 0.57 in 2008 (Hobbie et al., 2017), these relatively high values for this latitude reflect the site's unusually dense vegetation cover. At Cape Bounty, Melville Island (74º55′ N), long-term NDVI (1985-2015) increased significantly in mesic tundra (1.3% yr^{-1}) and semi-polar desert (0.82% yr^{-1}) linked to warmer summer temperatures and longer growing seasons (Edwards & Treitz, 2017). Banks Island (Nunavut; 73˚N) also exhibited a long-term (1984-2014) increase in vegetation productivity linked to an increase in the biomass of plant communities and mediated by terrain-controlled variation in soil moisture (Campbell et al., 2021).

The Fosheim Peninsula (80˚00'N) on Ellesmere Island in the Canadian high Arctic is a polar desert environment that is experiencing climate warming (Copland et al., 2020). Permafrost in this region is sensitive to changing climate conditions because the lowlands host ice-rich permafrost in the form of ice wedges and tabular massive ground ice (Pollard et al., 2015; Bernard-Grand'Maison and Pollard, 2018) with a thin organic layer and sparse vegetation cover (Ward-Jones et al., 2019). The numerous thaw slumps and active layer detachment slides that developed over the past decades, and the more recent melting of ice wedges, are an indication the sensitivity of the permafrost (Lewkowicz, 1990; Pollard, 2000 (Becker et al., 2016). This study aims to identify landscape changes across the Fosheim Peninsula using a dense stack of Landsat imagery. The objectives of this study are to (1) generate a 30-yearsLandsat time series (1994-2024) for the Fosheim Peninsula and quantify spectral trends in TC brightness, greenness and wetness; (2) classify landscape change from the Landsat time series using pixel-wise Mann-Kendell significance test and Theil-Sen trend metrics; and (3) map significant geomorphic and environmental processes driving observed change across the Fosheim Peninsula through the use of a Random Forest model.

2.2 Study Area

The Fosheim Peninsula is on Ellesmere Island (Nunavut, Canada) and covers an area of 4637.8 km^2. Physiographic regions include the Eureka Sound Lowland (<150 m), Black Top (<650 m),

Troelsen (<650 m), Hare Cape (<450 m) and Airfield (<600 m) ridges, Snow Goose Hill (<225 m), and the Sawtooth Mountain (<1100 m) (**Fig. 2.1**). Deglaciation in the region began between 10.3-8.7 ka BP and retreated inland to current extent on Ellesmere Island and Axel Heiberg Island (England et al., 2006). Marine inundation of the areas below 139-150 m a.s.l. occurred until 8.8-8.7 ka BP and covered roughly 1/3 of the peninsula (Bell, 1996). The surficial materials consist primarily of weathered bedrock, colluvium, blanket, and veneer till, glaciofluvial sediments in meltwater channels above marine limit and marine sediments (clay-silt) below marine limit (Hodgson and Nixon, 1998, Bell & Hodgson, 2000; Young & Woo, 2000). Minor surficial materials units are fluvial, eolian, organic deposits (Bell and Hodgson, 2000).

The region experiences a polar desert climate (Edlund et al., 2000). Meteorological data from the Eureka Weather Station, the only weather station on the peninsula, shows for the 1991-2020 period a mean annual air temperature (MAAT) of -18.1°C, and total annual precipitation of 77.6 mm y^{-1}, (Fig. 2; Government of Canada, 2026). Relative to the 1961-1990 climate normal, the MAAT and total precipitation for the 1991-2020 period have increased by 1.8°C and by 19 mm, respectively. Thawing Degree Days (TDD) have increased since the 1980s. The TDD for the 1961-1990 period averaged 349 but increased to 431 for the 1991-2020. Since 1999, eight years have experienced TDD greater than 500, (2005, 2007, 2009, 2011, 2012, 2015, 2019, and 2020), highlighting the increasing frequency of warm summers across the Fosheim Peninsula. Based on δD-$\delta^{18}O$ analyses of precipitation, the increase in precipitation is linked to increase in air temperature, reduction in sea ice extent and enhanced meridional transport of moisture (Copland et al., 2020).

Despite having a polar desert climate, the FP is classified as an enriched prostrate shrub zone, characterized as having the greatest diversity and density of vascular plant species of the Queen Elizabeth Islands (Edlund et al., 2000; Edlund & Alt, 1989). The main types of landcover include barren land (31.8%), polar grassland-lichen-moss (28.9%), polar barren-lichen-moss (26.4%), wetland (5.2%), water (0.5%), snow and ice (0.5%), and urban areas (0.2%) (Government of Canada, 2019). Hot Weather Creek supports dense woody vegetation below 300-500 m a.s.l. (i.e., S*alix arctica and Dryas integrifolia*), whereas across the peninsula plant diversity declines above ~180 m a.s.l. and woody species become sparse and stunted above 300 m a.s.l. with herbaceous species such as *Luzula confusa* and *Potentilla hyparctica* becoming abundant (Edlund et al., 2000).

The FP lies within the continuous permafrost zone, with permafrost being > 500 m thick (Pollard et al., 2015). The active layer thickness ranges between 30 and 100 cm, with an average of about 60 cm (Hodgson & Nixon, 1998). The mean annual ground temperature (measured at

depth of zero annual amplitude) is < −10ºC (Hjort et al., 2018). Ground ice is estimated to occupy 30%vol of the uppermost 6 m of permafrost (Couture & Pollard, 1998). Of that, 3.5%vol is estimated to be wedge ice and the remaining is tabular bodies of massive ice all below marine limit (Couture & Pollard, 1998). Ice wedges in the region initiated between 9-2.5 cal ka BP following land emergence (Campbell-Heaton et al., 2021). The tabular massive ice in the raised marine-deltaic sediments also formed during the same period from the freezing of glacial meltwater recharging an aquifer (Roy et al., 2023).

Tundra polygon is the main periglacial landform in the region, covering approximately 50% of the FP; they are nearly continuous in unconsolidated sediments below marine limit and along the foothills of Black Top, Troelsen, Hare Cape and Airfield ridges and Snow Goose Hill (Bell, 1992; Bernard-Grand'Maison and Pollard, 2018). Thaw slumps and active layer detachment slides are the dominate thermokarst landforms in the area (Lewkowicz, 1990; Pollard et al., 2015). Slump activity in the region is limited to raised marine-deltaic sediments, with a particularly high concentration of slumping and active layer slides occurring in Hot Weather Creek basin, Slidre river, around Eureka, and the southern portion of the peninsula (Pollard and Bell, 1998). The increasing MAAT over the past four decades has implications on the stability of permafrost in the FP (i.e., Pollard et al., 2015). In recent years, ice wedge melting in troughs of polygons within the lowlands were observed, along with active layer thickening, and an increase in active thaw slumps (Pollard et al., 2015; Ward Jones et al., 2020). The troughs of these tundra polygons experienced a substantial amount of degradation for a cold polar desert, including subsistence, increase in ponding water and an increase in ice-wedge melt out events (Ward Jones et al., 2020). However, troughs with a greater vegetation cover experienced less degradation than troughs with little to no vegetation due to the insulating property of vegetation (Becker et al., 2016; Ward Jones et al., 2020).

2.3 Methods

2.3.1 Imagery Acquisition

Landsat imagery for the Fosheim Peninsula was obtained from the USGS Collection 2 Level 1 archive through Google Earth Engine (GEE; Gorelick et al., 2017). A total of 204 Landsat 7 ETM+ and 8 OLI scenes were selected for the period of 1999 – 2024 using two criteria: (1) <10% cloud cover, and (2) acquisition within the peak growing season (July 10 – August 10; **Fig. 2.2**; Chander et al., 2009).

Each image within the annual image collection was masked for cloud and cloud shadow using the QA_PIXEL quality assurance band, with an additional 1-pixel edge mask applied to the cloud and cloud shadow mask to reduce residual contamination. To ensure radiometric consistency across sensors, Landsat 8 OLI reflectance values were converted to Landsat 7 ETM+ equivalents following Roy et al. (2016), and band names were harmonized accordingly. A Tasseled Cap (TC) transformation was applied to the image collection using coefficients from Huang et al. (2002) to derive the brightness, greenness and wetness indices (Crist, 1984). For each year, a single composite image was generated using the median pixel value, which reduces the influence of clouds, haze, and Landsat 7 scan-line gaps. The annual composites were downloaded and manually inspected; persistent cloud or striping artifacts were masked in 2002, 2005, 2009, 2011, 2017, and 2024 using ArcGIS Pro.

2.3.2 Landscape change detection

Long-term spectral trends were quantified using pixel-wise Theil-Sen regressions applied to the 1999-2024 TC composites. The TC indices can be used to assess current changes in the landscape and represent three key parameters that influence the response of permafrost to climate change (Frappier et al., 2023). Monotonic trends (showing a continuous, gradual increasing or decreasing trend) were first assessed with pixel-based Theil–Sen regressions following the methods of Fraser et al. (2012; 2014). In R (v. 4.5.1; R Core Team, 2025), a pixel-wise trend for each spectral index (TCB, TCW and TCG) was computed using the stack of TC transformed Landsat images for the study period (1999-2024). The results are raster images showing the direction and magnitude of changes in TCB, TCG, and TCW. The statistical significance of the Theil–Sen regressions were assessed using the Mann–Kendall test. Masking p values >0.05 from the TC trends reveals areas with significant trends in each of the three TC indices.

Many landscape changes are non-monotonic, and these can be detected using the Landsat Arctic RGB Change method (LARCH) of Fraser et al. (2014). Here, the values of the slope of the three TC indices trends from the stack of images were composited into a RGB image. The product is an image depicting the three-dimensional TC trajectory using additive color mixing and provides a qualitative representation of landscape changes and visualized with a linear histogram stretch within +/- 5 standard deviations (Frappier et al., 2023).

2.3.3 Classification of Landscape Changes

A landscape change map was produced from the TC trends and classified using a supervised Random Forest classification (Olthof and Fraser, 2014). Model training data was generated using

the TC slopes: brightness, greenness and wetness in ArcGIS Pro (v. 3.4). Class generation was supported by high-resolution satellite imagery available in the ArcGIS Pro Imagery basemap (Worldview-2 provided by Vantor for July 9 and 16, 2024, resolution 0.5m). A total of 5543 training points were created (**Table 2.1**): 1) Vegetation succession - surface brightening, 2) Vegetation colonization - surface darkening, 3) Active thermokarst disturbance - wetting, browning and darkening, 4) Upland greening - greening and drying, 5) Aridification - browning and drying, 6) Waterlogged soils & vegetation decline, 7) Anthropogenic change - runway, 8) stable (p-value >0.05), 9) Surface water decrease, 10) Surface water increase, 11) Bedrock outcrop, 12) Melt-driven wetting, 13) Earlier melting of ice/snow. An effort was also made to delineate bedrock exposures; however, distinguishing bedrock from thin, patchy surficial deposits proved challenging given the complex Quaternary history of the area. Training data was confined to a 10 km radius of the Eureka Weather station and supported by field-collected GPS data obtained in July 2023.

The landscape change classification model was generated in R (v4.5.1) using predictor layers from the trend analysis, Theil Sen slope, Man Kendell's tau and p-value were compiled for TCB, TCG and TCW. The intercept from each index was intentionally excluded as it produced large regions of missing data in the final classification. Multiple iterations of this modelling included landscape characteristics as model predictors such as elevation, slope, aspect and land class. However, we found that those predictors tended to obscure subtle transitions between similar geomorphic classes; for example, wetting versus drying phases on a deltaic plain. The model that only relied on the Tau, Slope and p-value metrics from the three Tassell-cap indices, produced the most spatially coherent and interpretable classification.

The landscape change model was trained using 70% of data and the remaining 30% to test the model's accuracy. Model was trained using the the Random Forest package (Liaw & Wiener, 2002). The model was created with 301 trees, an 'mtry' value of 3 and the seed was set to 123 to ensure reproducibility of results across multiple runs. Stratified sampling was used to ensure an adequate representation of all classes during training and evaluation; this was necessary to improve classification of classes with small sample size by reducing classification bias towards dominate classes. The model was evaluated using the testing subset through a confusion matrix and accuracy statistics. This model achieved an overall accuracy was 95.1% (k=0.93). Model importance scores indicated that slope variables dominated predictive power, led by wetness, with brightness and greenness contributing progressively less. Class-specific performance was consistently high (**Table 2.2**), with most class-sensitives above 0.90 and overall F1-score is 0.

The confusion matrix shows a strong discriminative capacity for all classes with limited cross confusion.

2.3.4 Multi-scale Image Analysis

Landscape changes identified from the analyses were visually compared against high-resolution imagery from Planet Scope (July 30th, 2022, 3m; Planet Labs PBC, 2024) and the ArcGIS Pro Imagery basemap (Worldview-2 provided by Vantor for July 9 and 16, 2024, resolution 0.5m). These images were used to support identification and interpretation of land change classes and to visually validate the results of the model. Field observations from summer 2018, 2019, 2022, and 2023 were used to validate the analyses.

2.4 Results

2.4.1 Significant changes in TCG, TCB and TCW

The Man Kendell and the Theil-Sen analysis revealed that 6.4% of the FP experienced significant changes in all three TC indices (**Fig. 2.3**). Individually, 79.4% of the landscape experienced significant change in TCG (79.3% positive trend, 0.08% negative trend), 44.5% experienced significant change in TCB (42.3% positive trend, 2.2% negative trend), and 35.7% in TCW (31.2% positive trend, 4.5% negative trend). Most of the FP experienced a positive trend in TCG. The negative trend in TCG is limited to the alluvial fan of Slidre river, and exposed bedrock areas on the ridges showed no change. The TCB had a positive trend mostly above marine limit (146 m a.s.l.), and along portions of Slidre river watershed. Negative trends in TCB all occurred below marine limit in the ESL and south of Romulus Lake. Finally, the positive trend in TCW occurred inland and below marine limit. The negative trends in TCW are in areas above marine limit and largely occur on the steep slopes of Blacktop Ridge.

Using the Canadian Land Classification (Government of Canada, 2019), 26% of the positive TCG trend occur within the barren land class, 22.8% and 21.4% within the polar barren-lichen-moss (PBLM) and polar grassland-lichen-moss classes (PGLM). For the TCB, 20.6% of the positive trend is within the PGLM class, and 1.9% of the negative trend is in barren land class. For the TCW, 15.6% of the positive trend occurs in the barren class, whereas 1.74% and 1.47% of the TCW negative trend (4.5% total area) falls within the PGLM and barren classes.

2.4.2 Classified Landscape Change

The landscape change map, in which non-significant changes and bedrock were masked, is shown in **Figure 2.4**. The three dominant changes in the area include aridification (3.7%), waterlogged soils and vegetation decline (2.6%), and vegetation succession (1.1%). All other changes represent < 1% of the study area. Aridification mostly occurred on steep slopes above marine limit and below marine limit along valley slopes. Waterlogged soils and vegetation decline occurred in flat, low sloped terrain. Finally, vegetation succession occurs largely below marine limit.

Non-monotonic Landscape Changes from LARCH

Hydrogeomorphic Changes

Slidre river, the largest river in the region, experienced substantial change in its delta where new sandbars and new channels developed (**Fig. 2.5**). Upstream, minor changes were observed in a cutbank caused by erosion. Hot Weather Creek, a tributary of Slidre River, showed only minor erosion in a cutbank near its outlet. Station Creek and Blacktop Creek both show varying degree of fluvial drying. The alluvial fan of Blacktop Creek showed signs of wetting, attributed to erosion observed in July 2022 and 2023. Finally, Gemini Creek shows mild drying and wetting.

Most lakes on the FP remained stable over the 1999-2024 period, with no evidence of widespread expansion or shrinking. Nine lakes were identified as experiencing partial or complete drainage. In the Hot Weather Creek basin, a lake that persisted through the early 2000s began contracting around 2020 and was nearly fully drained by 2024, leaving only moisture retained within the ice wedge troughs (**Fig. 2.6A**). In the northwest interior of the peninsula, another lake drained in 2016 (confirmed with high resolution imagery) with subsequent wetland development after drainage (**Fig 2.6B**). Finally, south of Romulous Lake, a small lake shows frequent fluctuation in water level with periods of high and low water levels over the study period, near complete drainage was observed in 2015 followed by partial replenishment in 2016 (**Fig. 2.6C**).

More than thirty lakes in the FP showed some evidence of expansion, and, in some instances, new thermokarst pond development. For example, Eastwind Lake, the second largest lake on the peninsula, **Fig. 2.6D**, showed a slight increase in lake level (blue/ purple) along its western and southern margins. Another example of lake expansion is found west of the Sawtooth Mountain range, where the lake expanded into ice wedge polygonal terrain (**Fig. 2.6E**). Finally, an ice-covered lake was identified in the LARCH composite (**Fig. 2.6F**). This lake is small (< 0.3 km^2) and located at 190 m a.s.l. in the Sawtooth Mountain range. The ice cover on this lake

persists late into the summer season. For example, the lake was covered by ice in 1999, 2009, 2017 and 2023, and was ice free in 2005, 2011 and in 2024. This variability it ice off timing is more likely attributed to the image capture timing over the local climate conditions.

Thermokarst Landforms

A total of 139 retrogressive thaw slumps were identified using the LARCH method (**Fig. 2.7**). This is likely an underestimation as only those greater than about three pixels (90 x 90 m) would be visible. Of the 139 slumps, 60 were active in July 2024 based on visual identification of dark sediments near headwalls, absence of vegetation and salt efflorescence near headwall. All slumps, except one, are all found below marine limit and on low slopes (8.0 ± 7.3°). Over the time-series, landscape change classes in the slump scar and debris tongue for some slumps ranged from active thermokarst phase with wetting of the sediments to an inactive phase with drying and desertification, and finally vegetation succession in the scar zone.

Individual ice wedge melt outs and active layer detachments were too small to be detected in this analysis. However, large continuous areas of the FP are covered by ice wedge polygons (IWP). To understand how large patches of ice wedge networks have responded over the study period, over 225 km^2 of IWP (or 10% of the area occupied by IWP), were manually delineated using high resolution imagery. The selected polygons spanned a range of elevations, spatial configurations, and degradation states. In the IWP located below Holocene marine limit exhibits a greater increase in greenness (TCG) and wetness (TCW). Those located above marine limit show a stronger increase in surface brightness. Thermokarst ponds are widespread throughout the study area appearing in ice wedge troughs.

Snow and ice

In the LARCH composite, complete loss of late lying snowpacks appears as bright green and whereas persistent snowbanks appear as bright pink. Observed changes are evident on Blacktop Mountain, Troelsen Ridge, and Hare Cape Ridge. In the Sawtooth Mountains, residual snow and ice show substantial reduction, particularly along the snowpack and glacier margins. On glacier surfaces, green areas occur at higher elevations and correspond to full loss of seasonal snow cover. Their spectral signatures show decreased surface brightness and decreased surface wetness, consistent with the transition from bright snow to exposed ice (~2200 ha). Pink area occur at lower elevations near glacier margins; spectral signature of these areas shows an increased surface moisture and decreased surface brightness, consistent with melting snow and ice (~2000 ha).

2.5 Discussion

2.5.1 Response of the Fosheim Peninsula to Warmer-Wetter Climate

The Fosheim Peninsula shows clear, spatially patterned shifts in greenness, brightness and wetness, with the majority of changes occurring as positive trends - 79.3% of the landscape exhibiting significant greening, 42.3% brightening and 31.2% wetting. These widespread positive trends indicate that vegetation production and surface moisture availability have increased across most terrain types. Barren regions of the Fosheim are experiencing widespread vegetation colonization expressed through significant trends in greening, wetting and surface darkening, consistent with the 26% of positive greening trends occurring within barren land. This pattern aligns with Bjorkman et al. (2018), who documented widespread increases in plant height across the tundra – including cold, low-moisture sites in the Canadian Arctic Archipelago –indicating that vegetation is responding strongly to a warming climate even in sparsely vegetated and moisture-limited terrain. Moreover, areas classified as polar grassland-lichen-moss show a slight drying trend, consistent with the 20.6% of positive TCB trends occurring within this class. This drying likely reflects improved drainage on upland terrain above marine limit, where coarse glaciofluvial and till deposits retain less moisture. Together, these patterns indicate a clear elevation-dependant response: lowland marine sediments are greening and wetting, while upland till and glaciofluvial terrain show weaker greening, but strong brightening associated with drying and early successional vegetation.

These elevation-structured trends are broadly consistent with observations from other regions of the High Arctic, where greening is the dominant long-term signal, but its magnitude varies with moisture availability and substrate. In Zackenburg (Greenland), Cape Bounty (Nu.), and Banks Island (NWT), increases in NDVI (Normalized Difference Vegetation Index) have been strongest in mesic or moisture-supported terrain, while drier desert and coarse substrates show more modest gains (Hobbie et al., 2017; Edwards & Treitz, 2017; Campbell et al., 2021). The Fosheim's spectral response fits within this regional context but highlights how surficial geology and ground ice conditions control landscape responses to warming.

The results from this study indicate that the region has undergone major hydrological reorganization. Slidre River shows substantial shifts in channel position, particularly at the outlet, expressed as red (drying) and blue (wetting) in the Landsat trend analysis. Further, the river shows evidence of fluvial geomorphological change associated with cutbank and point bar

development, an indicator of lateral erosion linked to permafrost thaw. These changes are suspected to be quite large to be identified with this analysis (30 m pixels). Smaller tributaries near the Eureka Weather Station (Station Creek, Blacktop Creek and Gemini Creek) show localized wetting or drying trends, several of which correspond to recent anthropogenic disturbances such as gravel extraction and water reservoir development.

LARCH confirm nine drained or partially drained lakes, each showing the red perimeter signature. Upon closer inspection, three of the drained lakes show clear evidence of ice-wedge controlled drainage, with polygonal terrain visible adjacent and within the former lake beds and drainage timing corroborated by Google Timelapse. Lake drainage timing aligns with regional climate anomalies, particularly the exceptionally warm summers of 2011, 2015 and 2020. Post drainage response varies among the lakes; responses include wetland formation, surface drying, waterlogged vegetation collapse and early vegetation succession, indicating diverse ecological trajectories following hydrological loss.

Eastwind Lake (North of Eureka Weather Station) currently shows a slight increase in area and small increases in polygon-related vegetation density. The lake, which is surrounded by polygonal terrain and situated in a flat basin, currently drains into a channel on the north end of the lake. On the southern end of the lake, ice wedge polygonal terrain is present and well developed. We suggest this area be closely monitored. If the ice wedge polygonal terrain on the southern edge of the lake degrades, the lake has a high chance of draining into Blacktop Creek watershed, potentially disrupting flow, streambank morphology, and downstream infrastructure (road and bridge).

Slump activity in the Eureka Sound Lowlands has been monitored since 1991 with the number of observed slumps increasing by 10% annually since 2005 (Pollard et al., 2015). Between 2011 and 2018, Ward Jones et al. (2019) observed an average headwall retreat rate of 6.2 m yr^{-1} with individual slump annual ranges up to 26 m yr^{-1} and maximum retreat for a few specific slumps observed as high as 79 m yr^{-1} over a seven year-period (Ward Jones et al., 2019). This high slump activity reflects the combined effects of melting massive intrasedimental ice and ice wedge ice (Grom, 2008). A total of 139 retrogressive thaw slumps were identified in the Fosheim Peninsula with 60 active in 2024. This is an underestimation, as the pixel size of the imagery limited identification to only large, well-established slumps.

The slump scars and debris tongue exhibit a range of change classes from active thaw to drying, desertification and vegetation recolonization – capturing the typical thermokarst disturbance trajectory. The Random Forest classification was successful in identifying these subtle transitions in classes for most thaw slumps, consistent with findings by Frappier et al.

(2023), who also noted a shift in identified change classes within individual slump features. In this study, regenerating thaw slumps were difficult to distinguish from the surrounding terrain because vegetation the area is sparse and low laying. This contrasts with Sub-Arctic Landsat trend analyses, where slump scars are more readily identifiable against denser tundra vegetation.

Ice wedge polygonal terrain (IWP) shows similar elevation-structured response. The manually delineated subset indicates that IWP below marine limit is experiencing stronger greening, consistent with enhanced vegetation productivity in the ice wedge troughs and aligning well with the local IWP conditions of Becker et al. (2017). Upland polygons show greater brightening, attributed to improved drainage from trough subsidence, increased surface exposure and vegetation succession. These findings are consistent with Ward Jones et al. (2020) who documented widespread ice-wedge degradation on the Fosheim peninsula is concentrated in polygon troughs, where thaw-driven subsidence and hydrological reorganization are most active.

Overall, the Fosheim Peninsula (FP) is experiencing a widespread greening; with positive trends linked to changes within the barren, polar grassland-lichen-moss (PGLM) and polar barren-lichen-moss (PBLM) land classes. Of the entire area, 13.9% of the FP, classified as PGLM, is showing a combined increasing trend in both greenness and brightness and a stable trend in wetness, indicating vegetation succession over dark surfaces of the region but not linked to moisture redistribution. Most of this change is located above marine limit and inland of the FP, likely linked to warmer air temperatures at higher elevations. Similarly, 13.4% of the FP is classified as barren landscapes and exhibiting positive trend in greening and wetness with a stable trend in surface brightness. Majority of this change is located below marine limit and is likely attributed to increase in active layer moisture linked to thawing of surficial ground ice. Most identified ground ice in the area exists below marine limit (Pollard, 2000) with deposits ranging from segregated ice to massive ice and ice wedge polygonal terrain. Previous work in the area has identified an increase in trough greening linked to thawing ice wedges (Becker et al., 2016).

2.5.2 The Fosheim Peninsula as a Predictor of Changes in the High Arctic

Many of the conceptual models currently used to understand Arctic landscape response to climate change have been developed from studies conducted in the Low Arctic, particularly in regions underlain by ice-rich glaciogenic sediments (Kokelj et al., 2013; 2015; Malone et al., 2013; Littlefair et al., 2017). These studies have exhibited strong causal links between permafrost degradation, thermokarst development, altered hydrology, and ecological change. However, the extent to which these observations can be applied across different geological settings remains uncertain. In practise, the impacts observed in glaciogenic terrain are often assumed to be

representative of permafrost landscapes more broadly, despite limited evidence in other ice-rich sedimentary environments. Therefore, the Fosheim Peninsula provides an opportunity to evaluate this assumption because much of the thermokarst activity occurs within ice-rich Holocene marine sediments (Bell, 1996; Bell & Hodgson, 2000; Pollard et al., 2015; Campbell-Heaton et al., 2021; Roy et al., 2023). Extensive networks of ice wedges, abundant intrasedimental ground ice, and widespread marine deposits create conditions that differ substantially from many of the better-studied Low Arctic settings. A guiding question for this research has been whether permafrost degradation in these marine environments produces similar landscape responses to those previously documented in glaciogenic terrains, or whether the distinct geological history of the region results in a fundamentally different trajectory of change.

The results of this study suggest that many first-order responses are similar to observations in the Low Arctic. In this paper we identified widespread thaw slump activity, lake drainage, changes in surface moisture, fluvial reorganization, and vegetation change across the Fosheim Peninsula. These responses are consistent with landscape transformations reported elsewhere in permafrost regions experiencing rapid warming (Kokelj et al., 2013; Malone et al., 2013; Lewkowicz & Way, 2019). The overall pattern indicates that ice-rich marine sediments are highly sensitive to climatic forcing and capable of undergoing substantial geomorphic and ecological reorganization. Implications of these findings extend beyond the Fosheim Peninsula. Extensive portions of the Canadian Arctic are underlain by ice-rich marine sediments deposited during post-glacial marine inundation (Dyke et al., 2005; O'Neill et al., 2019). The patterns observed on the Fosheim Peninsula suggest that these landscapes may respond to continued warming through similar combinations of thermokarst development, hydrological change, and vegetation restructuring. Consequently, the findings from this study may be more broadly transferrable to ice-rich marine terrain than previously recognized. This area may also provide insight into the future evolution of other regions of the Canadian Arctic Archipelago. Although Eureka currently experiences a relatively warm climate for the High Arctic, many nearby regions are experiencing similar climate trajectories (Smith et al., 2012; 2015; 2022). The widespread greening and brightening observed across the peninsula indicate that significant environmental change is occurring even in areas above marine limit where ground ice is less abundant and thermokarst activity is limited. These changes have important implications for the surface energy balance, active layer development, water redistribution, and ground thermal regimes because both vegetation expansion and changing surface reflectance can modify the transfer of energy into the ground (Chapin et al., 2005; Blok et al., 2010; Loranty et al., 2012). Together, the results indicate that major landscape reorganization is not confined to the Low Arctic or to glaciogenic terrain.

Instead, ice-rich marine environments can exhibit comparable responses, including thermokarst development, hydrological reorganization, and ecological transformation. As climate warming continues across the Arctic, the Fosheim Peninsula may therefore provide an early indication of the types of changes likely to emerge across other ice-rich regions of the Canadian Arctic Archipelago.

2.6 Conclusions

This study sought to determine the extent of landscape changes that occurred on the Fosheim Peninsula for 1999-2024 using the Landsat archive. Findings indicate the following:

- 6.4% of the peninsula experienced significant monotonic changes in all three TC indices; individually, 79.4% in greenness, 44.5% in brightness and 36.2% in wetness, as shown by Mann-Kendell and Theil-Sen estimators.
- Compared against the Canadian Land Classification, 26% of the positive TCG trend occur within the barren land class, 22.8% and 21.4% within the polar barren-lichen-moss (PBLM) and polar grassland-lichen-moss classes (PGLM).
- Landsat trend analysis identified substantial fluvial reorganization of the Slidre river because of fluvial erosion and braided stream activity. Station, Blacktop and Gemini-2 creek basins show landscape change associated with anthropogenic activities (aggregate extraction, airstrip maintenance and water storage pond development).
- Nine (9) drained or near drained lakes were identified during the study period with drainage linked to warm summer conditions and ice wedge degradation.
- Eastwind Lake shows signs of possible drainage redirection on the south end of the lake with possible drainage into Blacktop Creek watershed.
- A total of 139 retrogressive thaw slumps were identified for the entire period; this value is an underestimated of true number as imagery resolution limited identification. Of that, high-resolution imagery confirmed 60 active retrogressive thaw slumps in 2024.

2.7 Acknowledgements

This project was funded by grants from the Natural Science and Engineering Research Council (NSERC; DL), the Northern Scientific Training Program (NSTP; KCH), the Royal Canadian Geographical Society (RCGS; KCH) and the Association of Canadian Universities for Northern Studies (ACUNS; KCH). Incredible field logistical support was provided by the Polar Continental Shelf Program (Natural resources Canada) and in-field resource support from the staff at the Eureka Weather Station. Fieldwork could not have been completed without the help of

B. Lauriol, J. Prest, and the Eureka Weather Station staff. Thank you to Dr. Konrad Gajewski and Dr. Robert Fraser for constructive comments on earlier versions of this manuscript. PlanetScope Imagery was provided through the Planet Education and Research program via a University of Ottawa academic license.

2.8 References

Becker, M. S., Davies, T. J., & Pollard, W. H. (2016). Ground ice melt in the high Arctic leads to greater ecological heterogeneity. Journal of Ecology, 104(1), 114–124. https://doi.org/10.1111/1365-2745.12491

Bell, T. (1996). The last glaciation and sea level history of. Fosheim Peninsula, Ellesmere Island, Canadian High Arctic. Canadian Journal of Earth Sciences, 33, 1075–1086.

Bell, T., & Hodgson, D. A. (2000). Quaternary geology and glacial history of Fosheim Peninsula, Ellesmere Island, Nunavut. In Garneau, M. & Alt, B. T. (eds.), Environmental response to climate change in the Canadian High Arctic, Geological Survey of Canada, Bulletin, 529, 175-196. Natural Resources Canada. https://doi.org/10.4095/211957

Bernard-Grand'Maison, C., & Pollard, W. (2018). An Estimate of Ice Wedge Volume for a High Arctic Polar Desert Environment, Fosheim Peninsula, Ellesmere Island. The Cryosphere Discussions, 12, 1–28. https://doi.org/10.5194/tc-2018-29

Berner, L.T., Massey, R., Jantz, P., Forbes, B.C., Macias-Fauria, M., Myers-Smith, I., Kumpula, T., Gauthier, G., Andreu-Hayles, L., Gaglioti, B.V. and Burns, P. (2020). Summer warming explains widespread but not uniform greening in the Arctic tundra biome. *Nature communications*, *11*(1), pp.1-12.

Bi, J., Xu, L., Samanta, A., Zhu, Z. and Myneni, R., 2013. Divergent arctic-boreal vegetation changes between North America and Eurasia over the past 30 years. *Remote Sensing*, *5*(5), pp.2093-2112.

Bjorkman, A. D., Myers-Smith, I. H., Elmendorf, S. C., Normand, S., Rüger, N., Beck, P. S., ... & Weiher, E. (2018). Plant functional trait change across a warming tundra biome. *Nature*, *562*(7725), 57-62.

Blok, D., Heijmans, M. M., Schaepman-Strub, G., Kononov, A. V., Maximov, T. C., & Berendse, F. (2010). Shrub expansion may reduce summer permafrost thaw in Siberian tundra. Global Change Biology, 16(4), 1296-1305.

Box, J. E., Colgan, W. T., Christensen, T. R., Schmidt, N. M., Lund, M., Parmentier, F. J. W., ... & Olsen, M. S. (2019). Key indicators of Arctic climate change: 1971–2017. *Environmental Research Letters*, *14*(4), 045010.

Brooker, A., Fraser, R. H., Olthof, I., Kokelj, S. V., & Lacelle, D. (2014). Mapping the activity and evolution of retrogressive thaw slumps by tasselled cap trend analysis of a Landsat satellite image stack. *Permafrost and Periglacial Processes*, *25*(4), 243-256.

Campbell, T. K. F., Lantz, T. C., Fraser, R. H., & Hogan, D. (2021). High Arctic vegetation change mediated by hydrological conditions. Ecosystems, 24, 106-121.

Campbell-Heaton, K., Lacelle, D., Fisher, D., & Pollard, W. (2021). Holocene ice wedge formation in the Eureka Sound Lowlands, high Arctic Canada. Quaternary Research, 1–13. https://doi.org/10.1017/qua.2020.126

Cast, Z. I., Serreze, M., Cassano, E., & Barrett, A. (2025). Seasonal Characteristics and Trends in Precipitation Partitioning in the Arctic. *EGUsphere*, *2025*, 1-24.

Chander, G., Markham, B. L., & Helder, D. L. (2009). Summary of current radiometric calibration coefficients for Landsat MSS, TM, ETM+, and EO-1 ALI sensors. *Remote sensing of environment*, *113*(5), 893-903.

Chapin, F. S., Sturm, M., Serreze, M. C., McFadden, J. P., Key, J. R., Lloyd, A. H., ... & Welker, J. M. (2005). Role of land-surface changes in Arctic summer warming. science, 310(5748), 657-660.

Copland, L., Lacelle, D., Fisher, D., Delaney, F., Thomson, L., Main, B., & Burgess, D. (2020). Warmer–wetter climate drives shift in δ D–δ18O composition of precipitation across the Queen Elizabeth Islands, Arctic Canada. Arctic Science, 7(1), 136-157.

Couture, N. J., & Pollard, W. H. (1998). An assessment of ground ice volume near eureka, northwest territories. In Permafrost - Seventh International Conference, 55, 195–200.

Crist, E. P., & Cicone, R. C. (1984). A physically-based transformation of Thematic Mapper data--The TM Tasseled Cap. *IEEE Transactions on Geoscience and Remote sensing*, (3), 256-263.

Dou, T. F., Pan, S. F., Bintanja, R., & Xiao, C. D. (2022). More frequent, intense, and extensive rainfall events in a strongly warming Arctic. Earth's Future, 10(10), e2021EF002378.

Dyke, A. S., Dredge, L. A., & Hodgson, D. A. (2005). North American deglacial marine-and lake-limit surfaces. Géographie physique et Quaternaire, 59(2), 155-185.

Edlund, S. A., & Alt, B. T. (1989). Regional congruence of vegetation and summer climate patterns in the Queen Elizabeth Islands, Northwest Territories, Canada. Arctic, 42(1), 3–23. https://doi.org/10.14430/arctic1635

Edlund, S. A., Alt, B. T., & Garneau, M. (2000). Vegetation patterns on Fosheim Peninsula, Ellesmere Island, Nunavut. In Bulletin of the Geological Survey of Canada (Issue 529).

Edwards, R., & Treitz, P. (2017). Vegetation greening trends at two sites in the Canadian Arctic: 1984–2015. *Arctic, Antarctic, and Alpine Research*, *49*(4), 601-619.

England, J., Atkinson, N., Bednarski, J., Dyke, A. S., Hodgson, D. A., & Ó Cofaigh, C. (2006). The Innuitian Ice Sheet: configuration, dynamics and chronology. Quaternary Science Reviews, 25(7–8), 689–703. https://doi.org/10.1016/j.quascirev.2005.08.007

Frappier, R., Lacelle, D., & Fraser, R. H. (2023). Landscape changes in the Tombstone Territorial Park region (central Yukon, Canada) from multilevel remote sensing analysis. Arctic Science, 9(4), 838-855.

Fraser, R., Olthof, I., Carrière, M., Deschamps, A., & Pouliot, D. (2012). A method for trend-based change analysis in Arctic tundra using the 25-year Landsat archive. *Polar record*, *48*(1), 83-93.

Fraser, R., Olthof, I., Kokelj, S., Lantz, T., Lacelle, D., Brooker, A., ... & Schwarz, S. (2014). Detecting landscape changes in high latitude environments using landsat trend analysis: 1. Visualization. *Remote Sensing*, *6*(11), 11533-11557.

Gorelick, N., Hancher, M., Dixon, M., Ilyushchenko, S., Thau, D., & Moore, R. (2017). Google Earth Engine: Planetary-scale geospatial analysis for everyone. *Remote sensing of Environment*, *202*, 18-27.

Government of Canada, Natural Resources Canada. (2019a). CanVec Series [Geospatial data]. Canada Centre for Mapping and Earth Observation. https://open.canada.ca/data/en/dataset/7f245e4d-76c2-4caa-951a-45d1d2051333

Government of Canada, Natural Resources Canada. (2022). National Hydro Network (NHN) – GeoBase Series [Data set]. Government of Canada, Open Government Portal. https://open.canada.ca/data/en/dataset/a4b190fe-e090-4e6d-881e-b87956c07977

Government of Canada; Environment and Climate Change Canada. (2026). Historical climate data [Website]. https://climate.weather.gc.ca/historical_data/search_historic_data_e.html

Government of Canada; Natural Resources Canada; Canada Centre for Remote Sensing. (2019). *2015 Land Cover of Canada.* Government of Canada; Natural Resources Canada; Canada Centre for Remote Sensing.

Grom, J. (2008). Retrogressive thaw slump process and morphology, Eureka Sound Lowlands, Ellesmere Island, Nunavut, Canada (Master's thesis, McGill University).

Hamel Jomphe, E., Bayle, A., Lévesque, E., Johnson, C. A., Langlois, A., & Roy, A. (2026). Complementary insights into high Arctic greening from absolute and relative NDVI trends across the Canadian Arctic Archipelago. *Canadian Journal of Remote Sensing*, *52*(1), 2672167.

Hobbie, J. E., Shaver, G. R., Rastetter, E. B., Cherry, J. E., Goetz, S. J., Guay, K. C., ... & Kling, G. W. (2017). Ecosystem responses to climate change at a Low Arctic and a High Arctic long-term research site. *Ambio*, *46*(Suppl 1), 160-173.

Hodgson, D. A., & Nixon, F. M. (1998). Ground ice volumes determined from shallow cores from western Fosheim Peninsula Ellesmere Island, Northwest Territories. In Bulletin of the Geological Survey of Canada (Issue 507). Government of Canada.

Huang, C., Wylie, B., Yang, L., Homer, C., & Zylstra, G. (2002). Derivation of a tasselled cap transformation based on Landsat 7 at-satellite reflectance. *International journal of remote sensing*, *23*(8), 1741-1748.

Jones, B. M., Grosse, G., Farquharson, L. M., Roy-Léveillée, P., Veremeeva, A., Kanevskiy, M. Z., Gaglioti, B. v., Breen, A. L., Parsekian, A. D., Ulrich, M., & Hinkel, K. M. (2022). Lake and drained lake basin systems in lowland permafrost regions. Nature Reviews Earth & Environment, 3(1), 85–98. https://doi.org/10.1038/s43017-021-00238-9

Kauth, R. J., & Thomas, G. S. (1976). The tasselled cap--a graphic description of the spectral-temporal development of agricultural crops as seen by Landsat. In *LARS symposia* (p. 159).

Kokelj, S. V., Lacelle, D., Lantz, T. C., & Gergel, S. E. (2013). Rapid thawing of subarctic ice-rich permafrost: Impacts on hydrology, geomorphology, and vegetation. *Geophysical Research Letters, 40*(22), 5700–5705. https://doi.org/10.1002/2013GL057642

Kokelj, S., Tunnicliffe, J., Lacelle, D., Lantz, T. C., Chin, K. S., & Fraser, R. (2015). Increased precipitation drives mega slump development and destabilization of ice-rich permafrost terrain, northwestern Canada. *Global and Planetary Change*, *129*, 56–68. https://doi.org/10.1016/j.gloplacha.2015.02.008

Lewkowicz, A. G. (1990). Morphology, frequency and magnitude of active-layer detachment slides, Fosheim Peninsula, Ellesmere Island, NWT. In *Proceedings of the 5th Canadian permafrost conference* (Vol. 54, pp. 111-118). Université Laval: Québec.

Lewkowicz, A. G., & Way, R. G. (2019). Extremes of summer climate trigger thousands of thermokarst landslides in a High Arctic environment. *Nature Communications (Resubmitted December 2018)*, *10*(1), 1329. https://doi.org/10.1038/s41467-019-09314-7

Liaw, A., & Wiener, M. (2002). Classification and regression by randomForest (R package version 4.7-1.2). R News, 2(3), 18–22. https://CRAN.R-project.org/doc/Rnews/

Liljedahl, A. K., Boike, J., Daanen, R. P., Fedorov, A. N., Frost, G. V., Grosse, G., ... & Zona, D. (2016). Pan-Arctic ice-wedge degradation in warming permafrost and its influence on tundra hydrology. *Nature Geoscience*, *9*(4), 312-318.

Littlefair, C. A., Tank, S. E., & Kokelj, S. V. (2017). Retrogressive thaw slumps temper dissolved organic carbon delivery to streams of the Peel Plateau, NWT, Canada. Biogeosciences, 14(23), 5487-5505.

Loranty, M. M., & Goetz, S. J. (2012). Shrub expansion and climate feedbacks in Arctic tundra. Environmental Research Letters, 7(1), 011005.

Malone, L., Lacelle, D., Kokelj, S., & Clark, I. D. (2013). Impacts of hillslope thaw slumps on the geochemistry of permafrost catchments (Stony Creek watershed, NWT, Canada). Chemical Geology, 356, 38-49.

Olthof, I., & Fraser, R. H. (2014). Detecting landscape changes in high latitude environments using Landsat trend analysis: 2. Classification. *Remote Sensing*, *6*(11), 11558-11578.

O'Neill, H. B., Wolfe, S. A., & Duchesne, C. (2019). New ground ice maps for Canada using a paleogeographic modelling approach. The cryosphere, 13(3), 753-773.

Phoenix, G. K., Bjerke, J. W., Björk, R. G., Blok, D., Bryn, A., Callaghan, T. V., ... & Voigt, C. (2025). Browning events in Arctic ecosystems: Diverse causes with common consequences. *PLOS Climate*, *4*(1), e0000570.

Planet Labs PBC. (2024). *PlanetScope imagery* [Satellite imagery]. Planet Labs.

Pollard, W. (2000). Distribution and characterization of ground ice on Fosheim Peninsula, Ellesmere Island, Nunavut. In Garneau, M. & Alt, B. T. (eds.), Environmental response to climate change in the Canadian High Arctic, Geological Survey of Canada, Bulletin, 529, 175-196. Natural Resources Canada.

Pollard, W., Ward, M., & Becker, M. (2015). The Eureka Sound lowlands: an ice-rich permafrost landscape in transition. Proceedings of GeoQuebec.

R Core Team (2025). _R: A Language and Environment for Statistical Computing_. R Foundation for Statistical Computing, Vienna, Austria. <https://www.R-project.org/>.

Rantanen, M., Karpechko, A. Y., Lipponen, A., Nordling, K., Hyvärinen, O., Ruosteenoja, K., ... & Laaksonen, A. (2022). The Arctic has warmed nearly four times faster than the globe since 1979. *Communications earth & environment*, *3*(1), 168.

Roy, C., Campbell-Heaton, K., Lacelle, D., & Pollard, W. (2023). Massive ground ice of glacial meltwater origin in raised marine-deltaic sediments, Fosheim Peninsula, high Arctic Canada. *Quaternary Research*, *116*, 96-107.

Roy, D. P., Kovalskyy, V., Zhang, H. K., Vermote, E. F., Yan, L., Kumar, S. S., & Egorov, A. (2016). Characterization of Landsat-7 to Landsat-8 reflective wavelength and normalized difference vegetation index continuity. *Remote sensing of Environment*, *185*, 57-70.

Smith, S. L., Lewkowicz, A. G., & Duchesne, C. (2015). Variability and Change in Permafrost Thermal State in Northern Canada. *68e Conférence Canadienne de Géotechnique et 7e Conférence Canadienne Sur Le Pergélisol, 20 Au 23 Septembre 2015, Québec, Québec.*, *Figure 1*, 1–6.

Smith, S. L., O'Neill, H. B., Isaksen, K., Noetzli, J., & Romanovsky, V. E. (2022). The changing thermal state of permafrost. *Nature Reviews Earth & Environment*, *3*(1), 10–23. https://doi.org/10.1038/s43017-021-00240-1

Smith, S. L., Throop, J., & Lewkowicz, A. G. (2012). Recent changes in climate and permafrost temperatures at forested and polar desert sites in Northern Canada. *Canadian Journal of Earth Sciences*, *49*(8), 914–924. https://doi.org/10.1139/E2012-019

Walvoord, M. A., & Kurylyk, B. L. (2016). Hydrologic Impacts of Thawing Permafrost-A Review. Vadose Zone Journal, 15(6), vzj2016.01.0010. https://doi.org/10.2136/vzj2016.01.0010

Wang, J.A. & Friedl, M.A. (2019). The role of land cover change in Arctic-Boreal greening and browning trends. Environmental Research Letters, 14(12), p.125007.

Ward Jones, M. K., Pollard, W. H., & Amyot, F. (2020). Impacts of Degrading Ice-Wedges on Ground Temperatures in a High Arctic Polar Desert System. Journal of Geophysical Research: Earth Surface, 125(3). https://doi.org/10.1029/2019JF005173

Ward Jones, M. K., Pollard, W. H., & Jones, B. M. (2019). Rapid initialization of retrogressive thaw slumps in the Canadian high Arctic and their response to climate and terrain factors. Environmental Research Letters, 14(5). https://doi.org/10.1088/1748-9326/ab12fd

Webb, E. E., Liljedahl, A. K., Cordeiro, J. A., Loranty, M. M., Witharana, C., & Lichstein, J. W. (2022). Permafrost thaw drives surface water decline across lake-rich regions of the Arctic. Nature Climate Change, 12(9), 841–846. https://doi.org/10.1038/s41558-022-01455-w

Young, K. L., & Woo, M. K. (2000). Hydrological environment of the Hot Weather Creek basin, Ellesmere Island, Nunavut. Bulletin of the Geological Survey of Canada, 529, 347–360. https://doi.org/10.4095/211973

2.9 Captions

Table 1. Landscape change classes included is the number of training points (No. TP) per class and the mean index value per class.

Table 2. Confusion Matrix for Random Forest Model results for each land change class. Class-specific performance metrics for Random Forest model. Includes model sensitivity, precision, overall accuracy and f1 score also included.

Figure 2.1. Map of study area, (A) shows study site in relation to Canadian Arctic Archipelago and Canada; (B) shows Fosheim Peninsula, labelled, elevation (ArcticDEM 4) with maximum extent of marine inundation (150m asl in black). Data for large water bodies and water courses from Natural Resources Canada (Government of Canada, 2019a; 2022).

Figure 2.2. Annual image collection used for this analysis. Images filtered from July 10 (192) to August 10 (223), number of images per collection indicated at the top of figure.

Figure 2.3. Results of Mann-Kendell analysis; displayed is the significant ($p<0.05$) slope values. (A) illustrates the RGB (R = TC Brightness, G=TC Greenness and B=TC Wetness). (B) TC Greenness, (C) TC Wetness and (D) TC Brightness. Watercourses outlined in grey, marine limit (146m a.s.l.) denoted by black dashed line.

Figure 2.4. Results of Random Forest land change classification. Stable and bedrock classes are omitted.

Figure 2.5. LARCH result, map illustrating the RGB (Brightness slope – red, Greenness slope – green, and Wetness slope – blue) for the Fosheim peninsula (A) and subsequent focus areas (B-D). Extent labels correspond to features highlighted in Figures 6 and 7.

Figure 2.6. Examples of lake dynamics in the region. Visual comparison provided for LARCH RGB image, false-colour Landsat 1999 and 2023 and high-resolution planet imagery from July 30th, 2022 (5 m resolution), random forest land classification also included.

Figure 2.7. Locations of identified thaw slumps with dashed black line indicating approximate marine limit (145 m a.s.l.) overlain the elevation profile for the region (ArcticDEM 4).

Figure 2.8. Examples of active thaw slumps in the region. Visual comparison provided for LARCH RGB image, false-colour Landsat 1999 and 2023 and high-resolution planet imagery from July 30th, 2022 (5 m resolution). Random forest change classes and aerial image from July 2019.

2.10 Tables

Table 2.3. Landscape change classes included is the number of training points (No. TP) per class and the mean index value per class.

		Brightness			Greenness			Wetness		
Landscape Change Class	**No. TP**	**p-value**	**slope**	**tau**	**p-value**	**slope**	**tau**	**p-value**	**slope**	**tau**
1. Vegetation succession – surface brightening	635	0.007	-0.004	-0.518	0.000	0.002	0.727	0.000	0.005	0.666
2. Vegetation colonization – surface darkening	115	0.011	-0.001	-0.029	0.000	0.002	0.717	0.008	0.004	0.608
3. Active thermokarst disturbance – wetting, browning and darkening	97	0.036	-0.008	-0.497	0.003	0.003	0.658	0.005	0.008	0.602
4. Upland greening – greening and drying	407	0.012	0.003	0.479	0.000	0.002	0.711	0.007	0.002	0.558
5. Aridification – browning, brightening and drying	101	0.030	0.001	0.164	0.006	0.002	0.574	0.023	0.002	0.183
6. Waterlogged soils & vegetation decline	99	0.044	0.003	0.427	0.009	0.001	0.532	0.027	0.000	0.290
7. Anthropogenic change – runway development	113	0.059	-0.004	-0.528	0.009	0.001	0.535	0.001	0.008	0.755
8. Insignificant changes	2938	0.497	0.000	0.103	0.016	0.001	0.625	0.146	0.001	0.384
9. Surface Water Decrease	221	0.142	0.003	0.189	0.209	0.000	0.095	0.066	0.000	-0.055
10. Surface Water Increase	200	0.215	-0.007	-0.300	0.010	0.003	0.545	0.044	0.010	0.445
11. Bedrock outcrop	207	0.386	0.001	0.195	0.013	0.001	0.526	0.645	0.000	0.089
12. Melt-Driven Wetting	210	0.107	0.017	0.430	0.391	0.000	-0.043	0.402	0.000	-0.107
13. Earlier melting of ice/snow	200	0.571	0.001	0.065	0.216	0.003	0.317	0.238	-0.005	-0.245
Total:	5543									

Table 2.4. Confusion Matrix for Random Forest Model results for each land change class. Class-specific performance metrics for Random Forest model. Includes model sensitivity, precision, overall accuracy and f1 score also included.

		Reference													
		1	**2**	**3**	**4**	**5**	**6**	**7**	**8**	**9**	**10**	**11**	**12**	**13**	**Precision**
Prediction	**1**	**186**	8	1	0	2	0	0	0	0	0	0	0	0	94.4
	2	1	**18**	1	0	0	0	0	0	0	0	0	0	0	90
	3	0	0	**23**	0	0	0	0	0	0	2	0	0	0	92
	4	0	8	0	**121**	0	0	0	0	0	0	0	0	0	93.8
	5	2	0	2	0	**27**	0	0	0	0	0	0	0	0	87.1
	6	1	0	0	1	0	**23**	0	0	0	0	0	0	0	92
	7	0	0	0	0	0	0	**33**	0	1	0	0	0	0	97.1
	8	0	0	1	0	1	6	0	**875**	2	1	15	2	0	96.9
	9	0	0	0	0	0	0	0	2	**56**	0	0	0	0	96.6
	10	0	0	1	0	0	0	0	2	7	**57**	0	0	0	85.1
	11	0	0	0	0	0	0	0	2	0	0	**47**	0	0	95.9
	12	0	0	0	0	0	0	0	0	0	0	0	**57**	5	91.9
	13	0	0	0	0	0	0	0	0	0	0	0	4	**55**	93.2
	Sensitivity	97.9	52.9	79.3	99.2	90	79.3	100	99.3	84.8	95	75.8	90.5	91.7	
														Overall accuracy: 95.1%	
														Overall f-score: 0.9	

2.11 Figures

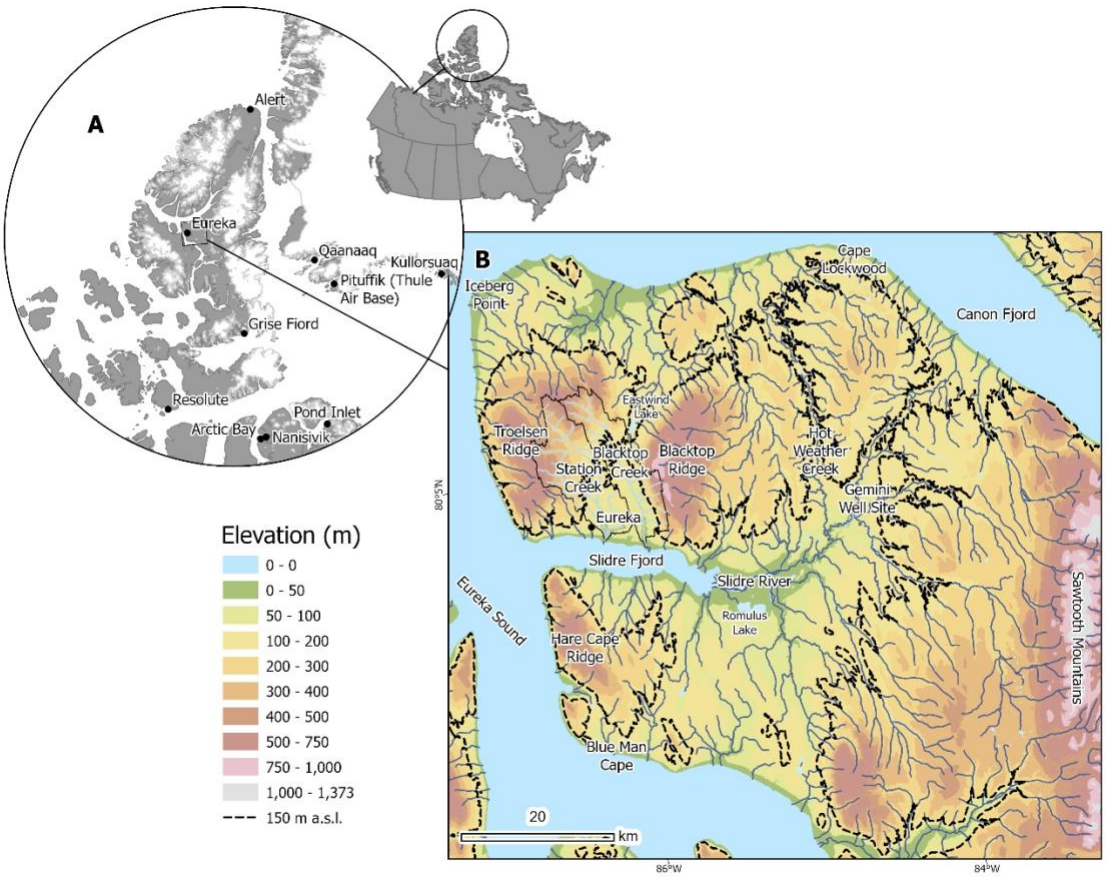


Figure 2.1. Map of study area, (A) shows study site in relation to Canadian Arctic Archipelago and Canada; (B) shows Fosheim Peninsula, labelled, elevation (ArcticDEM 4) with maximum extent of marine inundation (150m asl in black). Data for large water bodies and water courses from Natural Resources Canada (Government of Canada, 2019a; 2022).

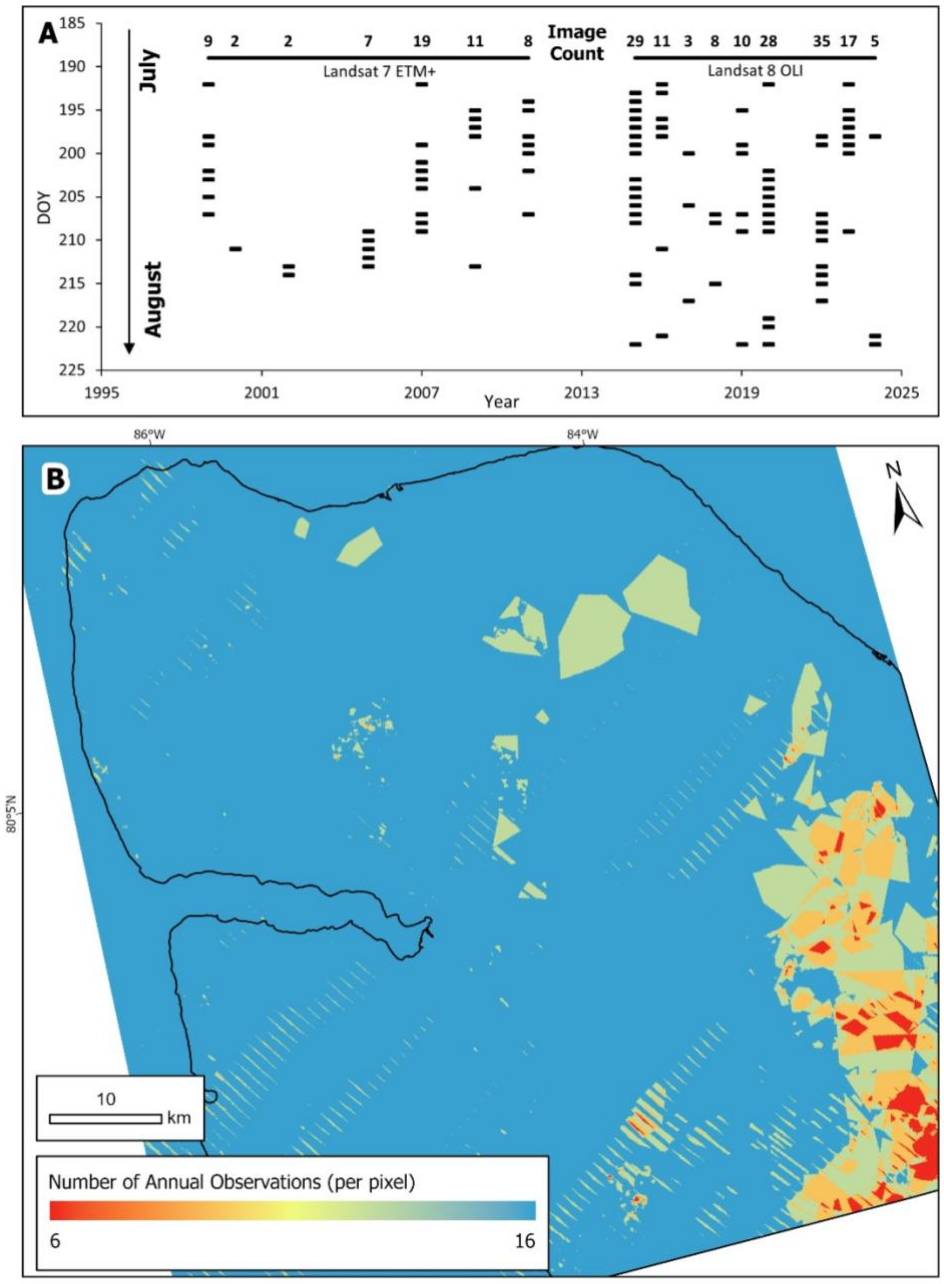


Figure 2.2. Annual image collection used for this analysis. Images filtered from July 10 (192) to August 10 (223), number of images per collection indicated at the top of figure.

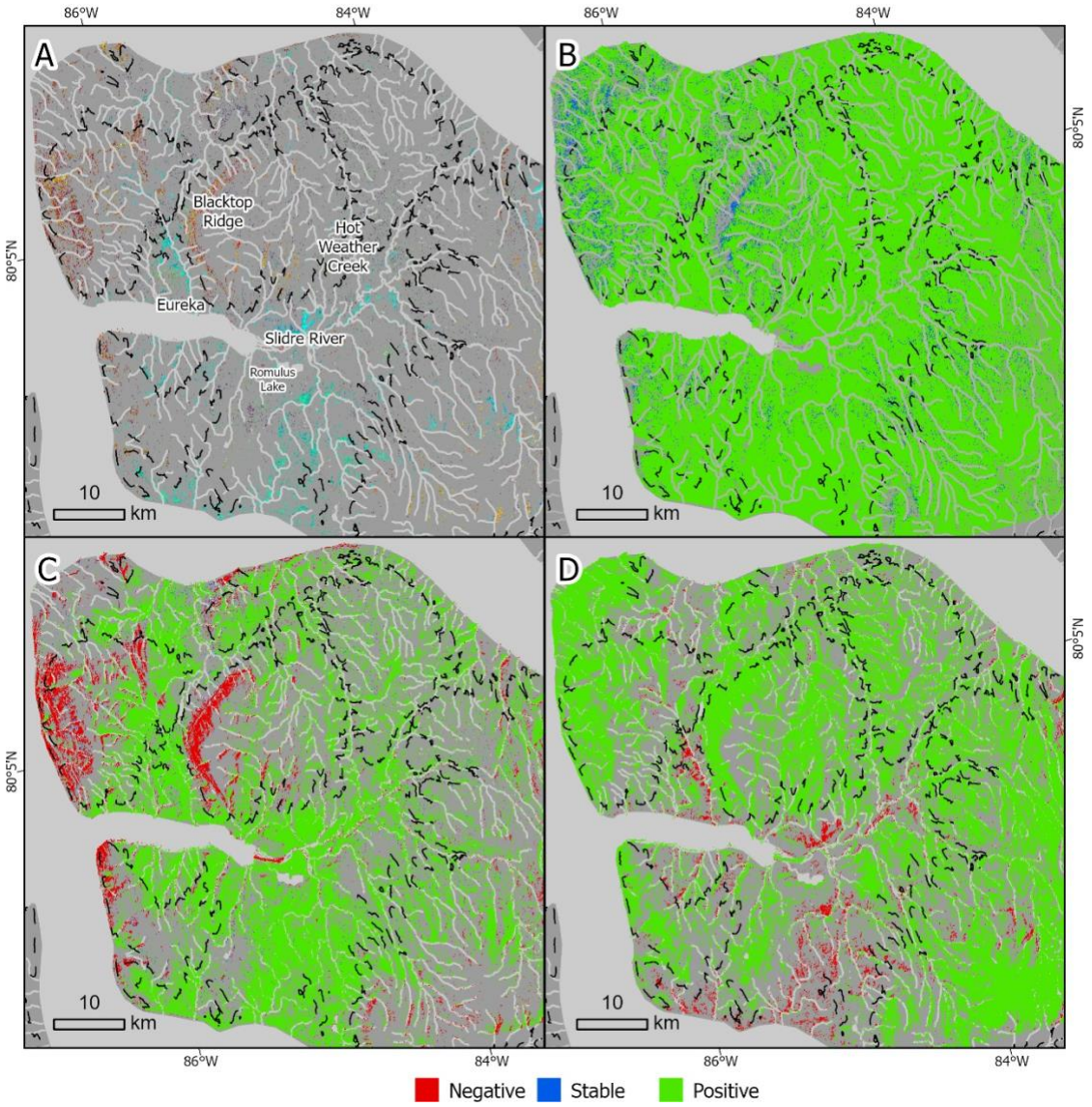


Figure 2.3. Results of Mann-Kendell analysis; displayed is the significant ($p<0.05$) slope values. (A) illustrates the RGB (R = TC Brightness, G=TC Greenness and B=TC Wetness). (B) TC Greenness, (C) TC Wetness and (D) TC Brightness. Watercourses outlined in grey, marine limit (146m a.s.l.) denoted by black dashed line.

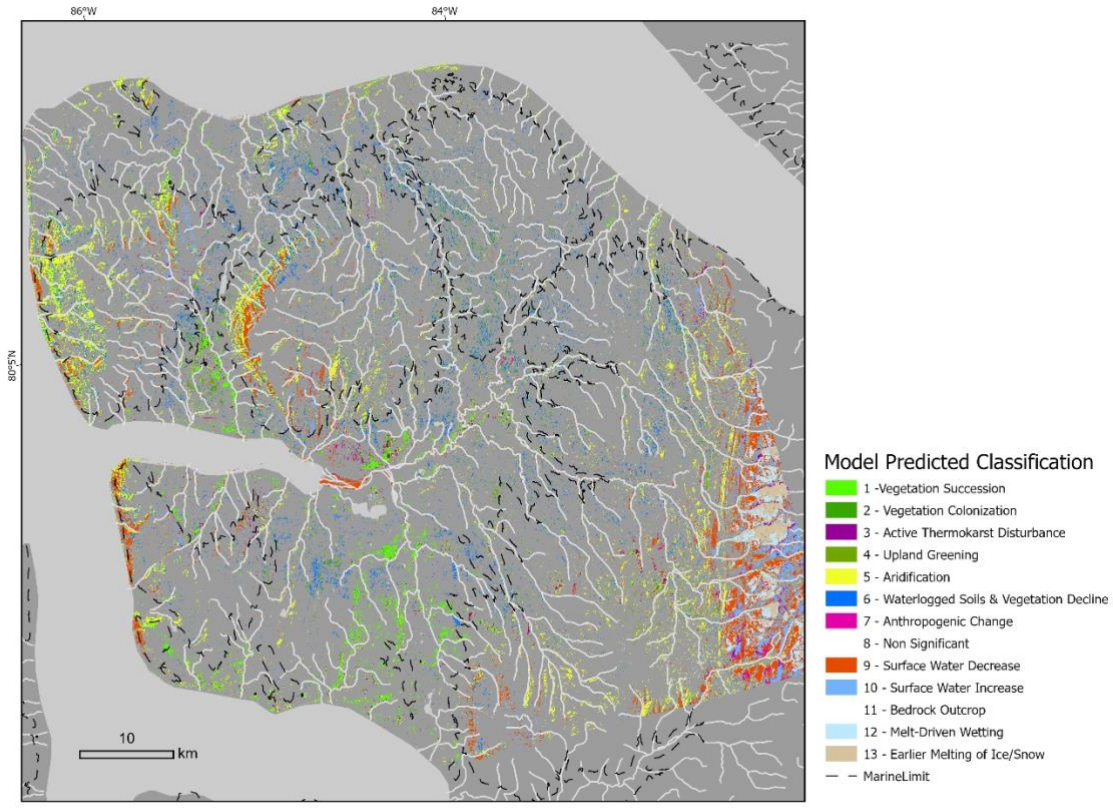


Figure 2.4. Results of Random Forest land change classification, marine limit denoted by dashed line. Stable and bedrock classes are omitted.

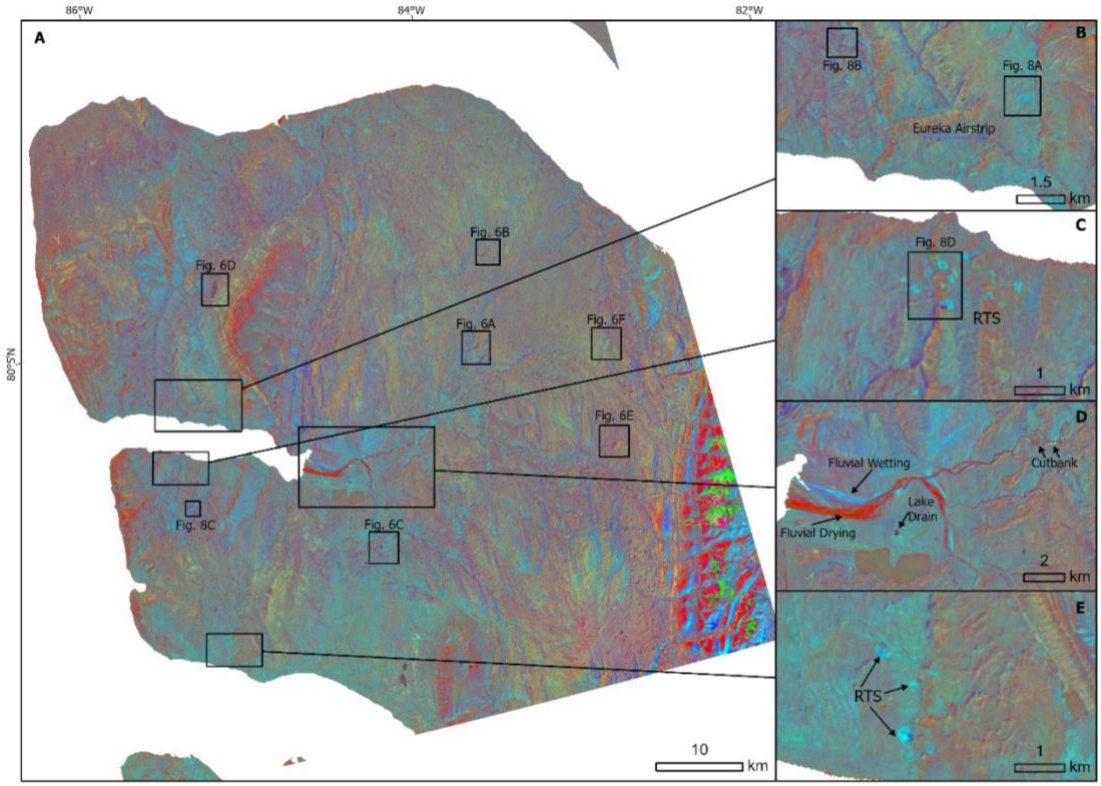


Figure 2.5. LARCH result, map illustrating the RGB (Brightness slope – red, Greenness slope – green, and Wetness slope – blue) for the Fosheim peninsula (A) and subsequent focus areas (B-D). Extent labels correspond to features highlighted in Figures 6 and 8.

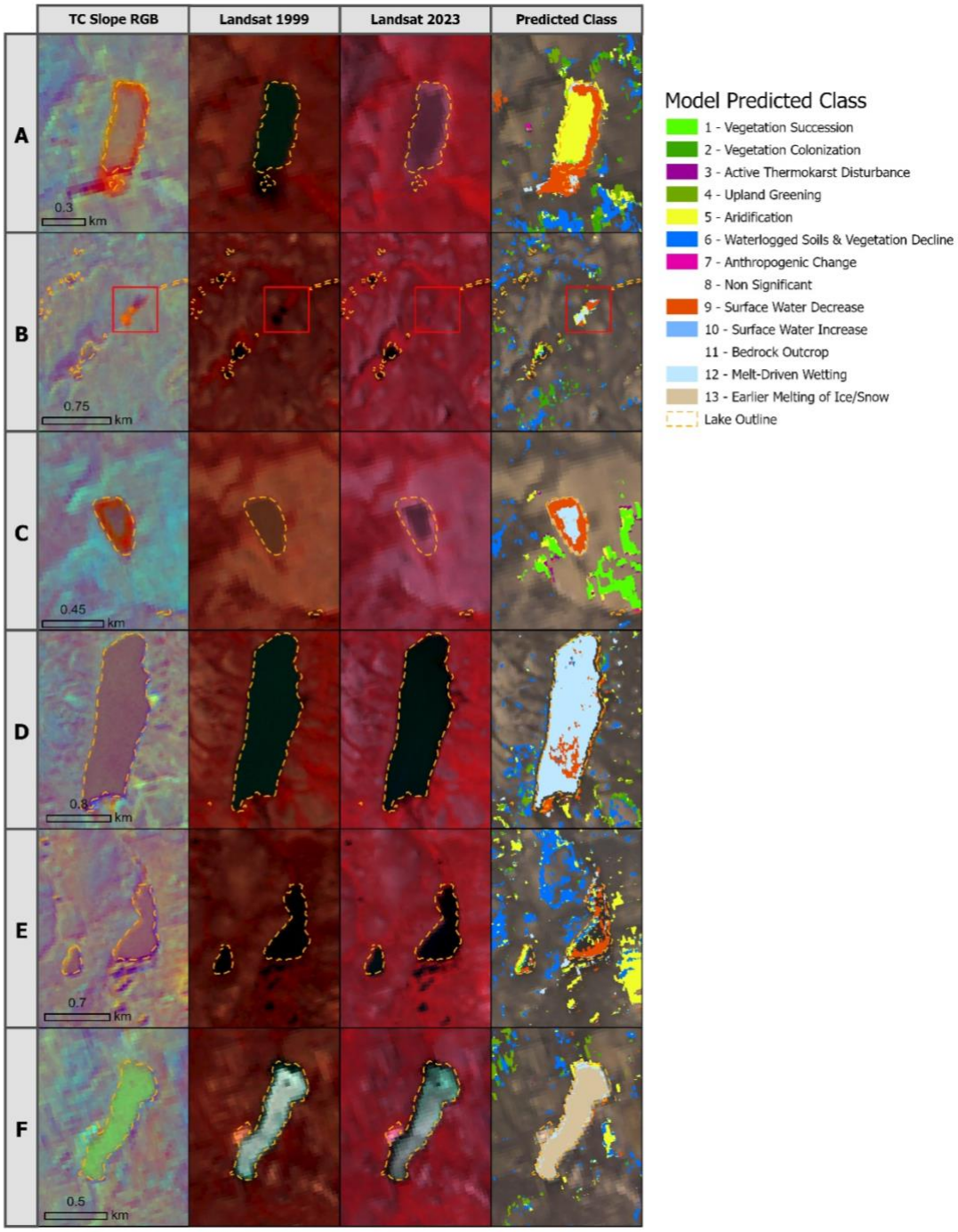


Figure 2.6. Examples of lake dynamics in the region. Visual comparison provided for LARCH composite results, false-colour Landsat 1999 and 2023 mosaic and model predicted landscape change classification. Lake dataset provided by Government of Canada (2022).

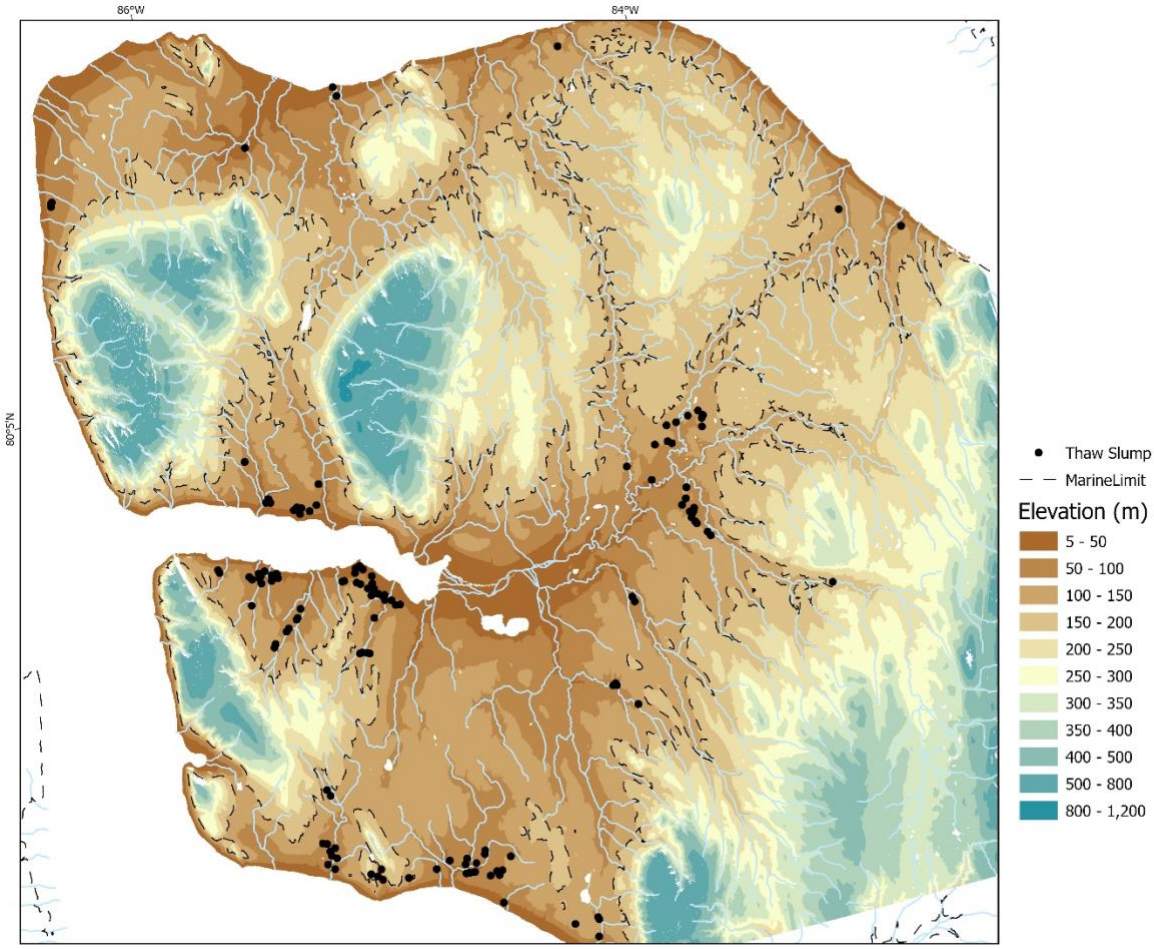


Figure 2.7. Locations of identified thaw slumps with dashed black line indicating approximate marine limit (145 m a.s.l.) overlain the elevation profile for the region (ArcticDEM 4).

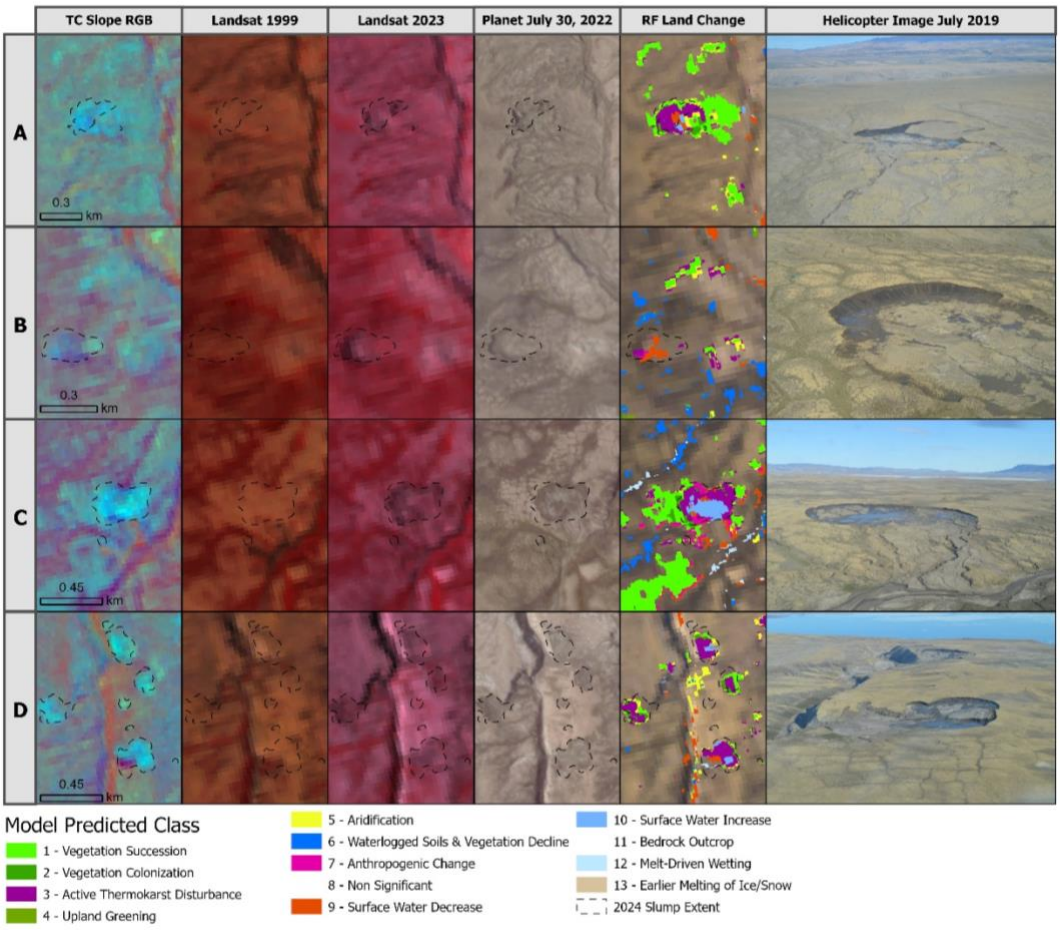


Figure 2.8. Examples of active thaw slumps in the region. Visual comparison provided for LARCH RGB image, false-colour Landsat 1999 and 2023 and high-resolution planet imagery from July 30th, 2022 (5 m resolution). Random forest change classes and aerial image from July 2019.

Chapter 3

Hydrochemistry of two High Arctic permafrost catchments with thaw slumps in raised marine-deltaic sediments, Eureka Sound Lowlands, Canada.

Kethra Campbell-Heaton[1], Denis Lacelle[1]

[1]Department of Geography, Environment and Geomatics, University of Ottawa, Ottawa, ON, Canada

Abstract

Retrogressive thaw slumps are one of the prevalent thermokarst features in Eureka, Nunavut (79.98°N, 85.95°W) and activity has increased over the last decade. Moisture from active thaw slumps either evaporates in-situ or flows along the surface as rillwash and outlet into a nearby creek. In July 2022 and 2023, we collected daily stream water samples above and below the input of active thaw slump rillwash (7 sites) to measure the direct, geochemical effects of thaw slump activity on two nival streams. The results showed no difference between sampled sites in the δD-$\delta^{18}O$ data. DOC concentrations from the studied streams are consistently low, below 2 ppm; active thaw slump rillwash samples are between 5.2 – 8.0 ppm. Concentrations of DOC between sites show a statistically significant difference for both creeks in all years. The molar ratio between sulphates and chloride (SO_4:Cl^-) in stream samples revealed a significant difference between the above and below slump stream sites. This research shows that retrogressive thaw slump activity in Eureka does impact stream chemistry and alters the streams' nutrient load.

Keywords. Permafrost thaw, geochemistry, water isotopes, Arctic hydrology, nival streams, dissolved organic carbon

3.1 Introduction

In the last decade, the increasing retrogressive thaw slump (RTS) activity in the Canadian Arctic has become a major concern (Lewkowicz & Way, 2019; Ward Jones et al., 2019). Known trigger mechanisms for thaw slumps includes: 1) undercutting of a steep bank by lateral stream erosion (Balser et al., 2014; Lewkowicz & Way, 2019); 2) thermally-driven lakeshore subsidence (Burn & Kokelj, 2009); 3) wave action (Lantuit & Pollard, 2008); and 4) extreme thaw or precipitation events (Lacelle et al., 2010). The key to these mechanisms is the disruption of the ground thermal regime and with that, the deepening of the permafrost table and subsequent exposure of ground ice. Thawing ground ice raises the moisture content of the soil and, on slopes inclined at 8-12° surfaces increases the chances of slope failure, slope runoff and downslope sediment transfer (Woo, 1990; Lacelle et al., 2015). RTS recession can last multiple decades and can re-activate if the remaining ground ice is disturbed (Mackay, 1966; Wolfe et al., 2001; Lantuit & Pollard, 2008). Active RTSs pose a significant risk to regional hydrology, infrastructure, atmospheric carbon concentrations and methylmercury (Dixon, 2013; Doré et al., 2016; Frey & McClelland, 2009; Kokelj et al., 2015; Ward Jones & Pollard, 2021).

The majority of the research on RTS activity and Arctic hydrology has been situated in the Western Canadian Arctic and Alaska. RTS in the Peel Plateau (NWT) significantly impact stream geochemistry by increasing the solute load well above the normal load in pristine streams (Malone et al., 2013). The molecular ratio between sulphate (SO_4) and chloride (Cl^-) is an effective tracer to identify RTS activity in freshwater streams where SO_4 concentrations are several magnitudes greater than pristine streams (Kokeji et al, 2005; 2013). Thaw-effected streams also exhibited diurnal fluctuations in water level, solute load, and sediment flux, attributed entirely to ground ice thaw (Kokeji et al., 2013). Lacelle et al (2019) showed that sediment in the thaw slump scar zone has a higher concentration of solutes than the undisturbed permafrost due to evaporation. Moreover, in North Slope Alaska, Bowden et al (2008) identified higher concentrations of ammonium, nitrate and phosphate downstream of active thermokarst features; authors note that a small increase in stream nutrient loading can stimulate primary and secondary production. Therefore, the moisture released from active thermokarst (slump activity) poses a high risk to freshwater invertebrate and vertebrate communities via changes to stream nutrient levels (Bowden et al., 2008; Lacelle et al., 2019).

In comparison, RTS activity in the Canadian High Arctic (Eureka, Nunavut) is directly influenced by increasing air temperature, as precipitation in the region is extremely low (<80 mm yr^{-1}; Ward Jones et al., 2019). Slump activity in the Eureka Sound Lowlands has been monitored since 1991 with the number of observed slumps increasing by 10% annually since 2005 (Pollard et

al., 2015). Between 2011 and 2018, average headwall retreat rate was 6.2 m yr^{-1} and a maximum retreat observed as high as 79 m yr^{-1} over a seven year-period (Ward Jones et al., 2019). High RTS activity is attributed to the combined effects of melting massive ice, intrasedimental ice and ice wedge ice (Grom, 2008). Ground ice in Eureka is estimated to constitute 30.8%$_{vol}$ of the upper 5.9 m of permafrost and in regions below marine limit (~146m a.s.l.) 48.6%$_{vol}$ of frozen materials is comprised of pore ice or ice lenses (Couture & Pollard, 1998). Wedge ice only comprises a small fraction of the total ground ice volume (3.3%$_{vol}$) however, the near purity of this type of ice makes it highly susceptible to any disturbance which can lead to ground subsidence or trigger a retrogressive thaw slump (Couture & Pollard, 1998).

There is currently no known information on the hydrological impact of thaw slumps to this polar desert watershed. This project investigates the hydrochemical impact of retrogressive thaw slumping on the regional hydrology and overall water quality in Eureka, Nunavut. We compare the water quality of two streams in Eureka (Blacktop creek and Station creek) above and below active thaw slump inputs (slump rillwash). Both streams are impacted by the input of rillwash from retrogressive thaw slumps. Since thaw slumps in the High Arctic behave differently than in the Western Canadian Arctic, our objective is to see how these polar desert, nival streams respond to the surface water input of thaw slumps. We will assess differences in dissolved organic carbon (DOC), stable water isotopes and major ions to further understand how these streams respond to current thermokarst pressures. Our work will provide context to how these streams will behave under stronger climate pressures and the long-term impact of this activity to local terrestrial and aquatic communities.

3.2 Study Area

The Fosheim Peninsula (FP) is an intermontane region located in the west-central section of Ellesmere Island and the south-eastern section of Axel Heiberg Island (**Fig. 1**). The region is surrounded by massifs exceeding 1000 meters above sea level (m a.s.l.) and hosts two main physiographic regions: the uplands that exceed 500 m a.s.l. and the Eureka Sound Lowland (ESL) that consists of flat to gently rolling terrain situated at elevations < 200 m a.s.l. The region is underlain by the Sverdrup Basin, a folded and faulted Carboniferous to Paleogene sedimentary bedrock comprised of sandstone, siltstone and shale strata (Bell, 1996; Hodgson and Nixon, 1998).

The Innuitian Ice Sheet covered most of the Queen Elizabeth Islands and reached its maximum extent at about 15,800 ^{14}C yr BP (Dyke et al., 2002; England et al., 2006). Deglaciation started between 10,300-8800 ^{14}C yr BP (England et al. 2006) and marine transgression followed until 8800-7800 ^{14}C yr BP; the Holocene marine limit is found between 139 and 150 m a.s.l. (Bell,

1996). The surficial sediments on the Fosheim Peninsula consist of weathered bedrock, till and glaciofluvial sediments above the marine limit and early Holocene-age marine and deltaic deposits below the marine limit interspersed with patches of fluvial and alluvial deposits and small areas of thin peat (Hodgson and Nixon, 1998; Bell and Hodgson, 2000). Solifluction, rill washing and slope failures reworked these deposits into colluvium deposits along hillslopes (Bell and Hodgson, 2000).

The Fosheim Peninsula is characterized by a polar desert climate, with cold winter and cool summer air temperatures. The 1991-2021 mean annual air temperature recorded at Eureka weather station is -18.0±1.2°C and the total annual precipitation was 77.0 ± 23.0 mm yr^{-1}, making it one of the coldest-driest places in Canada (Government of Canada, 2025). The typical vegetation consists of a *Salix-Dryas* community, occupying up to 50% of hummocky tundra and less than 20% on drier and more exposed slopes (Becker et al., 2016).

Climate and vegetation conditions ensure that permafrost is cold, continuous, and ~ 500 m thick (Pollard, 2000). The thickness of the active layer is typically 40-80 cm but varies due to microclimatic conditions. Permafrost is generally ice-rich as revealed by 152 boreholes drilled to depths of 8 m with average ice content of 53%$_{vol}$; the marine-deltaic deposits contained the highest amount of ice (average of 64%$_{vol}$; Hodgson and Nixon, 1998). The landscape is dominated by ice wedge polygons and they occupy ~ 50% of the ESL (Couture and Pollard, 1998; Bernard-Grand'Maison and Pollard, 2018). Based on $^{14}C_{DOC}$ dating, the ice wedges started to develop immediately after marine regression from spring meltwater and glacial meltwater (Campbell-Heaton et al., 2021). Thaw slumps and active layer detachment slides are also common (Lewkowicz, 1990, 2007; Pollard et al., 2015; Ward Jones et al., 2019, 2021). The slumps are mostly located around Eureka, in the Station Creek and Blacktop Creek watersheds, in Hot Weather Creek watershed, and in the Mokka Fjord region (Ward Jones et al., 2019). Thaw slumps often develop along an ice wedge network, but they also develop in areas underlain by tabular massive ice bodies that are found only within the fine-grained Holocene marine-deltaic sediments (Hodgson and Nixon, 1998; Pollard, 2000). Between 1989 and 2018, the number of active thaw slumps in the FP range from about 50 to about 240 each year and headwall retreat rates ranged from 3 to 15.5 m yr^{-1}, mostly in response to thaw degree days (Ward Jones et al., 2019). Vegetation re-colonization of slump scar is slowed by the high salinity of disturbed marine sediments and presence of efflorescence salts (Kokelj and Lewkowicz, 1999). Ice wedges in the area are still active (Ward Jones et al., 2020; Campbell-Heaton et al., 2021) and degrade due to warming air temperatures (Ward Jones et al., 2020).

3.3 Methods

3.3.1 Site Description

The Blacktop Creek watershed is approximately 98 km^2 and has colluvium above marine limit and colluviated fine-grained and glacio-marine sediments at lower elevations (Bell & Hodgson, 2000). The watershed has two active thaw slumps: Blacktop slump and Nunavut slump, see Table 1 for slump characteristics. Blacktop slump is at 65 m a.s.l. and measures about 97 m wide with a headwall less than 1 m high (including active layer). The headwall exposes an active layer about 60 cm thick, composed of massive ice (not visible in 2022 & 2023) and ice wedges. In 2022, only the top 2-5cm of a few affected ice wedges (1-2 wedges) were exposed. No flowing water was present, with only little to no stagnate water. Between 2011-18, the headwall of Blacktop slump retreated at an average rate of 8 m yr^{-1} (Ward Jones et al. 2019). However, in summer 2022 and 2023, the slump showed no signs of activity and no rillwash was observed along the slump floor. Nunavut slump, found at approximately 90 m a.s.l. is substantially larger; the slump measures about 230 m wide with a headwall about 5-6 m high. The headwall exposes an active layer 60 cm thick, the headwall is composed of segregated and reticulate ice in marine sediments (<1m), massive ice (~5m) and ice wedges. In summer 2022 and 2023, the headwall of this slump retreat by about 5 m and rillwash was observed along the slump floor.

The Station Creek watershed is approximately 111 km^2 and has colluvium above the marine limit and fine grained (glacio) marine sediments below marine limit. The watershed has six known thaw slumps that are active during warm summers (Ward Jones et al. 2019). Station creek slump is the largest of the six, measuring about 105 m wide. The 8-10 m high headwall exposes about 3 m of marine sediments containing reticulate ice overlying tabular massive ice with thin layers of marine sediments within its upper section. Between 2011-18, the headwall retreated at an average of 4.7 m yr^{-1}; however, in summer 2022 and 2023, this slump was inactive.

In July 2022, a small slump (BL slump) developed downstream (~10 m) of the Station Creek slump (within the same slump complex). This slump is ~100 m wide and 6-10 m high. The headwall exposes an active layer 60 cm thick and is composed of reticulate ice formed in marine sediments (4-5m thick) and massive ice (~5m). In 2023, this slump was active and the slump runoff completely blocked Station Creek, creating a pond upstream. In July 2023, another large thaw slump (CHP slump) was found 4.2 km upstream of the Eureka Weather Station. Satellite imagery shows that this slump initiated in 2012, see Table 1 for slump characteristics. The headwall of the slump is 490 m wide and 6-8 m tall. The headwall exposes an active layer ~60 cm thick and

comprised mostly of massive (3-4 m) and wedge ice (~1 m). In summer 2023, this slump was very active, with slump runoff flowing almost a kilometer before entering Station Creek.

3.3.2 Sample Collection

The geochemical characteristics of runoff along active slumps and their potential effect to the water quality of Station Creek and Blacktop Creek were assessed by sampling: i) pristine streams well upstream of slumps; ii) slump runoff along the slump floor of active slumps; iii) runoff from creeks downstream of the active slumps. To identify the source of solutes in the slump runoff, the geochemical composition of the various units exposed in the headwalls was determined.

Water samples from the various sites were collected daily. At each site, 60 ml of filtered water samples (0.45 mm cellulose nitrate filters) were collected for major and minor ions, δD-$\delta^{18}O$, DOC and $\delta^{13}C_{DOC}$. When possible, samples were collected at 10-15 cm depth in the water column. All samples were stored at 5°C in the field and shipped in coolers to the University of Ottawa (Ottawa, Canada) for analyses.

Six Solinst Levellogger 5 LTC sensors (Solinst Canada, 2024) were deployed in 2022 and 2023, with one positioned above an active thaw slump, one below and a third near the stream outlet in both streams. These dataloggers recorded the water level (m), temperature (°C) and conductivity (µS/cm) at a 30-minute interval. Each logger was housed in perforated PVC pipe to reduce solar heating and physical disturbance (Johnson & Wilby, 2013). In 2022, the loggers were attached to fine (1/8" or 0.3cm) metal cable and one wooden stake at the stream edge. The logger and casing were a fixed to a large rock (slightly bigger than a brick) and positioned in the thalweg of the stream. Rain events washed several of the loggers out of place, these were repositioned once identified back to their original location. In 2023, we used a two-cable system, one on either bank and a 3' (~90 cm) steel rod hammered into the creek bed at the thalweg. The combination of steel rod and cables kept the logger in place (loggers were zip-tied to the steel rod). Logger data was supplemented with manual readings from a YSI (Pro 20) meter, recorded when the grab sample was collected.

3.3.3 Laboratory Analyses

Geochemical and isotopic tracers were used to identify water sources and influence of retrogressive thaw slumps. Major and minor cations and anions were analyzed in the Geochemistry Laboratory, University of Ottawa. The cations (Ca^{2+}, Mg^{2+}, Na^{+}, K^{+}, Sr^{+}, Ba^{2+}) were acidified with ultra-pure nitric acid and analysed using an Agilent 4100 Microwave Plasma Emission Spectrometer. The anions (Cl^{-}, SO_4^{2-} and NO_3^{-}) were analyzed unacidified by ion chromatography with a Dionex ICS-

2100. Analytical precision is ± 5% for both cations and anions. Total dissolved solids (TDS) were calculated by the sum of all major ions. To facilitate a comparison between stream and melted ground ice samples, the results were converted to molar ratios with respect to Cl^- as conservative tracer.

The stable isotope ratios of oxygen ($^{18}O/^{16}O$) and hydrogen (D/H) were measured using a Los Gatos Research high precision water isotope analyzer. The instrument uses laser absorption for simultaneous measurement of $^{18}O/^{16}O$ and D/H ratios in liquid water samples (Berman et al. 2013). Results are expressed in δ notation, where δ represents the part-per-mile difference of $^{18}O/^{16}O$ and D/H in a sample relative to VSMOW (Vienna Standard Mean Ocean Water). Analytical precision for $\delta^{18}O$ and δD are ± 0.3‰ and ± 1‰ respectively. The deuterium-excess was calculated using the following equation ($D = \delta D - 8\delta^{18}O$; Dansgaard, 1969).

The DOC and its stable isotope ratio ($\delta^{13}C_{DOC}$) were analyzed in the Ján Veizer Stable Isotope Laboratory at the University of Ottawa. The DOC concentration and δ^{13}CDOC was measured by a wet TOC analyzer interfaced with a Thermo DeltaPlus XP isotope-ratio mass spectrometer using methods described by St-Jean (2003). The $^{13}C/^{12}C$ results are presented using the δ-notation relative to Vienna Pee-Dee Belemnite (VPDB). The analytical precision is ± 0.5 ppm for the concentrations and ± 0.2‰ for $\delta^{13}C$.

3.3.4 Data Analysis

All statistical analysis was computed in R (v. 4.5.1; R Core Team, 2025). Summary statistics were computed for each variable, with computations separated by year, stream, stream year and then individual site to determine if there were any obvious differences between years, streams and sites. Shapiro-Wilk tests were used to determine normality within the dataset, only DOC concentrations needed to be log-transformed. Correlations (Pearson) were conducted to identify relationships between variables, again these were separated by year, stream and site. Anova and Tukey HSD were then computed to identify differences between sites for each stream with the goal to identify which variables indicate the input of thermokarst effluent moisture.

3.4 Results

3.4.1 Potential Source Chemistry:

Ice wedges in the region were formed during the Holocene between 9-2.5 kyr BP from spring snowmelt (Campbell-Heaton et al., 2021). Tabular massive ice in the region was formed during the same period from ground water inclusion (Roy et al., 2023). Average concentration of Dissolved Organic Carbon (DOC) within studied ice wedges is 2.70±3.02 ppm (Campbell-Heaton et al.,

2021). Massive and intrasedimental ice has a much higher DOC concentration ranging between 1.01-31.61 ppm and averaged 6.67 ppm (Roy et al., 2023). Table 2 details the average concentration of major ions in massive ice samples and ice wedges from Roy (2018) and Campbell-Heaton (2020). Most reported concentrations are greater in the ice wedge samples than the massive ice. This difference is attributed to the moisture source of the respective ground ice types (i.e., meteoric, ground water).

Water quality monitoring was conducted in August 2010 of Station Creek to ensure it met the Canadian Drinking Water Quality Guidelines for use by Environment Canada's Weather Station (Arcadis Canada Inc., 2016). Recorded water temperature for Station Creek was 5.9°C, electrical conductivity was 797 µs/cm, pH 7.49, turbidity 3.27 NTU, TDS 544 mg/L, dissolved sodium ranged between 333 to 507 mg/L and aluminum 0.215 mg/L (Arcadis Canada Inc., 2016). All other water quality parameters for Station Creek were below the Aesthetic Objective (a threshold to monitor water quality). In July 2018, water samples were collected by K. Campbell-Heaton near the outlet of Station Creek and Blacktop Creek. Recorded $\delta^{18}O$ for Station Creek and Blacktop Creek is -25.25±0.11‰ and -23.90±0.12‰, d-excess is 1.88 and 1.15, respectively. Recorded dissolved organic carbon (DOC) concentrations for Station Creek and Blacktop Creek were 2.21 ppm and 1.84 ppm, respectively. Moreover, $\delta^{13}C$ values for Station Creek and Blacktop Creek are similar, -28.64‰ and -28.16‰. Both creeks were only sampled once in 2018. In addition, the 2018 stream samples were analyzed for major ions, see Table 2. Sodium (Na^{2+}), chloride (Cl^{-}) and sulphate (SO_4^{-2}) were the ions with the highest concentrations in both streams. In 2018 and 2019, the active layer in blacktop creek was sampled in five locations near active thaw slumps. Samples were collected every five centimetres to a maximum of 70 cm depth. Average DOC was 28.54 ppm, $^{13}C_{DOC}$: -24.89‰, and TDS: 128.94 ppm.

3.4.2 Geochemistry Of Ice-Rich Permafrost Exposed in Headwalls

The geochemical facies of the massive ice vary according to site elevation (Roy, 2018). At Dump and Station Creek (40-45 m a.s.l.), the ice is characterized by a NaCl geochemical facies, with Na/Cl molar ratios similar to Slidre Fiord and seawater, but with TDS concentrations of one to two orders of magnitude lower (average TDS of 868 ± 1990 and 310 ± 353 mg L^{-1}, respectively). The ice at the higher elevation site (Gemini, 115 to 120 m a.s.l.) is characterized with a Ca-SO_4 geochemical facies with a lower TDS (average of 28 ± 15 and 37 ± 10 mg L^{-1}, respectively). At both coring sites (G1 and G3), the TDS shows little variation with depth. The Na/Cl molar ratios of the massive ice at Gemini is higher than at Dump and Station Creek, but more similar to that of snow.

3.4.3 Hydrochemistry Of Slump Runoff and Streams

3.4.3.1 Interannual stream hydrochemistry variations

Dissolved organic carbon concentrations were lower in Blacktop creek (BC) than Station creek (SC) in both years, with average values for respective creeks in 2022, 0.89±0.32 ppm (n=36) and 1.27±0.42 ppm (n=38), and in 2023, 0.69±0.36 ppm (n=33) and 1.22±0.66 ppm (n=36). With respect to $^{13}C_{DOC}$, BC is consistently more enriched than SC with average values for respective creeks in 2022: -27.42±7.46 ‰ (n=36) and -27.64±7.34 ‰ (n=38) and in 2023: -26.10±13.16 ‰ (n=33) and -26.52±13.36 ‰ (n=36). Mean $\delta^{18}O$ in 2022 varies slightly between creeks with BC averaging -23.54±3.89 ‰ (n=36) and SC averaging -23.47±1.03 ‰ (n=38). In 2023, the variability is greater with a mean $\delta^{18}O$ for BC -26.91±0.80 ‰ (n=33) and -25.79±3.27 ‰ (n=36) for SC. Recorded conductivity for 2022 averages 169.64±68.34 µS cm-1 (n=1799) and 264.25±68.56 µS cm^{-1} (n=1737) for BC and SC respectively. In 2023, average conductivity is 221.40±45.73 µS cm^{-1} (n=2213) and 427.79±124.41 µS cm^{-1} (n=2156), for BC and SC respectively. Average TDS values for Blacktop creek in 2022 is 166.7±46.1 ppm and 212.9±49.5 ppm (n=41) for Station creek. In 2023, mean TDS for BC is 183.2±94.1 ppm (n=64) and 357.8±196.8 ppm (n=74) for SC. Sulphate comprises a large majority load, in 2022, the concentration of SO_4 in Blacktop creek is 94.6±20.8 ppm (n=37) and 120.0±31.2 ppm (n=41) for Station creek. In 2023, the average SO_4 concentration for BC 98.2±16.9 ppm (n=33) and 213.4±79.7 ppm (n=37) for SC. In 2022, the average concentration of calcium in Blacktop creek is 24.4±3.9 ppm (n=38) and 30.9±5.5 ppm (n=41) for Station creek. In 2023, concentrations are higher, 32.8±8.2 ppm (n=33) for BC and 49.2±18.7 ppm (n=37) for SC. Average chloride concentration between creeks is similar for 2022, with 19.6±9.0 ppm (n=38) and 18.8±7.5 ppm (n=41) for BC and SC, respectively. In 2023, the streams vary greatly from each other, BC averages14.1±7.7 ppm (n=33) and 36.1±26.1 ppm (n=37) for SC.

3.4.3.2 Hydrochemistry of undisturbed sites

The following details the hydro-chemical profile of the thaw-undisturbed sites. In 2022, only one site, Site 3 was considered thaw undisturbed within Blacktop Creek whereas in 2023, two undisturbed sites were monitored, Site 3 in BC and Site 7 in SC. In 2022, the average DOC was 0.72±0.16 ppm (n=10) for Site 3 (BC). Comparatively, in 2023, Site 3 (BC) had an average DOC of 0.66±0.07 ppm (n=8) whereas Site 7 (SC) had a mean DOC of 0.81±0.13 ppm (n=7). The mean $^{13}C_{DOC}$ of the undisturbed site (Site 3, BC) in 2022 was -27.10±0.82‰ (n=10). In 2023, Site 3 (BC) had an average $^{13}C_{DOC}$ of -26.52±1.30‰ (n=8), Site 7 (SC) averaged -27.21±0.23‰ (n=7). In 2022, Site 3 had an average $\delta^{18}O$ of -23.81±0.93 (n=10). In 2023, Site 3 had an average $\delta^{18}O$ of -

26.96±0.74 (n=16) and Site 7 had an average of -25.82±1.15‰ (n=14). In 2022, Site 3 had an average recorded conductivity of 134.25±68.90 µS cm^{-1} (n=533). In 2023, Site 3, had an average conductivity of 209.94±31.31 µS cm^{-1} (n=498) and Site 7 had an average conductivity of 454.81±81.80 µS cm^{-1} (n=563). Average TDS for Site 3 (BC) in 2022 was 169.21+-35.95ppm (n=10) and 232.37±44.17ppm (n=8) in 2023. At Site 7, average TDS was nearly double at 397.43±74.36 ppm (n=7). Sulphates compromise most of the TDS load, Site 3 in 2022 had an average concentration of 85.33±13.28 ppm (n=10), in 2023, the average concentration is 97.03±18.23 ppm (n=8). Site 7 (SC) in 2023 averaged 207.98±59.85 ppm (n=7).

3.4.3.3 Hydrochemistry of Slump Runoff:

Slump runoff was monitored in both years, Blacktop Creek (BC) had one active slump whereas Station Creek (SC) had two active thaw slumps. The slump runoff (SR) was far greater in SC than BC. Average dissolved organic carbon content for the BC SR was 6.13±1.15 ppm (n=5) and in SC slightly greater 6.63±0.69 ppm (n=4), $^{13}C_{DOC}$ is -27.08±1.04‰ (n=5) for BC and 26.77±1.47‰ (n=4) for SC. The average $\delta^{18}O$ is -25.07±0.71‰ (n=19) for BC and -26.90±3.26‰ (n=22) for SC. The conductivity of slump runoff (SR) from BC was higher than SC with values of 4228.00±747.73 µS cm^{-1} (n=18) and 3211.70±2367.44 µS cm^{-1} (n=20), respectively. TDS, however, was lower in BC than SC with average values of 4334.71±1730.24 ppm (n=9) and 4709.70±3241.77 ppm (n=14), respectively.

3.4.3.4 Hydrochemistry of Disturbed Sites:

In 2022, five down-stream of thaw disturbance sites were monitored, Sites 1 & 2 in BC and Sites 4-6 in SC. Sites 2 and 5 are located close (within 200m) to the disturbance whereas sites 1, 4 and 6 are located further downstream. In 2023, Site 2 was further subdivided (left and right sides) as it was visually evident that slump runoff was not horizontally mixed within the water column at this site. In Station Creek, Sites 4 and 5 were sampled and passively monitored using Solinist Levelloggers, whereas only grab samples were used in Site 6. An additional site was established in 2023, 5 SC, this site was established near Site 5 but featured a portion of the stream that did not interact with the slump runoff (a small braid off the main channel) this was only grab-sampled a handful of times.

In 2022, mean DOC from Blacktop Creek (BC) for Site 1 was 0.95±0.21 ppm (n=14), for Site 2 it was 0.97±0.24 ppm (n=12). In Station Creek for the same year, average DOC from collected samples at Site 4 was 1.26±0.31 ppm (n=14), 1.20±0.24 ppm (n=12) at Site 5 and 1.34±0.26 ppm (n=12) for Site 6. In 2023 the average DOC was lower than the previous year, Site

1 had an average of 0.69±0.24 ppm (n=9), Site 2 LS had an average of 0.73±0.10 ppm (n=8), Site 2 RS had an average of 0.68±0.15 ppm (n=8). In SC, Site 4 had an average of 1.44±0.41 ppm (n=9), 1.40+0.24 ppm (n=8) for Site 5, 1.06±0.35 ppm (n=4) for Site 5 SC, 1.24±0.17 ppm (n=8) for Site 6. ANOVA analysis showed a significant difference between sampled sites for Blacktop creek in 2022 only (p= 0.0116, F=5.112). Post-hoc Tukey HSD showed that the strongest difference is between the above slump site (3) and directly below the slump (2). In Station creek, no significant difference was identified for 2022 as all sites sampled were downstream. The following year shows a statistically significant (ANOVA) difference between the above and below slump sites (p = 0.0007, F = 6.383). Post-hoc Tukey test reveals that the greatest difference in DOC is between sites 7 and 4, (p = 0.0007).

In 2022 Blacktop creek (BC), mean $^{13}C_{DOC}$ for Site 1 was -27.37±1.94‰ (n=16), for Site 2 it was -27.75±1.08‰ (n=12). In Station creek (SC), average $^{13}C_{DOC}$ from site 4 was -27.62±1.05‰(n=14), from site 5 it was -27.41±0.77‰ (n=12) and -27.91±0.90‰ (n=12). In 2023 BC, the $^{13}C_{DOC}$ for all three sites was more enriched, Site 1 had an average of -25.94±0.63‰ (n=9), Site 2 LS had an average of -25.53±0.92‰ (n=8), Site 2 RS had an average of -26.42±0.60‰ (n=8). In SC, the stream was more enriched, average $^{13}C_{DOC}$ at Site 4 was -26.37±1.31‰ (n=9), Site 5 was -26.56±1.02‰ (n=8), site 5 SC was -25.55±1.03 (n=4), site 6 was -26.52±0.59‰ (n=8). No significant difference detected between sites for either year for both streams.

For BC in 2022, Site 2, had an average $\delta^{18}O$ of -23.51±1.12 (n=12) and Site 1 had an average of -23.39±0.93 (n=16). In SC, Site 6 had an average $\delta^{18}O$ of -23.47±0.98‰ (n=12), Site 5, had an average of -23.60±1.06‰ (n=12) and Site 4 had an average of -23.37±1.09‰ (n=17). In 2023 BC, at Site 2, the left side had an average $\delta^{18}O$ of -26.93±0.80 (n=16), the right an average of -26.92±0.68 (n=15). At Site 1, furthest downstream had an averaged of -26.85±1.00 (n=16). In SC, Site 6, had an average of -25.70±1.31‰ (n=17), site 5 had an average of -25.63±1.38‰ (n=16) and Site 5 SC (adjacent to Site 5, but not impacted by slump) had an average of -26.39 ± 0.76‰ (n=9). Site 4 furthest downstream had an average $\delta^{18}O$ of -25.71±1.63 (n=17). ANOVA analysis revealed no significant difference among any site in either creek for both years.

Conductivity 2022 BC Site 2 was 165.30±66.11 µS cm^{-1} (n=536) and furthest downstream, Site 1 averaged 198.75±55.37 µS cm^{-1} (n=728). In SC, Site 6 had an average recorded conductivity 262.32±62.07 µS cm^{-1} (n=529), lower in the reach directly below BL slump, Site 5 was 277.79±55.58 µS cm^{-1} (n=532) and furthest downstream, Site 4 averaged 386.91±169.86 µS cm^{-1} (n=1173). In 2023 BC, Site 2, located directly below the active slump averaged 244.73±47.77 µS cm^{-1} (n=725) and Site 1 was 200.34±39.60 µS cm^{-1} (n=532). In SC, Site 5, located directly below BL Slump averaged 511.32±152.60 µS cm^{-1} (n=703) and Site 4 was 468.52±150.07 µS cm^{-1}

(n=751). ANOVA analysis revealed a significant difference on measured conductivity for both streams in both years. Blacktop creek 2022 ($p=<2e^{-16}$; F=164.6) Tukey HSD showed a difference between all sites (1-3). Station creek 2022 ($p=<2e^{-16}$; F=965.7), significant difference between Site 5 & 4 and Site 6 & 4. Blacktop creek 2023 ($p=<2e^{-16}$; F=206.9), significant difference for all sites. Station creek 2023 ($p=<2e^{-16}$; F=118), significant difference for all sites but Site 7 and 4.

Total Dissolved Solids (TDS) in 2022 BC Site 2 was 190.43±42.27 ppm (n=12) and furthest downstream, Site 1 averaged 212.44±56.53 ppm (n=16). In SC, Site 6 had an average TDS 251.21±59.26 ppm (n=12), lower in the reach directly below BL slump, Site 5 was 237.58±55.20 ppm (n=12) and furthest downstream, Site 4 averaged 247.88±68.55 ppm (n=17). In 2023 BC, Site 2, located directly below the active slump averaged 201.14±38.43 ppm (n=8) on the left side of the stream, 220.20±41.78ppm (n=8) and Site 1 was 206.09±41.42 ppm (n=9). In SC, Site 5, located directly below BL Slump averaged 427.46±81.26 ppm (n=8), the adjacent site (5 SC) averaged 399.09±61.87 ppm (n=5) and Site 4 was 397.32±81.72 ppm (n=9). ANOVA analysis revealed no significant difference between studied sites for BC 2023 and SC 2022 and SC 2023. There was a significant difference in BC 2022 (p=0.013; F=4.918), Tukey revealed the significant difference between Site 1 and 3.

Sulphate was the dominate ion in both streams. Average concentration in 2022 BC Site 2 was 89.49±15.84 ppm (n=11) and furthest downstream, Site 1 averaged 103.88±24.42 ppm (n=16). In SC, Site 6 had an average SO_4 125.65±40.28 ppm (n=12), lower in the reach directly below BL slump, Site 5 was 113.88±21.52 ppm (n=12) and furthest downstream, Site 4 averaged 120.34±30.86 ppm (n=17). In 2023 BC, Site 2, located directly below the active slump averaged 94.98±16.78 ppm (n=8) on the left side of the stream, 94.91±17.15 ppm (n=8) and Site 1 was 105.10±16.49 ppm (n=9). In SC, Site 5, located directly below BL Slump averaged 288.08±87.70 ppm (n=8), the adjacent site (5 SC) averaged 179.96±61.76 ppm (n=5) and Site 4 was 218.12±100.58 ppm (n=9). No significant difference was found for either stream in either year.

Stream sodium, chloride, calcium and magnesium concentrations are reported in Table 3 for all sites (1-7) and the slump runoff. ANOVA analysis revealed a significant difference within Blacktop creek 2022 for sodium (p=0.0013, F=8.134) and chloride (p=0.0006, F=9.212) concentrations between sites 2 & 3 (p=0.01) and 1 & 3 (p=0.001) for sodium and between 3 & 1 (p=0.00068) and 3 & 2 (p=0.0053). Blacktop Creek 2023 had a significant difference between sites for chloride (p=0.0178; 1&3), calcium (p=0.00059; 1&3, 2 LS&3) and magnesium (p=0.0046; 1&3, 2 LS&3). No significant difference found for any of the ions for Station Creek in either year.

3.5 Discussion

3.5.1 Above Disturbance Stream Conditions

Dissolved organic carbon (DOC) content was very low compared to other High Arctic locations, with values ranging between 0.66-0.81 ppm. In Cape Bounty (74°54′N, 109°35′W). for example, undisturbed rivers have DOC values ranging from 1.14-4.14 ppm (Wang et al. 2018). As latitude decreases, DOC concentrations increase in undisturbed streams in the Peel Plateau, NWT, where DOC concentrations range between 6.6-26.1 ppm (Littlefair et al., 2017). Therefore, the very low DOC concentrations measured in Eureka reflect the region's low biological productivity.

The Local Meteoric Water Line (LMWL) for Eureka was established using the CNIP dataset, which includes monthly snow and rain samples collected between 1989 and 1993 (IAEA/WMO, 2018). The resulting LMWL is expressed as $\delta D = 7.43 \times \delta^{18}O - 9.14$. Stream samples from both study years plot below the LMWL, indicating isotopic fractionation from evaporation. In 2022, stream waters were more isotopically enriched, reflecting greater rainfall input during that season. In contrast, 2023 stream waters were more depleted, with consistent enrichment over time. No rain events were recorded by the Eureka Weather Station in 2023, indicating that the primary sources of stream water were snowmelt and thawing ground ice. Figure 2 shows δD–$\delta^{18}O$ data separated by year, stream, and sampling date. The 2022 samples plot closer to the LMWL and exhibit a more mixed signal, while the 2023 samples deviate further below the line, signifying stronger evaporative effects. Toward the end of the 2023 sampling period, Station Creek samples shift even farther from the LMWL, consistent with increased evaporation later in the season. The $\delta^{18}O$–δD range for Station Creek 2023 is greater than that of Blacktop Creek 2023, suggesting that SC23 became progressively more enriched through time—potentially due to enhanced evaporation under warmer, drier late-season conditions. Lamhonwah et al. (2016) identified a similar increasing trend through time with stream stable oxygen data in Cape Bounty, Melville Island, Nunavut. This trend is evident in all the study years (2006-2010, 2012, 2014) for June/July. They isolated no difference in ^{18}O between disturbed and undisturbed catchments (Lamhonwah et al., 2016).

Stream chemical composition of undisturbed sites (Fig. 3) show that Blacktop Creek is dominated by calcium, magnesium and sulphate ions, while Station Creek exhibits a similar composition with higher sodium concentrations. These solutes reflect the meltwater induced-dissolution of evaporite-rich Holocene marine and deltaic sediments that underlie the Eureka Sound Lowlands, which contain gypsum, anhydrite, halite, and associated efflorescent salts (Hodgson & Nixon, 1998; Kokelj & Lewkowicz, 1999; Bell & Hodgson, 2000). The elevated Ca-Mg-SO_4-Na

signature in both streams therefore reflects baseline geochemical inputs from marine-derived sediments and shallow ground ice, rather than thermokarst disturbance. In Fig. 4A, the undisturbed sites consistently show higher SO_4 : Cl^- molar ratio than disturbed sites, largely due to lower chloride concentrations. In 2022, $Na:Cl^-$ ratios at Blacktop Creek remained close to maritime precipitation (~0.86; Fig. 4B); while Station Creek approached ~2, consistent with continental precipitation (Möller, 1990). Variability is low across sites throughout the study period. In 2023, undisturbed sites generally exhibited higher $Na:Cl^-$ ratios, indicating a greater proportion of sodium, suggesting mobilization of sodium-rich salts from marine-deltaic sediments during early melt. A secondary peak is present around July 17th suggests an input of supra-permafrost ground water. Previous studies in area suggest that weathering of bedrock is low (Lewkowicz, 2001) with wind-blown snow being the primary driver of weathering. The results from 2023 suggest that weathering rates are greater, likely linked to the freeze-thaw of snowmelt at higher elevations in the basin. Future work is necessary on bedrock weathering processes in the area to determine if climate warming in the arctic will speed up weathering rates and result in changes to stream chemical composition and overall terrestrial/aquatic ecosystem functions.

3.5.2 Slump Runoff Conditions

The dissolved organic carbon content for slump runoff was higher than the undisturbed sites with slightly higher recorded levels for Station Creek, where DOC ranged between 5.2–8.0 ppm. This is with range comparative to other Subarctic regions. The Peel Plateau for example, has measured DOC concentrations range between 5.8-25 ppm (Littlefair et al., 2017). The dominate source of DOC in these slump runoff samples is old Holocene (2.5–11.5 k yr BP) massive and wedge ice. Previously sampled in 2017-2019; ice wedges and massive ground ice in the Eureka region have DOC concentrations between 0.88–48.7 mg L^{-1}, with DOC from leached active layer samples similarly low 39.5 ± 32.2 mg L^{-1} (Campbell-Heaton et al., 2021; Roy et al., 2023). $^{13}C_{DOC}$ is similar in disturbed and undisturbed sites and indicative of C3 vegetation source and the associated microbial processes (Raymond et al., 2007; Hindshaw et al., 2016). Conductivity and TDS are extremely high at both sites, the amount of runoff from slumps that make it to the streams is low and with high concentration of salts (~4‰ salinity), indicated by the very high concentrations of chloride and sodium. Further, the molar ratio of sodium and chloride averages is 0.69±0.11 for Blacktop Creek slump runoff and 0.75±0.12 for Station Creek slump runoff, and both sites have molar ratios slightly lower than the reference seawater ratio of~0.86 (Millero et al., 2008). This is indicative of thawing marine sediments. Salt efflorescence is a common occurrence in the area,

especially below Holocene marine limit, and largely linked to permafrost disturbance (Kokelj & Lewkowicz, 1999).

3.5.3 Below Disturbance Stream Conditions

Dissolved organic carbon (DOC) concentration in both streams is low compared to other High Arctic locations. Wang et al. (2018) reported an average DOC concentration of 4.8±1.6 ppm for disturbed stream sites at Cape Bounty (74°54′N, 109°35′W), much greater than the disturbed sites at Eureka. Statistically significant differences were observed between disturbed and undisturbed sites for Blacktop Creek in 2022 and Station Creek in 2023, indicating that slump runoff contributed enough DOC to alter stream DOC composition. This difference was not observed in Blacktop 2023 which can be attributed to overall slump activity, as the exposure of ground ice in the headwall was visibly smaller, suggesting that this feature is transitioning toward stabilization. There is some evidence that the stream DOC concentrations decline as distance from the sample site to the point source increases. This is clearer in the Blacktop Creek data between Site 1 and 2, however the difference is very little and could simply be attributed to an increase in discharge at the lower site. Overall, reported effects of thermokarst activity on Arctic stream DOC vary, with some studies noting enrichment following disturbance and others the opposite (Lafrenière and Lamoureux, 2019). This variability likely reflects differences in DOC biolability. Vonk et al. (2013) found that DOC derived from old permafrost had a high biolability, rapidly converting to CO_2. Spencer et al. (2015) similarly observed greater DOC loss in thaw-affected streams relative to unaffected systems. The transformation of permafrost-derived DOC to CO_2 poses concerns for carbon fluxes, as ancient carbon is converted more rapidly than modern sources (Vonk et al., 2013), with photochemical oxidation under sunlight increasing microbial conversion rates by up to 40% (Cory et al., 2013). Future research should investigate how continuous 24-hour summer sunlight influences the photochemical conversion of DOC from old versus modern carbon sources. Despite the low carbon stocks characteristic of the high Arctic, prolonged solar exposure may further reduce DOC availability in streams by promoting rapid oxidation before the organic material reaches the stream channel.

The $^{13}C_{DOC}$ of the disturbed sites do not significantly differ from the undisturbed sites and are within normal range compared to larger Arctic rivers (Raymond et al., 2007). The recorded stream values are indicative of DOC sourced from C3 vegetation, and the associated microbial processing of carbon fixed by the Calvin-Benson-Bassham cycle (Hindshaw et al., 2016). Although not observed at this High Arctic location, Hindshaw et al. (2016) report highly depleted stream

values (~-43.8‰) in Svalbard, indicative of a partial contribution of methane-derived carbon - a likely product of permafrost thaw.

No statistically significant differences were detected in stable isotope composition between above- and below-slump sites for either stream or year. This lack of difference suggests that rillwash contributions from thaw slumps were isotopically minor relative to total stream discharge and therefore undetectable in the isotope record. However, regression analyses of δD versus $\delta^{18}O$ indicate variations in slope and intercept among years and sites. Downstream of slump-affected reaches, slope values were consistently lower than those of undisturbed sites, with the exception of Blacktop Creek 2022 (Site 1), where the furthest downstream site exhibited the highest slope (7.2). The same site maintained a higher slope in 2023 compared to the slump-impacted site. These patterns may reflect the introduction of new water sources, such as snowmelt, or differing evaporation-to-input ratios among sites. The consistently lower slope values in disturbed downstream sites likely indicate stronger evaporative enrichment, consistent with the isotopic evidence of water–energy balance shifts caused by permafrost disturbance. Future work should focus on resolving the relative contributions of snowmelt, rainfall, and ground-ice melt across seasons while better constraining evaporative enrichment processes to more precisely link observed deviations from the LMWL to permafrost driven changes in High Arctic stream hydrology.

Stream conductivity is significantly different between disturbed and undisturbed sites for both streams in both years, indicating that slump runoff consistently changes the stream chemistry. In 2022, the stream samples sites located the furthest down the reach (sites 1 and 4) had the highest conductivity values whereas in 2023, the opposite occurred where conductivity was higher nearest the point source and lower further down the reach. This difference can be attributed to the variable climate: 2022 was a cooler wetter year with more rain events, while 2023 was drier and warmer. Therefore, the intra-site conductivity observations from 2022 can be attributed to rain events, slope runoff and slump input whereas the 2023 intra-stream observations are solely linked to slump input. A similar gradient was observed by Littlefair et al. (2017) in the Peel Plateau where stream conductivity levels near the point source were 9x greater than pristine streams further downstream which showed only 2x increase. Comparatively, stream conductivity values in undisturbed sites in Eureka are still high and do not show the same magnitude of change as Littlefair et al. (2017) this can be attributed to local surficial geology.

Stream TDS increased in 2023 compared to 2022, with intra-stream differences between disturbed and undisturbed only significant for Blacktop Creek in 2022. No significant differences were observed for the other stream-years. These patterns suggest that while TDS increased interannually, likely reflecting differences in climate, permafrost thaw and evaporative

concentration, spatial variation along the streams was generally minimal. Sulphates accounted for most TDS concentrations in both streams, highlighting their dominate role in solute dynamics (Fig. 5). These results are similar to those of Lamhonwah et al. (2016), who identified a statistical difference in TDS between permafrost-thaw disturbed and undisturbed catchments (one sample site per basin) in Cape Bounty. Major ion results show that sulphate concentrations were consistently higher in Station Creek than in Blacktop Creek. Among all sampling years and sites, the only significant difference in sulphate concentration between disturbed and undisturbed reaches occurred at Blacktop Creek in 2022 ($p = 0.05$, ANOVA). A post-hoc Tukey HSD test yielded a marginal p-value (0.06) between Sites 3 and 1, which is not significant at $\alpha = 0.05$ but near the threshold, indicating a weak but suggestive difference. Overall, sulphate concentrations did not vary systematically between thaw slump–affected and unaffected sites. Consistent with observations from the NWT (Kokelj et al., 2005; 2013), we found significant differences in SO_4^{-2}:Cl^- ratios between slump-affected and unaffected sites for both years (Fig. 4). Unaffected sites had approximately twice the molar ratio of affected sites, driven primarily by the large increases in Cl^- concentrations downstream of active slumps. The highest average chloride concentrations were recorded at Site 5 in 2023 (49.91 ± 29.8 ppm), with a maximum of 109.3 ppm observed at Site 4 on July 21. Station Creek also exhibited higher mean Cl^- concentrations than Blacktop Creek (36.05 ± 26.8 ppm and 14.1 ± 4.1 ppm, respectively), corresponding to the presence of two active thaw slumps in Station Creek versus one weakly active feature in Blacktop Creek. In 2022, stream Cl^- concentrations were similar between streams (18.76 ± 7.46 ppm for Station Creek; 19.64 ± 8.12 ppm for Blacktop Creek).

These findings contrast with those reported by Kokelj et al. (2013) in the Northwest Territories, where slump-affected streams exhibited sulphate concentrations several orders of magnitude higher than unaffected systems. Their study also documented elevated calcium and magnesium in disturbed streams, patterns not observed in Eureka. One-way ANOVA results showed no significant differences in Ca or Mg concentrations for BC22, SC22, or SC23. In BC23, both ions differed significantly between disturbed and undisturbed sites, but concentrations were higher in the undisturbed reaches. This reversal may suggest a localized input source—potentially related to rillwash chemistry—or hydrological dissolution effects during active thaw periods that warrant further investigation. In contrast, chloride and sodium concentrations were markedly higher at slump-affected sites across both streams, directly influenced by slump runoff. However, only Blacktop creek showed a significant difference between disturbed and undisturbed sites in both years.

3.6 Conclusion

An analysis of permafrost-affected streams in Eureka, Ellesmere Island, Nunavut reveals distinct biogeochemical responses to thaw slumps. The major findings are summarized as follows:

- DOC Response: Active retrogressive thaw slumps increase dissolved organic carbon (DOC) concentrations downstream, though absolute DOC levels remain low due to limited organic matter and rapid photochemical degradation (Campbell-Heaton et al., 2021; Vonk et al., 2013). As slump activity declines, stream DOC concentrations return to pre-disturbance levels, highlighting the transient nature of carbon fluxes.
- Stable Water Isotopes: Stable isotopes ($\delta^{18}O$ and δD) show minimal differentiation between disturbed and undisturbed sites, suggesting that slump rillwash constitutes a minor fraction of total discharge. Seasonal variations primarily reflect evaporation and snowmelt inputs rather than thaw-derived contributions.
- Major Ion Chemistry: Elevated chloride concentrations and low SO_4^{2-}:Cl^- ratios in slump-affected streams act as reliable tracers of thermokarst activity, reflecting the influence of marine salts within permafrost rather than mineral weathering or organic matter leaching (Couture & Pollard, 1998).
- Spatial and Temporal Variability: Stream responses to thaw slumps are site- and year-specific, influenced by the activity level of slumps, local surficial geology, and climate conditions such as rainfall, temperature, and evaporation.
- Latitudinal Variability: DOC concentrations and chemical signatures in Eureka streams are lower than in more southern Arctic locations (Wang et al., 2018; Littlefair et al., 2017), consistent with the high Arctic's low productivity and limited carbon stocks.
- Implications for Arctic Carbon Cycling: The data suggest that permafrost thaw in the High Arctic primarily affects solute chemistry rather than carbon export or stream water isotopes. Thermokarst disturbances thus have localized but measurable effects on biogeochemistry, with broader implications for understanding carbon cycling under a warming climate.

Collectively, these findings indicate that permafrost thaw in the High Arctic affects stream systems primarily through solute enrichment rather than carbon export or hydrological mixing. The geochemical expression of thermokarst disturbance in Eureka is thus characterized by low organic carbon availability, isotopic signals dominated by evaporation, and ion chemistry reflective of marine silt and ice melt. As permafrost landscapes in this region continue to evolve under a warming climate, such responses may intensify but are unlikely to mirror the more carbon-rich and

hydrologically connected systems of subarctic or boreal regions. Future studies should integrate continuous hydrological monitoring, radiocarbon dating of dissolved carbon, and year-round isotope analyses to better constrain the timing, persistence, and fate of thaw-derived solutes and carbon. Understanding the interplay between geomorphic processes, carbon dynamics, and hydrology in these extreme northern systems will be critical for predicting the evolving biogeochemical role of the High Arctic in a warming world.

3.7 Acknowledgments

This project was funded by grants from the Natural Science and Engineering Research Council of Canada (NSERC; DL), the Northern Scientific Training Program (NSTP; KCH), the Royal Canadian Geographical Society (RCGS; KCH) and the Association of Canadian Universities for Northern Studies (ACUNS; KCH). Incredible field logistical support was provided by the Polar Continental Shelf Program (Natural resources Canada). Fieldwork could not have been completed without the help of B. Lauriol, J. Prest, and the Eureka Weather Station staff. Thank you to Dr. Konrad Gajewski for constructive comments on an earlier version of this manuscript.

3.8 References

Alt, B. T., & Maxwell, B. (2000). Overview of the modern arctic climate. Bulletin of the Geological Survey of Canada, (529), 17–36.

Arcadis Canada Inc. (2016). Environmental Impact Assessment - High Arctic Weather Station Project Improvements (Issue September).

Balser, A. W., Jones, J. B., & Gens, R. (2014). Timing of retrogressive thaw slump initiation in the Noatak Basin, northwest Alaska, USA. *Journal of Geophysical Research: Earth Surface*, *119*(5), 1106–1120. https://doi.org/10.1002/2013JF002889

Becker, M. S., Davies, T. J., & Pollard, W. H. (2016). Ground ice melt in the high Arctic leads to greater ecological heterogeneity. Journal of Ecology, 104(1), 114–124. https://doi.org/10.1111/1365-2745.12491

Bell, T. (1996). The last glaciation and sea level history of. Fosheim Peninsula, Ellesmere Island, Canadian High Arctic. Canadian Journal of Earth Sciences, 33, 1075–1086.

Bell, T., & Hodgson, D. A. (2000). Quaternary geology and glacial history of Fosheim Peninsula, Ellesmere Island, Nanavut. In Bulletin of the Geological Survey of Canada. https://doi.org/10.4095/211957

Bernard-Grand'Maison, C., & Pollard, W. (2018). An Estimate of Ice Wedge Volume for a High Arctic Polar Desert Environment, Fosheim Peninsula, Ellesmere Island. The Cryosphere Discussions, 12, 1–28. https://doi.org/10.5194/tc-2018-29

Bowden, W. B., Gooseff, M. N., Balser, A., Green, A., Peterson, B. J., & Bradford, J. (2008). Sediment and nutrient delivery from thermokarst features in the foothills of the North Slope, Alaska: Potential impacts on headwater stream ecosystems. *Journal of Geophysical Research: Biogeosciences*, *113*(G2).

Burn, C. R., & Kokelj, S. v. (2009). The environment and permafrost of the Mackenzie Delta area. *Permafrost and Periglacial Processes*, *20*(2), 83–105. https://doi.org/10.1002/ppp.655

Campbell-Heaton, K. (2020). *Ice wedge activity in the Eureka Sound Lowlands, Canadian High Arctic* (Master's dissertation, Université d'Ottawa/University of Ottawa).

Campbell-Heaton, K., Lacelle, D., Fisher, D., & Pollard, W. (2021). Holocene ice wedge formation in the Eureka Sound Lowlands, high Arctic Canada. *Quaternary Research*, *102*, 175-187.

Cory, R. M., Crump, B. C., Dobkowski, J. A., & Kling, G. W. (2013). Surface exposure to sunlight stimulates CO2 release from permafrost soil carbon in the Arctic. *Proceedings of the National Academy of Sciences*, *110*(9), 3429-3434.

Couture, N. J., & Pollard, W. H. (1998). An assessment of ground ice volume near eureka, northwest territories. *In Permafrost - Seventh International Converence*, *55*, 195–200.

Dansgaard, W. (1964). Stable isotopes in precipitation. Tellus, 16(4), 436–468. https://doi.org/10.3402/tellusa.v16i4.8993

Dixon, J. C. (2013). Response of Periglacial Geomorphic Processes to Global Change. *Treatise on Geomorphology*, *13*, 176–189. https://doi.org/10.1016/B978-0-12-374739-6.00351-1

Doré, G., Niu, F., & Brooks, H. (2016). Adaptation Methods for Transportation Infrastructure Built on Degrading Permafrost. *Permafrost and Periglacial Processes*, *27*(4), 352–364. https://doi.org/10.1002/ppp.1919

Dyke, A. S., Andrews, J. T., Clark, P. U., England, J. H., Miller, G. H., Shaw, J., & Veillette, J. J. (2002). The Laurentide and Innuitian ice sheets during the Last Glacial Maximum. Quaternary Science Reviews, 21.

Edlund, S. A., & Alt, B. T. (1989). Regional congruence of vegetation and summer climate patterns in the Queen Elizabeth Islands, Northwest Territories, Canada. Arctic, 42(1), 3–23. https://doi.org/10.14430/arctic1635

Edlund, S. A., Alt, B. T., & Garneau, M. (2000). Vegetation patterns on Fosheim Penisula, Ellemere Island, Nunavut. In Bulletin of the Geological Survey of Canada

Embry, A., & Beauchamp, B. (2008). Chapter 13 Sverdrup Basin. Sedimentary Basins of the World, 5(C), 451–471. https://doi.org/10.1016/S1874-5997(08)00013-0

England, J, Atkinson, N., Bednarski, J., Dyke, A. S., Hodgson, D. A., & Ó Cofaigh, C. (2006). The Innuitian Ice Sheet: configuration, dynamics and chronology. Quaternary Science Reviews, 25(7–8), 689–703. https://doi.org/10.1016/j.quascirev.2005.08.007

French, H. M. (2018). *The Periglacial Environment*. John Wiley & Sons.

Frey, K. E., & McClelland, J. W. (2009). Impacts of permafrost degradation on arctic river biogeochemistry. *Hydrological Processes*, *23*(1), 169–182. https://doi.org/10.1002/hyp.7196

Government of Canada. (2025). Historical Climate Data. Retrieved from https://climate.weather.gc.ca/historical_data/

Grom, J. D. (2008). Retrogressive thaw slump process and morphology. *Eureka Sound Lowlands, Ellesmere Island, Nunavut, Canada [MS thesis]: Montreal, McGill University*.

Hindshaw, R. S., Lang, S. Q., Bernasconi, S. M., Heaton, T. H. E., Lindsay, M. R., & Boyd, E. S. (2016). Origin and temporal variability of unusually low δ13C-DOC values in two High Arctic catchments. *Journal of Geophysical Research: Biogeosciences*, *121*(4), 1073-1085.

Hjort, J., Karjalainen, O., Aalto, J., Westermann, S., Romanovsky, V. E., Nelson, F. E., … Luoto, M. (2018). Degrading permafrost puts Arctic infrastructure at risk by mid-century. Nature Communications, 9(1). https://doi.org/10.1038/s41467-018-07557-4

Hodgson, D. A., & Nixon, F. M. (1998). Ground ice volumes determined from shallow cores from western fosheim peninsula ellesmere island, northwest territories. In Bulletin of the Geological Survey of Canada. Ottawa: Government of Canada.

IAEA/WMO. (2018). *Global Network of Isotopes in Precipitation (GNIP) database* [Data set]. International Atomic Energy Agency / World Meteorological Organization. https://www.iaea.org/water

Johnson, M. F., & Wilby, R. L. (2013). Shield or not to shield: Effects of solar radiation on water temperature sensor accuracy. *Water*, *5*(4), 1622-1637.

Kokelj, S. v, Tunnicliffe, J., Lacelle, D., Lantz, T. C., Chin, K. S., & Fraser, R. (2015). Increased precipitation drives mega slump development and destabilization of ice-rich permafrost terrain, northwestern Canada. *Global and Planetary Change*, *129*, 56–68. https://doi.org/10.1016/j.gloplacha.2015.02.008

Kokelj, S. V., & Lewkowicz, A. G. (1999). Salinization of permafrost terrain due to natural geomorphic disturbance, Fosheim Peninsula, Ellesmere Island. Arctic, 372-385.

Kokelj, S. V., Jenkins, R. E., Milburn, D., Burn, C. R., & Snow, N. (2005). The influence of thermokarst disturbance on the water quality of small upland lakes, Mackenzie Delta region, Northwest Territories, Canada. *Permafrost and Periglacial Processes*, *16*(4), 343-353.

Kokelj, S. V., Lacelle, D., Lantz, T. C., Tunnicliffe, J., Malone, L., Clark, I. D., & Chin, K. S. (2013). Thawing of massive ground ice in mega slumps drives increases in stream sediment and solute flux across a range of watershed scales. *Journal of Geophysical Research: Earth Surface*, *118*(2), 681-692.

Lacelle, D., Bjornson, J., & Lauriol, B. (2010). Climatic and geomorphic factors affecting contemporary (1950-2004) activity of retrogressive thaw slumps on the Aklavik Plateau, Richardson Mountains, NWT, Canada. *Permafrost and Periglacial Processes*, *21*(1), 1–15. https://doi.org/10.1002/ppp.666

Lacelle, D., Brooker, A., Fraser, R. H., & Kokelj, S. V. (2015). Distribution and growth of thaw slumps in the Richardson Mountains–Peel Plateau region, northwestern Canada. Geomorphology, 235, 40-51.

Lacelle, D., Fontaine, M., Pellerin, A., Kokelj, S. V., & Clark, I. D. (2019). Legacy of holocene landscape changes on soil biogeochemistry: a perspective from paleo-active layers in Northwestern Canada. *Journal of Geophysical Research: Biogeosciences*, *124*(9), 2662-2679.

Lafrenière, M. J., & Lamoureux, S. F. (2019). Effects of changing permafrost conditions on hydrological processes and fluvial fluxes. *Earth-science reviews*, *191*, 212-223.

Lamhonwah, D., Lafrenière, M. J., Lamoureux, S. F., & Wolfe, B. B. (2016). Multi-year impacts of permafrost disturbance and thermal perturbation on High Arctic stream chemistry. Arctic Science, 3(2), 254-276.

Lantuit, H., & Pollard, W. H. (2008). Fifty years of coastal erosion and retrogressive thaw slump activity on Herschel Island, southern Beaufort Sea, Yukon Territory, Canada. *Geomorphology*, *95*(1–2), 84–102. https://doi.org/10.1016/j.geomorph.2006.07.040

Lewkowicz, A. G. (1990). Morphology, frequency and magnitude of active-layer detachment slides, Fosheim Peninsula, Ellesmere Island, NWT. In Proceedings of the 5th Canadian permafrost conference (Vol. 54, pp. 111-118). Université Laval: Québec.

Lewkowicz, A. G. (2001). Temperature regime of a small sandstone tor, latitude 80 N, Ellesmere Island, Nunavut, Canada. Permafrost and Periglacial Processes, 12(4), 351-366.

Lewkowicz, A. G. (2007). Dynamics of active-layer detachment failures, Fosheim peninsula, Ellesmere Island, Nunavut, Canada. Permafrost and Periglacial Processes, 18(1), 89-103.

Lewkowicz, A. G., & Way, R. G. (2019). Extremes of summer climate trigger thousands of thermokarst landslides in a High Arctic environment. *Nature Communications (Resubmitted December 2018)*, *10*(1), 1329. https://doi.org/10.1038/s41467-019-09314-7

Littlefair, C. A., Tank, S. E., & Kokelj, S. V. (2017). Retrogressive thaw slumps temper dissolved organic carbon delivery to streams of the Peel Plateau, NWT, Canada. *Biogeosciences*, *14*(23), 5487-5505.

Mackay, J. R. (1966). Segregated epigenetic ice and slumps in permafrost, Mackenzie Delta area, N.W.T. *Geographical Bulletin*, *8*, 59–80. https://cir.nii.ac.jp/crid/1570854174364600320.bib?lang=en

Malone, L., Lacelle, D., Kokelj, S., & Clark, I. D. (2013). Impacts of hillslope thaw slumps on the geochemistry of permafrost catchments (Stony Creek watershed, NWT, Canada). *Chemical Geology*, *356*, 38-49.

Miall, A. D. (1986). Eureka Sound Group. Bullitin of Canadian Petroleum Geology, 34(2), 240–270.

Millero, F. J., Feistel, R., Wright, D. G., & McDougall, T. J. (2008). The composition of Standard Seawater and the definition of the Reference-Composition Salinity Scale. *Deep Sea Research Part I: Oceanographic Research Papers*, *55*(1), 50-72.

Möller, D. (1990). The Na/Cl ratio in rainwater and the seasalt chloride cycle. Tellus B, 42(3), 254-262.

Pollard, W. (2000). Distribution and characterization of ground ice on Fosheim Peninsula, Ellesmere Island, Nunavut. In Garneau, M. & Alt, B. T. (eds.), Environmental response to climate change in the Canadian High Arctic, Geological Survey of Canada, Bulletin, 529, 175-196. Natural Resources Canada.

Pollard, W., Ward, M., & Becker, M. (2015). The Eureka Sound lowlands: an ice-rich permafrost landscape in transition. *Proceedings of GeoQuebec*.

R Core Team (2025). _R: A Language and Environment for Statistical Computing_. R Foundation for Statistical Computing, Vienna, Austria. <https://www.R-project.org/>.

Raymond, P. A., McClelland, J. W., Holmes, R. M., Zhulidov, A. V., Mull, K., Peterson, B. J., ... & Gurtovaya, T. Y. (2007). Flux and age of dissolved organic carbon exported to the Arctic Ocean: A carbon isotopic study of the five largest arctic rivers. *Global Biogeochemical Cycles*, *21*(4).

Roy, C. (2018). Origin of massive ground ice in the Eureka Sound Lowlands, Nunavut. Master's Thesis, McGill University.

Roy, C., Campbell-Heaton, K., Lacelle, D., & Pollard, W. (2023). Massive ground ice of glacial meltwater origin in raised marine-deltaic sediments, Fosheim Peninsula, high Arctic Canada. *Quaternary Research*, *116*, 96-107.

Simon, K. M., James, T. S., & Dyke, A. S. (2015). A new glacial isostatic adjustment model of the Innuitian Ice Sheet, Arctic Canada. Quaternary Science Reviews. https://doi.org/10.1016/j.quascirev.2015.04.007

Solinst Canada Ltd. (2024, October 18). *Levelogger 5 LTC: Data sheet* [PDF]. https://www.solinst.com/products/data/3001-ltc.pdf

Spencer, R. G., Mann, P. J., Dittmar, T., Eglinton, T. I., McIntyre, C., Holmes, R. M., ... & Stubbins, A. (2015). Detecting the signature of permafrost thaw in Arctic rivers. *Geophysical Research Letters*, *42*(8), 2830-2835.

St-Jean, G. (2003). Automated quantitative and isotopic (13C) analysis of dissolved inorganic carbon and dissolved organic carbon in continuous-flow using a total organic carbon analyser. Rapid Communications in Mass Spectrometry, 17(5), 419–428. https://doi.org/10.1002/rcm.926

Vonk, J. E., Mann, P. J., Davydov, S., Davydova, A., Spencer, R. G., Schade, J., ... & Holmes, R. M. (2013). High biolability of ancient permafrost carbon upon thaw. *Geophysical Research Letters*, *40*(11), 2689-2693.

Wang, J. J., Lafreniere, M. J., Lamoureux, S. F., Simpson, A. J., Gelinas, Y., & Simpson, M. J. (2018). Differences in riverine and pond water dissolved organic matter composition and sources in Canadian high Arctic watersheds affected by active layer detachments. *Environmental science & technology*, *52*(3), 1062-1071.

Ward Jones, M. K., & Pollard, W. H. (2021). Daily field observations of retrogressive thaw slump dynamics in the Canadian high arctic. *Arctic*, *74*(3), 339–354. https://doi.org/10.14430/arctic73377

Ward Jones, M. K., Pollard, W. H., & Amyot, F. (2020). Impacts of degrading ice-wedges on ground temperatures in a high Arctic polar desert system. *Journal of Geophysical Research: Earth Surface*, *125*(3), e2019JF005173.

Ward Jones, M. K., Pollard, W. H., & Jones, B. M. (2019). Rapid initialization of retrogressive thaw slumps in the Canadian high Arctic and their response to climate and terrain factors. *Environmental Research Letters*, *14*(5). https://doi.org/10.1088/1748-9326/ab12fd

Wolfe, S. A., Kotler, E., & Dallimore, S. R. (2001). Surficial characteristics and the distribution of thaw landforms (1970 to 1999), Shingle Point to Kay Point, Yukon Territory. *Geological Survey of Canada, Open File*, *4088*.

Woo, M. (1990). Consequences of Climatic Change for Hydrology in Permafrost Zones. *Journal of Cold Regions Engineering*, *4*(1), 15–20. https://doi.org/10.1061/(asce)0887-381x(1990)4:1(15)

3.9 Captions

Table 3.1. Slump characteristics, approximate size in hectares evaluated via satellite imagery, status and approximate straight-line distance to the respective stream. Evaluated 2023 from high-resolution imagery.

Table 3.2. Average concentration of major ions for massive ice and ice wedges for Eureka, Nunavut. Concentrations reported in mg/L, massive ice samples collected in July 2017, ice wedges collected in July 2019.

Table 3.3. Average ion concentrations (Cl^-, Ca, Mg and Na) for undisturbed, thaw runoff and disturbed study sites within the Blacktop and Station creek watersheds. Ion concentrations in ppm.

Figure 3.1. Site map of Eureka and surrounding area. Extent of Station Creek watershed outlined by large black dashes, small black dashes indicate the extent of Blacktop creek watershed. Marine limit (~146 m asl) outlined by grey dashed lines. Elevation presented in meters above sea level. Slumps monitored in this study are indicated with a black star.

Figure 3.2. $\delta^{18}O$~D for Station creek and Blacktop creek in 2022 and 2023. Data is coloured by sampling day (dark - early to light -late) and symbol (circle/triangle) represents disturbed and undisturbed sites. Local Meteoric water line (LMWL; blue; IAEA/WMO, 2018) and Global Meteoric Water Line (GMWL; black).

Figure 3.3. Scholler plot of major ions from stream chemistry for Station creek and Blacktop creek. Plots divided by disturbance and coloured by site, mean value presented per ion, mean Total Dissolved Solids (TDS) per site also included.

Figure 3.4. Time series of molar ratio between (A) sulphate and chloride and (B) sodium and chloride for Station creek and Blacktop creek for July 2022 and 2023. Data is divided by disturbance (shape) and sampling location (colour).

Figure 3.5. Time series of stream chloride (Cl^-), sulphate (SO_4) and TDS concentrations (mg/L) for July 2022 and 2023.

3.10 Tables

Table 3.1. Slump characteristics, approximate size in hectares evaluated via satellite imagery, status and approximate straight-line distance to the respective stream. Evaluated 2023 from high-resolution imagery.

Slump Name	Area (Ha)	Status	Distance to Stream (m)
Nunavut Slump	4.5	Active	700
Blacktop Slump	1.1	Inactive	720
BL Slump	0.1	Active	70
CHP Slump	3.5	Active	950

Table 3.2. Average concentration of major ions for massive ice and ice wedges for Eureka, Nunavut. Concentrations reported in mg/L, massive ice samples collected in July 2017, ice wedges collected in July 2019.

Ion	Massive Ice	Ice Wedge
Ca (mg/l)	11.64	16.90
Mg (mg/l)	4.72	7.39
K (mg/l)	5.17	4.22
Na (mg/l)	33.78	43.70
SO_4 (mg/l)	12.93	50.03
Cl (mg/l)	58.41	57.10
TDS	**132.79**	**180.64**

Table 3.3. Average ion concentrations (Cl^-, Ca, Mg and Na) for undisturbed, thaw runoff and disturbed study sites within the Blacktop and Station creek watersheds. Ion concentrations in ppm.

			No. Samples	Chloride	Calcium	Magnesium	Sodium
Blacktop Creek	Undisturbed	3 2022	10	11.88±2.44	23.29±3.74	13.50±2.41	10.29±2.21
		3 2023	8	10.92±2.05	39.30±4.65	19.40±0.81	22.43±8.05
	Thaw runoff	BC		2360.70±944.34	139.03±40.54	125.44±52.76	1113.37±476.64
	Disturbed	2 2022	12	21.78±7.62	23.95±3.45	14.14±2.34	15.37±3.71
		2 2023 LS	8	14.68±3.52	29.24±9.48	15.20±5.77	14.96±8.91
		2 2023 RS	8	13.59±3.73	36.36±5.26	17.42±0.94	19.41±7.17
		1 2022	16	23.02±7.78	25.42±4.22	15.13±2.83	16.43±4.72
		1 2023	9	16.89±4.58	26.56±5.18	14.04±1.24	14.41±6.27
Station Creek	Undisturbed	7 2023	7	19.64±7.16	53.78±24.38	21.63±11.5	38.07±30.41
	Thaw runoff	SC		2556.38±1848.74	112.8±63.42	110.71±77.02	1290.22±898.79
	Disturbed	6 2022	12	20.07±8.89	30.75±5.46	14.47±2.51	25.16±7.00
		6 2023	8	32.90±18.80	48.41±24.65	19.09±11.51	33.11±26.76
		5 2022	12	16.42±3.45	31.05±5.15	14.89±2.41	24.51±4.86
		5 2023	8	49.91±29.84	47.27±16.32	19.85±7.89	31.65±18.12
		5 2023 SC	5	22.88±9.94	58.28±17.56	24.81±8.68	47.02±25.87
		4 2022	17	19.49±8.41	30.88±5.96	14.93±2.88	25.42±6.95
		4 2023	9	46.60±37.14	42.96±9.27	18.95±3.05	25.48±11.83

3.11 Figures

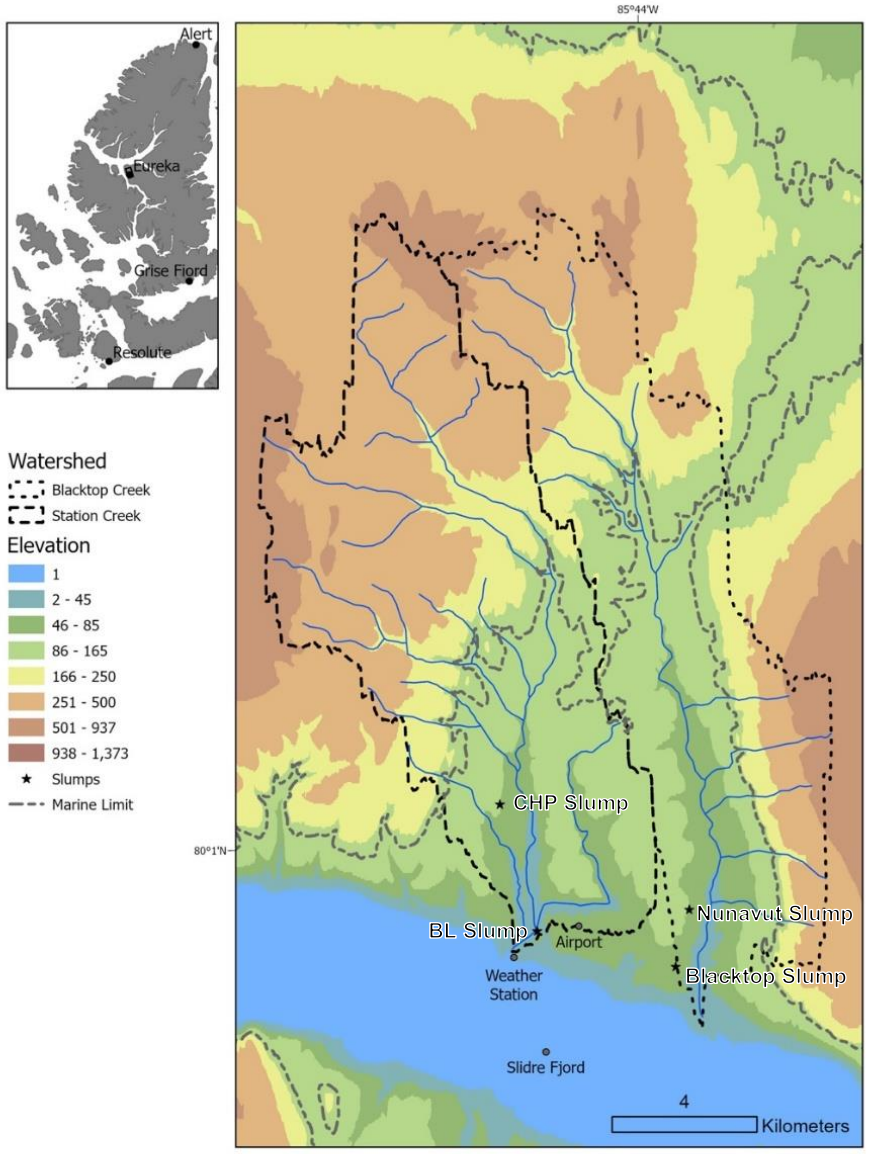


Figure 3.1. Site map of Eureka and surrounding area. Extent of Station Creek watershed outlined by large black dashes, small black dashes indicate the extent of Blacktop creek watershed. Marine limit (~146 m asl) outlined by grey dashed lines. Elevation presented in meters above sea level. Slumps monitored in this study are indicated with a black star.

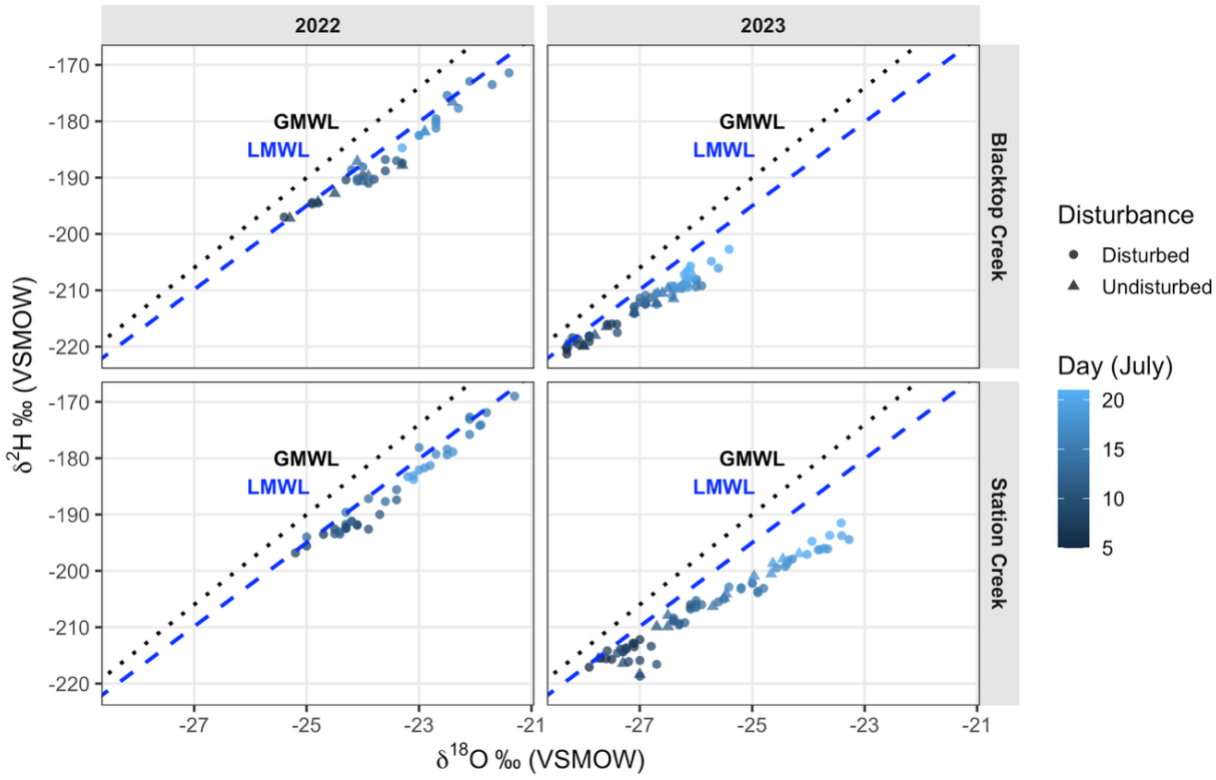


Figure 3.2. $\delta^{18}O$~D for Station creek and Blacktop creek in 2022 and 2023. Data is coloured by sampling day (dark - early to light -late) and symbol (circle/triangle) represents disturbed and undisturbed sites. Local Meteoric water line (LMWL; blue; IAEA/WMO, 2018) and Global Meteoric Water Line (GMWL; black).

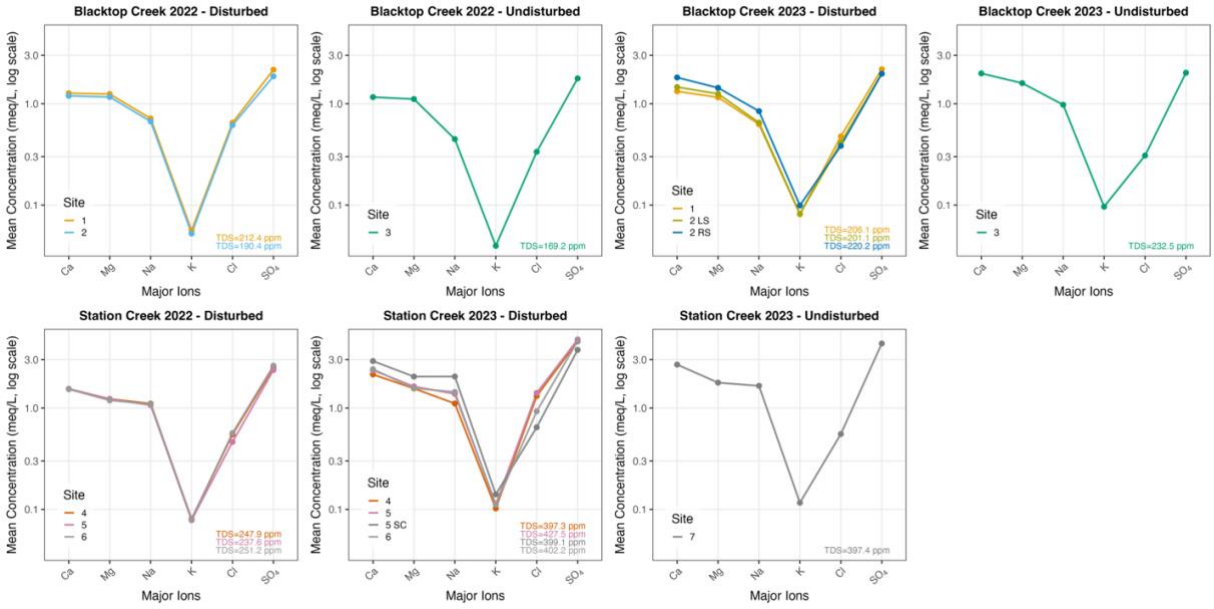
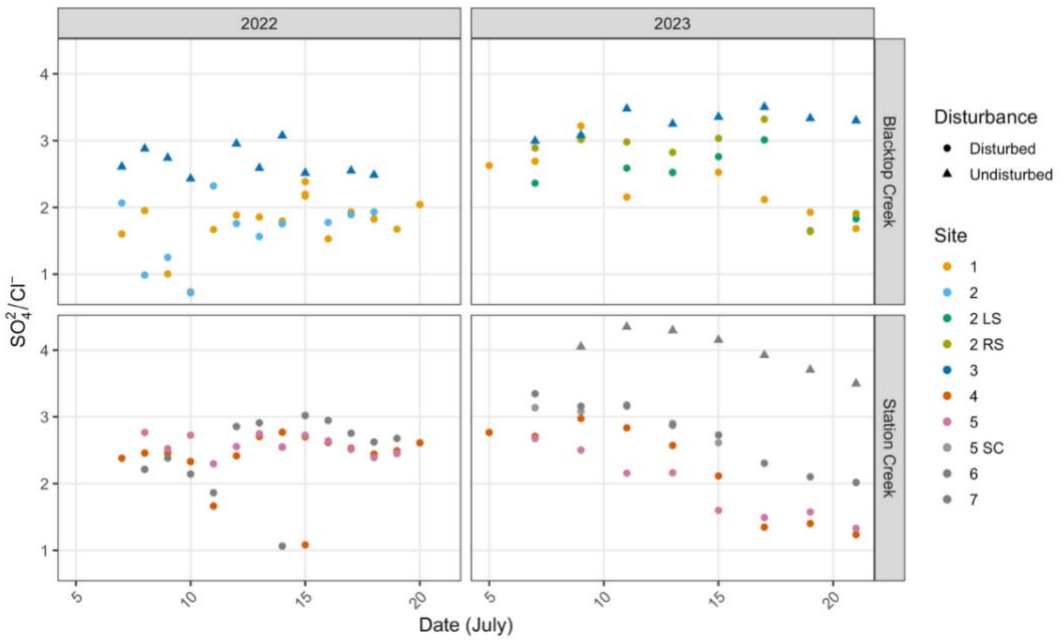


Figure 3.3. Scholler plot of major ions from stream chemistry for Station creek and Blacktop creek. Plots divided by disturbance and coloured by site, mean value presented per ion, mean Total Dissolved Solids (TDS) per site also included.

A



B

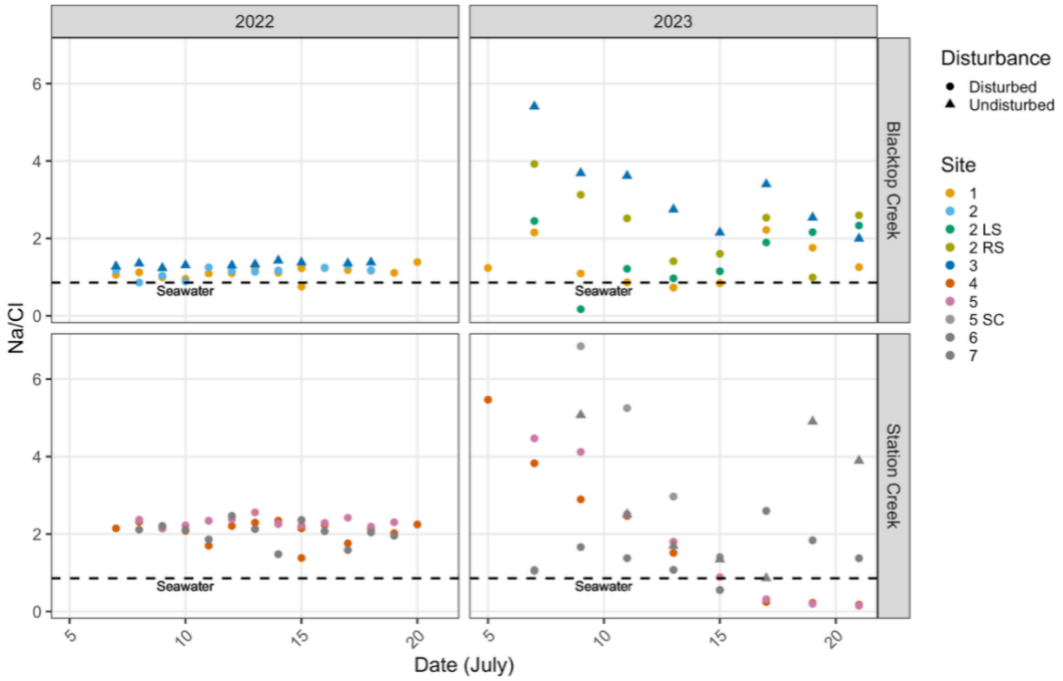


Figure 3.4. Time series of molar ratio between (A) sulphate and chloride and (B) sodium and chloride for Station creek and Blacktop creek for July 2022 and 2023. Data is divided by disturbance (shape) and sampling location (colour).

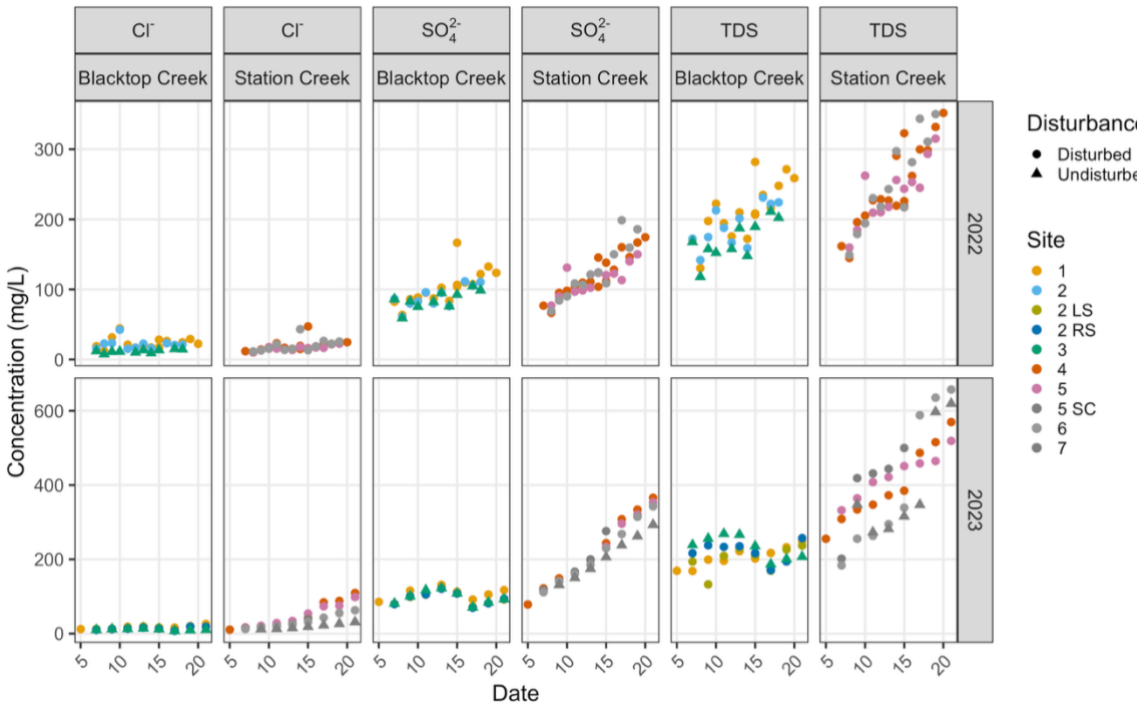


Figure 3.5. Time series of stream chloride (Cl^-), sulphate (SO_4) and TDS concentrations (mg/L) for July 2022 and 2023.

Chapter 4

Impact of Climate and Permafrost Thaw Disturbances on High Arctic Nival Stream Summer Regimes; Case Study from Eureka, Nunavut.

Kethra Campbell-Heaton[1], Denis Lacelle[1]

[1]Department of Geography, Environment and Geomatics, University of Ottawa, Ottawa, ON, Canada

Abstract

High Arctic streams remain underrepresented in hydrological research due to their remoteness. This study presents stream temperature, discharge, and suspended sediment load data from two nival-dominated streams near Eureka, Nunavut (79.98°N, 85.95°W), collected over two contrasting summers: a cold–wet 2022 and a warm–dry 2023. Stream conditions were monitored with Solinst Levelogger-5 sensors recording temperature, water level, and conductivity at 30-minute intervals, with three loggers deployed per stream. Daily suspended sediment samples and 7–10 manual discharge measurements were collected at seven sites along the study reaches. Mean stream temperature was ~3°C warmer in 2023 than in 2022, with intra-stream variability governed primarily by fluvial geomorphology and temperature inversion rather than thermokarst activity. Climate–temperature relationships shifted between years, from strong air temperature control in the cold–wet year (avg. among sites $r = 0.76$) to stronger solar radiation influence in the warm–dry year (avg. among sites $r = 0.56$). Discharge was greater and more variable in 2022, while suspended sediment and dissolved particulate loads were significantly elevated downstream of thaw slumps during the dry 2023 season ($p < 0.05$ for both streams). Collectively, these results show that climate regime strongly mediates the thermal and sedimentary behaviour of High Arctic streams, emphasizing the need for sustained monitoring to capture interannual variability.

Keywords. High Arctic streams, Nival-Streams, Discharge, Sediment load, Climate variability, Thermokarst.

4.1 Introduction

Nival streams are predominantly snowmelt fed, characterized by high spring freshets, intermittently peaked by summer rain events, and which taper off quickly to low baseflow or no flow in the winter. The majority (90%) of continuously monitored (by the Canadian Hydrometric Service) nival streams are in Atlantic Canada near the St. Lawrence (Zaerpour et al., 2021). In the Arctic and Subarctic, nival streams are affected by permafrost, which restricts ground water movement and as a result, baseflow. Nival Subarctic streams can be characterized as *winter-dry* or *perennial*: winter-dry streams cease flowing during the winter resulting in dry, ice-less riverbeds, whereas larger Subarctic rivers maintain low winter baseflow, often beneath ice cover (Church, 1974). The freshet of Arctic nival streams is typically the most severe flooding as rain events in the Arctic are less intense and infrequent (Church, 1974). This spring flood is the main mechanism for sediment transport in High Arctic nival streams (McDonald & Lamoureux, 2009; Woo, 2012).

With climate change, Western Arctic nival streams are responding to an earlier spring runoff (Dery et al., 2009). This has also been observed in the High Arctic (Melville Island), Favaro and Lamoureux (2015) recorded a decline in snowmelt driven runoff and stream sediment yield between 2010 and 2012. This decline is attributed the presence of snowbanks in the stream channel which buffer the stream bed and bank from erosion during the bulk melt period (Favaro & Lamoureux, 2015). In that year, the sediment yield of the stream was greater post-melt due to permafrost degradation and related localized disturbances (Favaro & Lamoureux, 2015). However, the effect of permafrost disturbance on stream sediment yield is suspected to be much weaker than the shift towards a pluvial-dominated hydrological regime in the high arctic (Beel et al, 2018). More recent research from this region is showing a shift in hydrological regime from nival to pluvial and nival dominated, a shift which is ubiquitous to watersheds in the high and low Arctic (Beel et al., 2021). A warmer, wetter thaw season is increasing the stream's erosive power later in the year, resulting in greater sediment and carbon transfer (Beel et al., 2021). This increase in summer and fall rain events is expected to have a significant effect on landscape change, stream sediment yield and carbon exchange than arctic greening and thermokarst activity (Beel et al., 2018; 2021).

This study will focus on stream response to climate and thermokarst pressures in two nival, polar desert streams located in Eureka, Nunavut (80˚00'N, 85˚56'W). Data was collected over two summers, July 2022 and July 2023, each with different climates. Both streams are affected by active thaw slumps which range in life stage (just initiated to ceased). The objective of this study is threefold: 1) determine the streams' temperature response to climatic pressures, 2) establish a rating curve for each stream and 3) determine the effects of thaw slumping to stream solute and sediment load. This study will provide valuable information on the stream-climate response of these hard to

access high arctic streams, the influence of thermokarst activity and the potential repercussions to aquatic and terrestrial communities.

4.2 Study Site

The study site, Eureka, is located on the Fosheim peninsula on the south-western side of Ellesmere Island. Situated within an intermontane area, Eureka is surrounded on three sides by tall mastifs (>1000 m a.s.l.). Deglaciation of the region began 10.3-8.7 ka BP and ice retreated inland to current extents on Ellesmere and Axel Heiberg Island (England et al., 2006). Marine inundation occurred until 8.8-7.8 ka BP and covered approximately 1/3 of the peninsula. Modern Holocene marine limit varies between 139 -150 m asl on the FP; near the Eureka Weather station, the marine limit reaches 143 m asl (Bell, 1996).

Surficial materials consist of weathered bedrock, blanket and veneer till, glaciofluvial in meltwater channels above marine limit and Holocene marine sediments (clay – silt) below marine limit (Hodgson and Nixon, 1998, Bell & Hodgson, 2000; Young & Woo, 2000). Minor surficial units on the FP are fluvial, eolian, organic deposits and colluvium (Bell and Hodgson, 2000).

The Eureka Sound Lowlands is a polar desert (Edlund et al., 2000), with a cold winter and cool summer temperatures and little precipitation. Between 1991-2021, the mean annual air temperature (MAAT) for Eureka was -18.0±1.2°C (Government of Canada, 2025). The MAAT at Eureka shows strong inter-annual variations and has experienced a general increase in MAAT since the 1980s at a rate of 0.53°C decade^{-1} over the period 1980-2019. Average annual precipitation for Eureka is low (1991-2021: 77.0 ± 23.0 mm y-1, with ~80% falling as snow; Fig. 2; Government of Canada, 2025). The average snow depth in Eureka is 12.1 ± 8.3 cm between 1991-2021 (Government of Canada, 2025). Maximum snow depths are reached in early April and decrease rapidly with spring snowmelt (Alt & Maxwell, 2000). Rainfall events are typically low (<0.03 mm) but can reach >10 mm. Total precipitation increased at a rate of 1.26 mm decade^{-1} over the period 1950 to 2019. The low precipitation around Eureka is attributed to the surrounding topography which blocks cold ocean air masses and creates a rain-shadow (Edlund & Alt, 1989; Bell, 1996; Alt & Maxwell, 2000). The FP is classified as Enriched Prostrate Shrub Zone, characterized as having the greatest diversity and density of vascular plant species of the Queen Elizabeth Islands (Edlund et al., 2000; Edlund & Alt, 1989).

The Eureka Sound Lowlands is located within the continuous permafrost zone, with permafrost >500m thick (Pollard et al., 2015). The active layer depth is between 10 and 100 cm and averages ~60 cm (Hodgson & Nixon, 1998). Tundra polygon (formed by ice wedge activity) is the main periglacial landform in the region, covering approximately 50% of the Fosheim

Peninsula, with the majority found within marine limit (140m a.s.l.; Bernard-Grand'Maison and Pollard, 2018). Thaw slumps and active layer detachment slides are the other main permafrost landforms found in the area. Ground ice in the Fosheim region is estimated to occupy 30% vol of the uppermost 6 m of permafrost (Couture & Pollard, 1998). Of that, 3.5% vol is estimated to be wedge ice and the remaining occurs mostly as tabular bodies of massive ice (Couture & Pollard, 1998).

The increasing MAAT over the past 40 years has implications on the stability of permafrost in the Eureka Sound Lowlands (ex. Pollard et al., 2015). Tundra polygons and ice wedges were found to be degrading at a rate synchronous with the active layer thickening; the number of active thaw slumps have also been increasing (Pollard et al., 2015). The troughs of tundra polygons in the Eureka Sound Lowlands experienced a significant amount of degradation for a cold polar desert, such changes include trough subsidence, increase in ponding water and an increase in melt out events (Ward Jones et al., 2020). Permafrost in this region is highly responsive to changing climate conditions because of the thin (if any) organic soil layer and low vegetation cover (Ward-Jones et al., 2019).

4.2.1 Watershed Characteristics

This project focuses on two streams in the Eureka area: Blacktop Creek (BC) and Station Creek (SC). The watersheds for these streams are adjacent each other and similar in size, BC has an approximate area of 98 km^2 and SC approximate area of 111 km^2. Watershed size was calculated using ArcGIS Pro Watershed tool from the Spatial Analyst extension; actual catchment might be greater/smaller in person. Maximum elevation in the watersheds differ, BC has a maximum elevation of 820 m a.s.l. and SC has a maximum elevation of 660 m a.s.l. Both watersheds have similar surficial materials, in high elevations (above marine limit) the primary material is colluvial rubble and fine grained (glacio) marine sediments at lower elevations (below marine limit). Percent of the watersheds that are below marine limit for Blacktop creek and Station creek is 37% and 33%, respectively. Within this zone, as the stream reaches the fjord, the streams transition from weathered river stone to braided streams with large amounts of fine sediments. Permafrost thaw is a contributing factor to water and sediment redistribution in both watersheds. The main thaw feature is retrogressive thaw slumps; both watersheds are impacted by thaw slumping to varying degrees. Blacktop creek watershed has two known slumps, one of which was not active in during the period of study. Station creek also has two known active thaw slumps, and six inactive slumps (Ward Jones et al., 2019). Chemical effects to stream quality from slump runoff for this period is detailed in Chapter 4.

4.3 Methods

4.3.1 Passive Stream Monitoring

4.3.1.1 Logger deployment:

Six Solinst Levellogger 5 LTC sensors (Solinst Canada, 2024) were deployed in 2022 and 2023; one was positioned above an active thaw slump, one below and a third near the stream outlet in both streams. These dataloggers recorded the water level (m), temperature (°C) and conductivity (µS/cm) at a 30-minute interval. Each logger was housed in perforated PVC pipe to reduce solar heating and physical disturbance (Johnson & Wilby, 2013). In 2022, the loggers were attached to fine (1/8") metal cable and one wooden stake at the stream edge. The logger and casing were fixed to a large rock (slightly bigger than a brick) and positioned in the thalweg of the stream. Rain events washed several of the loggers out of place, these were repositioned once identified back to their original location. In 2023, we used a two-cable system, one on either bank and a 3' steel rod hammered into the creek bed at the thalweg. The combination of steel rod and cables kept the logger in place (loggers were zip-tied to the steel rod). We did find that we had to lower the logger after approximately a week after installed as the water level had dropped enough to reveal the logger casing. These manual adjustments to the logger in the stream were obvious in the water level data, the following section details how the data was adjusted to accommodate these manual adjustments.

4.3.1.2 Water-level data processing:

Arctic rivers exhibit large seasonal and episodic variability in discharge and particulate export (Holmes et al., 2012; McClelland et al., 2016). Therefore, stage data were screened for abrupt, non-hydrological step-changes associated with occasional logger displacement during high flows. In 2022, the loggers were occasionally found 1-2 meters downstream after a rain event. Sudden changes in water level where level was >2 cm than the previous reading was classified as artificial (anomalous events) and corrected using a segment-based cumulative offset procedure (full workflow in Appendix S1). This approach restored continuity while preserving natural hydrologic variability.

4.3.2 Total Suspended Sediment and Total Dissolved Particulates

Traditional studies of Arctic stream sediments will filter water samples prior to gravimetric analysis, measuring only suspended solids while excluding dissolved particulates (i.e., Forbes & Lamoureux, 2005; Favaro & Lamoureux, 2015; Beel et al., 2018). However, in High Arctic nival streams influenced by permafrost thaw, both ultra-fine suspended material and dissolved

particulates contribute to total sediment flux and can be missed by filtered methods (Kokelj et al., 2013; Coch et al., 2020). To capture the full spectrum of particulate transport, we measured total solids gravimetrically without pre-filtration. This approach preserves ultrafine particulates (<0.45um), including colloidal material which has been shown to be chemically and ecologically significant in Arctic aquatic ecosystems (Manasypov et al., 2023), providing a more complete representation of total particulate load (TSS + TDP).

Stream water samples were collected at the stream's thalweg at each site into 50-60mL plastic tubes, sealed and shipped back to the University of Ottawa where they were stored at 4℃. Samples were weighted to 0.0001 gram in the original sample bottle without the lid, placed in an oven at 60℃ for 1 week or until completely dry. Samples were reweighed then washed with soap and warm water (soaked for 20 mins) and transferred to ultrasonic bath to remove any remaining material. Each bottle was visually checked for sediment before the ultrasonic bath. Bottles were then placed back in the oven at 60℃ to dry for 2-3 hours or until completely dry and weighed again. The amount of water was calculated by subtracting the weight of the bottle from the wet and dry weight then subtracting the dry weight from the wet weight, water weight was converted to volume (L) by assuming 1g=1mL and dividing by 1000. Weight of sediment was calculated by subtracting the clean bottle weight from the dried sample weight. Then converted to sediment load (mg/L) by multiplying the sediment weight by 1000 (g > mg) and dividing by the water volume of sample.

This method is different than most Arctic studies which examine suspended sediment load which collects 1L samples, pre-weighs filters and uses the dried filtered sample weight. The filtered water is used for other analysis. In our case, the sampled amount was smaller, but this method allows for no loss of ultra fine-grained material and, we had already reserved samples for other analyses, so we had no need for the collected water. The remaining weight provides the combined Total Suspended Solids (TSS) and the Total Dissolved Solids (TDS).

4.3.3 Manual Discharge

At each site, the goal was to collect ten manual discharge measurements throughout the course of the study period to compliment continuous water-level data. The stream was subdivided into 10 sections, and the velocity was measured at 60% depth using a Geopacks Stream Flow-meter, recorded three times per section to calculate the average velocity (m/s). All stream sections were shallower than 1 meter. Discharge was then determined via the velocity-area method (Hendriks, 2010). Although labour-intensive, frequent and numerous discharge measurements improve the accuracy of the streams' rating curve, particularly important for High Arctic streams where flow is highly variable (Favaro & Lamoureux, 2015). Measurement frequency varied between study years

with fewer measurements in 2022. Observed variations in discharge were influenced by rainfall, stream geomorphology, and localized thermokarst activity.

Stage-discharge relationships were established for each site using the manual recorded discharge measurements and the concurrent water level data from Solinst LevelLogger 5 LTC (Solinst, 2024). A rating curve was created for each site, and the stage-discharge relationship was established using the following equation.

$$Q=a(h-h_0)^b \quad \text{Eq. 2}$$

Where Q is the discharge, a and b are coefficients determined with the rating curve, h is the stage and h_0 is the stage height with zero flow (Hendriks, 2010). Each site and year was treated individually due to differences in hydrologic behaviour and flow regime. Model fit was evaluated by comparing predicted and measured discharges, with deviations associated with localized thaw slump activity and rain events. The majority of rating curves had an error rate below 10%.

4.3.4 Data Analysis

The remainder of the data analysis was conducted in R (Version 2025.05.0+496; R Core Team, 2025). Summary statistics were calculated using the R base packages and plots were created using the package GGPLOT2. One-way ANOVA was used to test for significant differences between mean daily water temperature and daily sediment load among sites within each stream and year. Post-hoc Tukey HSD test was applied to identify which pairs of sites differed significantly. Exploratory relationships between stream temperature and climate variables were assessed using Pearson correlation in R (using function "cor()"). Because the hourly environmental data exhibit temporal autocorrelation and the study period is short, correlation coefficients likely overestimate statistical significance. Accordingly, correlations are interpreted as indicators of thermal coupling rather than causal relationships. With longer time series, future work could apply time-series models such as ARIMA (ie., Docherty et al., 2019) to more formally account for serial dependence.

Climate data (air temperature, precipitation, relative humidity) were obtained from Environment Canada at two elevations in Eureka (Station: 10 m a.s.l. and Airport: 80 m a.s.l.; Government of Canada, 2025). Solar position (elevation and azimuth) was calculated using NOAA's solar position calculator (Cornwall et al., 2025). Potential incoming shortwave radiation at the top of the atmosphere was then estimated from solar elevation using a solar constant of 1361 W m^{-2}, consistent with the formulations embedded in the NOAA algorithm. Correlation matrices were generated to identify relationships between stream temperature, climate and solar forcings. Analyses focussed on data from two specific intervals: 2022-07-08 11:30 to 2022-07-18 16:30 and

2023-07-09 17:30 to 2023-07-20 9:30. This was because each logger was started and stopped at different periods.

4.4 Results & Discussion

4.4.1 Temperature Response of Two Nival-Dominated Streams.

Mean stream temperature differed substantially between the two years, with 2022 being ~3°C cooler than 2023 (10.3±2.7°C and 13.0±2.3°C, respectively). In both years, Station Creek and Blacktop Creek only vary by ~0.3°C from each other. The two creeks can get quite warm; maximum recorded water temperature over the two years was 19.7°C at station 4 on July 16th, 2022. Water temperature varies between sites along the stream (Fig. 4.2D & E). In 2022, Blacktop Creek (BC) mean water temperature was coldest at the thaw undisturbed location, Site 3 (10.1±2.9°C, n=728), nearly identical to Site 2 (10.1±2.9°C, n=536) whereas Site 1, the furthest most downstream site was slightly warmer (10.2±2.8 °C, n=533). In 2022, Station Creek (SC) was warmer with mean water temperature at Site 6 being 10.3±2.8°C, at Site 5 10.3±2.8°C, and Site 4 10.2±2.7°C. All sites are down stream of slump activity, and the coldest site is the furthest downstream (Site 4). In 2023, BC Site 3 had a mean temperature 13.7±2.2°C, Site 2 13.8±2.3°C and Site 1 13.6±2.1°C. Comparatively, at SC Site 7, temperature was 13.8±1.8°C, Site 5 13.5±2.2°C and Site 4 was 12.8±2.1°C. A one-way ANOVA tested whether mean daily summer temperature differed among sites within each stream year. Mild short-range autocorrelation was detected within model residuals, an expected result for environmental time series and does not invalidate ANOVA on daily means. Only Station Creek in 2023 showed a significant difference between sites ($F = 3.263$, $p=0.051$). Tukey HSD post-hoc comparisons indicated that Site 7 (undisturbed) differed significantly from Site 4 (thaw disturbed, located far from source). However, Site 7 (undisturbed) did not differ from Site 5 (directly thaw disturbed, located close to source), suggesting that thaw disturbance alone does not explain spatial daily temperature patterns within the stream reach.

The observed spatial patterns in stream temperature are more likely controlled by local geomorphology, elevation and temperature inversion rather than by thaw-slump influence. Similar controls have been documented for nival streams in Greenland where the spatial and temporal variability in stream temperature is largely related to climate conditions, geology and local geomorphology (Docherty et al., 2018). In 2022, Blacktop creek warmed slightly as it reaches the outlet, whereas Station Creek shows the opposite trend (Figure 4.3). This contrast is consistent with their differing geomorphic settings: Blacktop Creek's broad, low-gradient alluvial fan provides greater sun exposure whereas Station Creek's is narrower and more confined, lowering solar

heating. Air temperature patterns support this interpretation. In 2022, air temperatures recorded at the airport and station differ only slightly (Fig. 4.2B), indicating a weak inversion and suggesting that intra-stream temperature differences were driven primarily by geomorphology. In contrast, 2023 exhibited a stronger temperature inversion with markedly cooler temperatures near the fjord. Similarly, stream temperatures were both cooler in their downstream sites. The effect was strongest at Station Creek, Site 4, an already shaded, geomorphologically constrained reach which results in temperatures more than a degree lower than upstream sites. Together, these results show that intra-stream temperature patterns in the Eureka region vary from year to year and are not consistently influenced by nearby thaw slumps. Instead, interannual climate conditions (especially the strength of temperature inversions) and reach-scale geomorphic controls dominate spatial variations in stream temperature, consistent with findings from similar High Arctic nival streams (Docherty et al., 2018).

4.4.2 Stream Temperature Climate Forcings

Each site exhibited clear diurnal variations in stream temperature (Fig. 4.2A-E). Stream temperatures were compared against air temperature, precipitation, relative humidity and solar position to evaluate climate controls between patterns. Relative humidity was included as an indirect indicator of atmospheric moisture conditions that often coincide with cloudiness and reduced solar input to these shallow streams (Docherty et al., 2019). Correlation matrices indicated the strength of coupling between stream temperature and climate variables for each year.

In 2022, the strongest correlation exists between the stream temperature and air temperature recorded at the 80 m a.s.l. location (average 0.76 across six sites; Fig. 4.4A). Air temperature recorded at the station (10 m a.s.l.) also shows a strong positive relationship with stream temperature (avg. 0.67). In 2022, dew point temperature and relative humidity (recorded at both elevations) showed moderate but opposite signed relationships with stream temperature – dew point was positively correlated (DP_{10m}: 0.49, DP_{80m}: 0.46) and relative humidity was negatively correlated (RH_{10m}: -0.47, RH_{80m}: -0.45). In contrast, top of atmosphere radiation showed only a weak relationship with stream temperature (0.10; Fig. 4C). These patterns are consistent for nival-fed streams where permafrost restricts ground water movement and limits baseflow. In Greenland, Docherty et al (2019) found that climate variables, particularly air temperature and solar radiation, have strong positive influence on nival stream temperatures.

In 2023, stream temperatures at low elevation sites in both streams (Sites 1, 4 and 5) showed strong positive correlations with the air temperature at both the airport (avg. 0.58 across sites; Fig. 4.4B) and station (avg. 0.48 across sites) and moderate negative relationships with

relative humidity (airport = avg. -0.55; station = avg -0.48). Stream temperatures at upstream sites (2, 3 and 7) were weakly positively correlated (avg. 0.35; Fig. 4.4B) with airport air temperature and weakly negatively correlated with the airport relative humidity (avg. -0.33). No relationship was identified between the station air temperature or relative humidity data and the stream water temperature at these upstream sites, likely attributed to the higher elevation of these sites. Notably, all sites exhibited a consistently strong positive correlation with top of atmosphere solar radiation (avg. 0.56 among sites; Fig. 4.4D). These findings align with the warm-dry conditions of July 2023 which had a much lower record of precipitation (9.5mm), lower mean relative humidity (72%) and higher mean air temperature (airport: 11.1℃, station: 7.9℃). Under clear-sky conditions, solar forcing variables exhibited a stronger influence over stream temperatures.

Together, these results show that the strength and direction of climate controls on stream temperature vary between years depending on prevailing weather conditions while still confirming that nival stream temperatures are largely governed by air temperature and solar radiation (Docherty et al., 2019). Previous studies have solely used air temperature to predict stream temperature (etc. Stefan & Preud'homme, 1993; Mohseni & Stefan, 1999) but these models have been found to under-predict the maximum and minimum stream temperatures when applied beyond the study year (Arismendi et al., 2014). This deviation is attributed to other factors such as solar radiation and climate (Arismendi et al., 2014). Our findings from Eureka reinforce this limitation: stream temperature and air temperature are highly related but to varying degrees between years. Understanding this variability is crucial for anticipating how High Arctic streams will respond to ongoing climate change. Recent work in Svalbard, for example, detected a diurnal warming trend of 0.5-3.5℃ per decade in stream temperature (Majerska et al., 2024). Such changes in water temperature could impact nutrient uptake and biological community structures in streams (Docherty et al., 2018). Given the lack of long-term stream temperature records across the Canadian High Arctic, expanding monitoring efforts would substantially improve our ability to detect and interpret future thermal shifts in these sensitive systems.

4.4.3 Stage-Discharge Relationship of Nival Dominated Streams

Table 1 contains the stage-discharge relationships for each site and, Fig. 4.2F & G illustrates the reconstructed discharge for both streams. In 2022, too few manual discharge measurements were collected to create robust rating curves for most sites, only sites 1 (Blacktop Creek) and 4 (Station Creek) produced useable results. In 2023, the flow meter malfunctioned near the end of the field season impacting the accuracy of all estimated measurements beyond this date.

Across both years, manual discharge measurements were consistently greater in Blacktop Creek than Station Creek. Discharge was also greater in July 2022 than July 2023, consistent with the occurrence of rain events in that season. Based on the furthest downstream sites, Blacktop Creek 2022 had an average discharge of 0.77±0.53 m^3/s (Site 1); Station Creek in the same year had an average measured discharge of 0.59±0.57 m^3/s (Site 4). In 2023, Site 3 (above slump), Blacktop Creek, had an average discharge of 0.20±0.15 m^3/s, Site 2 (directly below the slump) had an average discharge of 0.38±0.14 m^3/s, and Site 1, furthest downstream, had an average discharge of 0.40±0.42 m^3/s. Comparatively, Station Cree Site 7, (which was unaffected by thaw), had an average discharge of 0.06±0.03 m^3/s; Site 5 directly downstream of a slump was 0.18±0.12 m^3/s and Site 4, furthest downstream, had an average discharge of 0.14±0.18m^3/s. Measured stream level declined at an average rate of -2.92±0.1 cm/day for Blacktop Creek sites and -3.59±0.26 cm/day for Station Creek sites in 2022. This variability is attributed to the high frequency of rain events. In contrast, the average rate of water level decline for Blacktop creek sites was -0.67±0.05 cm/day and -0.55±0.08 cm/day for Station creek in July 2023. Together, the higher discharges and greater water-level recession of July 2022, compared to the subdued July 2023 hydrological data, points to a hydrological system that responds quickly to rainfall but stabilized under melt-controlled conditions, findings consistent with other Arctic studies (Forbes & Lamoureux, 2005; Beel et al., 2018).

The estimated discharge was differenced against the actual discharge to determine fit of each site's stage-discharge model (i.e., rating curve). The models fit to the 2023 data performed substantially better than those fit to data from 2022, a difference attributed to the absence of rain events. Within the stream itself, the stability of the rating curve is largely controlled by disturbance, a finding consistent with other Arctic catchments where thermokarst disturbance events significantly increase particulate flux and destabilize hydrological regimes (Beel et al., 2020; Kokelj et al., 2021). For example, between the two modelled 2022 sites (1 and 4), Site 1 showed a smaller prediction error, likely because it was less affected by active thaw slumping and associated sediment pulses. Site 4 showed the poorest prediction of discharge; this is attributed to the rain events as well as the slump activity. Active thaw slumps upstream can deliver episodic sediment and water pulses, temporarily altering channel hydraulics and flow pattens (Kokelj et al., 2021). These findings highlight the importance of considering both geomorphology and direct thermokarst interactions when interpreting Arctic stream discharge, particularly the distinction between direct and indirect slump influences.

4.4.4 Suspended Sediment and Dissolved Particulate Load of Nival Fed, RTS Impacted Streams

Suspended sediment (SS) and dissolved particulate (DP) concentrations were measured in nival-fed, RTS-impacted streams to evaluate the influence of thaw slumps on sediment transport, see Fig. 2H & I. In 2022, mean SS and DP concentrations in Blacktop Creek (BC) ranged from 327.8 ± 193.2 mg/L to 580.2 ± 549.7 mg/L across sites. Station Creek (SC) exhibited slightly lower or comparable SS and DP values (433.0 ± 129.7 mg/L to 470.2 ± 379.7 mg/L). The SS+DP load (mg/L) for stream sites in 2022 did not significantly differ among disturbed and undisturbed sites, this is attributed to the frequency of rain events which overshadowed direct thermokarst inputs.

In 2023, differences between sites became more pronounced. In BC, SS and DP ranged from 168.0 ± 21.7 mg/L at site 3 to 322.7 ± 75.0 mg/L at Site 1. For SC, concentrations varied from 411.9 ± 105.9 mg/L at site 7 to 1105.4 ± 610.1 mg/L at site 5. Significant differences (one way ANOVA) in daily SS+DP load (mg/L) were identified between thaw-affected and unaffected sites in both streams (p-value =0.008, f=6.4 for BC, p-value=0.001, f=9.1 for SC). Tukey HSD post-hoc tests showed that in Blacktop Creek, Site 3 (undisturbed) differed significantly from both disturbed sites (Sites 1 and 2) demonstrating the strong influence of slump runoff on SS and DP concentrations. In Station Creek, Site 7 (undisturbed) differed significantly from Site 5 (disturbed) and Site 5 differed significantly from Site 4 (disturbed), but Site 7 and Site 4 did not differ. This indicates that thermokarst inputs elevate SS and DP concentrations at the disturbance point, with loads diminishing downstream as water level and transport capacity declines. Similar increases in suspended sediment load associated with thaw slump runoff have been documented in other Arctic systems (Kokelj et al., 2013).

Stream sediment-discharge relationships showed weak and inconsistent hysteresis patterns across both streams in both years (Fig. 4.5). In Blacktop creek 2022, sediment loads were higher on the rising limb, but the limb x discharge relationship was not significant. Hysteresis was not detectable in SC 2022 on either creek in 2023, indicating it is not a consistent control on sediment transport in these nival-dominated, thaw-disturbed streams. Stream sediment-discharge relationships for nival-fed streams have been known to display different hysteresis behaviour based on snowmelt timing and sediment availability (Favaro & Lamoureux, 2015) and permafrost disturbances can alter particulate and dissolved fluxes across multiple years (Beel et al., 2020).

Overall, these results are comparative to those of Beel et al. (2018) which identified pluvial activity to be the more important driver behind stream suspended sediment and discharge compared against the influence of active layer detachments. This study shows that the cause of elevated suspended sediment (SS) and dissolved particulates (DP) can vary between years because of

climate conditions. In warm-dry years, the fluctuations in stream SS and DP levels - particularly in regions like Eureka - is likely attributed to the high degree of thaw slump activity. In colder-wetter climates, detection of thaw slump activity is more difficult with pluvial and nival processes dominating sediment mobilization. Together, these results suggest that weak and inconsistent hysteresis in Eureka streams reflect the combined effects of variable sediment supply from thaw slumps and shifting hydrological forcing (nival/pluvial).

4.5 Conclusion

This study focuses on stream characteristics for two nival streams in the Canadian High Arctic. Findings show the following:

- Stream temperature in July 2022 was on average 3℃ cooler than the following year with a maximum observed stream temperature of nearly 20℃ in 2022.
- Within-reach comparison showed that local thermokarst activity had no influence on temperature but rather, stream temperature differences were controlled by geomorphology, elevation and air temperature inversion. Results are highly variable between years but similar between streams.
- Stream temperatures also exhibit a diurnal pattern, which was more prominent in 2023. A correlation analysis revealed a strong positive relationship between stream temperature and air temperatures in 2022 and a moderate-strong positive relationship between stream temperature and incoming top of atmosphere solar radiation in 2023.
- Stream discharge was greater in July 2022 for both streams due to the occurrence of rain events. Over the course of both summers, stream level declined at an average rate of 3.25 cm per day for 2022 and 0.61 cm per day for 2023.
- The accuracy of the sites' rating curve was largely governed by the site's geomorphology. With one site (Site 5) directly impacted by thermokarst activity (debris intrusion) and naturally had the least accuracy in predicted discharge.
- Suspended and dissolved particulate load was similar between streams in 2022 and shows no significant difference between disturbed and undisturbed sites. Comparatively, both streams show a statistical difference in 2023 between disturbed and undisturbed sites.
- Results show that stream suspended sediment and dissolved particulate load was largely governed by climate, then magnified by thermokarst activity.

Overall, these findings demonstrate the value of sustained High Arctic stream monitoring. High resolution data not only captures the interannual variability of these streams but also reveals subtle

changes linked to thermokarst processes, reinforcing the need for sustained monitoring in a rapidly changing environment.

4.6 Acknowledgments

This project was funded by grants from the Natural Science and Engineering Research Council (NSERC; DL), the Northern Scientific Training Program (NSTP; KCH), the Royal Canadian Geographical Society (RCGS; KCH) and the Association of Canadian Universities for Northern Studies (ACUNS; KCH). Incredible field logistical support was provided by the Polar Continental Shelf Program (Natural resources Canada). Fieldwork could not have been completed without the help of B. Lauriol, J. Prest, and the Eureka Weather Station staff. Thank you to Dr. Konrad Gajewski for constructive comments on earlier versions of this manuscript. PlanetScope Imagery was provided through the Planet Education and Research program through a University of Ottawa academic license.

4.7 References

Alt, B. T., & Maxwell, B. (2000). Overview of the modern arctic climate. Bulletin of the Geological Survey of Canada, 529, 17–36.

Arismendi, I., Safeeq, M., Dunham, J. B., & Johnson, S. L. (2014). Can air temperature be used to project influences of climate change on stream temperature? *Environmental Research Letters*, *9*(8), 084015.

Beel, C. R., Heslop, J. K., Orwin, J. F., Pope, M. A., Schevers, A. J., Hung, J. K. Y., ... & Lamoureux, S. F. (2021). Emerging dominance of summer rainfall driving High Arctic terrestrial-aquatic connectivity. Nature Communications, 12(1), 1448.

Beel, C. R., Lamoureux, S. F., & Orwin, J. F. (2018). Fluvial response to a period of hydrometeorological change and landscape disturbance in the Canadian High Arctic. Geophysical Research Letters, 45(19), 10-446.

Beel, C. R., Lamoureux, S. F., Orwin, J. F., Pope, M. A., Lafrenière, M. J., & Scott, N. A. (2020). Differential impact of thermal and physical permafrost disturbances on High Arctic dissolved and particulate fluvial fluxes. *Scientific Reports*, *10*(1), 11836.

Bell, T. (1996). The last glaciation and sea level history of. Fosheim Peninsula, Ellesmere Island, Canadian High Arctic. Canadian Journal of Earth Sciences, 33, 1075–1086.

Bell, T., & Hodgson, D. A. (2000). Quaternary geology and glacial history of Fosheim Peninsula, Ellesmere Island, Nanavut. In Bulletin of the Geological Survey of Canada (Issue 529). https://doi.org/10.4095/211957

Bernard-Grand'Maison, C., & Pollard, W. (2018). An Estimate of Ice Wedge Volume for a High Arctic Polar Desert Environment, Fosheim Peninsula, Ellesmere Island. The Cryosphere Discussions, 12, 1–28. https://doi.org/10.5194/tc-2018-29

Church, M. (1974). Hydrology and permafrost with reference to northern North America. In Permafrost Hydrology, Proceedings of Workshop Seminar (pp. 7-20). Ottawa: Canadian National Committee of the International Hydrological Decade.

Coch, C., Ramage, J. L., Lamoureux, S. F., Meyer, H., Knoblauch, C., & Lantuit, H. (2020). Spatial variability of dissolved organic carbon, solutes, and suspended sediment in disturbed low Arctic coastal watersheds. *Journal of Geophysical Research: Biogeosciences*, *125*(2), e2019JG005505.

Cornwall, C., Horiuchi, A., & Lehman, C. (2025). Solar position calculator. Retrieved from https://gml.noaa.gov/grad/solcalc/azel.html

Couture, N. J., & Pollard, W. H. (1998). An assessment of ground ice volume near eureka, northwest territories. In Permafrost - Seventh International Converence, 55, 195–200.

Déry, S. J., K. Stahl, R. D. Moore, P. H. Whitfield, B. Menounos, and J. E. Burford (2009), Detection of runoff timing changes in pluvial, nival, and glacial rivers of western Canada, Water Resour. Res., 45, W04426, doi:10.1029/2008WR006975.

Docherty, C. L., Dugdale, S. J., Milner, A. M., Abermann, J., Lund, M., & Hannah, D. M. (2019). Arctic river temperature dynamics in a changing climate. *River Research and Applications*, *35*(8), 1212-1227.

Docherty, C. L., Riis, T., Hannah, D. M., Rosenhøj Leth, S., & Milner, A. M. (2018). Nutrient uptake controls and limitation dynamics in north-east Greenland streams. *Polar Research*, *37*(1), 1440107.

Edlund, S. A., & Alt, B. T. (1989). Regional congruence of vegetation and summer climate patterns in the Queen Elizabeth Islands, Northwest Territories, Canada. *Arctic*, *42*(1), 3–23. https://doi.org/10.14430/arctic1635

Edlund, S. A., Alt, B. T., & Garneau, M. (2000). Vegetation patterns on Fosheim Peninsula, Ellesmere Island, Nunavut. In Bulletin of the Geological Survey of Canada (Issue 529).

England, J., Atkinson, N., Bednarski, J., Dyke, A. S., Hodgson, D. A., & Ó Cofaigh, C. (2006). The Innuitian Ice Sheet: configuration, dynamics and chronology. Quaternary Science Reviews, 25(7–8), 689–703. https://doi.org/10.1016/j.quascirev.2005.08.007

Favaro, E. A., & Lamoureux, S. F. (2015). Downstream patterns of suspended sediment transport in a High Arctic river influenced by permafrost disturbance and recent climate change. Geomorphology, 246, 359-369.

Forbes, A. C., & Lamoureux, S. F. (2005). Climatic controls on streamflow and suspended sediment transport in three large middle arctic catchments, Boothia Peninsula, Nunavut, Canada. *Arctic, Antarctic, and Alpine Research*, *37*(3), 304-315.

Government of Canada. (2025). Historical Climate Data. Retrieved from https://climate.weather.gc.ca/historical_data/

Hendriks, M. (2010). *Introduction to physical hydrology*. Oxford University Press.

Hodgson, D. A., & Nixon, F. M. (1998). Ground ice volumes determined from shallow cores from western Fosheim Peninsula Ellesmere Island, Northwest Territories. In Bulletin of the Geological Survey of Canada (Issue 507). Government of Canada.

Holmes, R. M., McClelland, J. W., Peterson, B. J., Tank, S. E., Bulygina, E., Eglinton, T. I., ... & Zimov, S. A. (2012). Seasonal and annual fluxes of nutrients and organic matter from large rivers to the Arctic Ocean and surrounding seas. Estuaries and Coasts, 35(2), 369-382.

Johnson, M. F., & Wilby, R. L. (2013). Shield or not to shield: Effects of solar radiation on water temperature sensor accuracy. *Water*, *5*(4), 1622-1637.

Kokelj, S. V., Kokoszka, J., van Der Sluijs, J., Rudy, A. C., Tunnicliffe, J., Shakil, S., ... & Zolkos, S. (2021). Thaw-driven mass wasting couples slopes with downstream systems, and effects propagate through Arctic drainage networks. The Cryosphere, 15(7), 3059-3081.

Kokelj, S. V., Lacelle, D., Lantz, T. C., Tunnicliffe, J., Malone, L., Clark, I. D., & Chin, K. S. (2013). Thawing of massive ground ice in mega slumps drives increases in stream sediment and solute flux across a range of watershed scales. *Journal of Geophysical Research: Earth Surface*, *118*(2), 681-692.

Majerska, M., Osuch, M., & Wawrzyniak, T. (2024). Long-term patterns and changes of unglaciated High Arctic stream thermal regime. Science of the Total Environment, 923, 171298.

Manasypov, R. M., Lim, A. G., Krickov, I. V., Raudina, T. V., Kurashev, D. G., Shirokova, L. S., & Pokrovsky, O. S. (2023). Colloids in thermokarst lakes along a permafrost and climate gradient of permafrost peatlands in Western Siberia using in situ dialysis procedure. *Water*, *15*(9), 1783.

McClelland, J. W., Holmes, R. M., Peterson, B. J., Raymond, P. A., Striegl, R. G., Zhulidov, A. V., ... & Griffin, C. G. (2016). Particulate organic carbon and nitrogen export from major Arctic rivers. *Global biogeochemical cycles*, *30*(5), 629-643.

McDonald, D. M., & Lamoureux, S. F. (2009). Hydroclimatic and channel snowpack controls over suspended sediment and grain size transport in a High Arctic catchment. *Earth Surface Processes and Landforms*, *34*(3), 424-436.

Mohseni, O., & Stefan, H. G. (1999). Stream temperature/air temperature relationship: a physical interpretation. *Journal of hydrology*, *218*(3-4), 128-141.

Planet Labs PBC. (2024). *PlanetScope imagery* [Satellite imagery]. Planet Labs.

Pollard, W., Ward, M., & Becker, M. (2015). The Eureka Sound lowlands : an ice-rich permafrost landscape in transition. 68e Conférence Canadienne de Géotechnique et 7e Conférence Canadienne Sur Le Pergélisol, 20 Au 23 Septembre 2015, Québec, Québec.

Porter, C., Morin, P., Howat, I., Noh, M.-J., Bates, B., Peterman, K., Keesey, S., et al. (2023). *ArcticDEM*, *Version 4.1* [Digital elevation model]. Harvard Dataverse. https://doi.org/10.7910/DVN/3VDC4W (Accessed: April 2025).

R Core Team (2025). _R: A Language and Environment for Statistical Computing_. R Foundation for Statistical Computing, Vienna, Austria. <https://www.R-project.org/>.

Solinst Canada Ltd. (2024). *Levelogger 5 LTC: Data sheet* [PDF]. https://www.solinst.com/products/data/3001-ltc.pdf

Stefan, H. G., & Preud'homme, E. B. (1993). Stream temperature estimation from air temperature 1. *JAWRA Journal of the American Water Resources Association*, *29*(1), 27-45.

Ward Jones, M. K., Pollard, W. H., & Amyot, F. (2020). Impacts of Degrading Ice-Wedges on Ground Temperatures in a High Arctic Polar Desert System. Journal of Geophysical Research: Earth Surface, 125(3). https://doi.org/10.1029/2019JF005173

Ward Jones, M. K., Pollard, W. H., & Jones, B. M. (2019). Rapid initialization of retrogressive thaw slumps in the Canadian high Arctic and their response to climate and terrain factors. Environmental Research Letters, 14(5). https://doi.org/10.1088/1748-9326/ab12fd

Woo, M. K. (2012). Chapter 9: Rivers in Cold Regions. In *Permafrost Hydrology* (pp. 407-454).

Young, K. L., & Woo, M. K. (2000). Hydrological environment of the Hot Weather Creek basin, Ellesmere Island, Nunavut. Bulletin of the Geological Survey of Canada, 529, 347–360. https://doi.org/10.4095/211973

Zaerpour, M., Hatami, S., Sadri, J., & Nazemi, A. (2021). A global algorithm for identifying changing streamflow regimes: application to Canadian natural streams (1966–2010). Hydrology and Earth System Sciences, 25(9), 5193-5217.

4.8 Captions

Table 4.1. Stage-Discharge equation components, number of manual measurements and the average difference between the estimated and measured discharge. Note, if the number of manual measurements is 5 or less, they were not included.

Figure 4.1. Study site (A) Canadian Arctic Archipelago; (B) watershed extent with elevation underlay, dashed black line indicates marine limit; (C) sample locations, true colour composite satellite image underlain. Satellite image captured July 30, 2022, by Planet Labs PBC (2024). Ephemeral creeks represented by blue dashed line, continuous flowing streams by the solid blue line; (D) images of sample locations, site numbers correspond numbers in Fig, 1C. Images were taken in July 2023, photo credit Jacob Prest. All images are taken downstream.

Figure 4.2. Climate and stream component comparison left panel illustrates July 2022, right July 2023. A) Solar elevation and Azimuth (calculated using NOAA Solar Calculator); B) Hourly Air temperature (°C) recorded at Eureka Weather Station (black) and Eureka Air Strip (red; data collected from Government of Canada); C) Hourly precipitation (mm) collected at Weather station (data collected from Government of Canada); D) Blacktop Creek recorded stream temperature (30 min interval); E) Station Creek recorded stream temperature (30 min interval); F) Blacktop Creek calculated discharge (m^3/s); G) Station Creek calculated discharge (m^3/s); H) Blacktop Creek sediment and dissolved particulate load (mg/L); I) Station Creek sediment and dissolved particulate load (mg/L).

Figure 4.3. Mean annual stream temperature (labelled) for each study site overlying the lidar-derived elevation (ArcticDEM) for (A) 2022 and (B) 2023, Site 7 in inset map. (C) shows watershed extent with digital elevation model, dashed line indicates extent of marine sediments (~146 m asl).

Figure 4.4. Hourly stream temperature for 2022 and 2023 against recorded air temperature (°C; A & B) and estimated top of atmosphere (TOA) solar radiation (W m^{-2}; C & D).

Figure 4.5. Log-transformed stream sediment and dissolved particulate load against log-transformed stream discharge. Data illustrated per year, per stream.

4.9 Tables

Table 4.1. Stage-Discharge equation components, number of manual measurements and the average difference between the estimated and measured discharge. Note, if the number of manual measurements is 5 or less, they were not included.

Site	Equation Components	Measured average discharge (m^3/s)	No. manual measurements	Model Error
1	h_0 = 0.115 (2022), 0.243 (2023) C = 6.4442 (2022), 25.4653 (2023) b = 0.7282 (2022), 1.9610 (2023)	22: 0.77±0.53; 23:0.40±0.42	2022: 7, 2023: 9	2022: 7% 2023: 8.1%
2	h_0 = 0.07 C = 4.9225 b =1.3385	0.38±0.14	2023: 9,	5.2%
3	h_0 = 0.135 C = 22.0512 b = 2.5220	0.20±0.15	2023:9	9.4%
4	h_0 =0.055 (2022), 0.10 (2023) C = 2.8697 (2022), 16.6542 (2023) b = 0.6501 (2022), 2.7173 (2023)	22:0.59±0.57 23:0.14±0.18	2022:7, 2023:9	2022: 39.3% 2023: 9.7%
5	h_0 = 0.05 C = 279.3 b = 4.29	0.18±0.12	2023: 8	11.4%
7	h_0 = 0.137 C = 362.614 b = 3.4391	0.06±0.03	2023: 6	10%

4.10 Figures

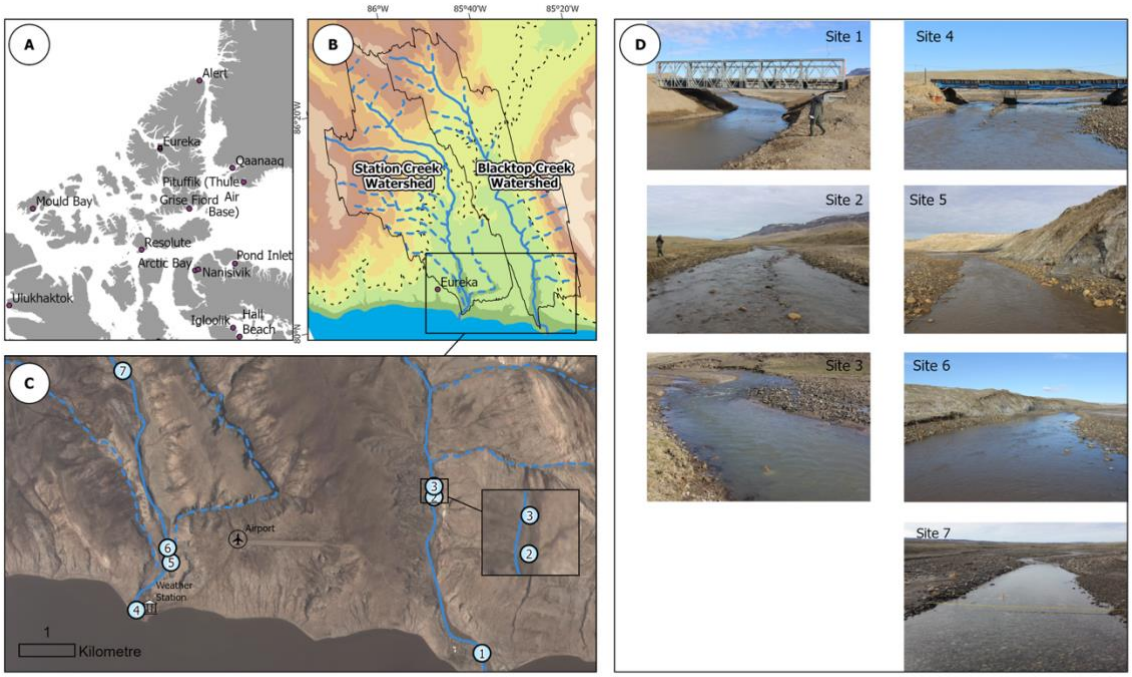


Figure 4.1. Study site (A) Canadian Arctic Archipelago; (B) watershed extent with elevation underlay, dashed black line indicates marine limit; (C) sample locations, true colour composite satellite image underlain. Satellite image captured July 30, 2022, by Planet Labs PBC (2024). Ephemeral creeks represented by blue dashed line, continuous flowing streams by the solid blue line; (D) images of sample locations, site numbers correspond numbers in Fig, 1C. Images were taken in July 2023, photo credit Jacob Prest. All images are taken downstream.

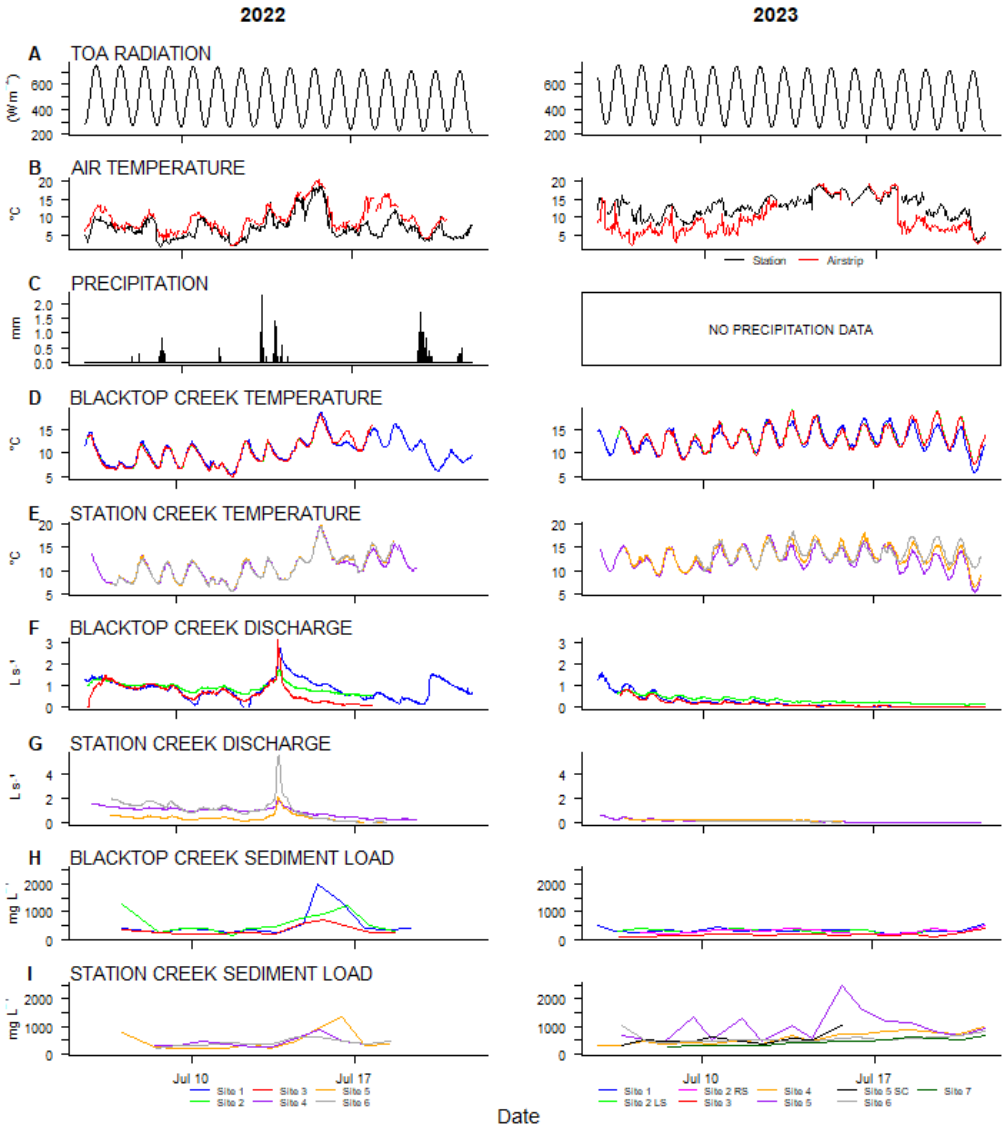


Figure 4.2. Climate and stream component comparison left panel illustrates July 2022, right July 2023. A) TOA Radiation (W m^{-2}); B) Hourly Air temperature (°C) recorded at Eureka Weather Station (black) and Eureka Air Strip (red; data collected from Government of Canada); C) Hourly precipitation (mm) collected at Weather station (data collected from Government of Canada); D) Blacktop Creek recorded stream temperature (30 min interval); E) Station Creek recorded stream temperature (30 min interval); F) Blacktop Creek calculated discharge (m^3/s); G) Station Creek calculated discharge (m^3/s); H) Blacktop Creek sediment and dissolved particulate load (mg/L); I) Station Creek sediment and dissolved particulate load (mg/L).

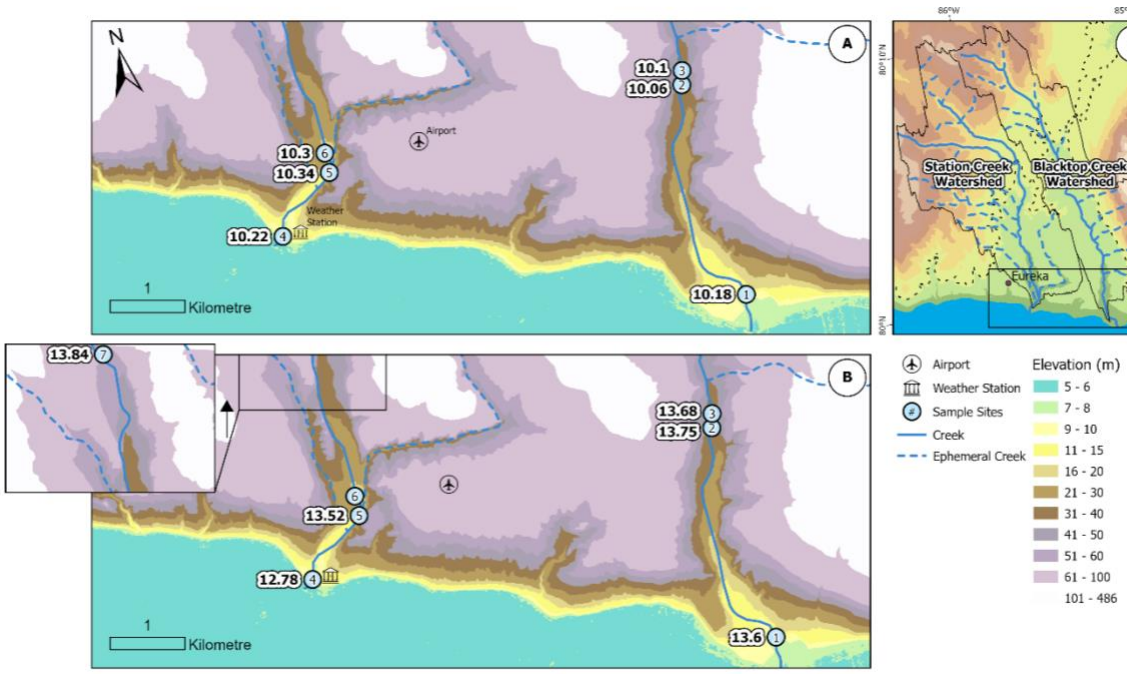


Figure 4.3. Mean annual stream temperature (labelled) for each study site overlying the lidar-derived elevation (ArcticDEM Version 4.1; Porter et al., 2023) for (A) 2022 and (B) 2023, Site 7 in inset map. (C) shows watershed extent with digital elevation model, dashed line indicates extent of marine sediments (~146 m asl).

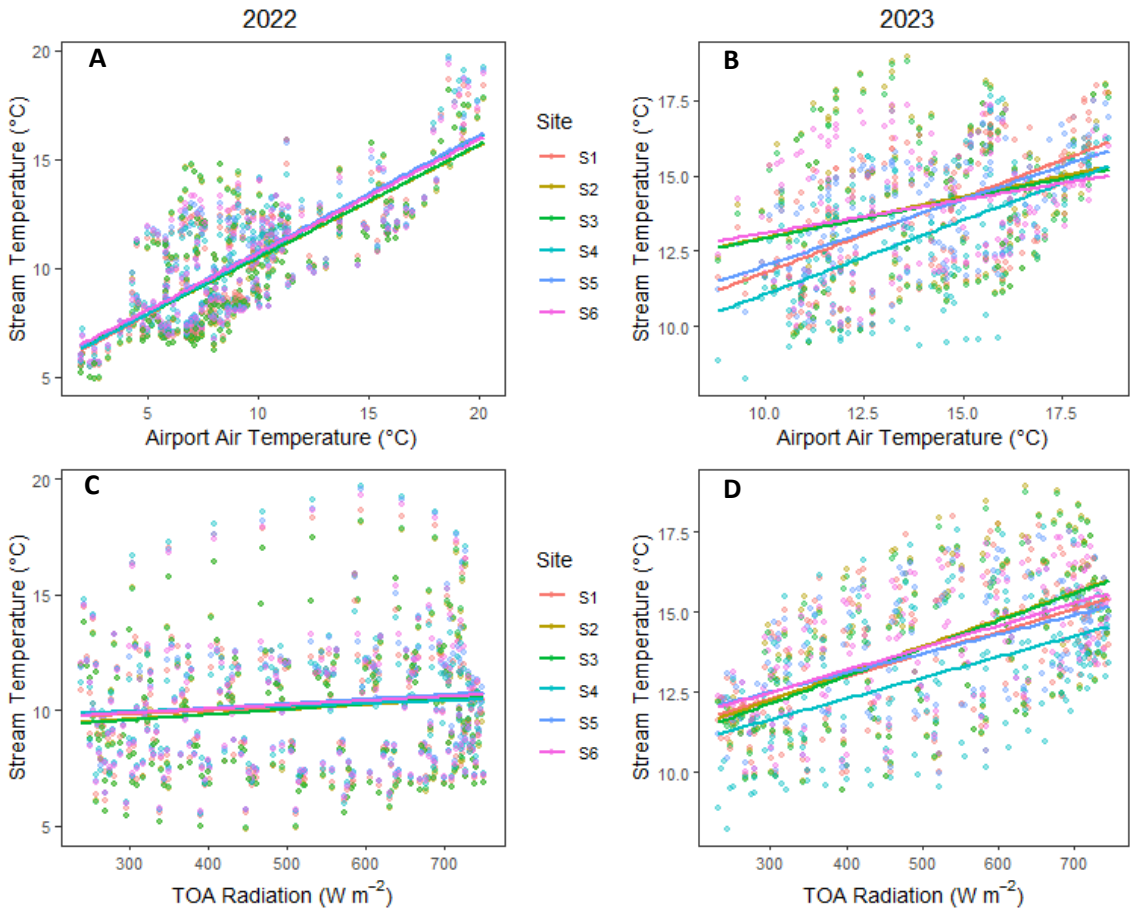


Figure 4.4. Hourly stream temperature for 2022 and 2023 against recorded air temperature (°C; A & B) and estimated top of atmosphere (TOA) solar radiation (W m^{-2}; C & D).

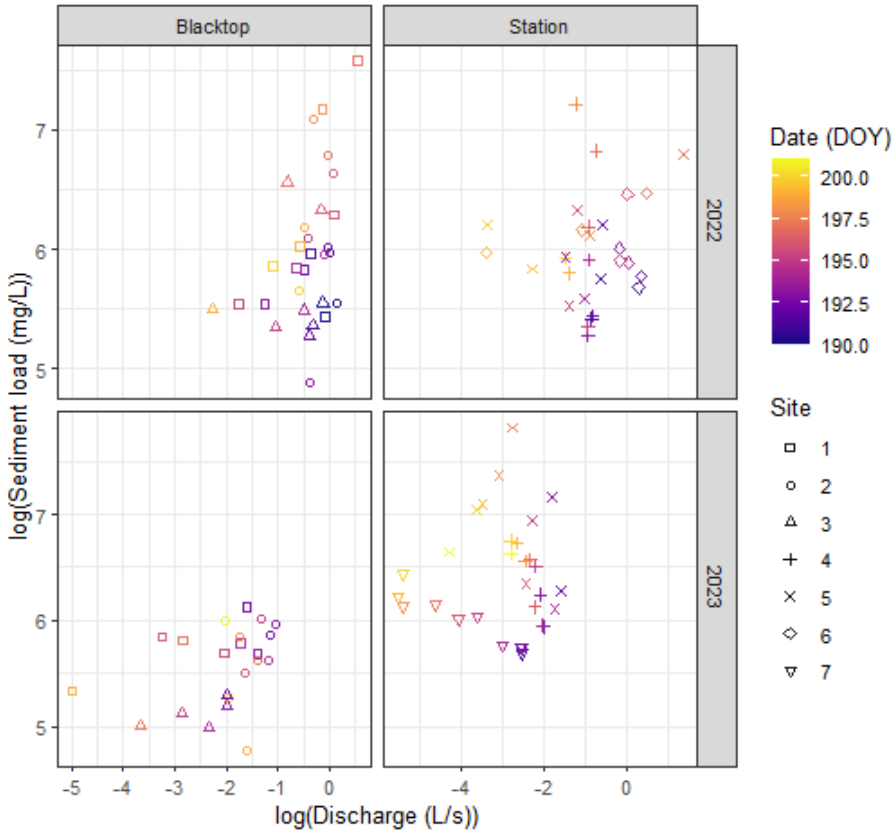


Figure 4.5. Log-transformed stream sediment and dissolved particulate load against log-transformed stream discharge. Data illustrated per year, per stream.

Chapter 5

5.1 Summary and Conclusions

Much of the Canadian Arctic is underlain by permafrost, and national scale mapping indicates that a large proportion of this region contains medium to very high ground ice content, with ice volumes frequently exceeding ~30-60% within the first 5m of permafrost (O'Neill et al., 2019). Surficial permafrost, rich in ground ice, is particularly susceptible to warming climates, especially areas which have a little to no vegetation cover or have been disturbed through vegetation removal or infrastructure development (roads, buildings etc.). Retrogressive thaw slump activity, a byproduct of thawing ice-rich permafrost, is increasing across the Canadian Arctic (Lewkowicz & Way, 2019; Ward Jones et al., 2019; van der Sluijs et al., 2023; Dai et al., 2025). Climate drivers of thaw slump activity are latitude dependent and Dai et al (2025) identified an inflection point of 71°N across the circumpolar Arctic. South of this latitude, thaw slump activity is precipitation-driven, whereas to the north, activity becomes temperature-driven (Dai et al., 2025). Much of what is known about the hydrological effects of thaw slumping to arctic streams is limited to the Western Canadian Arctic and Alaska, where higher precipitation and warmer summer conditions amplify solute and sediment delivery to streams (Kokelj et al., 2005; 2013; Malone et al., 2013; Littlefair et al., 2017). In contrast, the hydrological impact of thaw slumps in polar desert settings remain largely unexamined.

The Fosheim Peninsula, situated in a polar desert environment, host some of the highest densities of thaw slump in the Canadian High Arctic, driven by the abundant massive ground ice, marine-deltaic sediments and rapid warming (Pollard et al., 2015; Ward Jones et al., 2019). Previous research in the area has focused on mapping thaw slump activity, quantifying headwall retreat, characterizing ground-ice composition, documenting ice-wedge degradation and assessing vegetation succession following disturbance (Couture & Pollard, 1998; Pollard et al., 2015; Becker et al., 2016; Bernard-Grand'Masion & Pollard, 2018; Ward Jones et al., 2020; Roy et al., 2023). Collectively, these studies provide a strong permafrost and geomorphology framework, but none have examined how these thermokarst features influence local hydrology or stream biogeochemistry. As a result, the linkages between landscape change and nival stream behaviour remain poorly understood. Thus, this thesis's primary goal was to use remote sensing products and conduct laboratory analysis on samples collected during the 2022-2023 Eureka field seasons to fill these knowledge gaps.

Analysis of a 25-year Tasseled Cap trend shows that 79.3% of the Fosheim Peninsula experienced significant positive change (greening), 42.3% in brightness and 31.2% in wetness (Chapter 2). These widespread positive trends indicate that vegetation production and surface moisture availability have increased across most terrain types. Barren regions of the Fosheim are experiencing widespread vegetation colonization, as shown by significant trends in greening, wetting and surface darkening, consistent with the 26% of positive greening trends occurring within barren land. LARCH visual analysis identified substantial fluvial reorganization of the Slidre river because of fluvial erosion and braided stream activity. Station, Blacktop and Gemini-2 Creek basins show landscape change associated with anthropogenic activities (aggregate extraction, airstrip maintenance and water storage pond development). Moreover, nine drained or near drained lakes were identified during the study period with drainage linked to warm summer conditions and ice wedge degradation. Finally, a total of 139 retrogressive thaw slumps were activated during the entire period although this value is an underestimation of the true number as imagery resolution limited identification. High-resolution imagery confirmed 60 active retrogressive thaw slumps in 2024. A comparison to climate records from Eureka shows that since 1999, eight years have experienced TDD greater than 500, highlighting the increasing frequency of warm summers that enhance thaw conditions across the Fosheim Peninsula. The results from this chapter reinforce previous research show that the Fosheim Peninsula is undergoing substantial thermokarst change, attributed to temperature-driven retrogressive thaw slump activity.

Stream geochemistry analysis of two nival streams in Eureka, Nunavut (Chapter 3) shows that active retrogressive thaw slumps increase the dissolved organic carbon (DOC) concentrations in affected streams (undisturbed streams ranged between 0.66-0.81 ppm whereas disturbed sites ranged between 0.64-1.44 ppm). As slump activity declined, the DOC concentrations of the streams returned to pre-disturbance levels, highlighting the transient nature of carbon fluxes. Stable water isotopes (δD-$\delta^{18}O$) between disturbed and undisturbed sites show minimal differentiation, suggesting that slump rillwash constitutes a minor fraction of total discharge. Moreover, disturbed sites show elevated chloride concentrations and low SO_4:Cl^- ratios, reflecting the influence of marine salts within permafrost rather than mineral weathering or organic matter leaching (Couture & Pollard, 1998). Major ion concentrations at Eureka's disturbed sites do not match those recorded in the Western Arctic (Kokelj et al., 2013), demonstrating that thaw slumps can alter stream geochemistry in distinct ways depending on regional context. Moreover, the DOC and signatures in Eureka streams are lower than in more southern Arctic locations (Wang et al., 2018; Littlefair et al., 2017), consistent with the high Arctic's low productivity and limited carbon stocks. The results of this chapter suggest that permafrost thaw in the High Arctic primarily affects solute chemistry

rather than carbon export or stream δD-δ^{18}O and highlights the need for expanded pan-Arctic investigations into slump-driven geochemical change.

Finally, analysis of stream characteristics of two nival-dominated streams in Eureka revealed that stream temperature in July 2022 was on average 3℃ cooler than the following year. A maximum stream temperature of nearly 20℃ was observed in 2022. Within-reach comparison showed that local thermokarst activity had little influence on temperature but rather, stream temperature differences were controlled by geomorphology, elevation and air temperature inversion. Results are highly variable between years but similar between streams. Stream temperatures exhibit a diurnal pattern, which was more prominent in 2023 even under continuous daylight conditions. Correlation analysis revealed a strong positive relationship between stream temperature and air temperatures in 2022 and a moderate-strong positive relationship between stream temperature and top of atmosphere solar radiation in 2023. Stream discharge was greater in July 2022 for both streams due to the occurrence of rain events. Over the course of both summers, stream level declined an average rate of 3.25 cm per day in 2022 and 0.61 cm per day in 2023. The accuracy of the sites' rating curve was largely governed by the site's geomorphology. Site 5 for example was directly impacted by thermokarst activity (debris intrusion) and therefore had the least accuracy in predicted discharge. Suspended and dissolved particulate load was similar between streams in 2022 and shows no significant difference between disturbed and undisturbed sites, however, both streams showed a statistical difference in 2023 between disturbed and undisturbed sites. Thaw disturbance is only detectable within the Station Creek sediment flux measurements in both years, a result of high thaw activity. Stream particulate load is largely governed by climate, magnified by thermokarst activity. Overall, results demonstrate the value of sustained High Arctic stream monitoring. The high-resolution data collected in this chapter captured both the interannual variability between the same stream in different years and revealed the subtle stream changes linked to thermokarst activity, reinforcing the need for sustained monitoring in a rapidly changing environment.

5.2 Limitations and Future Research Directions

The landscape-change analysis presented in Chapter 2 is subject to several methodological limitations. First, the 30 m spatial resolution of Landsat imagery restricts the minimum detectable feature size to approximately 8100 m^2 (three pixels by three pixels), meaning that smaller-scale disturbances such as new thaw slumps, ice-wedge melt-outs, and active layer detachments are underrepresented. Although higher resolution imagery would improve feature detection but would come at the cost of losing the multi-decadal temporal record provided by the Landsat archive.

Further, the training data used for the Random Forest classification were limited to a 10 km radius around the Eureka Weather Station, reflecting the spatial constraints of field campaigns in 2022 and 2023. As a result, several classes, specifically classes 9-13, are less well-represented and their accuracy would benefit from additional ground-truthing. Extrapolation of these classes across the remainder of the Fosheim Peninsula assumes consistent spectral-process relationships, an assumption that is reasonable at the scale of the peninsula but may not hold across broader regions of the Canadian Arctic Archipelago. Finally, although the LARCH analysis proved highly effective for identifying both monotonic and non-monotonic landscape changes, accurate interpretation requires extensive cross-comparison with high-resolution imagery and supporting field observations, as emphasized in previous applications of the method (Fraser et al., 2014; Frappier et al., 2023). Used in isolation, LARCH may yield ambiguous results; its strength lies in being combined with the individual Mann-Kendell trend indices and the supervised landscape classification outputs. Future research may apply this combined framework to other regions of the Canadian Arctic undergoing rapid environmental change to compare rates of greening, drying and moisture redistribution. Additional work could also subdivide the Landsat time series into shorter intervals (5-10 years) to examine how the initiation, progression and surface expression of landscape change have evolved over the entire period.

Chapter 3 is constrained by several limitations that should be considered when interpreting the results. First, the scale of this study is necessarily local: the two nival streams examined provide detailed insight into thermokarst-hydrology interactions in the Eureka Sound Lowlands, but they do not represent the full range of hydrological responses across the Canadian Arctic Archipelago, particularly given the region's unique polar desert climate and marine-deltaic geological setting (Hodgson and Nixon, 1998; Bell and Hodgson, 2000). A broader and longer-term monitoring program, potentially using a less intensive and automated sampling protocol, would help build a more comprehensive understanding of how High Arctic streams respond to ongoing climate pressures. In addition, the nival aspect of these streams introduces sampling challenges. As stream levels declined steadily during both field campaigns, late-season channel contraction altered thalweg position and mixing patterns, especially at downstream sites. This complexity required sampling both sides of Blacktop Creek at Site 2 in 2023, and similar issues may arise in other nival catchments where flow structure and mixing evolve as discharge diminishes (Woo, 2012). Furthermore, the temporal window of this study is limited by logistical constraints, capturing only the peak summer period in Eureka. Extending the observations into the spring freshet and fall freeze-back period would provide a more complete picture of seasonal hydrological and geochemical dynamics. Finally, this work did not assess the biological consequences of

thermokarst-derived solutes in sediments. Given evidence that thermokarst activity can alter nutrient availability and influence aquatic ecosystem (Bowden et al., 2008; Kokelj et al., 2015), future studies should examine how slump derived inputs affect downstream aquatic and terrestrial communities in the High Arctic.

In the final chapter (Chapter 4) there are several limitations that shape the interpretation of this study's findings. First, as mentioned in the above paragraph, the monitoring period was short, only capturing brief early to mid-summer intervals and limiting the ability to infer longer-term or seasonal climate-stream interactions. Therefore, developing a local, sustained monitoring program for one or both streams in Eureka, possibility supported by the year-round presence of staff at the Eureka Weather Station, would substantially improve temporal coverage. Moreover, the instrument constraints affected data continuity in this study. In 2022, loggers were displaced downstream following heavy rain events which led to manual adjustment to logger data (Appendix III), and, in 2023, the flowmeter stopped functioning late in the season and reduced the robustness of some stage-discharge relationships – particularly those for low flow events. The stream total suspended sediment sampling protocol also imposed constraints. Although the combined TSS+TDS gravimetric method was effective given the logistical challenges of working in a remote High Arctic setting (i.e., sample shipping and lack of laboratory equipment), it did not partition dissolved and particulate fractions. Future work could integrate conductivity and TDS measurements from Chapter 3 to separate dissolved and particulate loads and evaluate how thermokarst activity influences each component. Beyond the methodological considerations, the spatial scale of this study is necessarily limited. However, two small nival streams cannot represent the full diversity of hydrological response across the High Arctic, particularly given the strong influence of local geology, permafrost conditions and the thermokarst activity documented elsewhere in the region (Chapter 2; Pollard et al., 2015; Ward Jones et al., 2019). Expanding the monitoring network to additional watersheds in the High Arctic would help build a more holistic understanding of how thermokarst pressures shape stream regimes across the different landscape contexts. Finally, there is a need for integrated climate-hydrology-geomorphology modelling that links air temperature, solar radiation, stream temperature, discharge and sediment dynamics to predict future stream behaviour under a shifting High Arctic climate. Such models would complement field observations and help clarify how thermokarst-driven stream changes alter High Arctic aquatic ecosystems, particularly given that it has been shown that thermokarst activity alters stream sediment and nutrient delivery and disrupts aquatic communities at more southern Arctic locations (Bowden et al., 2008; Kokelj et al 2015).

Overall, this thesis establishes a footing for contemporary High Arctic stream studies. The constraints identified across chapters underscores the need for sustained multi-site and multi-season monitoring to fully comprehend how thermokarst activity shapes High Arctic streams and aquatic communities – an imperative made more urgent as climate change continues to intensify in these remote regions.

5.3 Key Contributions

The following list details the main research findings of this PhD project (outlined in Section 1.4) which are novel scientific contributions to the study of High Arctic landscape change, permafrost-hydrology interactions, and the climate sensitivity of High Arctic nival streams in Eureka.

1. The first long-term, peninsula scale quantification of High Arctic greening, brightening and wetting.
2. Identification of major geomorphic reorganization, including river migration and lake drainage.
3. Demonstration that LARCH and Random Forest together provide a reliable framework for High Arctic change detection.
4. First detailed hydrochemical assessment of slump-impacted streams in a polar-desert setting.
5. Evidence that High Arctic thaw slumps influence stream chemistry differently than Western Arctic thaw slumps.
6. Identification of clear above-below disturbance differences with daily stream measurements using ANOVA.
7. First multi-year comparison showing climate-regime-dependent thermal controls in High Arctic nival streams.
8. Demonstration that geomorphology and temperature inversion – not thaw slumps – control spatial temperature patterns in nival streams.
9. Evidence that thaw slump activity strongly increases sediment and particulate loads during warm and dry years.

5.4 References

Becker, M. S., Davies, T. J., & Pollard, W. H. (2016). Ground ice melt in the high Arctic leads to greater ecological heterogeneity. Journal of Ecology, 104(1), 114–124. https://doi.org/10.1111/1365-2745.12491

Bell, T., & Hodgson, D. A. (2000). Quaternary geology and glacial history of Fosheim Peninsula, Ellesmere Island, Nanavut. In Bulletin of the Geological Survey of Canada. https://doi.org/10.4095/211957

Bernard-Grand'Maison, C., & Pollard, W. (2018). An Estimate of Ice Wedge Volume for a High Arctic Polar Desert Environment, Fosheim Peninsula, Ellesmere Island. The Cryosphere Discussions, 12, 1–28. https://doi.org/10.5194/tc-2018-29

Bowden, W. B., Gooseff, M. N., Balser, A., Green, A., Peterson, B. J., & Bradford, J. (2008). Sediment and nutrient delivery from thermokarst features in the foothills of the North Slope, Alaska: Potential impacts on headwater stream ecosystems. *Journal of Geophysical Research: Biogeosciences*, *113*(G2).

Church, M. (1974). Hydrology and Permafrost with Reference to Northern North America. In *Proceedings of workshop seminar "Permafrost Hydrology"*. (pp. 7-15). Ottawa: Canadian National Committee of the International Hydrological Decade.

Couture, N. J., & Pollard, W. H. (1998). An assessment of ground ice volume near eureka, northwest territories. *In Permafrost - Seventh International Conference*, *55*, 195–200.

Dai, C., Ward Jones, M. K., van der Sluijs, J., Nesterova, N., Howat, I. M., Liljedahl, A. K., ... & Sriram, S. (2025). Volumetric quantifications and dynamics of areas undergoing retrogressive thaw slumping in the Northern Hemisphere. *Nature Communications*, *16*(1), 6795.

Frappier, R., Lacelle, D., & Fraser, R. H. (2023). Landscape changes in the Tombstone Territorial Park region (central Yukon, Canada) from multilevel remote sensing analysis. Arctic Science, 9(4), 838-855.

Fraser, R., Olthof, I., Kokelj, S., Lantz, T., Lacelle, D., Brooker, A., ... & Schwarz, S. (2014). Detecting landscape changes in high latitude environments using landsat trend analysis: 1. Visualization. Remote Sensing, 6(11), 11533-11557

Hodgson, D. A., & Nixon, F. M. (1998). Ground ice volumes determined from shallow cores from western fosheim peninsula ellesmere island, northwest territories. In Bulletin of the Geological Survey of Canada. Ottawa: Government of Canada.

Kokelj, S. V., Jenkins, R. E., Milburn, D., Burn, C. R., & Snow, N. (2005). The influence of thermokarst disturbance on the water quality of small upland lakes, Mackenzie Delta region, Northwest Territories, Canada. Permafrost and Periglacial Processes, 16(4), 343-353.

Kokelj, S. V., Lacelle, D., Lantz, T. C., Tunnicliffe, J., Malone, L., Clark, I. D., & Chin, K. S. (2013). Thawing of massive ground ice in mega slumps drives increases in stream sediment and solute flux across a range of watershed scales. *Journal of Geophysical Research: Earth Surface*, *118*(2), 681-692.

Lewkowicz, A. G., & Way, R. G. (2019). Extremes of summer climate trigger thousands of thermokarst landslides in a High Arctic environment. *Nature Communications (Resubmitted December 2018)*, *10*(1), 1329. https://doi.org/10.1038/s41467-019-09314-7

Littlefair, C. A., Tank, S. E., & Kokelj, S. V. (2017). Retrogressive thaw slumps temper dissolved organic carbon delivery to streams of the Peel Plateau, NWT, Canada. *Biogeosciences*, *14*(23), 5487-5505.

Malone, L., Lacelle, D., Kokelj, S., & Clark, I. D. (2013). Impacts of hillslope thaw slumps on the geochemistry of permafrost catchments (Stony Creek watershed, NWT, Canada). *Chemical Geology*, *356*, 38-49.

O'Neill, H. B., Wolfe, S. A., and Duchesne, C. (2019). New ground ice maps for Canada using a paleogeographic modelling approach, The Cryosphere, 13, 753–773, doi:10.18739/A22V2C974.

Pollard, W., Ward, M., & Becker, M. (2015). The Eureka Sound lowlands : an ice-rich permafrost landscape in transition. *68e Conférence Canadienne de Géotechnique et 7e Conférence Canadienne Sur Le Pergélisol, 20 Au 23 Septembre 2015, Québec, Québec.*, *Figure 1*.

Roy, C., Campbell-Heaton, K., Lacelle, D., & Pollard, W. (2023). Massive ground ice of glacial meltwater origin in raised marine-deltaic sediments, Fosheim Peninsula, high Arctic Canada. *Quaternary Research*, *116*, 96-107.

van der Sluijs, J., Kokelj, S. V., & Tunnicliffe, J. F. (2023). Allometric scaling of retrogressive thaw slumps. *The Cryosphere*, *17*(11), 4511-4533.

Wang, J. J., Lafreniere, M. J., Lamoureux, S. F., Simpson, A. J., Gelinas, Y., & Simpson, M. J. (2018). Differences in riverine and pond water dissolved organic matter composition and sources in Canadian high Arctic watersheds affected by active layer detachments. Environmental science & technology, 52(3), 1062-1071.

Ward Jones, M. K., Pollard, W. H., & Amyot, F. (2020). Impacts of Degrading Ice-Wedges on Ground Temperatures in a High Arctic Polar Desert System. Journal of Geophysical Research: Earth Surface, 125(3). https://doi.org/10.1029/2019JF005173

Ward Jones, M. K., Pollard, W. H., & Jones, B. M. (2019). Rapid initialization of retrogressive thaw slumps in the Canadian high Arctic and their response to climate and terrain factors. *Environmental Research Letters*, *14*(5). https://doi.org/10.1088/1748-9326/ab12fd

Woo, M. K. (2012). *Permafrost Hydrology.* Springer Science & Business Media. https://doi.org/10.1007/978-3-642-23462-0

Appendix A: Data Download

The data used in this thesis can be acquired from this link. The folder contains all csv files used for analysis for Chapters 3 and 4. Please cite appropriately when using the data. Contact author if link is no longer available.

Appendix B: Chapter 2 Code

Appendix I
Code for Chapter 2
Google Earth Engine Colab File here.
Man-Kendell:

```
# Install if needed
install.packages(c("terra", "zyp", "Kendall")
# Load libraries
library(terra)
library(zyp)
library(Kendall)
years <- c(1999,2000,2002,2005,2007,2009,2011,2013, 2015,2016,2017,2018, 2019, 2020, 2022,
2023, 2024)
indices<-c("TC_Brightness","TC_Greenness", "TC_Wetness")
# Folder where your rasters are stored
input_folder <- "F:\\Indices Eureka\\SR TC TS\\Landsat_TC_ready"
output_folder <- "F:\\Indices Eureka\\SR TC TS\\Landsat_TC_MKOutput"
# Optional: water mask raster (1=water, 0=land)
#water_mask <- rast("F:\\Indices Eureka\\water_mask (1).tif")
compute_trend <- function(pixel_values, years) {
  if (all(is.na(pixel_values))) return(c(slope=NA, intercept=NA, tau=NA, p=NA))
  ts_fit <- zyp.sen(pixel_values ~ years)
  mk <- Kendall::MannKendall(pixel_values)
  c(
    slope = ts_fit$coefficients[2],
    intercept = ts_fit$coefficients[1],
    tau = mk$tau[1],
    p = mk$sl[1]
  )
}
compute_trend_block <- function(x) {
  t(apply(x, 1, function(pixel) compute_trend(pixel, years)))
}
for (idx in indices) {
  message("Processing ", idx, " ...")
  # Load raster stack for that index
  raster_files <- paste0(input_folder, idx, "_", years, ".tif")
  index_stack <- rast(raster_files)
  # Optional: apply water mask (mask out where water==1)
 # index_stack <- mask(index_stack, water_mask, maskvalues=1)
  # Apply pixel-wise Mann-Kendall + Theil-Sen
  result <- app(index_stack, compute_trend_block)
  names(result) <- c("slope","intercept","tau","pvalue")
  # Save result
  out_path <- paste0(output_folder, idx, "_MK_Trend.tif")
  writeRaster(result, out_path, overwrite=TRUE)
  message("Finished: ", idx)
}
```

Random Forest Modelling:

```
### Random Forest Code
library(sf)
library(dplyr)
library(randomForest)
library(terra)
library(caret)
#### Predictors : ####
pred_folder <- "F:\\Indices Eureka\\RF MODEL\\Inputs"
pred_files <- list.files(pred_folder, pattern = "\\.tif$", full.names = TRUE)
pred_files
r <- rast(pred_files[2])
names(r)
master_raster<-rast(pred_files[2])
master_crs<-crs(master_raster)
#### Extract data: ####
training_points <- st_read("F:\\Indices Eureka\\ModeltrainingData_feb2326.shp")
training_points<-st_transform(training_points, master_crs)
####load_predictors ####
load_predictors <- function(files) {
  ras_list <- list()
  for (f in files) {
    r <- rast(f)
    # Fix broken factor levels safely
    if (length(levels(r)) > 0) {
      levels(r) <- NULL
    }
    base <- tools::file_path_sans_ext(basename(f))
    bn <- names(r)
    # Multi-band TC trend rasters
    if (all(c("slope", "intercept", "tau", "pvalue") %in% bn)) {
      for (band in c("slope", "intercept", "tau", "pvalue")) {
        single_r <- r[[band]]
        names(single_r) <- paste0(base, "_", band)
        ras_list[[paste0(base, "_", band)]] <- single_r
      }
    } else {
      # Single-band predictors
      names(r) <- base
      ras_list[[base]] <- r
    }
  }

  do.call(c, ras_list)
}
predictors <- load_predictors(pred_files)
sapply(predictors,nlyr)
# write each predictor layer individually
for (nm in names(predictors)) {
```

```
  writeRaster(predictors[[nm]],
              filename = file.path("F:/Indices Eureka/RF MODEL/CleanPredictors2",
                                   paste0(nm, ".tif")),
              overwrite = TRUE)
}
pred_files <- list.files("F:/Indices Eureka/RF MODEL/CleanPredictors2",
                         pattern = "\\.tif$", full.names = TRUE)
predictors_clean <- lapply(pred_files, rast)
names(predictors_clean) <- tools::file_path_sans_ext(basename(pred_files))
master_r <- predictors_clean[["elevation"]]
aligned <- lapply(predictors_clean, \(r) project(r, master_r))
aligned <- lapply(aligned, \(r) crop(r, master_r))  # optional, but keeps extents clean

names(aligned) <- names(predictors_clean)
sapply(aligned, nlyr)
####
pred_stack <- aligned[[1]]

for (i in 2:length(aligned)) {
  pred_stack <- c(pred_stack, aligned[[i]])
}
class(pred_stack)
nlyr(pred_stack)
names(pred_stack)
#### FILL NA FOR SLOPE + ASPECT ####
# Fill slope NA with 0 (flat terrain)
if ("slope" %in% names(pred_stack)) {
  pred_stack$slope <- terra::ifel(is.na(pred_stack$slope), 0, pred_stack$slope)
}
# Fill aspect NA with 0 (undefined on flat terrain)
if ("aspect" %in% names(pred_stack)) {
  pred_stack$aspect <- terra::ifel(is.na(pred_stack$aspect), 0, pred_stack$aspect)
}
 # OPTIONAL: remove MK intercept layers entirely
pred_stack <- pred_stack[[!grepl("intercept", names(pred_stack))]]
#### write each predictor layer individually ####
for (nm in names(pred_stack)) {
  writeRaster(pred_stack[[nm]],
              filename = file.path("F:/Indices Eureka/RF MODEL/AlignedPredictors",
                                   paste0(nm, ".tif")),
              overwrite = TRUE)
}
pred_stack<-list.files("F:/Indices Eureka/RF MODEL/AlignedPredictors",
                       pattern = "\\.tif$", full.names = TRUE)
pred_stack<-rast(pred_stack)
crs(pred_stack)

#### stack: ####
pts_v <- vect(training_points)
pts_v<-project(pts_v, pred_stack)
vals <- terra::extract(pred_stack, pts_v, bind=TRUE)
```

```
vals_full <- cbind(pts_v, vals[,-1])
write.csv(vals_full, "C:\\Users\\Kethr\\OneDrive\\Desktop\\PhD\\data_points_training_MS2.csv")
pts_sf <- st_as_sf(vals_full, coords = c("x", "y"), crs = crs(pred_stack))
#check duplicates:
preds <- predictor_sets$set2
dup_idx <- duplicated(pts_sf[, preds])
sum(dup_idx)
grep("landcover", names(aligned), value = TRUE)
####Create Predictor sets: ####
predictor_sets <- list(
   # 1) ALL TC indices (slope + intercept + tau) + geomorph + land class
 #    +slope+aspect+elevation+surficial material
 set1 = c(
  "Landclass_2015",
 "TC_Brightness_MK_Trend_slope",
 "TC_Brightness_MK_Trend_tau",
 "TC_Brightness_MK_Trend_pvalue",
 "TC_Greenness_MK_Trend_slope",
 "TC_Greenness_MK_Trend_tau" ,
 "TC_Greenness_MK_Trend_pvalue" ,
 "TC_Wetness_MK_Trend_slope",
 "TC_Wetness_MK_Trend_tau",
 "TC_Wetness_MK_Trend_pvalue"
 ),
 # 6)  ALL TC indices (slope + intercept + tau) + land class
 #    +slope+aspect+elevation+surficial material
 set2 = c(
  "Landclass_2015",
 "TC_Brightness_MK_Trend_slope",
    "TC_Brightness_MK_Trend_tau",
 "TC_Brightness_MK_Trend_pvalue",
 "TC_Greenness_MK_Trend_slope",
 "TC_Greenness_MK_Trend_tau" ,
 "TC_Greenness_MK_Trend_pvalue" ,
 "TC_Wetness_MK_Trend_slope",
  "TC_Wetness_MK_Trend_tau",
 "TC_Wetness_MK_Trend_pvalue",
  "aspect","slope",
  "elevation"
),
set3 = c(
  "TC_Brightness_MK_Trend_slope",

  "TC_Brightness_MK_Trend_tau",
  "TC_Brightness_MK_Trend_pvalue",
  "TC_Greenness_MK_Trend_slope",

  "TC_Greenness_MK_Trend_tau" ,
  "TC_Greenness_MK_Trend_pvalue" ,
  "TC_Wetness_MK_Trend_slope",
```

```
    "TC_Wetness_MK_Trend_tau",
    "TC_Wetness_MK_Trend_pvalue"
      )
)
#### Train function ####
train_rf <- function(data,
                     response_col,
                     predictors,
                     ntree = 201,
                     mtry = 3,
                     test_split = 0.3,
                     seed = 123) {
  # Drop geometry and select relevant columns
  df <- data %>%
    st_drop_geometry() %>%
    dplyr::select(all_of(c(response_col, predictors)))
  # Convert response to factor
  df[[response_col]] <- as.factor(df[[response_col]])
  df <- na.omit(df)
  # Create 70/30 train-test split
  set.seed(seed)
  train_index <- createDataPartition(df[[response_col]], p = 1 - test_split, list = FALSE)
  training_set <- df[train_index, ]
  testing_set  <- df[-train_index, ]
  # Class counts for stratified RF sampling
  class_counts <- table(training_set[[response_col]])
  # Train the Random Forest
  rf_model <- randomForest(
    x = training_set[, predictors],
    y = training_set[[response_col]],
    ntree = ntree,
    mtry = mtry,
    importance = TRUE,
    strata = training_set[[response_col]],
    sampsize = as.vector(class_counts)
  )
  # Optional: evaluate on test set
  test_pred <- predict(rf_model, testing_set[, predictors], type= 'response')
  test_prob <- predict(rf_model, testing_set[, predictors], type= 'prob')
  confusion <- confusionMatrix(test_pred, testing_set[[response_col]])
  # Return model and evaluation
  list(
    model = rf_model,
    training_set = training_set,
    testing_set = testing_set,
    confusion_matrix = confusion,
    test_probabilities = test_prob,
    variable_importance = importance(rf_model)
  )
}
models <- list()
```

```
vals_df<-as.data.frame(vals_full,na.rm=FALSE)
colSums(is.na(vals_df[, predictor_sets$set1]))
for (name in names(predictor_sets)) {
  message("Training model: ", name)
  preds <- predictor_sets[[name]]
  models[[name]] <- train_rf(
    data = vals_df,         # corrected argument name
    response_col = "ClassID",
    predictors = preds,
    ntree = 301
  )
  # Optional: print accuracy
  acc <- models[[name]]$confusion_matrix$overall["Accuracy"]
  message("Accuracy for ", name, ": ", round(acc, 3))
}
models[["set1"]][["confusion_matrix"]][["overall"]]
predicted_rasters <- list()
output_folder <- "F:\\Indices Eureka\\RF MODEL\\RasterOutputs3"
for (name in names(models)) {
  rf_model <- models[[name]]$model
  preds <- predictor_sets[[name]]
  # Subset raster stack to only predictors used in this model
  pred_stack_subset <- pred_stack[[preds]]
  # Predict
  predicted_rasters[[name]] <- terra::predict(pred_stack_subset, rf_model, type="response",
na.rm=TRUE)# false?
  # Optionally save
  writeRaster(predicted_rasters[[name]] ,
              filename = file.path("F:\\Indices Eureka\\RF MODEL\\RasterOutputs_v2",
                                   paste0(name,"predicted_res.tif")),
              overwrite=TRUE)
}
predicted_rasters[[name]] <- terra::predict(pred_stack_subset, rf_model, type="response",
na.rm=TRUE)# false?
# Optionally save
writeRaster(predicted_rasters$set2,
            filename = file.path("F:\\Indices Eureka\\RF MODEL\\RasterOutputs_v2",
                                 paste0("predicted_set2_v3res.tif")),
            overwrite=TRUE)
  saveRDS(models, "F:/Indices Eureka/RF MODEL/models_all_sets_v4.rds")
models<-readRDS("F:/Indices Eureka/RF MODEL/models_all_sets_v4.rds")
accuracy_table <- data.frame(
  Model = names(models),
  Accuracy = sapply(models, function(m) m$confusion_matrix$overall["Accuracy"])
)
write_csv(accuracy_table,
          "F:/Indices Eureka/RF MODEL/Model_Accuracy_v4.csv")
conf_list <- lapply(models, function(m) {
  as.data.frame.matrix(m$confusion_matrix$table)
})
write_xlsx(conf_list,
```

```
        "F:/Indices Eureka/RF MODEL/Confusion_Matrices_v3.xlsx")
varimp_list <- lapply(models, function(m) {
  as.data.frame(m$variable_importance)
})
write_xlsx(varimp_list,
        "F:/Indices Eureka/RF MODEL/Variable_Importance_v3.xlsx")
varimp_list <- lapply(names(models), function(nm) (
  imp <- models[[nm]]$model$importance   # <-- use the real importance
  df <- as.data.frame(imp)
  df$Predictor <- rownames(df)
  # Put Predictor first
  df <- df[, c("Predictor", setdiff(colnames(df), "Predictor"))]

  df
})
names(varimp_list) <- names(models)
write_xlsx(varimp_list,    "F:/Indices Eureka/RF
MODEL/Variable_Importance_AllModels.xlsx")
library(writexl)
export_list <- list(
  Accuracy = accuracy_table,
  Confusion_Matrices = conf_list,
  Variable_Importance = varimp_list
)
# Flatten nested lists for writexl
flat_export <- c(
  list(Accuracy = accuracy_table),
  setNames(conf_list, paste0("Conf_", names(conf_list))),
  setNames(varimp_list, paste0("VarImp_", names(varimp_list)))
)
write_xlsx(flat_export,
        "F:/Indices Eureka/RF MODEL/All_Model_Results.xlsx")
Eureka Climate trends:

install.packages("weathercan",
              repos = c("https://ropensci.r-universe.dev",
                        "https://cloud.r-project.org"))
install.packages("tidyhydat", repos = "https://dev.ropensci.org")
install.packages("PIC", reps = "https://github.com/iffylaw/PIC.git")


library('devtools')
install_github("iffylaw/PIC")

#load required packages
library(weathercan)
library(tidyverse)
library(ggthemes)
library(dplyr)
library(ggplot2)
stations_dl() #update the server
```

```
eur <- stations_search(name="Eureka", interval="day")
alert<-stations_search(name="Alert", interval="day")

list(eur$station_id)
list(alert$station_id)

#gather up the data
eur_fin <- weather_dl(station_ids = c(1750,50737),
                      interval="day",
                      string_as = NULL)
eur_fin2 <- weather_dl(station_ids = c(53598,53599),
                      interval="day",
                      string_as = NULL)

#subset(year=="2022" & year=="2023") %>%

alert_weather<-weather_dl(station_ids=c(1731, 42463),
                          interval="day",
                          string_as = NULL)

#filter to remove NA
eur_filter = eur_fin %>%
  filter(!if_all(15:37, ~is.na(.))) %>%
  distinct(across(11:37), .keep_all = T) %>%
  mutate(loc="Station")
#%>%
 # subset(month=="07")

eur_filter2 = eur_fin2 %>%
  filter(!if_all(15:37, ~is.na(.))) %>%
  distinct(across(11:37), .keep_all = T) %>%
  mutate(loc="Airport")

alert_filter<-alert_weather%>%
  filter(!if_all(15:37, ~is.na(.))) %>%
  distinct(across(11:37), .keep_all = T)
#### Quick stats
names(climate)
# 1. Compute annual mean temperature for each year
annual_temp <- climate %>%
  group_by(year) %>%
  summarise(
    mean_annual_temp = mean(mean_monthly_temp, na.rm = TRUE),
    sd_annual_temp = sd(mean_monthly_temp, na.rm = TRUE),
    .groups = "drop"
  )

# 2. Identify the last 60 years in the dataset
# (so we can split into two 30-year periods)
max_year <- max(annual_temp$year, na.rm = TRUE)
```

```
period_recent  <- (max_year - 29):max_year
period_previous <- (max_year - 59):(max_year - 30)

# 3. Compute 30-year means
recent_mean <- annual_temp %>%
  filter(year %in% period_recent) %>%
  summarise(mean_recent = mean(mean_annual_temp, na.rm = TRUE),
            sd_recent = sd(mean_annual_temp, na.rm = TRUE))

previous_mean <- annual_temp %>%
  filter(year %in% period_previous) %>%
  summarise(mean_previous = mean(mean_annual_temp, na.rm = TRUE))

# 4. Compute the change between the two 30-year periods
trend_30yr <- tibble(
  mean_previous_30yr = previous_mean$mean_previous,
  mean_recent_30yr   = recent_mean$mean_recent,
  difference         = recent_mean$mean_recent - previous_mean$mean_previous
)

trend_30yr

library(trend)

mk <- mk.test(annual_temp$mean_annual_temp)
ts <- sens.slope(annual_temp$mean_annual_temp)

# Theil–Sen slope is °C per year
slope_per_year <- ts$estimates

# Convert to °C per decade
slope_per_decade <- slope_per_year * 10
slope_per_decade

period_previous

library(dplyr)

# 1. Compute annual total precipitation for each year
annual_precip <- climate %>%
  group_by(year) %>%
  summarise(
    total_annual_precip = sum(total_monthly_precip, na.rm = TRUE),
    .groups = "drop"
  )

# 2. Identify the last 60 years in the dataset
max_year <- max(annual_precip$year, na.rm = TRUE)

period_recent   <- (max_year - 29):max_year
period_previous <- (max_year - 59):(max_year - 30)
```

```
# 3. Compute 30-year totals (means of annual totals)
recent_mean <- annual_precip %>%
  filter(year %in% period_recent) %>%
  summarise(mean_recent = mean(total_annual_precip, na.rm = TRUE),
            sd_recent = sd(total_annual_precip, na.rm = TRUE))

previous_mean <- annual_precip %>%
  filter(year %in% period_previous) %>%
  summarise(mean_previous = mean(total_annual_precip, na.rm = TRUE))

# 4. Compute the change between the two 30-year periods
precip_trend_30yr <- tibble(
  mean_previous_30yr = previous_mean$mean_previous,
  mean_recent_30yr   = recent_mean$mean_recent,
  difference         = recent_mean$mean_recent - previous_mean$mean_previous
)

precip_trend_30yr

####


ggplot(monthly_anoms, aes(x = month, y = temp_anomaly, group = year, colour =
factor(decade))) +
  geom_hline(yintercept = 0, colour = "black", linewidth = 1) +
  geom_line(linewidth = 0.8, alpha = 0.8) +
  scale_colour_viridis_d(option = "turbo", name = "Decade") +
  labs(
    title = "Monthly Temperature Anomalies by 30-Year Period",
    x = "Month",
    y = "Temperature Anomaly (°C)"
  ) +
  facet_wrap(~ period_30yr, ncol = 1, scales = "free_y") +
  theme_bw() +
  theme(
    legend.position = "top",
    panel.grid.minor = element_blank()
  )
#####  Seasonal Annomaly
monthly_anoms <- monthly_anoms %>%
  mutate(
    season = case_when(
      month %in% c(12, 1, 2) ~ "DJF",
      month %in% c(3, 4, 5)  ~ "MAM",
      month %in% c(6, 7, 8)  ~ "JJA",
      month %in% c(9, 10, 11) ~ "SON"
    ),
    # shift December to next year for proper DJF grouping
    season_year = if_else(month == 12, year + 1, year)
  )
```

```
seasonal_climate <- monthly_anoms %>%
  group_by(season_year, season) %>%
  summarise(
    seasonal_temp = mean(mean_monthly_temp, na.rm = TRUE),
    .groups = "drop"
  )

seasonal_clim <- seasonal_climate %>%
  group_by(season) %>%
  summarise(
    mean_seasonal_temp = mean(seasonal_temp, na.rm = TRUE),
    .groups = "drop"
  )

seasonal_anoms <- seasonal_climate %>%
  left_join(seasonal_clim, by = "season") %>%
  mutate(
    seasonal_anomaly = seasonal_temp - mean_seasonal_temp,
    decade = (season_year %/% 10) * 10
  )

ggplot(seasonal_anoms, aes(x = season_year, y = seasonal_anomaly, colour = factor(decade))) +
  geom_hline(yintercept = 0, colour = "black", linewidth = 1) +
  geom_line(linewidth = 1) +
  geom_point(size = 2) +
  scale_colour_viridis_d(option = "turbo", name = "Decade") +
  facet_wrap(~ season, ncol = 2) +
  labs(
    title = "Seasonal Temperature Anomalies by Year",
    x = "Year",
    y = "Temperature Anomaly (°C)"
  ) +
  theme_bw() +
  theme(
    legend.position = "top",
    panel.grid.minor = element_blank()
  )

##### seasonal air temperature
monthly_climate <- monthly_climate %>%
  mutate(
    year  = as.numeric(year),
    month = as.numeric(month)
  )
monthly_climate_alert <- monthly_climate_alert %>%
  mutate(
    year  = as.numeric(year),
    month = as.numeric(month)
  )
```

```
monthly_climate <- monthly_climate %>%
  mutate(
    season = case_when(
      month %in% c(12, 01, 02) ~ "DJF",
      month %in% c(03, 04, 05) ~ "MAM",
      month %in% c(06, 07, 08) ~ "JJA",
      month %in% c(09, 10, 11) ~ "SON"
    ),
    season_year = if_else(month == 12, year + 1, year)
  )

monthly_climate_alert <- monthly_climate_alert %>%
  mutate(
    season = case_when(
      month %in% c(12, 01, 02) ~ "DJF",
      month %in% c(03, 04, 05) ~ "MAM",
      month %in% c(06, 07, 08) ~ "JJA",
      month %in% c(09, 10, 11) ~ "SON"
    ),
    season_year = if_else(month == 12, year + 1, year)
  )

seasonal_temp <- monthly_climate %>%
  group_by(station_id, season_year, season) %>%
  summarise(
    seasonal_temp = mean(mean_monthly_temp, na.rm = TRUE),
    .groups = "drop"
  )

seasonal_temp <- seasonal_temp %>%
  mutate(decade = (season_year %/% 10) * 10)


seasonal_temp_alert <- monthly_climate_alert %>%
  group_by(station_id, season_year, season) %>%
  summarise(
    seasonal_temp = mean(mean_monthly_temp, na.rm = TRUE),
    .groups = "drop"
  )

seasonal_temp_alert <- seasonal_temp_alert %>%
  mutate(decade = (season_year %/% 10) * 10)

a<-seasonal_temp[c(4:318),]
b<-seasonal_temp_alert[c(3:313),]

seasonal<-rbind(a,b )
names(seasonal)

seasonal$station_id <-factor(seasonal$station_id)
```

```
#colour = factor(decade)

Seaonal<-ggplot(seasonal, aes(x = season_year, y = seasonal_temp,
                              color=station_id, group=station_id)) +
  geom_line(linewidth = 0.75, aes(linetype=station_id)) +
  facet_wrap(~ season, ncol = 2, scales = "free_y") +
  scale_y_continuous(labels = scales::number_format(accuracy = 1)) +
  scale_color_manual(
    values = c(
      "1750"  = "black",
      "50737" = "black",
      "1731"  = "red",
      "42463" = "red"
    )
  ) +
  scale_linetype_manual(
    values = c(
      "1750"  = 1,
      "50737" = 2,
      "1731"  = 1,
      "42463" = 2
    )
  ) +
  labs(
    x = "Year",
    y = "Seasonal Mean Temperature (°C)"
  ) +
  theme_bw() +
  theme(
    legend.position = "top",
    panel.grid.minor = element_blank(),
    axis.text=element_text(colour="black")

  )
Seaonal

unique(seasonal$station_id)

seasonal_means<-write.csv(seasonal_temp, "/Users/kethracampbell-
heaton/Library/CloudStorage/OneDrive-
Personal/Desktop/PhD/Eureka_Cliamte_Season_4725.csv")

names(monthly_climate)

monthly_all<-rbind(monthly_climate[c(4:318),-2], monthly_climate_alert[c(3:313),])

seasonal_TDD_eu <- monthly_climate[c(4:318),] %>%
  group_by(station_id, season_year, season) %>%
  summarise(
    seasonal_tdd1 = mean(TDD, na.rm = TRUE),
    .groups = "drop"
```

```
  )

seasonal_TDD_al <- monthly_climate_alert[c(3:313),] %>%
  group_by(station_id, season_year, season) %>%
  summarise(
    seasonal_tdd1 = mean(TDD, na.rm = TRUE),
    .groups = "drop"
  )

# Filter for May–October
tdd_plot_data_eu <- monthly_climate %>%
  filter(month %in% 6:8)

# Create month labels
tdd_plot_data_eu$month <- factor(
  tdd_plot_data_eu$month,
  levels = 6:8,
  labels = c( "June", "July", "August")
)
tdd_plot_data_eu$station_id<-as.factor(tdd_plot_data_eu$station_id)

# Filter for May–October
tdd_plot_data_al <- monthly_climate_alert %>%
  filter(month %in% 6:8)

# Create month labels
tdd_plot_data_al$month <- factor(
  tdd_plot_data_al$month,
  levels = 6:8,
  labels = c( "June", "July", "August")
)
tdd_plot_data_al$station_id<-as.factor(tdd_plot_data_al$station_id)

# Plot
TDDeu<-ggplot(tdd_plot_data_eu, aes(x = year, y = TDD, color = month)) +
  geom_line(linewidth = 1, aes(linetype = station_id)) +
  scale_color_manual(
    values = c(
      "June" = "darkblue",
      "July" = "darkgreen",
      "August" = "purple"
    )
  ) +scale_linetype_manual(
    values = c(
      "1750"  = 1,
      "50737" = 2
    )
  )+ guides(linetype="none")+

  labs(
    x = "Year",
```

```
    y = "TDD",
    color = NULL,
    title = "Eureka, Nu"
  ) +
  theme_bw(base_size = 14) +
  theme(
    panel.grid = element_blank(),           # remove grid lines
    axis.text = element_text(color = "black"),
    axis.title = element_text(color = "black"),
    legend.position = c(0.05, 0.95),        # inside plot, top-left
    legend.justification = c("left", "top"),
    legend.background = element_rect(fill = alpha("white", 0.7) )
  )
TDDeu

TDDal<-ggplot(tdd_plot_data_al, aes(x = year, y = TDD, color = month)) +
  geom_line(linewidth = 1, aes(linetype = station_id)) +
  scale_color_manual(
    values = c(
      "June" = "darkblue",
      "July" = "darkgreen",
      "August" = "purple"
    )
  )+ scale_linetype_manual(
    values = c(
      "1731"  = 1,
      "42463" = 2
    ) )+
  guides(linetype="none")+
  labs(
    x = "Year",
    y = "TDD",
    color = NULL,
    title="Alert, Nu"
  ) +
  theme_bw(base_size = 14) +
  theme(
    panel.grid = element_blank(),           # remove grid lines
    axis.text = element_text(color = "black"),
    axis.title = element_text(color = "black"),
    legend.position = c(0.05, 0.95),        # inside plot, top-left
    legend.justification = c("left", "top"),
    legend.background = element_rect(fill = alpha("white", 0.7) )
  )+  scale_y_continuous(limits = c(0, 309),
                         breaks = c(100, 200, 300))

TDDal
Seaonal

grid.arrange(Seaonal,grid.arrange(TDDeu, TDDal, ncol=2), ncol=1 )
```

```
julyTDD<-subset(tdd_plot_data_eu, tdd_plot_data_eu$month=="July")
mean(julyTDD$TDD[c(53:79)])
sd(julyTDD$TDD[c(53:79)])
```

Appendix C: Chapter 3 Code

Code for Chapter 3
Creating Plots:
Stable water isotopes:

```
 EurekaStream.dat<-  EurekaStream.dat %>%
   mutate(
     Site_clean = str_remove_all(Site.., "\\s+"),  # remove spaces
     Disturbance = case_when(
       Site_clean %in% c("3", "7") ~ "Undisturbed",
       TRUE ~ "Disturbed"
     )
   )

 iso<-EurekaStream.dat %>%
   ggplot(aes(x = Processed.Delta.18O, y = Processed.Delta.2H, color = Day,shape=Disturbance
)) +
   geom_point(size = 2, alpha = 0.8) +
   #geom_smooth(method = "lm", se = FALSE, linetype = "dashed") +
   facet_grid(Creek ~ Year, labeller = labeller(Creek = stream_labels)) +
   labs(
     x = expression(delta^{18}*O~"\u2030 (VSMOW)"),
     y = expression(delta^{2}*H~"\u2030 (VSMOW)"),
     color = "Day (July)"
   ) +
   #scale_color_manual(values = site_colors) +
   theme_bw(base_size = 14) +
   theme(
     legend.position = "right",
     strip.background = element_rect(fill = "grey90", color = NA),
     strip.text = element_text(face = "bold"),
     panel.grid.minor = element_blank(),
     plot.margin = margin(5, 50, 5, 5)
   ) +

   # --- GMWL ---
   geom_abline(intercept = 10, slope = 8, color = "black", linetype = "dotted", size = 1) +
   annotate("text", x = -25, y = -180, label = "GMWL", color = "black", size = 4, fontface =
"bold") +

   # --- LMWL ---
   geom_abline(intercept = -9.140, slope = 7.434, color = "blue", linetype = "dashed", size = 1) +
   annotate("text", x = -25.5, y = -185, label = "LMWL", color = "blue", size = 4, fontface =
"bold")

 png("18O~D_sites.png", width = 10, height = 6, units = "in", res = 300)
 print(iso)
 dev.off()

## Manuscript scheoller
```

```
{
library(ggplot2)
library(dplyr)
library(gridExtra)
library(RColorBrewer)

# Update creek names in site_means
site_means <- site_means %>%
  mutate(Creek = case_when(
    Creek == "stationcreek" ~ "Station Creek",
    Creek == "blacktop" ~ "Blacktop Creek",
    TRUE ~ Creek
  ))

# Define ion order
ion_levels <- c("Ca", "Mg", "Na", "K", "Cl", "SO4")
ion_labels <- c(
  "Ca",
  "Mg",
  "Na",
  "K",
  "Cl",
  expression(SO[4])
)
# Color-blind friendly (Okabe–Ito) palette
okabe_ito <- c(
  "#E69F00", # orange
  "#56B4E9", # sky blue
  "#009E73", # bluish green
  "#A6A300", # darker yellow-green (better contrast)
  "#0072B2", # blue
  "#D55E00", # vermillion
  "#CC79A7", # reddish purple
  "#999999"  # grey
)
# Assign colors to sites
sites <- unique(site_means$Site)
site_colors <- setNames(okabe_ito[seq_along(sites)], sites)

# Compute global y-axis limits
y_min <- min(site_means$mean_meqL, na.rm = TRUE)
y_max <- max(site_means$mean_meqL, na.rm = TRUE)

# Use site_means across all creeks/sites/years
y_global_min <- min(site_means$mean_meqL, na.rm = TRUE)
# Ensure >0 for log scale
y_global_min <- ifelse(y_global_min <= 0,
min(site_means$mean_meqL[site_means$mean_meqL > 0], na.rm = TRUE), y_global_min)

y_global_max <- max(site_means$mean_meqL, na.rm = TRUE)
```

```
plot_scholler_panel <- function(df, creek, year, dist_type, y_min, y_max) {

  df_sub <- df %>%
    filter(Creek == creek, Year == year, Disturbance == dist_type) %>%
    filter(!is.na(Ion))

  # Get mean TDS per site
  tds_df <- df_sub %>%
    distinct(Site, mean_TDS)
  n_sites <- nrow(tds_df)
  # Vertical spacing — adjust as needed
  y_range <- log10(y_max) - log10(y_min)
  spacing_factor <- 0.08  # vertical space between labels
  y_stagger <- 10^(log10(y_min) + (0:(n_sites - 1)) * spacing_factor)
  # Reverse order so they stack upward
  tds_df$y_pos <- rev(y_stagger)
  tds_df$x_pos <- length(ion_levels) - 0.2  # near last ion, slightly inside

  ggplot(df_sub, aes(x = Ion, y = mean_meqL, group = Site, color = Site)) +
    geom_line(linewidth = 0.8, alpha = 0.9, show.legend = TRUE) +
    geom_point(size = 2, show.legend = TRUE) +
    # --- TDS text (non-overlapping, bottom-right) ---
    geom_text(
      data = tds_df,
      aes(x = x_pos, y = y_pos,
          label = paste0("TDS=", round(mean_TDS, 1), " ppm"),
          color = Site),
      hjust = 0.75, size = 3
    ) +

    scale_color_manual(values = site_colors) +
    guides(color = guide_legend(
      title = "Site",
      override.aes = list(linetype = 1, shape = 16, size = 0)
    )) +
    scale_x_discrete(limits = ion_levels, labels = ion_labels) +
    scale_y_log10(limits = c(y_min, y_max)) +
    labs(
      title = paste(creek, year, "-", dist_type),
      x = "Major Ions",
      y = expression("Mean Concentration (meq/L, log scale)")
    ) +
    theme_bw(base_size = 12) +
    theme(
      legend.position = c(0.05, 0.05),  # bottom-left
      legend.justification = c("left", "bottom"),
      legend.background = element_rect(fill = alpha("white", 0.75), color = NA),
      legend.key.size = unit(0.4, "cm"),
      legend.text = element_text(size = 9),
      panel.grid.minor = element_blank(),
      axis.text.x = element_text(angle = 45, hjust = 1),
```

```
    plot.title = element_text(size = 12, face = "bold", hjust = 0.5)
  )
}
# Generate all Schöller plots
creek_year_dist <- site_means %>% distinct(Creek, Year, Disturbance)
plot_list <- list()
for(i in 1:nrow(creek_year_dist)) {
  c <- creek_year_dist$Creek[i]
  y <- creek_year_dist$Year[i]
  d <- creek_year_dist$Disturbance[i]

  p <- plot_scholler_panel(site_means, c, y, d, y_min = y_global_min, y_max = y_global_max)
  plot_list[[i]] <- p
}
# Arrange plots in 4x2 grid
grid_arrange <- grid.arrange(grobs = plot_list, nrow = 2, ncol = 4)

library(gridExtra)

# Arrange plots but save as a single grob
grid_grob <- arrangeGrob(grobs = plot_list, nrow = 2, ncol = 4)

# Export as PNG
ggsave("scholler_plots.png", grid_grob, width = 16, height = 8, dpi = 300)
  }
##############
  ## TIME SERIES
  library(ggplot2)
library(dplyr)
library(scales)
library(RColorBrewer)
ions_of_interest <- c("Cl", "SO4", "TDS")
# Ensure Ion factor
data_long$Ion <- factor(data_long$Ion, levels = ions_of_interest)

# Labeller function for Ion
# Define ion labels correctly for label_parsed
ion_labels <- c(
  "Cl"  = "'Cl'^'-'",      # chloride (Cl⁻)
  "SO4" = "'SO'[4]^'2-'",  # sulfate (SO₄²⁻)
  "TDS" = "'TDS'"          # plain TDS
)

# Color-blind friendly (Okabe–Ito) palette
okabe_ito <- c(
  "#E69F00", "#56B4E9", "#009E73", "#A6A300",
  "#0072B2", "#D55E00", "#CC79A7", "#999999"
)
sites <- unique(site_means$Site)
site_colors <- setNames(okabe_ito[seq_along(sites)], sites)
```

```
# Point shapes for Disturbance
dist_shapes <- c("Disturbed" = 16, "Undisturbed" = 17)  # circle vs triangle

# Compute global y-limits per Ion
y_limits <- data_long %>%
  filter(Ion %in% ions_of_interest) %>%
  group_by(Ion) %>%
  summarise(
    ymin = min(Concentration, na.rm = TRUE),
    ymax = max(Concentration, na.rm = TRUE),
    .groups = "drop"
  )
y_min_lookup <- setNames(y_limits$ymin, y_limits$Ion)
y_max_lookup <- setNames(y_limits$ymax, y_limits$Ion)
get_y_limits <- function(ion) c(y_min_lookup[ion], y_max_lookup[ion])

# Plot
time_series_plot <- data_long %>%
  filter(Ion %in% ions_of_interest) %>%
  ggplot(aes(x = Day, y = Concentration, color = Site, shape = Disturbance)) +
  geom_point(size = 2) +  # no lines
  facet_grid(
    Year ~ Ion + Creek,
    scales = "free_y",
    labeller = labeller(
      Creek = Creek.labs,
      Ion   = as_labeller(ion_labels, label_parsed)
    )) +
  scale_color_manual(values = site_colors) +
  scale_shape_manual(values = dist_shapes) +
  theme_bw(base_size = 13) +
  theme(
    legend.position = "right",             # outside on the right
    legend.justification = c("left", "top"),
    legend.background = element_rect(fill = alpha("white", 0.75), color = NA),
    legend.key.size = unit(0.4, "cm"),
    legend.text = element_text(size = 10),
    axis.text.x = element_text(angle = 45, hjust = 1),
    strip.text = element_text(size = 11),
    panel.grid.minor = element_blank(),
    plot.title = element_text(size = 14, face = "bold", hjust = 0.5),
    plot.margin = margin(5, 50, 5, 5)     # extra right margin for legend
  ) +
  labs(
    title = "Temporal Dynamics of Key Solutes by Creek and Year",
    x = "Date",
    y = "Concentration (mg/L)")
time_series_plot
# Example: your plot is called p
png("Ionsthroughtime_sites.png", width = 10, height = 6, units = "in", res = 300)
print(time_series_plot)
```

```
dev.off()

data$nacl<-data$Na_meq/data$Cl_meq

# Typical seawater Na/Cl molar ratio
sw_ratio <- 0.86  # example value, adjust if needed

  b<-  ggplot(data, aes(x = Day, y = nacl, color = Site, shape = Disturbance)) +
    geom_point(size = 2) +  # no lines
    scale_color_manual(values = site_colors) +
    scale_shape_manual(values = dist_shapes) +
    theme_bw(base_size = 13) +
    theme(
      legend.position = "right",             # outside on the right
      legend.justification = c("left", "top"),
      legend.background = element_rect(fill = alpha("white", 0.75), color = NA),
      legend.key.size = unit(0.4, "cm"),
      legend.text = element_text(size = 10),
      axis.text.x = element_text(angle = 45, hjust = 1),
      strip.text = element_text(size = 11),
      panel.grid.minor = element_blank(),
      plot.title = element_text(size = 14, face = "bold", hjust = 0.5),
      plot.margin = margin(5, 50, 5, 5)     # extra right margin for legend
    ) +
    labs(
      x = "Date (July)",
      y = "Na/Cl")+
    facet_grid(Creek~Year, labeller = labeller(Creek = stream_labels))+
    geom_hline(yintercept = sw_ratio, linetype = "dashed", color = "black", size = 0.7)+
    geom_text(
      aes(x = 10, y = sw_ratio - 0.2, label = "Seawater"),  # adjust x and y for positioning
      inherit.aes = FALSE,
      color = "black",
      size = 3)
  b
  png("NaCl_MR_throughtime_sites.png", width = 10, height = 6, units = "in", res = 300)
  print(b)
  dev.off()
######
  data <- data %>%
    mutate(SO4_Cl = (SO4 / 96.06) / (Cl / 35.45))
  c<-ggplot(data, aes(x = Day, y = SO4_Cl, color = Site, shape = Disturbance)) +
    geom_point(size = 2) +
    #geom_line(aes(group = interaction(Site, Disturbance)), alpha = 0.4) +
    scale_color_manual(values = site_colors) +
    scale_shape_manual(values = dist_shapes) +
    facet_grid(Creek ~ Year, labeller = labeller(Creek = stream_labels)) +
    labs(x = "Date (July)", y = expression(SO[4]^2/Cl^-~ "") )+
    #geom_hline(yintercept = 0.05, linetype = "dashed", color = "black") +  # seawater reference
    #annotate("text", x = Inf, y = 0.05, label = "Seawater", hjust = 1.1, vjust = -0.5, size = 3) +
    theme_bw(base_size = 13) +
```

```
  theme(
    legend.position = "right",
    axis.text.x = element_text(angle = 45, hjust = 1),
    strip.text = element_text(size = 11),
    panel.grid.minor = element_blank(),
    plot.title = element_text(size = 14, face = "bold", hjust = 0.5)
  )

png("So4CL_MR_throughtime_sites.png", width = 10, height = 6, units = "in", res = 300)
print(c)
dev.off()
```

Appendix D: Chapter 4 Code

Water-Level Time Series Correction

Rationale

During field deployment in 2022, several water-level loggers were displaced by high flows and required repositioning. These movements produced abrupt, non-hydrologic step-changes in the recorded stage data. Correction was required to reconstruct a continuous stage record suitable for rating-curve development and hydrological analysis.

Identification of Non-Natural Level Changes

Raw water-level data were first differenced ($\Delta h = h_i - h_{i-1}$) to separate natural hydrologic variability from abrupt mechanical disturbances.

- Natural changes (e.g., rising/falling limb of a hydrograph) produced smooth, autocorrelated Δh patterns.
- Non-natural changes resulting from logger movement appeared as isolated, single-interval anomaly, termed anomalous events.

A threshold of $\Delta h > \pm 0.02$ m (2 cm) was used to classify anomalous events. This value corresponded to the maximum rate of natural stage change observed under normal hydrologic conditions during rain events and melt pulses. All identified anomalies were single-time-step events, consistent with sudden physical displacement rather than natural hydrological forcing.

Segmentation of the Time Series

After detecting each anomalous Δh event, the dataset was segmented at the timestamp of the disturbance. For a sequence of n disturbances:

- Segment 1 = original data
- Segment 2 = data following disturbance 1
- Segment 3 = data following disturbance 2
- … continued through segment n + 1

Each segment thus represented a period when the logger position was stable.

S3.4 Offset Correction Procedure

To restore continuity:

1. For each anomalous event, the magnitude of the step-change (the Δh anomaly) was recorded.
2. Downstream segments were adjusted by subtracting the cumulative offset generated by all preceding disturbances.
3. If two or more disturbances occurred, offsets were compounded such that:
   Corrected h = recorded h – $\Sigma(\text{offset}_1 \ldots \text{offset}_i)$
   where offset_i is the i-th anomaly.

4. Corrections were applied iteratively until continuity was achieved across all segments.

This method preserves the shape of the hydrograph within each stable period while restoring realistic transitions between segments.

Verification

Corrected time series were visually inspected to ensure:

- Removal of artificial jumps
- Preservation of natural rising/falling limbs
- No introduction of negative water levels
- Continuity during low-flow periods

For 2023, logger stability was high and corrections were rarely required.

Example Calculation:

Table D1. Sample of data from Site 1 for July 7, 2022 for 14:00-23:00. Includes logger-recorded (after pressure adjustments) water level, the time of the recording, the difference in water level from previous measurement (Δh) and the calculated manual adjusted water level. Bold number indicates the anomalous event.

Logger-Recorded Level (m)	Date-Time	Difference from previous measurement (Δh; m)	Adjusted Level (m)
0.2136	7/7/2022 14:00	-0.0012	0.2136
0.2158	7/7/2022 14:30	0.0022	0.2158
0.2144	7/7/2022 15:00	-0.0014	0.2144
0.218	7/7/2022 15:30	0.0036	0.218
0.2251	7/7/2022 16:00	0.0071	0.2251
0.2264	7/7/2022 16:30	0.0013	0.2264
0.2314	7/7/2022 17:00	0.005	0.2314
0.2347	7/7/2022 17:30	0.0033	0.2347
0.2458	7/7/2022 18:00	0.0111	0.2458
0.2425	7/7/2022 18:30	-0.0033	0.2425
0.1941	7/7/2022 19:00	**-0.0484**	0.2425
0.1828	7/7/2022 19:30	-0.0113	0.2312
0.1813	7/7/2022 20:00	-0.0015	0.2297
0.187	7/7/2022 20:30	0.0057	0.2354
0.1861	7/7/2022 21:00	-0.0009	0.2345
0.1806	7/7/2022 21:30	-0.0055	0.229
0.173	7/7/2022 22:00	-0.0076	0.2214
0.1798	7/7/2022 22:30	0.0068	0.2282
0.1831	7/7/2022 23:00	0.0033	0.2315
0.1859	7/7/2022 23:30	0.0028	0.2343

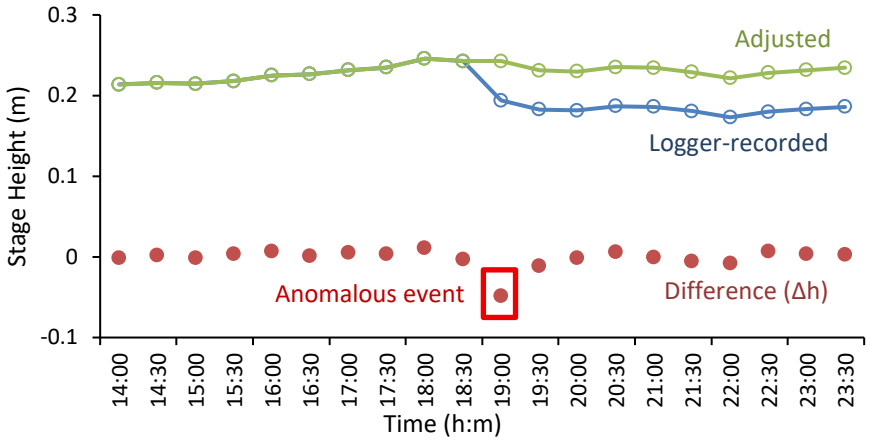


Figure D1. Sample stream water level data for Site 1 on July 7, 2022, from 14:00 to 23:00. Logger-recorded water level (m) outlined in blue, adjusted level in green, difference in orange, anomalous event indicated by red box.

Anomalous event offset = -0.0484 m

All values after 19:00 are corrected for offset:

Recorded water level – Anomalous offset = Adjusted water level

Therefore, for 19:00: 0.1941- (-0.0484) = 0.2425
19:30: 0.1828 - (-0.0484) = 0.2312
20:00: 0.1813 - (-0.0484) = 0.2297 and so on.

This method catches when the logger is displaced in the stream by high flow events and manual re-adjustments (occasionally necessary when water level drops rapidly in nival-fed streams). This method does smooth over some event data where the manual adjustments are made but, preserves most of the data signal.

Code for Chapter 4:
Parsing two datasets together to get the discharge measurement for each sediment reading:

```
### Stream sediment load work
library(fuzzyjoin)
library(data.table)
library(dplyr)
library(lubridate)

setwd("C:\\Users\\Kethr\\OneDrive\\Desktop\\PhD\\Working Folder\\Eureka Data\\Stream Discharge\\Stage Discharge")
EurekaStream.dat <- read.csv("C:\\Users\\Kethr\\OneDrive\\Desktop\\PhD\\Working Folder\\Eureka Data\\CumulativeData\\EurekaData_051724.csv")
log.dat<-read.csv("LoggerData_combined.csv")

# Prepare datasets
EurekaStream_small <- EurekaStream.dat %>%
  mutate(DateTime = as.POSIXct(paste(Date, time), format = "%m/%d/%Y %H:%M")) %>%
  select(Site.and.Year, DateTime, SedimentLoad_mgL = sediment.load..mg.L., StreamConductivity = cond) %>%
```

```
  na.omit()

# Create DateTime in log_small
log_small <- log.dat %>%
  mutate(
    # Combine date and time into POSIXct
    #DateTime = as.POSIXct(Date.and.time, format = "%Y-%m-%d %H:%M:%S")
    # If Date.and.time is not complete, use Date + Time:
     DateTime = as.POSIXct(paste(Date, Time), format = "%m/%d/%Y %H:%M")
  ) %>%
  select(Site.and.Year, DateTime, Discharge_ls, LogConductivity = Conductivity)

# Convert to data.table
setDT(EurekaStream_small)
setDT(log_small)

# 4 Function to get nearest logger row per EurekaStream row
get_nearest_logger <- function(sample_dt, logger_dt, max_diff_mins = 25) {
  # Add an ID for sample rows
  sample_dt[, sample_id := .I]

  # Cross join by Site.and.Year
  combined <- logger_dt[sample_dt, on = .(Site.and.Year2), allow.cartesian = TRUE]

  # Compute time difference in minutes
  combined[, time_diff := abs(as.numeric(difftime(DateTime, i.DateTime, units="mins")))]

  # Keep only logger rows within max_diff_mins
  combined <- combined[time_diff <= max_diff_mins]

  # Take the nearest logger row per sample
  nearest <- combined[, .SD[which.min(time_diff)], by = sample_id]

  # Merge nearest logger info back to EurekaStream
  result <- merge(sample_dt, nearest[, .(sample_id, Discharge_ls, LogConductivity)], by = "sample_id",
all.x = TRUE)

  # Clean up
  result[, sample_id := NULL]
  return(result)
}
log_small$Site.and.Year2<-log_small$Site.and.Year
EurekaStream_small[, Site.and.Year2 := gsub(" (LS|RS|SC) ", " ", Site.and.Year)]


# 5 Apply function
merged_small <- get_nearest_logger(EurekaStream_small, log_small, max_diff_mins = 25)

# 6 Keep desired columns
merged_small <- merged_small %>%
  select(Site.and.Year, DateTime, SedimentLoad_mgL, Discharge_ls, LogConductivity,
StreamConductivity)

# Remove the middle stream code (LS, RS, SC)
#this gets a lot of the data but still not enough. Will need to manually edit now
write.csv(merged_small, "StreamSedimentLoadxDischarge_4.csv")
```

Code for the giant multiplot figure:

```
## Goal of this script is to create a master
## figure shwoing both years of data for btoh streams.

## Packages
library(ggplot2)
library(tidyverse)
library(gridExtra)
library(cowplot)
library(dplyr)
library(zoo)
library(grid)
library(ggnewscale)
library(ggtext)

library(shadowtext)
library(patchwork)
library(ggpubr)
library(GGally)


## Data - stream temp, discharge, conductivity?, sediment load, air temp, rain,

#stream temperature - SITE
#climate forcing - temp, ppt solar
#discharage
#suspended sediment

setwd("/Users/kethracampbell-heaton/Library/CloudStorage/OneDrive-
Personal/Desktop/PhD/Chapters/Streams x Climate")

logger22<-read.csv("/Users/kethracampbell-heaton/Library/CloudStorage/OneDrive-
Personal/Desktop/PhD/Chapters/Streams x Climate/Logger2022.csv")
logger23<-read.csv("/Users/kethracampbell-heaton/Library/CloudStorage/OneDrive-
Personal/Desktop/PhD/Chapters/Streams x Climate/Logger2023.csv")

solar22<-read.csv("/Users/kethracampbell-heaton/Library/CloudStorage/OneDrive-
Personal/Desktop/PhD/Chapters/Streams x Climate/SolarElevation2022.csv")
solar23<-read.csv("/Users/kethracampbell-heaton/Library/CloudStorage/OneDrive-
Personal/Desktop/PhD/Chapters/Streams x Climate/SolarElevation2023.csv")

climate22<-read.csv("/Users/kethracampbell-heaton/Library/CloudStorage/OneDrive-
Personal/Desktop/PhD/Chapters/Streams x Climate/EurekaClimate2022.csv")
climate23<-read.csv("/Users/kethracampbell-heaton/Library/CloudStorage/OneDrive-
Personal/Desktop/PhD/Chapters/Streams x Climate/EurekaClimate2023.csv")

EurekaStream.dat <- read.csv('/Users/kethracampbell-heaton/Library/CloudStorage/OneDrive-
Personal/Desktop/PhD/Working Folder/Eureka Data/CumulativeData/EurekaData_051724.csv')
SedimentLoad.dat<-read.csv('/Users/kethracampbell-heaton/Library/CloudStorage/OneDrive-
Personal/Desktop/PhD/Working Folder/Eureka Data/Stream Discharge/Stage
Discharge/StreamSedimentLoadxDischarge.csv')

##### READ DATA IN WINDOWS ####
```

```
logger22<-read.csv("C:/Users/Kethr/OneDrive/Desktop/PhD/Chapters/Streams x Climate/Logger2022.csv")
logger23<-read.csv("C:\\Users\\Kethr\\OneDrive\\Desktop\\PhD\\Chapters\\Streams x Climate\\Logger2023.csv")

solar22<-read.csv("C:\\Users\\Kethr\\OneDrive\\Desktop\\PhD\\Chapters\\Streams x Climate\\SolarElevation2022.csv")
solar23<-read.csv("C:\\Users\\Kethr\\OneDrive\\Desktop\\PhD\\Chapters\\Streams x Climate\\SolarElevation2023.csv")

climate22<-read.csv("C:\\Users\\Kethr\\OneDrive\\Desktop\\PhD\\Chapters\\Streams x Climate\\EurekaClimate2022.csv")
climate23<-read.csv("C:\\Users\\Kethr\\OneDrive\\Desktop\\PhD\\Chapters\\Streams x Climate\\EurekaClimate2023.csv")

EurekaStream.dat<-read.csv("C:/Users/Kethr/OneDrive/Desktop/PhD/Working Folder/Eureka Data/CumulativeData/EurekaData_051724.csv")
SedimentLoad.dat<-read.csv("C:/Users/Kethr/OneDrive/Desktop/PhD/Working Folder/Eureka Data/Stream Discharge/Stage Discharge/StreamSedimentLoadxDischarge_4.csv")


#######

SedimentLoad.dat<-SedimentLoad.dat[c(1:174),]

climate22_stat<-climate22[c(145:528),]
climate22_ap<-climate22[c(889:1249),]

climate23_stat<-climate23[c(112:491),] #3pm july 5 to july 21 at 10am
climate23_ap<-climate23[c(856:1235),]

solar22$TOA_rad<-1361 * sin(solar22$Solar.Elevation.corrected.for.atm.refraction..deg. * pi/180)
solar23$TOA_rad<-1361 * sin(solar23$Solar.Elevation.corrected.for.atm.refraction..deg. * pi/180)



### Data Date formatting ###
# Convert to Date (if not already)
EurekaStream.dat$Date2 <- as.Date(EurekaStream.dat$Date)

# Check what years exist
unique(format(EurekaStream.dat$Date2, "%Y"))

dt <- as.POSIXct(as.character(EurekaStream.dat$Date.time..LST.),
format = "%m/%d/%Y %H:%M",
tz = "")

library(lubridate)

dt <- mdy_hm(as.character(EurekaStream.dat$Date.time..LST.))
summary(dt)  # Should show proper POSIXct values


solar22$Day <- yday(as.POSIXct(solar22$Date.and.Time.UTC6))
solar23$Day <- yday(as.POSIXct(solar23$Date.time.UTC6))
```

```
logger22$Day <- yday(as.POSIXct(logger22$Date.and.Time.UTC6))
logger23$Day <- yday(as.POSIXct(logger23$Date.and.Time.UTC6))

### Make one solid date range for plotting nicely

doy_range <- range(
  solar22$Day, solar23$Day,
  climate22_stat$day, climate23_stat$day,
  logger22$Day, logger23$Day,
  sed22_blacktop$Day, sed23_blacktop$Day,
  sed22_station$Day, sed23_station$Day,
  na.rm = TRUE
)

doy_ticks <- pretty(doy_range, n = 6)


## Figure

######

library(lubridate)
library(RColorBrewer)

# ---- Axis helpers ----
y_ticks_n <- function(lim, n = 4, digits = NULL) {
  ticks <- pretty(lim, n = n)
  if (!is.null(digits)) ticks <- round(ticks, digits)
  ticks
}

add_x_axis <- function(x, show_labels = FALSE) {
  ax <- pretty(x, n = 5)
  axis(1, at = ax, labels = if (show_labels) ax else FALSE)
}

# Keep only rows with sediment
sed <- EurekaStream.dat[!is.na(dt) & !is.na(EurekaStream.dat$sediment.load..mg.L.), ]
sed$DateTime <- dt[!is.na(dt) & !is.na(EurekaStream.dat$sediment.load..mg.L.)]

# Extract year
sed$Year <- year(sed$DateTime)

# Split
sed22 <- sed[sed$Year == 2022, ]
sed23 <- sed[sed$Year == 2023, ]


# Convert sediment datetime
sed22$DateTime <- mdy_hm(as.character(sed22$Date.time..LST.))
sed23$DateTime <- mdy_hm(as.character(sed23$Date.time..LST.))

# Split sediment by stream (assumes Creek.Name.Year identifies stream)
sed22_blacktop <- sed22[grep("blacktop 2022", sed22$Creek.Name.Year), ]
sed22_station  <- sed22[grep("stationcreek 2022", sed22$Creek.Name.Year), ]
sed23_blacktop <- sed23[grep("blacktop 2023", sed23$Creek.Name.Year), ]
```

```
sed23_station  <- sed23[grep("stationcreek 2023", sed23$Creek.Name.Year), ]

# Unique sites and colors
sites22_bt <- unique(sed22_blacktop$Site..)
sites22_st <- unique(sed22_station$Site..)
sites23_bt <- unique(sed23_blacktop$Site..)
sites23_st <- unique(sed23_station$Site..)

cols_bt <- c(
  "1" = "blue",
  "2" = "green",
  "3" = "red")
cols_bt23 <- c(
  "1" = "blue",
  "2 LS" = "green",
  "2 RS" = "magenta",
  "3" = "red")
cols_st23 <-  c(
    "4"    = "orange",
    "5"    = "purple",
    "5 SC" = "black",
    "6"    = "darkgrey",
    "7"  = "darkgreen"
  )
cols_st22 <- c(
  "4"    = "orange",
  "5"    = "purple",
  "6"    = "darkgrey"
)

{
  # Layout 9 rows x 2 columns
layout(matrix(1:18, ncol=2, byrow=TRUE))
par(oma=c(4,5,3,3), mar=c(1.5,4,1.2,2), las=1)

# --------------------------
# Compute y-limits per row
ylim_solar_elev <- range(c(solar22$TOA_rad,
                      solar23$TOA_rad), na.rm=TRUE)
#ylim_solar_az   <- range(c(solar22$Solar.Azimuth.Angle..deg.cw.from.N.,
                #       solar23$Solar.Azimuth.Angle..deg.cw.from.N.), na.rm=TRUE)
ylim_air_temp   <- range(c(climate22_stat$temp, climate22_ap$temp,
                      climate23_stat$temp, climate23_ap$temp), na.rm=TRUE)
ylim_precip     <- range(climate22_stat$precip_amt, na.rm=TRUE)
ylim_blacktop_t <- range(c(logger22$S1.Temperature, logger22$S2.Temperature,
logger22$S3.Temperature,
                      logger23$S1.Temperature, logger23$S2.Temperature, logger23$S3.Temperature),
na.rm=TRUE)
ylim_station_t  <- range(c(logger22$S4.Temperature, logger22$S5.Temperature,
logger22$S6.Temperature,
                      logger23$S4.Temperature, logger23$S5.Temperature, logger23$S7.Temperature),
na.rm=TRUE)
ylim_blacktop_q <- range(c(logger22$S1.Discharge_ls, logger22$S2.Discharge_ls,
logger22$S3.Discharge_ls,
                      logger23$S1.Discharge_ls, logger23$S2.Discharge_ls, logger23$S3.Discharge_ls),
na.rm=TRUE)
```

```
ylim_station_q  <- range(c(logger22$S4.Discharge_ls, logger22$S5.Discharge_ls,
logger22$S6.Discharge_ls,
                          logger23$S4.Discharge_ls, logger23$S5.Discharge_ls, logger23$S7.Discharge_ls),
na.rm=TRUE)
#ylim_sed       <- range(c(sed22$sediment.load..mg.L., sed23$sediment.load..mg.L.), na.rm=TRUE)
ylim_sed <- range(
  sed22_blacktop$sediment.load..mg.L.,
  sed23_blacktop$sediment.load..mg.L.,
  sed22_station$sediment.load..mg.L.,
  sed23_station$sediment.load..mg.L.,
  na.rm = TRUE
)

panel_labels <- LETTERS[1:10]

# --------------------------
# 1. Solar Elevation
  yt_az <- y_ticks_n(ylim_solar_az, n = 4)

plot(as.POSIXct(solar22$Date.and.Time.UTC6), solar22$TOA_rad,
    type="l", bty="L", ylab="(W"~m^{-2}*")", ylim=ylim_solar_elev, xaxt="n")

mtext(toupper("TOA Radiation"), side=3, line=0, adj=0.01, cex=0.9)
mtext(panel_labels[1], side=3, line=0, adj=-0.1, font=2, cex=0.9)
add_x_axis(x = as.POSIXct(solar22$Date.and.Time.UTC6), show_labels = FALSE)
#axis(side=4)

#par(new=TRUE)
#plot(as.POSIXct(solar22$Date.and.Time.UTC6), solar22$Solar.Azimuth.Angle..deg.cw.from.N.,
 #    type="l", bty="L", ylab="(W"~m^{-2}*")", axes=FALSE, ylim=ylim_solar_az, col="darkkhaki")
#mtext(toupper("Solar azimuth"), side=3, line=0, adj=0.01, cex=0.9)
#mtext(panel_labels[2], side=3, line=0, adj=-0.1, font=2, cex=0.9)
#axis(side=4, at = yt_az)
#mtext("AZIMUTH (DEG)", side = 4, line = 2.5, cex = 0.8)


plot(as.POSIXct(solar23$Date.time.UTC6), solar23$TOA_rad,
    type="l", bty="L", ylab="", ylim=ylim_solar_elev, xaxt="n")

#par(new=TRUE)
#plot(as.POSIXct(solar23$Date.time.UTC6), solar23$Solar.Azimuth.Angle..deg.cw.from.N.,
   # type="l", bty="L", ylab="", ylim=ylim_solar_az, xaxt="n",axes=FALSE , col="darkkhaki")
#axis(side=4, at = yt_az)
add_x_axis(x = as.POSIXct(solar23$Date.time.UTC6), show_labels = FALSE)

#legend('bottom',
   #   inset = c(0,-0.3),
    #  legend = c("Elevation", "Azimuth"),
     # col = c("black", "darkkhaki"),
      # #lty = 1,
       #horiz = TRUE,
       #bty = "n",
       #cex = 0.8,
       #xpd=NA)

# --------------------------
```

```
# 2. Air Temperature
plot(as.POSIXct(climate22_stat$Date.and.Time.UTC6), climate22_stat$temp, type="l", bty="L",
    ylab="°C", ylim=ylim_air_temp, xaxt="n")
lines(as.POSIXct(climate22_ap$Date.and.Time.UTC6), climate22_ap$temp, col="red")
mtext(toupper("Air temperature"), side=3, line=0, adj=0.01, cex=0.9)
mtext(panel_labels[2], side=3, line=0, adj=-0.1, font=2, cex=0.9)
add_x_axis(x = as.POSIXct(climate22_stat$Date.and.Time.UTC6), show_labels = FALSE)

plot(as.POSIXct(climate23_stat$Date.and.time.UTC6), climate23_stat$temp, type="l", bty="L",
    ylab="", ylim=ylim_air_temp, xaxt="n")
lines(as.POSIXct(climate23_ap$Date.and.time.UTC6), climate23_ap$temp, col="red")
add_x_axis(x = as.POSIXct(climate23_stat$Date.and.time.UTC6), show_labels = FALSE)

legend("bottom",
      inset=c(0, -0.3),
      legend = c("Station", "Airstrip"),
      col = c("black", "red"),
      lty = 1,
      lwd = 1,
      horiz = TRUE,
      cex = 0.8,
      bty = "n",
      xpd=NA)

# ---------------------------
# 3. Precipitation
plot(as.POSIXct(climate22_stat$Date.and.Time.UTC6), climate22_stat$precip_amt,
    type="h", bty="L", ylab="mm", ylim=ylim_precip, xaxt="n")
mtext(toupper("Precipitation"), side=3, line=0, adj=0.01, cex=0.9)
mtext(panel_labels[3], side=3, line=0, adj=-0.1, font=2, cex=0.9)
add_x_axis(x = as.POSIXct(climate22_stat$Date.and.Time.UTC6), show_labels = FALSE)
plot.new()
box()
text(0.5, 0.5, "NO PRECIPITATION DATA", cex=0.9)
# ---------------------------
# 4. Blacktop Creek Temperature

yt_bt_t <- y_ticks_n(ylim_blacktop_t, n = 5)
yt_st_t <- y_ticks_n(ylim_station_t,  n = 5)


plot(as.POSIXct(logger22$Date.and.Time.UTC6), logger22$S1.Temperature, type="l",
    col="blue", bty="L", ylab="°C", ylim=ylim_blacktop_t, xaxt="n", yaxt="n")
lines(as.POSIXct(logger22$Date.and.Time.UTC6), logger22$S2.Temperature, col="green")
lines(as.POSIXct(logger22$Date.and.Time.UTC6), logger22$S3.Temperature, col="red")
mtext(toupper("Blacktop Creek temperature"), side=3, line=0, adj=0.01, cex=0.9)
mtext(panel_labels[4], side=3, line=0, adj=-0.1, font=2, cex=0.9)
axis(2, at = yt_bt_t)
add_x_axis(x = as.POSIXct(logger22$Date.and.Time.UTC6), show_labels = FALSE)


plot(as.POSIXct(logger23$Date.and.Time.UTC6), logger23$S1.Temperature, type="l",
    col="blue", bty="L", ylab="", ylim=ylim_blacktop_t, xaxt="n", yaxt="n")
lines(as.POSIXct(logger23$Date.and.Time.UTC6), logger23$S2.Temperature, col="green")
lines(as.POSIXct(logger23$Date.and.Time.UTC6), logger23$S3.Temperature, col="red")
axis(2, at = yt_bt_t)
```

```
add_x_axis(x = as.POSIXct(logger23$Date.and.Time.UTC6), show_labels = FALSE)


# ---------------------------
# 5. Station Creek Temperature
plot(as.POSIXct(logger22$Date.and.Time.UTC6), logger22$S4.Temperature, type="l",
    col="purple", bty="L", ylab="°C", ylim=ylim_station_t, xaxt="n", yaxt="n")
lines(as.POSIXct(logger22$Date.and.Time.UTC6), logger22$S5.Temperature, col="orange")
lines(as.POSIXct(logger22$Date.and.Time.UTC6), logger22$S6.Temperature, col="darkgrey")
mtext(toupper("Station Creek temperature"), side=3, line=0, adj=0.01, cex=0.9)
mtext(panel_labels[5], side=3, line=0, adj=-0.1, font=2, cex=0.9)
axis(2, at = yt_bt_t)


add_x_axis(x = as.POSIXct(logger22$Date.and.Time.UTC6), show_labels = FALSE)
plot(as.POSIXct(logger23$Date.and.Time.UTC6), logger23$S4.Temperature, type="l",
    col="purple", bty="L", ylab="", ylim=ylim_station_t, xaxt="n", yaxt="n")
lines(as.POSIXct(logger23$Date.and.Time.UTC6), logger23$S5.Temperature, col="orange")
lines(as.POSIXct(logger23$Date.and.Time.UTC6), logger23$S7.Temperature, col="darkgrey")
axis(2, at = yt_st_t)
add_x_axis(x = as.POSIXct(logger23$Date.and.Time.UTC6), show_labels = FALSE)


# ---------------------------
# ---------------------------
# 6. Blacktop Creek Discharge

yt_bt_q <- y_ticks_n(ylim_blacktop_q, n = 4, digits = 0)

plot(as.POSIXct(logger22$Date.and.Time.UTC6), logger22$S1.Discharge_ls, type="l",
    col="blue", bty="L", ylab="L s⁻¹", ylim=ylim_blacktop_q, xaxt="n", yaxt="n")
lines(as.POSIXct(logger22$Date.and.Time.UTC6), logger22$S2.Discharge_ls, col="green")
lines(as.POSIXct(logger22$Date.and.Time.UTC6), logger22$S3.Discharge_ls, col="red")

mtext(toupper("Blacktop Creek discharge"), side=3, line=0, adj=0.01, cex=0.9)
mtext(panel_labels[6], side=3, line=0, adj=-0.1, font=2, cex=0.9)
axis(2, at = yt_bt_q, labels = yt_bt_q)
add_x_axis(x = as.POSIXct(logger22$Date.and.Time.UTC6), show_labels = FALSE)

plot(as.POSIXct(logger23$Date.and.Time.UTC6), logger23$S1.Discharge_ls, type="l",
    col="blue", bty="L", ylab="", ylim=ylim_blacktop_q, xaxt="n", yaxt="n")
lines(as.POSIXct(logger23$Date.and.Time.UTC6), logger23$S2.Discharge_ls, col="green")
lines(as.POSIXct(logger23$Date.and.Time.UTC6), logger23$S3.Discharge_ls, col="red")
axis(2, at = yt_bt_q, labels = yt_bt_q)
add_x_axis(x = as.POSIXct(logger23$Date.and.Time.UTC6), show_labels = FALSE)

# ---------------------------
# 7. Station Creek Discharge
yt_st_q <- y_ticks_n(ylim_station_q, n = 4, digits = 0)

plot(as.POSIXct(logger22$Date.and.Time.UTC6), logger22$S4.Discharge_ls, type="l",
    col="purple", bty="L", ylab="L s⁻¹", ylim=ylim_station_q, xaxt="n",yaxt="n")
lines(as.POSIXct(logger22$Date.and.Time.UTC6), logger22$S5.Discharge_ls, col="orange")
lines(as.POSIXct(logger22$Date.and.Time.UTC6), logger22$S6.Discharge_ls, col="darkgrey")

mtext(toupper("Station Creek discharge"), side=3, line=0, adj=0.01, cex=0.9)
```

```
mtext(panel_labels[7], side=3, line=0, adj=-0.1, font=2, cex=0.9)
axis(2, at = yt_st_q, labels = yt_st_q)
add_x_axis(x = as.POSIXct(logger22$Date.and.Time.UTC6), show_labels = FALSE)

plot(as.POSIXct(logger23$Date.and.Time.UTC6), logger23$S4.Discharge_ls, type="l",
    col="purple", bty="L", ylab="", ylim=ylim_station_q, xaxt="n",yaxt="n")
lines(as.POSIXct(logger23$Date.and.Time.UTC6), logger23$S5.Discharge_ls, col="orange")
lines(as.POSIXct(logger23$Date.and.Time.UTC6), logger23$S7.Discharge_ls, col="darkgrey")
axis(2, at = yt_st_q, labels = yt_st_q)
add_x_axis(x = as.POSIXct(logger23$Date.and.Time.UTC6), show_labels = FALSE)

# -------------------------
# 8. Blacktop Creek Sediment Load

sed22_blacktop$datetime <- as.POSIXct(
  sed22_blacktop$Date.time..LST.,
  format = "%m/%d/%Y %H:%M",
  tz = "UTC"
)

xlimcl_bt22 <- range(climate23_stat$Date.and.time.UTC6, na.rm = TRUE)
xlimcl_bt22

xlim_bt22 <- range(sed22_blacktop$datetime, na.rm = TRUE)

plot(xlim_2022 <- as.POSIXct(c("2022-07-05 10:30",
                               "2022-07-22 00:00"),
                             tz = "UTC"),
    ylim_sed,
    type = "n",
    bty = "L",
    ylab = expression("mg L"^{-1}*""),
    xaxt = "n")

for(i in seq_along(sites22_bt)) {
  s <- sites22_bt[i]
  subdat <- sed22_blacktop[sed22_blacktop$Site.. == s, ]

  lines(subdat$datetime,
        subdat$sediment.load..mg.L.,
        col = cols_bt[i],
        lwd = 1)
}

axis(1,
  at = as.POSIXct(c("07/10/2022 00:00", "07/17/2022 00:00"),format = "%m/%d/%Y %H:%M", tz =
"UTC"),
  labels = c("", "")
)
mtext(toupper("Blacktop creek sediment load"), side=3, line=0, adj=0.01, cex=0.9)
mtext(panel_labels[8], side=3, line=0, adj=-0.1, font=2, cex=0.9)

##

sed23_blacktop$datetime <- as.POSIXct(
  sed23_blacktop$Date.time..LST.,
```

```
  format = "%m/%d/%Y %H:%M",
  tz = "UTC"
)
plot(range(sed23_blacktop$datetime, na.rm=TRUE),
     ylim_sed,
     type="n",
     bty="L",
     ylab="",
     xaxt="n")

for(i in seq_along(sites23_bt)) {
  s <- sites23_bt[i]
  subdat <- sed23_blacktop[sed23_blacktop$Site.. == s, ]
  lines(subdat$datetime,
        subdat$sediment.load..mg.L.,
        col = cols_bt23[i],
        lwd = 1,
        type = "l",
        pch = 16,
        cex = 0.8)
}
axis(1,
     at = as.POSIXct(c("07/10/2023 00:00", "07/17/2023 00:00"),format = "%m/%d/%Y %H:%M", tz =
"UTC"),
     labels = c("", "")
)



# ---------------------------
# 9. Station Creek Sediment Load

sed22_station$datetime <- as.POSIXct(
  sed22_station$Date.time..LST.,
  format = "%m/%d/%Y %H:%M",
  tz = "UTC"
)

xlim_range<-range(logger22$Date.and.Time.UTC6)
xlim_range

plot(xlim_2022 <- as.POSIXct(c("2022-07-05 10:30",
                               "2022-07-22 00:00"),
                             tz = "UTC"),
     ylim_sed,
     type="n",
     bty="L",
     ylab=expression("mg L"^{-1}*""),
     xaxt="n")

for(i in seq_along(sites22_st)) {
  s <- sites22_st[i]
  subdat <- sed22_station[sed22_station$Site.. == s, ]
  lines(subdat$datetime,
        subdat$sediment.load..mg.L.,
        col = cols_st22[i],
```

```
       lwd = 1,
       type = "l",
       pch = 16,
       cex = 0.8)
}

mtext(toupper("Station creek sediment load"), side=3, line=0, adj=0.01, cex=0.9)
mtext(panel_labels[9], side=3, line=0, adj=-0.1, font=2, cex=0.9)
axis(1,
    at = as.POSIXct(c("07/10/2022 00:00", "07/17/2022 00:00"),format = "%m/%d/%Y %H:%M", tz =
"UTC"),
    labels = c("Jul 10", "Jul 17")
)


legend("bottom",
      inset = c(0, -0.8),
      legend = paste("Site", 1:6),
      col    = c("blue", "green", "red", "purple", "orange", "darkgrey"),
      lty    = 1,
      lwd    = 1,
      horiz  = FALSE,
      ncol=3,
      cex    = 0.75,
      bty    = "n",
      xpd    = NA)
###
sed23_station$datetime <- as.POSIXct(
  sed23_station$Date.time..LST.,
  format = "%m/%d/%Y %H:%M",
  tz = "UTC"
)

plot(range(sed23_station$datetime, na.rm=TRUE),
    ylim_sed,
    type="n",
    bty="L",
    ylab="",
    xaxt="n")

for(i in seq_along(sites23_st)) {
  s <- sites23_st[i]
  subdat <- sed23_station[sed23_station$Site.. == s, ]
  lines(subdat$datetime,
       subdat$sediment.load..mg.L.,
       col = cols_st23[i],
       lwd = 1,
       type = "l",
       pch = 16,
       cex = 0.8)
}
axis(1,
    at = as.POSIXct(c("07/10/2023 00:00", "07/17/2023 00:00"),format = "%m/%d/%Y %H:%M", tz =
"UTC"),
    labels = c("Jul 10", "Jul 17")
)
```

```
 # -------------------------
# Global labels
mtext("Date", side=1, outer=TRUE, line=2)
mtext("2022", side=3, outer=TRUE, at=0.25, line=1.2, font=2)
mtext("2023", side=3, outer=TRUE, at=0.75, line=1.2, font=2)


legend("bottom",
       inset = c(0, -0.8),
       legend = paste("Site", c("1","2 LS", "2 RS", "3", "4", "5", "5 SC", "6", "7")),
       col    = c("blue", "green","magenta",  "red", "orange","purple", "black","darkgrey","darkgreen"),
       lty    = 1,
       lwd    = 1,
       horiz  = FALSE,
       cex    = 0.75,
       ncol=5,
       bty    = "n",
       xpd    = NA)

}
Climate interactions & stream temp plot:
############### scatter plots
## 2022 and 2023 Air temp (airport) and stream temp, 2 plots, sites coloured
names(data)
names(data22)

data$TOA_rad <- 1361 * sin(data$Solar.Elevation.corrected.for.atm.refraction..deg. * pi/180)
data22$TOA_rad <- 1361 * sin(data22$Solar.Elevation.corrected.for.atm.refraction..deg. * pi/180)
## 2022 and 2023 solar azimuth and stream temp, 2 plots, sites coloured.
library(tidyverse)
library(lubridate)
library(gridExtra)

# Reshape 2023 data to long format
data_long_23 <- data %>%
  select(Date.and.Time.UTC6, A.temp,TOA_rad,A.rel_hum, matches("^S[0-9]\\.Temperature$")) %>%
  pivot_longer(cols = matches("^S[0-9]\\.Temperature$"),
               names_to = "Site",
               values_to = "StreamTemp")%>%
  mutate(Site = str_remove(Site, "\\.Temperature"))

# Reshape 2022 data to long format
data_long_22 <- data22 %>%
  select(Date.and.Time.UTC6, A.temp,TOA_rad,A.rel_hum, matches("^S[0-9]\\.Temperature$")) %>%
  pivot_longer(cols = matches("^S[0-9]\\.Temperature$"),
               names_to = "Site",
               values_to = "StreamTemp")%>%
  mutate(Site = str_remove(Site, "\\.Temperature"))
# Plot
airtemp22<- ggplot(data_long_22, aes(x = A.temp, y = StreamTemp, colour = Site)) +
  geom_point(alpha = 0.4, size = 1.2) +
  geom_smooth(method = "lm", se = FALSE) +
  labs(
    x = "Airport Air Temperature (°C)",
    y = "Stream Temperature (°C)",
```

```
    title = "                    2022",
    colour = "Site"
  ) +
  theme_bw(base_size = 12)+
  theme(
    panel.grid.major = element_blank(),
    panel.grid.minor = element_blank()
  )
# Plot
airtemp23<-ggplot(data_long_23, aes(x = A.temp, y = StreamTemp, colour = Site)) +
  geom_point(alpha = 0.4, size = 1.2) +
  geom_smooth(method = "lm", se = FALSE) +
  labs(
    x = "Airport Air Temperature (°C)",
    y = "Stream Temperature (°C)",
    title = "                    2023",
    colour= "Site"
  ) +
  theme_bw(base_size = 12)+
  theme(
    panel.grid.major = element_blank(),
    panel.grid.minor = element_blank()
  )

# Plot
sol22<- ggplot(data_long_22, aes(x = TOA_rad, y = StreamTemp, colour = Site)) +
  geom_point(alpha = 0.4, size = 1.2) +
  geom_smooth(method = "lm", se = FALSE) +
  labs(
    x = expression("TOA Radiation (W"~m^{-2}*")"),
    y = "Stream Temperature (°C)",
    #title = "Relationship Between Airport Air Temperature and Stream Temperature (2022)",
    colour = "Site"
  ) +
  theme_bw(base_size = 12)+
  theme(
    panel.grid.major = element_blank(),
    panel.grid.minor = element_blank()
  )
# Plot
sol23<-ggplot(data_long_23, aes(x = TOA_rad, y = StreamTemp, colour = Site)) +
  geom_point(alpha = 0.4, size = 1.2) +
  geom_smooth(method = "lm", se = FALSE) +
  labs(
    x = expression("TOA Radiation (W"~m^{-2}*")"),
    y = "Stream Temperature (°C)",
    #title = "Relationship Between Airport Air Temperature and Stream Temperature (2023)",
    colour= "Site"
  ) +
  theme_bw(base_size = 12)+
  theme(
    panel.grid.major = element_blank(),
    panel.grid.minor = element_blank()
  )
```

```
grid.arrange(airtemp22, airtemp23, sol22,sol23, ncol=2, nrow=2)
```